JNC TN7400 2003-004

Mizunami Underground Research Laboratory Project
Results from 1996-1999

(Revised edition)

May 2001

Tono Geoscience Center
Japan Nuclear Cycle Development Institute

Contents

JNC TN7400 2003-004
May 2001

Mizunami Underground Research Laboratory Project Results from 1996-1999 (Revised edition)

Abstract

Tono Geoscience Center (TGC), Japan Nuclear Cycle Development Institute (JNC) has been carrying out a wide range of geoscientific research in order to build a firm scientific and technological basis for geological disposal. One of the major components of the ongoing geoscientific research program is the Mizunami Underground Research Laboratory (MIU) Project in the Tono area, central Japan. The R&D work for the MIU Project has the following main goals:

- To establish comprehensive techniques for investigating the geological environment
- To acquire data on the deep geological environment
- To develop a range of engineering techniques for deep underground application

The development of the MIU will occur in three overlapping Phases over a 20-year life cycle: Phase I (Surface-based Investigation Phase) began in 1996; Phase II (Construction Phase) and Phase III (Operation Phase) have yet to start.

The Shobasama Site has been studied in detail by surface-based geological, geophysical, hydrogeological, hydrochemical and rock mechanical investigations in the reporting period. Ground geophysical surveys, hydrological monitoring and multi-disciplinary borehole investigations have been carried out in the three 1,000 m deep boreholes drilled for the MIU Project in the reporting period. Based on the information obtained, geological, hydrogeological and hydrochemical models and rock mechanics conceptual models have been constructed. Groundwater flow simulations have been carried out in order to evaluate the validity of the hydrogeological modeling method. These investigations have facilitated the accumulation of technical knowledge and expertise on the methodologies and techniques needed to characterize the deep geological environment.

The results of these R&D activities have been used in the Second Progress Report on Research and Development for the Geological Disposal of HLW, commonly known as the H12 Report, submitted by JNC to the Japanese Government in 1999. The results have also been widely utilized by various research institutes, including universities. JNC will continue the research to provide a scientific and technological basis for safety regulations and repository siting.

This report is also available in Japanese: JNC Technical Report, JNC TN7400 2001-001.

1 Introduction

The Atomic Energy Commission of Japan formulated the 'Long-term Program for Research, Development and Utilization of Nuclear Energy' [1] (henceforth 'Long-term Program') in June 1994 with a subsequent revision in November 2000. This program laid down basic policy, stipulating that 'scientific research on deep geological environment as the basis for research and development of geological disposal should be advanced'. The Japan Nuclear Cycle Development Institute (JNC) has been promoting and carrying out scientific research on deep geological environments under the name 'geoscientific research'. The Long-term Program presented the following policy perspectives for underground research facilities to emphasize their importance.

- Deep underground research facilities play an important role in research relating to geological disposal. They allow us to understand the characteristics of the geological environment and to improve the reliability of the models used for performance assessment of disposal systems. They also provide opportunities for comprehensive research that will contribute to overall understanding of Japan's deep geological environment.
- It is recommended that more than one facility should be constructed, considering the range of characteristics and features of Japan's geology and other relevant factors.
- It is important to plan underground research facilities on the basis of results obtained from research and development work already carried out, particularly the results of scientific studies of the deep geological environment. Such a plan for underground research facilities should be clearly separated from the development of an actual repository.

Based on the basic policy outlined above, JNC began the Mizunami Underground Research Laboratory (MIU) Project. This report is a summary of the geoscientific research activities and the results for the period from 1996 FY to 1999 FY ('Phase I-a', See Section 3.2) of the MIU Project. The research was performed according to the 'Master Plan of the Mizunami Underground Research Laboratory' (henceforth 'Master Plan') [2] and the annual plan of the geoscientific research [3~7] for the MIU Project.

The revision to the Long-term Program in November 2000, stipulated that:

- Based on the results of past research, JNC should steadily carry on research and development activities to evaluate the reliability of geological disposal technologies and to establish a safety assessment method, using research facilities for the deep geological environment. The research facilities for deep geological environments will serve not only as a place for scientific investigations, but also as a place for deepening public understanding of research and development activities related to the geological disposal of nuclear waste.

2 Overview of the geoscientific research in the MIU Project

The MIU Project is located at the Shobasama Site in Akeyo-cho, Mizunami City, Gifu Prefecture. The geoscientific research carried out for the MIU Project is primarily focused on the study of the granite at the site; granite being a widely distributed crystalline rock type in Japan. Fortuitously, JNC had carried out an extensive geoscientific research program in and around the nearby Tono Mine. This research could be readily expanded to the benefit of the overall program.

By adopting a repetitive site investigation approach consisting of survey, prediction, and verification of the underground geological environment, JNC intends to confirm the applicability and accuracy of the investigation methods and the validity of the assessment of the geological environment. The project is divided into the following three Phases extending over a 20 years schedule (Figure 2.1).

Phase I (Surface-based Investigation Phase)
The multidisciplinary approach to geoscientific characterization from the surface has been implemented. Ultimately, all aspects of the geological environment deep underground as well as the effects on that environment of shaft excavation in Phase II will be predicted based on the surface-based investigations. Input to design of the facilities and scoping of the underground experimental activities has begun in Phase I.

Phase II (Construction Phase)
Site characterization and monitoring of the geological environment will continue during construction. During this Phase direct observations of the geological environment in the subsurface together with monitoring data will be used to test and assess the accuracy of the predictions made in Phase I about the geological environment and the effects of shaft excavation on that environment. During this Phase all new information will be combined with the existing knowledge on the geological environment to develop predictive models of the conditions expected to occur in the research galleries and the response to the excavations in Phase III. More detailed planning of Phase III activities will begin during this Phase.

Phase III (Operation Phase)
Detailed investigations, likely at several scales, with the intent to develop a detailed database and knowledge of the geological environment in the galleries are to be performed. The opportunity to develop geological information at scales of interest and in a variety of geological settings or conditions pertinent to the development of disposal technology are possible because of depth related variations in structural style and the hydrogeological and mechanical conditions. The facility layout will allow the study of processes that occur naturally in the subsurface, such as movement of solute in groundwater and other processes induced by excavation such as rock failure due to stress adjustment. Importantly, the accuracy of the predictions of the geological environment made in Phases I and II can be assessed, leading to improved models and expertise. In addition, the usefulness of the engineering techniques employed in the excavation deep underground can be assessed.

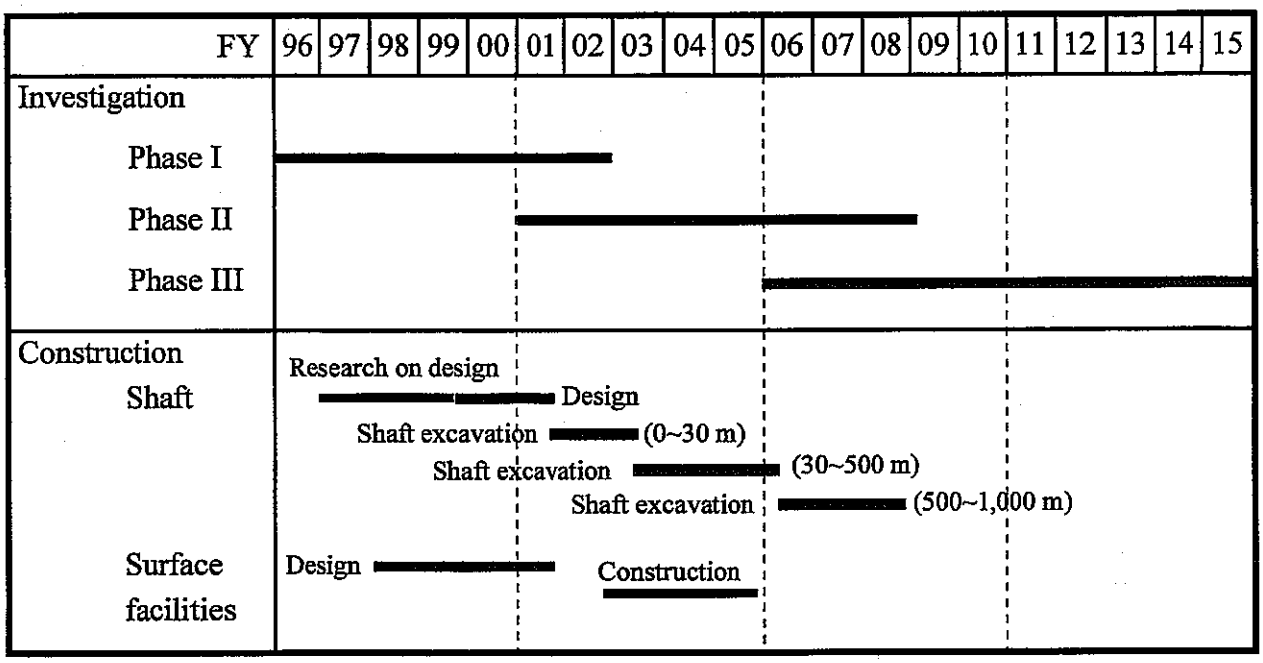

Figure 2.1 Schedule [8)]

2.1 Goals

The MIU Project is a study of a geological environment that has an appropriate extent and depth and has not been disturbed by human activities. The Project is expected to contribute to research and development for geological disposal as well as contributing to academic research on the deep geological environment in Japan. For this reason, it is essential that research should be comprehensive, systematic and relevant. Furthermore, the research is intended to not only develop an understanding of the geological environment and the effects of shaft and drift excavation on that environment but also at developing the methodology, applicable equipment and expertise for characterization of the subsurface.

In consideration of the above, goals of the entire MIU Project have been established. In addition, because the research activities differ from Phase to Phase, specific goals have been set for each Phase in order to give focus and direction to the research.

2.1.1 The goals of the MIU Project [2]

① To establish comprehensive techniques for investigating the geological environment

The first goal is to systematically combine the fundamental methodologies applied, developed and improved in JNC's geoscientific research and to provide comprehensive and integrated investigation strategies. These strategies are intended to demonstrate the effectiveness of a series of techniques for reliably investigating, predicting and modeling the characteristics of the deep geological environment and for evaluating the models of the geological environment. The reliability of the investigation techniques used and resultant data quality will be studied. It is expected that the techniques developed during the project will provide the technical basis for a variety of investigations.

② To acquire data on the deep geological environment

The second goal is to acquire high-quality data on the deep geological environment. These data, which will be backed up with results of geoscientific studies both in Japan and abroad, will be used to improve the reliability of conceptual models of the deep geological environment in Japan. They will also be used to evaluate engineering methods and equipment for the later Phases of underground construction and operations. The integrated dataset produced, which will include relevant results of geoscientific studies performed abroad, will provide a basis for other components of the R&D program for geological disposal in Japan.

③ To develop a range of engineering techniques for deep underground application

The third goal is to evaluate techniques for design and construction of large-scale underground facilities and to clarify the potential long-term effects of these techniques on the geological environment (e.g., possible interactions between construction materials and groundwater and/or bedrock.). Studies will also be carried out on the infrastructure for managing safety in such underground facilities.

2.1.2 The goals of Phase I [2]

① To acquire data on the undisturbed geological environment with surface-based investigation methods and to predict the characteristics of the geological environment and the effects of construction of underground facilities

These data will be used to construct geological, hydrogeological, hydrochemical and rock mechanical models for predicting the geological properties that will be encountered and the effects of construction in the next Phases.

② To establish methodologies for evaluating predictions

Criteria and detailed methodologies will be specified for checking the plausibility of predictions made in this Phase for comparison with the data obtained in the subsequent Construction Phase.

③ To formulate detailed design concepts for the underground facilities and to establish detailed research plans for the Construction Phase

Based on the data obtained in this Phase, as well as on modeling results, a detailed design concept for the underground facilities will be formulated and detailed investigation plans will be established for the construction Phase.

The goals ① and ② of the Phase I are set to achieve the goals ① and ② of the entire MIU Project. In the same way, the goal ③ of the Phase I is set to achieve the goal ③ of the entire MIU Project.

2.2 Applicability of the results

The results of the MIU Project will be categorized and reorganized from the viewpoint of geological disposal and provided to the Japanese national repository project and input to the development of safety regulations [8]. Coordination of the related organizations has advanced lately,* since the Long- term Program was revised and the implementing organization of the repository project, NUMO, was established in 2000. Therefore, based on this situation, re-examination on the organization and presentation of results would be done to advance the technology transfer.

2.3 Topography and geology

The MIU Project is being implemented at the Shobasama Site, a 14-hectare site owned by JNC. The Tono area, where the Shobasama Site is located, is bounded in the northwest by the Mino-Hida Mountains and in the southeast by the Mikawa Mountains. Topographically, the Tono area forms a roughly boat-shaped,

* Since the Japanese version of this report was written.

elongate topography with the axes of the linear ridges and valleys extending northeast-southwest between the two Mountains, as is shown in Figure 2.2. The Kiso River forms a deep valley cutting through the northern mountains. The boundary between the southeastern mountains and the boat-shaped hills is clearly marked by the northeast-southwest oriented Byobusan Fault, named after nearby Mt.Byobusan (794.1 m). This fault can be identified in the northeast by the presence of a steep cliff with talus deposits, although the steep cliff is less distinct toward the southwest. In the central part of this region, the Toki River flows from northeast to southwest. Terraces developed along the Toki River and its tributaries are composed of flat-lying, alluvial deposits.

The geology of the Tono area consists of sedimentary rocks of the Mino Belt (Jurassic to Cretaceous), granites and rhyolite (Cretaceous), and later sedimentary rocks (Miocene and Pliocene).

The sedimentary rocks of the Mino Belt are mostly sandstone, mudstone and chert with a strike of NE-WSW and represent repeated sequence of Triassic to Late Jurassic strata [9].

Nohi Rhyolite occurs in Kamado district, Mizunami City in the northeastern part of the Tono area and to the east of it. It is composed of monolithologic, welded tuff, and is intruded by Toki Granite in Mizunami City [10].

Granites are mainly the Ryoke Granite type and distributed in the Mino-Mikawa Plateau. The Toki Granite, 10 km in diameter, is exposed in the Toki-Mizunami Basin and intrudes into sedimentary rocks of the Mino Belt discordantly. The Toki Granite is regarded as a part of the Naegi-Agematsu Granite Complex located to the east. NNW quartz porphyry dikes [11] are intrusive into the Toki Granite near Toki City and in Mizunami City.

Miocene sedimentary strata (Mizunami and Kani Groups) unconformably overlie the basement rocks in the Toki-Mizunami and Kani basins. The Mizunami Group is divided into Toki Lignite-bearing Formation, Hongo Formation, Akeyo Formation and Oidawara Formation. As a whole, there is a trend of upward fining and wider distribution indicating transgression. The thickness of the Mizunami Group in the south of Toki-Mizunami Basin is over 300 m. The Pliocene Seto Group consists mainly of gravels (Toki Gravel) of chert and Nohi Rhyolite. A clay bed (Tokiguchi Formation) occurs in the lower horizon of Seto Group. [12]

There is a clear relationship between the geology and topography. The mountainous regions, hilly regions and hilltops correspond to Mesozoic basement rocks, Neogene/Quaternary sedimentary rocks and the Pliocene Seto Group (Toki Gravel), respectively [13].

The area is divided into several regional scale blocks formed by faulting and tilting movements. Geologically important faults include the Byobusan and Kasahara Faults occurring between Nakatsugawa-Tajimi (strike: NE-SW), Enasan Fault parallel to the above but to the south, and Sanageyama Fault along the east side of Mt.Sanageyama. All of these faults form steep cliffs. The Ako and Hanadate Faults crosscut the Byobusan Fault and the Kasahara Fault, nearly perpendicularly, to the north [14]. In Mizunami Basin are the Tsukiyoshi Fault (strike: EW) and the Yamada Fault Zone (strike: NE-SW to WSW) [12].

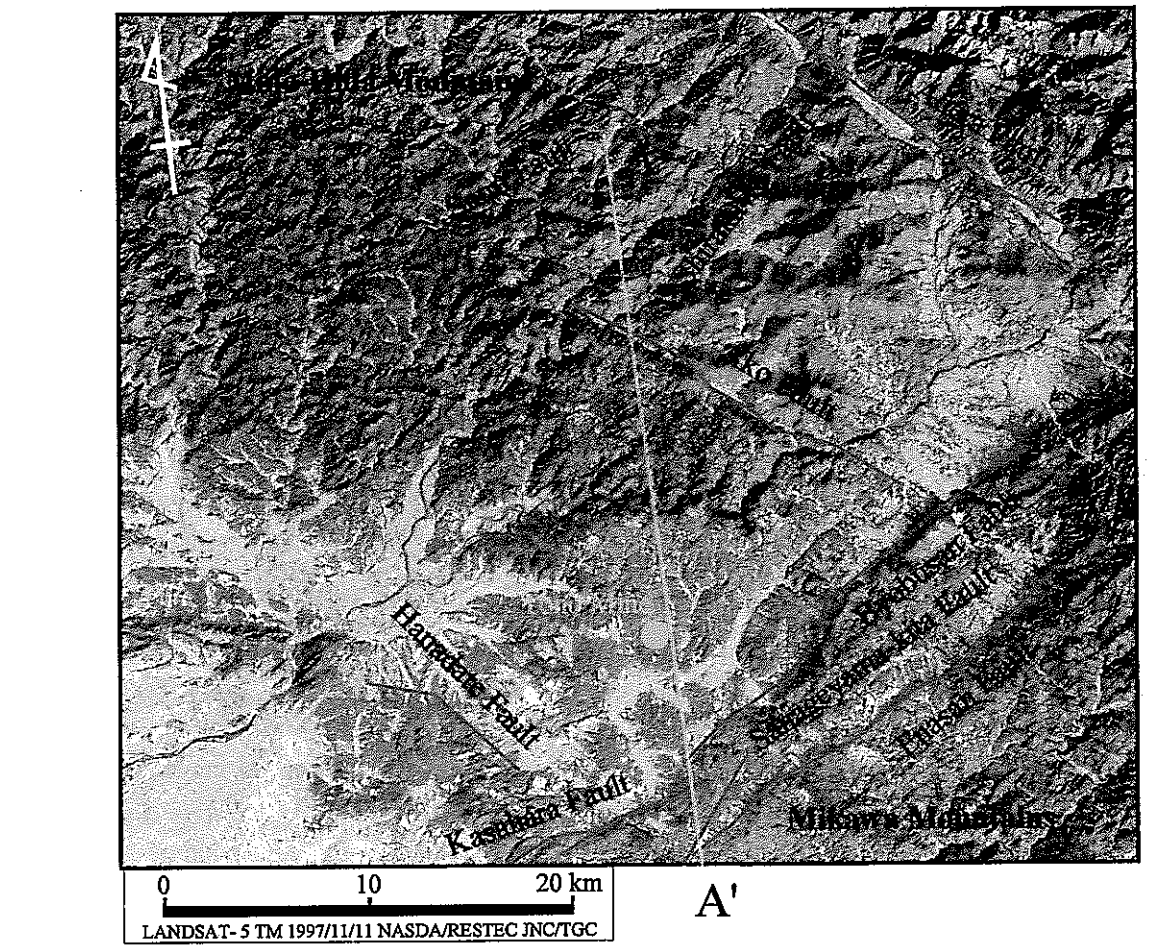

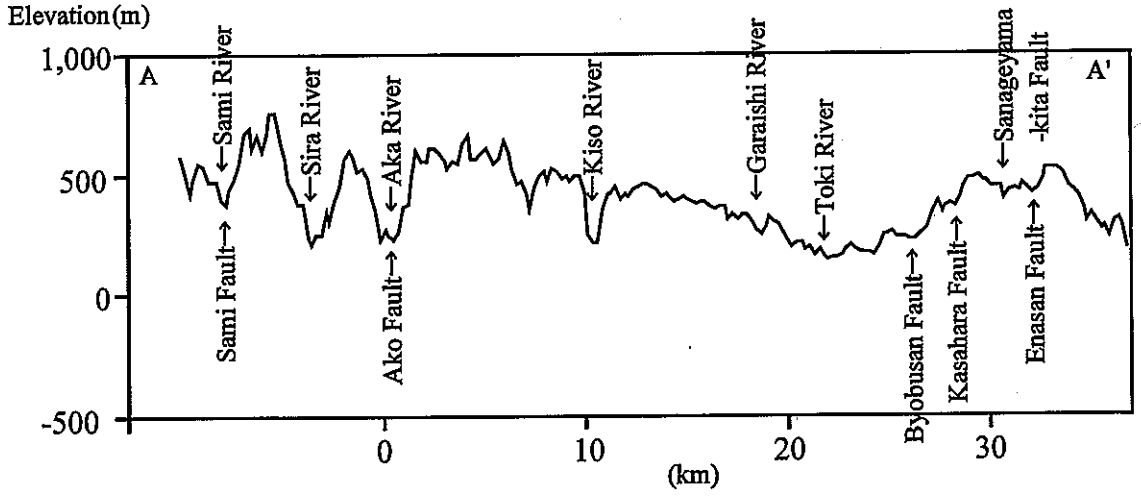

Figure 2.2 Topography of the Tono area (LANDSAT photograph and cross section)

The Shobasama Site is located in the hilly country between the Kiso and Toki Rivers, where the Mizunami and Seto Groups overlie the Toki Granite. Geology in the vicinity of the Shobasama Site is shown in Figure 2.3.

2.4 Planned facilities

Planned facilities for the MIU Project consist of the surface facilities, two shafts and the research galleries (Figure 2.4). According to the construction program of facilities decided by 1999 FY, the following shafts and research galleries are planned.

- A Main Shaft for access to about 1,000 m depth
- A Ventilation Shaft
- Two principal levels for research galleries at different depths (Main and Middle Stages)
- A spiral ramp to avoid premature disturbance of the Tsukiyoshi Fault by the Main Shaft intersection. The ramp will allow excavations to step out from the fault into the less disturbed part of the hanging wall and preparation for detailed investigations of the fault.

According to results from previous investigations, fracture frequencies are lowest between 400 m and 700 m depth. Fracture frequencies are higher above and below this range. The high fracture frequency below 800 m depth may be related to Tsukiyoshi Fault deformation. Thus, the research galleries at the Main and Middle Stages mentioned above are planned to be excavated at about 500 m and 1,000 m depths, which will allow detailed investigations in two different structural domains.

Planned facilities at surface consist of research and administration buildings, sample storage facility, an equipment maintenance facility, the shaft head frames, a muck deposit and a wastewater treatment facility.

The design of facilities will be optimized as the data are accumulated in Phase I, and as Phase II provides more detail on the subsurface.

2.5 Project site

As described above, the MIU Project is located at the Shobasama Site, owned by JNC (Figure 2.5). In order to improve the accuracy of all predictions including groundwater flow simulations carried out in the MIU Project, the study area should be established with consideration of the topography and properties of the geological environment. Thus, the results of the Regional Hydrogeological Study Project (RHS Project), which completely encompasses the Shobasama Site, can be fully utilized [15].

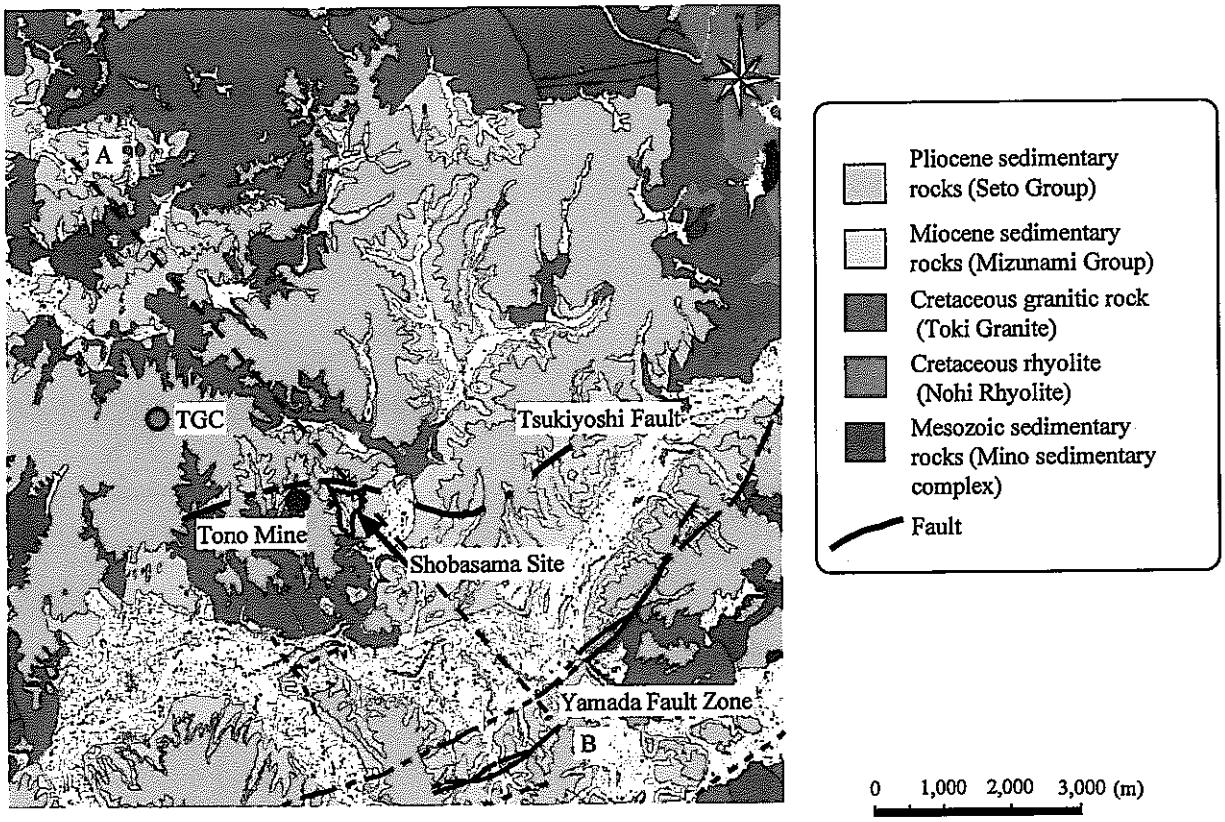

(a) Geological map

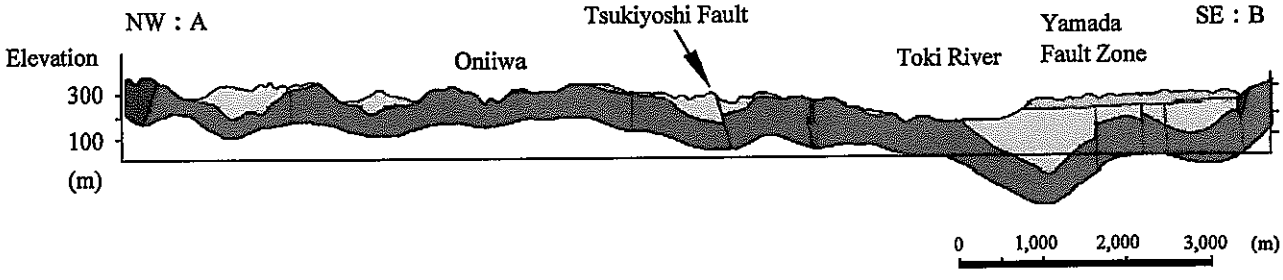

(b) Cross section of the line A-B in the geological map

Figure 2.3 Geology in the vicinity of the Shobasama Site

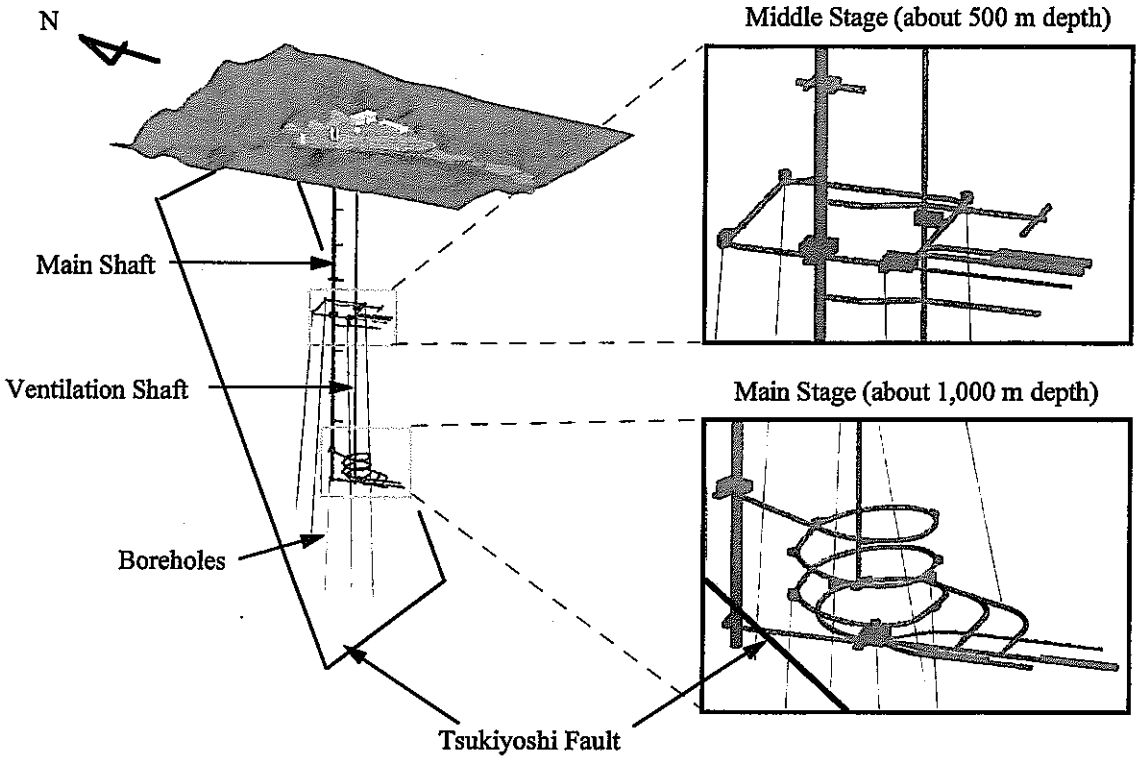

Figure 2.4 MIU conceptual design

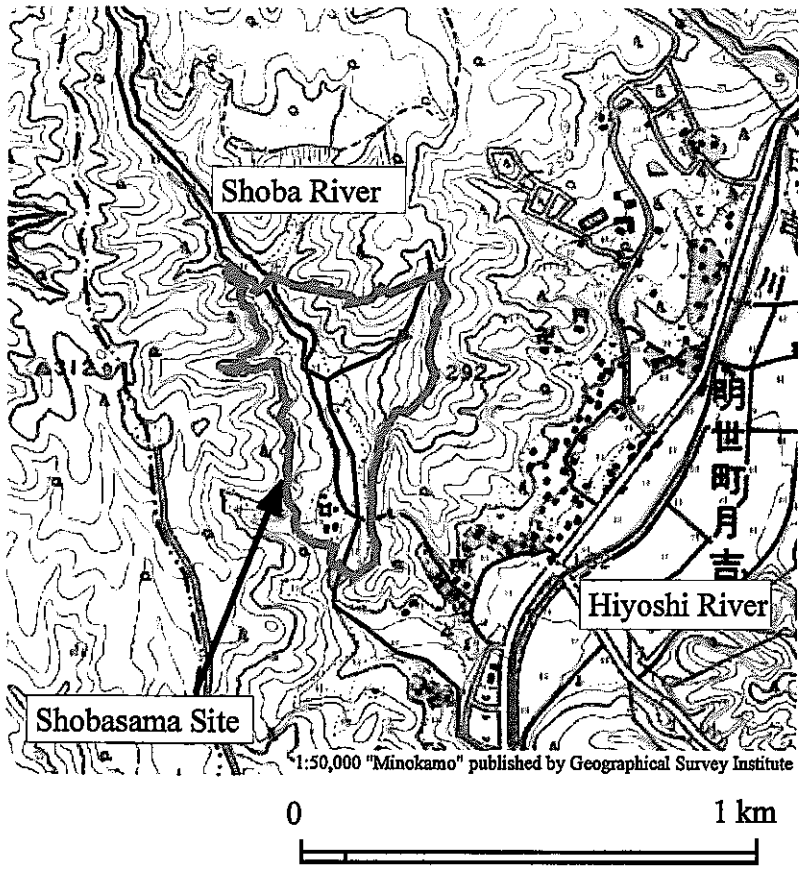

Figure 2.5 Location map of the Shobasama Site

3 Overview of Phase I-a

3.1 Approach to the investigations in Phase I

Also, an assessment of (a) the amount of data that can or should be acquired, i.e., the data requirements for each of the investigations and the investigations to be performed in terms of the type, detail and scope are related to (b) the quality and accuracy of the results needed for analysis and modeling. For this reason, a cyclical approach to the investigations, data analyses and evaluations were established, (Figure 3.1). This approach to assessment of data requirements and investigations has been done repetitively during this Phase.

The approach to the surface-based investigations and techniques applied in Phase I was as follows:

- Obtain data on the geological environment from surface utilizing a multi-disciplinary approach,
- Construct models of the geological environment,
- Predict the effects of shaft excavation on the geological environment.

The applicability of the techniques employed can be evaluated by a comparison of the predictions and the actual observations made during shaft excavation in Phase II.

3.2 Phase I-a and I-b [7]

The most important aspect of Phase I is to develop the expertise and techniques required to investigate, analyze and evaluate the geological environment to 1,000 m depth. Phase I was divided into Phases a and b to facilitate data analysis and the iterative approach to model development. Conceptual models of the geological environment were constructed in Phase I-a (1996-1999) from the data generated prior to and during the period of this report. Thereafter, the cycle of investigation, analysis and evaluation would be repeated in the 2nd half of Phase I (Phase I-b, starting 2000 FY) to examine the above-mentioned correlation between data requirements and investigations and the quality and accuracy of the investigation results.

In Phase I-a data obtained from the multi-disciplinary surface-based investigations were used to develop the geological, hydrogeological, hydrochemical and rock mechanics conceptual models (Figure 3.2).

The Phase I-b investigation plans are based on the results of the investigations in Phase I-a and in consideration of various research restrictions such as schedule and budget. Phase I-a models are to be revised according to the results of the analyses and evaluations made during the Phase I-b. The repetition of the cycle shown in Figure 3.1 enables us to understand how the models are improved by the revision and the correlation between quantity and quality of the data and the investigations.

Furthermore, by assessing and validating the revised models in subsequent Phases, it is expected that the usefulness of the surface-based investigations and associated analyses and evaluations can be assessed. Consequently, it may be possible to determine data requirements and the variety and scope of investigations for model construction.

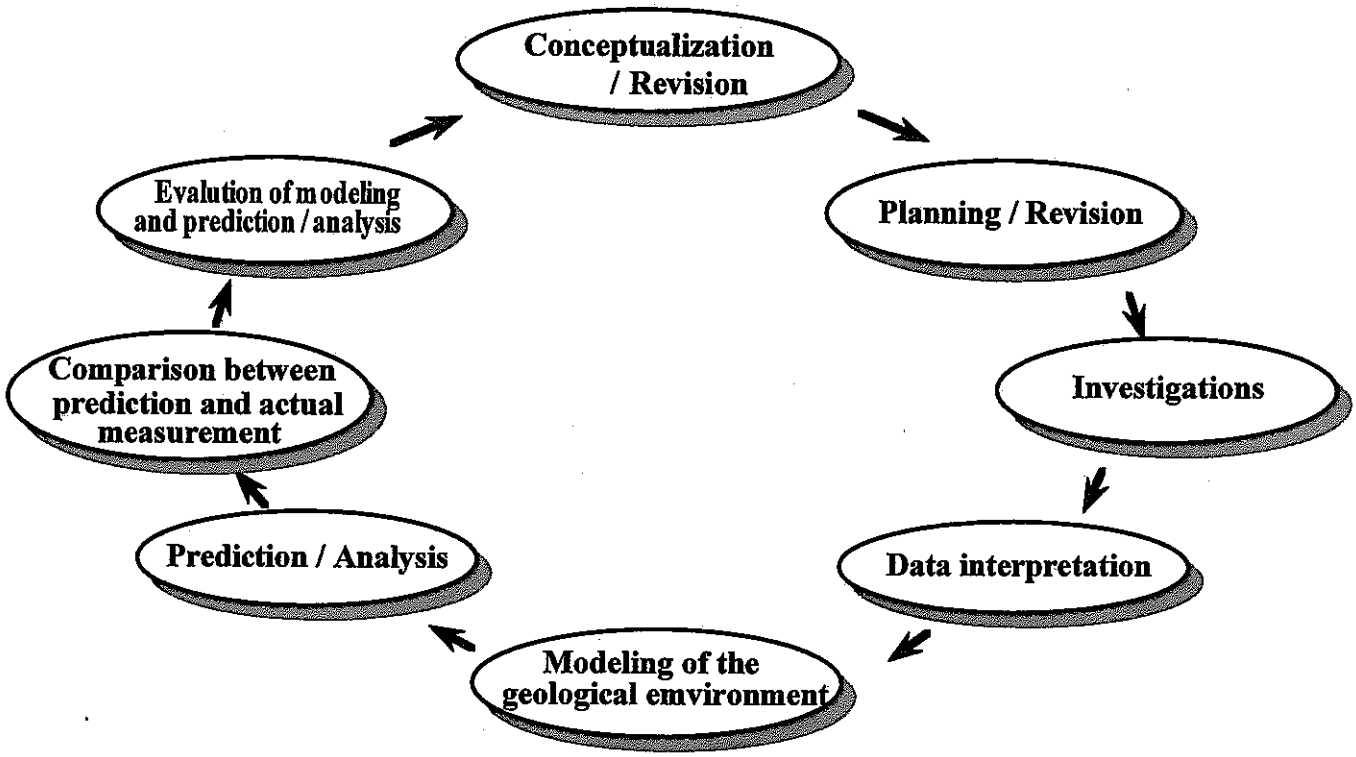

Figure 3.1 Approach to investigations, analysis and modeling

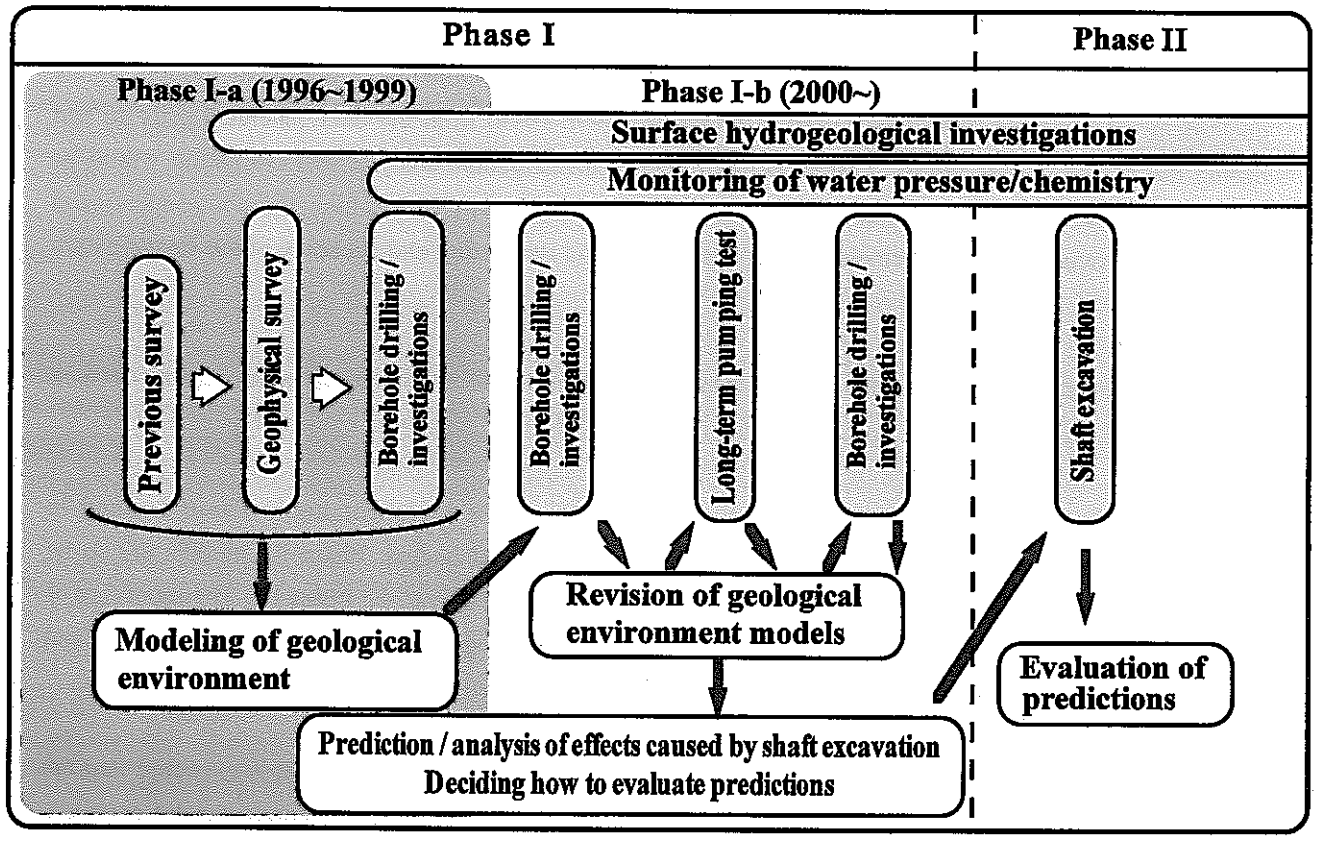

Figure 3.2 Research plan of the Phase I of the MIU Project

3.3 Overview of the investigations carried out in Phase I-a

Major investigations performed in Phase I-a include geophysical surveying, i.e., electro-magnetic and reflection seismic surveys, hydrological investigations and drilling of three 1000 m deep boreholes, MIU-1, 2 and 3. Investigations also included detailed core logging, structural analysis, BTV surveying, geophysical logging, hydraulic testing and in situ stress measurements (hydraulic fracturing tests) in the boreholes. Chemical and mineralogical analyses, determination of rock mechanical properties of the rock mass and of in situ stress by acoustic emission (AE) and deformation rate analysis (DRA) tests was done using core samples. Long-term monitoring of pore water pressure was carried out in boreholes drilled before the MIU Project commenced. Tables 3.1 and 3.2 and Figure 3.3 show the activities and purpose of the investigations, the outline of the borehole investigations and the location where investigations were carried out, respectively.

In order to understand and illustrate the geological environment underlying the Shobasama Site, four models were constructed; geological, hydrogeological, hydrochemical and rock mechanics conceptual models. Construction of each model was done iteratively, in two Stages. In the first stage, only data obtained from literature surveys and the results of earlier geoscientific research, excluding data from the MIU Project, were used. Following model construction, the models were revised using new data from the MIU Project.

· Geology

Models were constructed for two areas: the Shobasama Site and an area encompassing the Shobasama Site of about 4 km × about 6 km (Figure 3.4). The latter area was established for groundwater flow simulations.

For each area, two models were constructed. The first model was constructed using data obtained from literature surveys and the earlier geoscientific research, which excludes MIU Project results. The second model was constructed with the data from Phase I-a added to the data used for the first model.

· Hydrogeology

Two models were constructed for the above-mentioned more regional area encompassing the Shobasama Site (about 4 km × about 6 km) with the purpose of improving the accuracy of groundwater flow simulations.

The first model was constructed using data obtained from literature surveys and the earlier geoscientific research, which excludes MIU Project results. The second one was constructed adding data from the Shobasama Site to the data used for the first model. Groundwater flow simulations were also carried out.

· Hydrochemistry

Using data obtained from literature surveys and the earlier geoscientific research, a hydrochemical model was constructed. Groundwater sampling and analyses were planned to be carried out in and after 2000 FY.

Using those data, the hydrochemical model would be improved.

· Rock mechanics

The conceptual model was constructed only for the Shobasama Site. It was done in distinct stages as understanding was developed from successive boreholes at the Shobasama Site. First, the data obtained from geoscientific research and from MIU-1 were used. Next, the model was revised by adding data from MIU-2 and finally the model was revised with data from MIU-3.

In the final Phase I-a model, the rock mass has been divided into zones according to physical/mechanical properties and in situ stress.

· Investigation techniques and equipment

The MIU Project plays a role as a site for the application and testing of investigation techniques and equipment developed by TGC. TGC applies existing and developmental investigation techniques and equipment to actual investigations and to the extent possible adapts and improves them.

Additionally, literature surveys of overseas research experience are carried out to examine the evaluation techniques and methods used; for example, for the prediction of effects caused by shaft and drift excavations.

Furthermore, the basic concepts utilized in designing of facilities are examined to develop the engineering technologies needed for the deep underground.

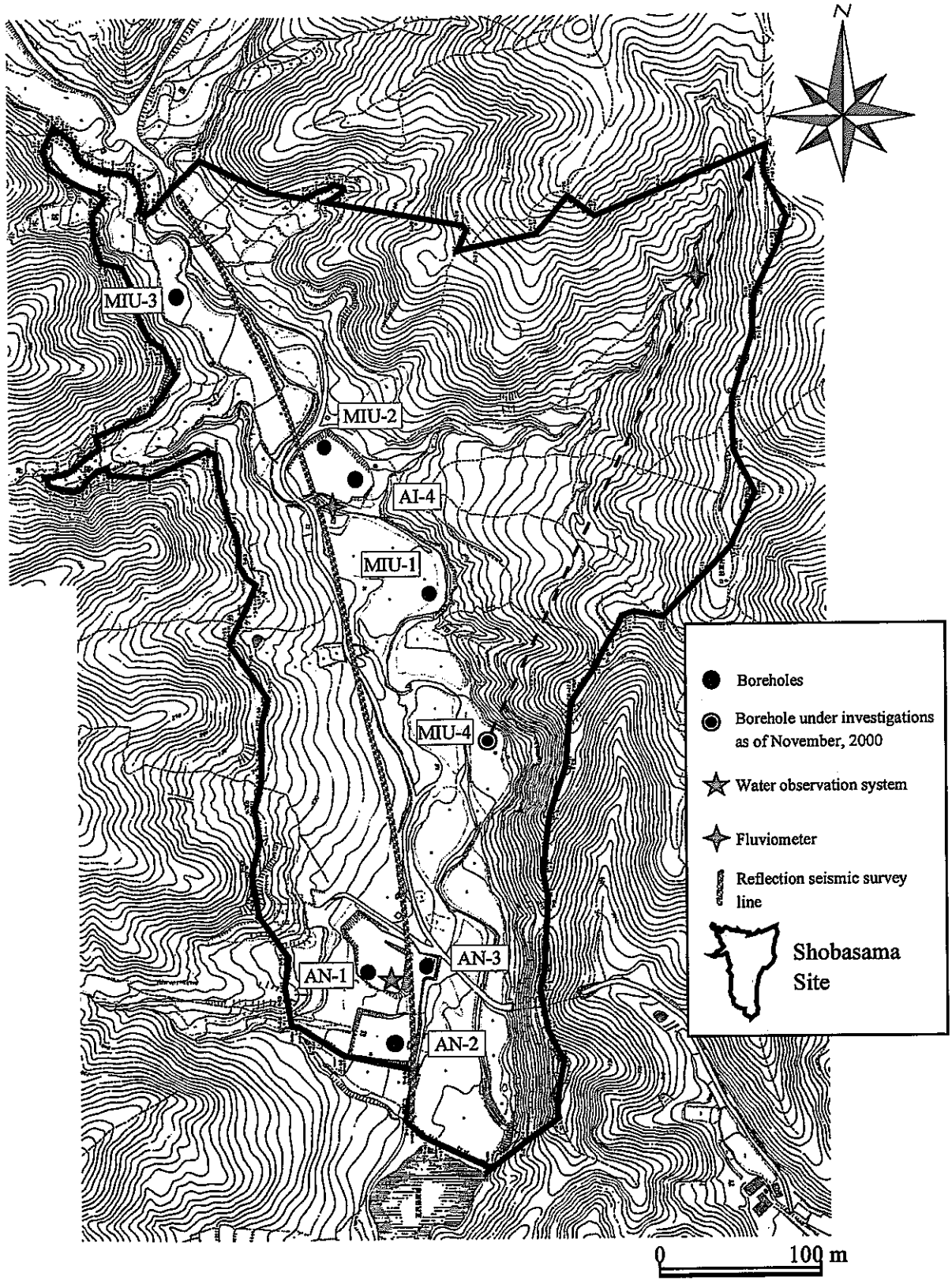

Figure 3.3 Location map of boreholes in the Shobasama Site

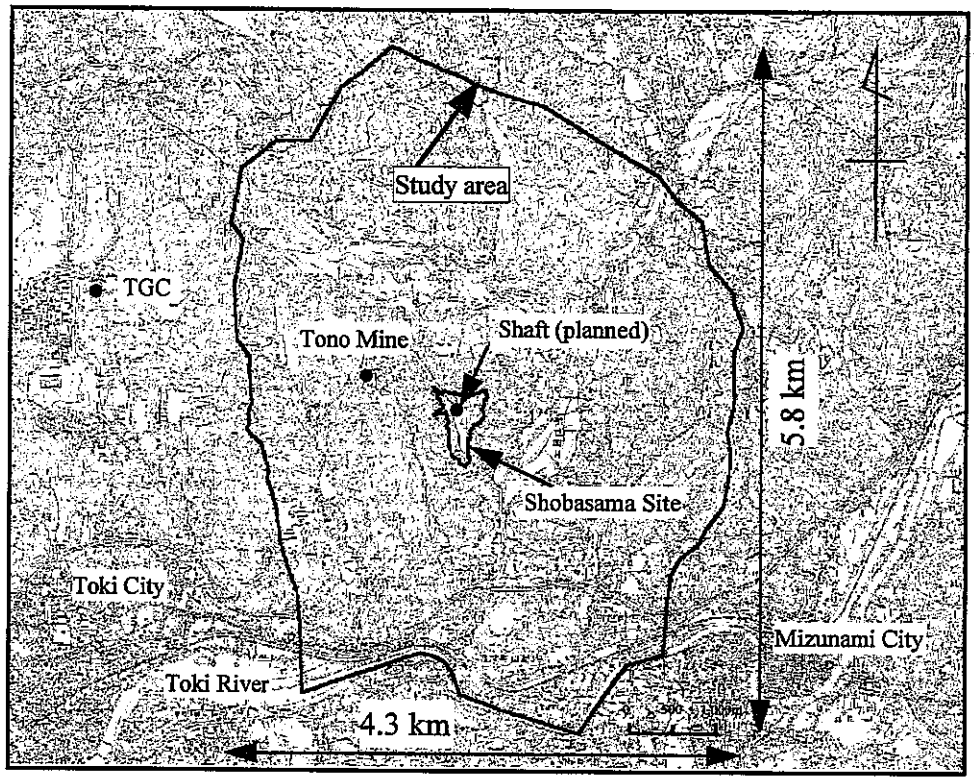

Figure 3.4 Location map of study area and Shobasama Site

Table 3.1 Details of investigations in Phase I-a
(1996 FY to 1999 FY)

Discipline/ Activity	Method	Purpose
Surface hydrological investigations	· **Meteorological observations** · **Water level observations** · **Soil moisture observations**, etc.	Estimate groundwater recharge rate
Water level monitoring	· **Seepage observations** (AN-1, AN-3)	Obtain data on steady state (static) groundwater levels and its response to borehole drilling.
	· **MP observations** (AN-1)	Obtain in situ data on steady state pore water pressures and changes caused by borehole drilling.
Geophysical surveying	· **Electric survey** (Resistivity method, 1 survey line, 200 m) · **Electromagnetic survey** (Magnetotelluric, MT) · **Reflection seismic survey** (1 survey line, 600 m)	Estimate distribution and continuity of unconformity, geological structure, alteration zone and fracture zone, etc.
Borehole investigations Existing boreholes · AN-1(about 1,000 m) · AN-3(about 400 m) New boreholes · MIU-1,2 and 3 (about 1,000 m) Geology Hydrogeology Hydrochemistry Rock mechanics	· **Geological survey** Detailed core logging, structural analysis, optical microscopy, Geophysical surveying, BTV investigations, etc.	Confirm geology and geological structures, (fractures, faults and dykes) which act as groundwater flow paths.
	· **Hydraulic testing - hydrogeology** Permeability tests (pulse/slug) (in 3 holes × about 30 intervals) Pumping test (3 holes × 10 intervals)	Obtain in-situ data of hydraulic conductivity of groundwater flowpaths and changes in hydraulic conductivity with depth.
	· **Geochemical Analysis** Rock (core) sample analysis (3 holes)	Understand geochemistry of geological formations and changes in geochemical properties with depth.
	· **Rock mechanical tests** Physical/Mechanical tests (3 holes × 10 locations) In situ stress measurement (3 holes × 10 locations)	Understand physical/mechanical properties of granite and changes with depth.

Table 3.2 Details of borehole investigations in MIU-1, 2 and 3 boreholes

		MIU-1	MIU－2	MIU-3
Depth (m)		1011.8	1012.0	1014.0
Diameter		HQ (about 100 mm)	HQ (about 100 mm)	HQ (about 100 mm)
Drilling fluid		Fresh water	Fresh water	Fresh water
Geophysical logging*		○	○	○
BTV investigations		○	○	○
Pumping tests (100 m intervals (no. of intervals)		10	10	11
Single borehole hydraulic tests, 6.5m intervals (no. of intervals)		30	30	23
Flowmeter logging		○	○	○
Mineralogical test**		○	○	○
Age dating (using rock core: Fission track method)		○	×	×
Physical/ mechanical property test (no.of tests)	Apparent density	180	20	40
	Effective porosity	180	20	40
	Water content	180	20	40
	Seismic wave velocity	180	20	40
	Uniaxial compression test	90	20	10
	Brazilian test	30	40	10
	Triaxial compression test	90	10	10
In situ stress measurement (number of measurements)	AE/DRA	10	20	10
	Hydraulic fracturing	-	10	10

*: Electrical, Micro resistivity, Density, Neutron, Gamma ray, Acoustic, Temperature, Caliper and borehole deviation

** : Modal/chemical composition analysis

4 Main results from Phase I-a

In this Chapter the results from the respective disciplines of geology (Section 4.1), hydrogeology (Section 4.2), hydrochemistry (Section 4.3) and rock mechanics (Section 4.4) are presented. Sections 4.5 and 4.6 present techniques and equipment and modeling predictions, respectively.

4.1 Geological investigations

4.1.1 Overview

4.1.1.1 Objectives

The objectives of geological investigations were established to meet the overall goals of the MIU Project and its Phases, as follows [7].

① Data acquisition and analysis of the geology and the geological structures from surface to deep underground at the Shobasama Site

② Construction of the geological model by analysis and integration of the data and assessing its accuracy

③ Developing methodology for systematic investigation and analysis of geology and geological structures

4.1.1.2 Overview of the investigations

In Phase I-a, as the first step to achieve these objectives, it was necessary to investigate the geology and the geological structures in the Shobasama Site and from this knowledge to construct the geological model. The data collection and analysis are described below. As stated previously, the geological models are constructed for two areas. The larger area, (about 4 km×about 6 km) was established for the performance of and to improve the accuracy of groundwater flow simulations. The other, within the larger area, is the Shobasama Site. The knowledge obtained through the geological investigations forms the basis of the models for hydrology, hydrochemistry and rock mechanics. Accuracy in the geological model will carry forward to the other models and result in more robust site models.

Two models were constructed for each area, so that an assessment of (a) the amount of data that can or should be acquired, i.e., the data requirements for the investigations and the investigations to be performed in terms of the type, detail and scope are related to (b) the quality and accuracy of the results needed for analysis and modeling. The first model was constructed using only the data from literature surveys and the earlier geoscientific research, excluding the new research for the MIU Project. The data predates the reporting period of this report. The second model is constructed using the data obtained from Phase I-a, the MIU Project data for this reporting period, in addition to the data used for the first model.

4.1.1.3 Construction of geological models

As stated above, the geological model will form the basis of the models for the other disciplines. Therefore, in addition to the importance of accuracy in the geological model, the methodologies for constructing the other models and their data requirements should be taken into consideration when constructing the geological model.

For example, there are two approaches to developing hydrogeological models of groundwater flow; a continuum model, postulating the rock mass as a porous and homogeneous continuous medium and a discrete fracture model, characterized by the inclusion of fractures in the rock mass. For the groundwater flow simulation in Phase I-a the continuum model was adopted largely due to lack of information on distribution of fractures and their permeability, as well as constraints on time required for analyzing the several kilometre square rock mass as a fractured rock mass. Assuming that the hydrogeological model was to be constructed as a continuum model, construction of geological model requires the following conditions.

① Division of the sedimentary rocks into geological units on the assumption that physical properties are uniform, that is, homogeneous in the same sedimentary formation.
② Specify the location, continuity and width of and structural discontinuities such as faults that extend throughout the entire model area.
③ Divide crystalline rocks into geological/structural domains which have statistically significant differences in fracture density or preferred orientations and that can be treated as homogeneous in terms of hydraulic conductivity and transmissivity.

Geological model was constructed in the following order.

① Definition of the geological units based on the known geology
② Define the boundaries between geological units and their characteristics
③ Construct the model using 3-D visualization software, Section 4.1.1.4 below.

4.1.1.4 Visualization of geological model

The geological model forms the basis of the models for hydrogeology, hydrochemistry and rock mechanics. The 3-D visualization of the geological model through computer graphics can make it easy to share and to integrate the necessary information for constructing the above models.

EarthVision, 3-D visualization software produced by Dynamic Graphics Inc., was used for visualization of the geological model. The software forms a 3-D geological model of the rock mass, including capability to show estimated shapes of discontinuity planes such as the boundaries between geological formations and large faults, and combining these discontinuities, taking relationships such as position in space and development process into consideration [16,17].

This software is used to construct models in other major projects for geological disposal, such as at

Sellafield (Nirex), Wellengerg (Nagra), Äspö HRL (SKB) and Yucca Mountain (USGS, USDOE) [18].

Minimum tension theory based on spline interpolation is one of the functions of EarthVision. It is applied to estimate the ground surface, geological boundaries and fault planes. This method interpolates between adjacent data with the smoothest curved surface by an n-dimensional polynomial formula based on the input data of positions and directions [19].

4.1.2 Geological results – JNC's geoscientific research prior to Phase I-a of the MIU Project

The geology and geological structures in and around the Shobasama Site were investigated prior to the MIU Project in what is termed in this report "other geoscience research". This research includes surveys on the Tsukiyoshi uranium deposits [20,21], the RHS Project [15], the Shaft Excavation Effect Experiment [22], investigations in the Tono Mine and historic geological knowledge available from literature surveys. Following is an overview on the other geoscience research.

4.1.2.1 Lineament definition, analysis and interpretation [15]

It is generally accepted that a lineament refers to a linear topographic feature (sometimes a geophysical linear) possibly related to an underlying structure such as a fault, fracture zone or lithologic contact. Generally, a linear topographic feature is visible on aerial photographs or satellite imagery such as Landsat or SPOT [23]. Structures such as faults and fracture zones often, though not always, have a linear topographic expression. Therefore, lineament analyses may provide a rapid method to develop knowledge of the location of individual structures and also, from a statistical analysis of lengths and trends, can provide a basis for conceptualization of structural patterns and a preliminary indication of regional deformation.

In the RHS Project, TGC used Landsat Thematic Mapper multi-spectral imagery with a ground level resolution of 30 m (1:200,000 scale) covering an area of 50 km square. As shown in Figure 4.1(1), 1,276 lineaments were identified, including ones coincident with known active faults [14] such as the Adera Fault, Ako Fault, Hanadate Fault, Shirakawa Fault, Byobusan Fault, Kasahara Fault, Enasan Fault and Sanageyama-Kita Fault.

These faults form a grid-like pattern and are interpreted to form the boundaries of several large blocks. The trends of lineaments in each fault-bounded block, the intra-block, were compared statistically. It was clear that, as is shown in Figure 4.1(1), there are differences in the distribution patterns of lineament trends among the blocks. This may suggest that, if we assume the lineament is a reflection of discontinuities such as faults, there are regional differences in tectonic patterns related to variations in stress conditions and deformation in the blocks. The reasons for the inter-block variations are not clear: they could be due to stress redistribution during tectonic events resulting in different deformation patterns or due to the underlying geology. Nevertheless, from conceptualization of geological models and a predictive perspective, the lineaments are useful. In addition, whether related to stress redistribution or internal geological fabrics, each block can be assumed to have had a slightly different evolution of the geological

structures [24].

In the RHS Project, more detailed lineament interpretations have been carried out in the larger area around Tono Mine and the Shobasama Site; the area bounded by the Ako, Byobusan, Hanadate and Shirakawa Faults (Figure 4.1(1)). Because observations and results might be different if imagery with different scales and availability of stereoscopic views are used, analysis at this scale was done using three kinds of imagery.

(a) Landsat TM imagery (1/200,000)
(b) French SPOT satellite photographs (High Resolution Visible Imaging System) with ground resolution of 20 m (1:100,000 scale)
(c) Stereoscopic aerial photographs (1:40,000 scale)

The results were compiled and analyzed separately. As a result, in this area many large and small lineaments were recognized, including lineaments coincident with the active faults such as the Byobusan, Kasahara and Ako Faults. More than ten lineaments longer than 3 km [23] were recognized in the Tono Mine area. These are considered to correspond to faults or fracture zones because of their length and continuity. In addition, NW-SE, NS and NNE-SSW trending lineaments are prominent. Some correspond to known faults [20] such as the Yamada Fault Zone and the Shizuki Fault.

As a result, ten blocks with unique patterns in lineament orientation distributions were recognized. Structural discontinuities such as faults and joint zones are considered to have formed due to variations in tectonic stress distributions resulting in slightly different deformation patterns. Therefore, each of the ten blocks is regarded as having been subjected to somewhat unique stress conditions and deformation. Those ten blocks are shown in Figure 4.1(2) [25]. The Shobasama Site is located in the 'f' block in this Figure.

4.1.2.2 Ground geological surveys

Ground geological surveying is intended to obtain basic data on geology and geological structures by surface mapping and observation to produce geological maps. The geological map is the fundamental tool for displaying geological knowledge and thus is the keystone to development of the geological model.

The Shobasama Site and the neighboring areas have had a geological map [15, 26] produced in the RHS Project. These maps depict the lithological variety and internal structure (faults and fractures) in the Toki Granite. As well, some excellent geological maps produced for earlier mapping projects are available [12,13, 20, 21].

Geology [13, 15, 20, 21, 26]

The geology, as it is known from the earlier work, is as follows. The basement is composed of Paleozoic and Mesozoic formations intruded by granites. The basement is unconformably overlain by Neogene to Quaternary Mizunami Group sedimentary rocks (Figure 2.3 (a)) in the vicinity of the Shobasama Site. The Mizunami Group is in turn overlain by the Seto Group with a distinct unconformity.

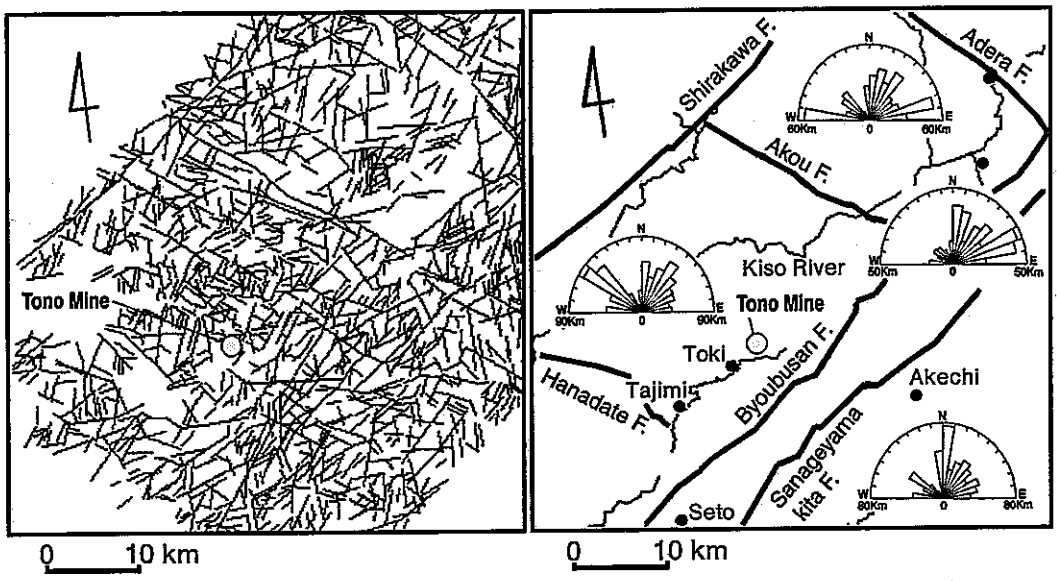

Figure 4.1(1) Lineament interpretation in the Tono district and lineament rose diagram for each fault-bounded block (top)

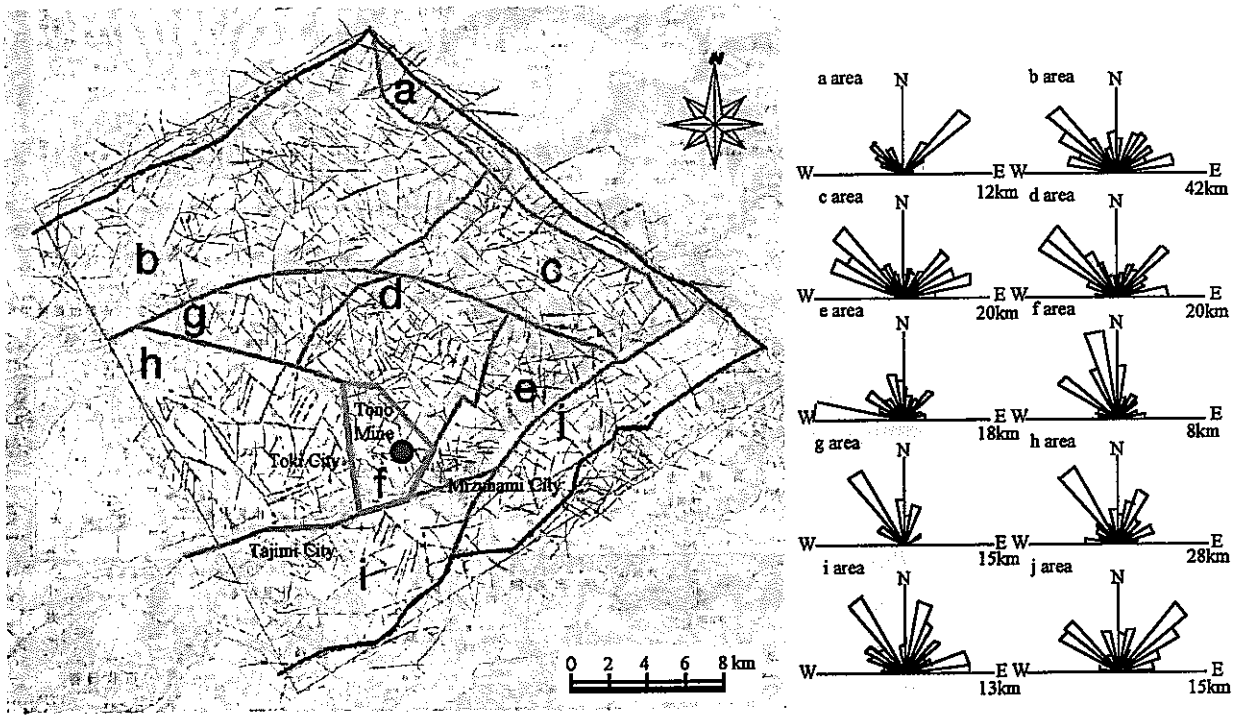

Figure 4.1(2) Division based on the result of the lineament interpretation and rose diagram

Basement rocks

At the Shobasama Site and the surrounding area, the Toki Granite forms the basement rock. The Toki Granite intrudes sedimentary rocks of the Mino Belt on its south, west and north sides. On its northeast and southeast sides, the granite intrudes the Nohi Rhyolite. The Toki Granite adjoins and is probably related to a Ryoke Granite known as the Sumikawa Granite. The intrusive contacts of the Toki Granite with sedimentary rocks of the Mino Belt and the Nohi Rhyolite are clearly defined at surface, and the nature of the contacts is well known. On the other hand, the contact with the Sumikawa Granite cannot be confirmed at surface because both granites are lithologically quite similar.

The Toki Granite is divided into three textural facies based on grain-size;: coarse-grained, medium-grained and fine-grained biotite granite. The center of the granite (Hiyoshi district of Mizunami City to Jorinji district of Toki City) is fine to medium-grained biotite granite. It is surrounded by coarse-grained biotite granite. Near the contact with the sedimentary rocks of the Mino Belt, especially at the contact, the Toki Granite tends to be fine-grained. This is confirmed at Takodo district of Mizunami City where a transition from coarse- to medium- to fine-grained is observed.

Sedimentary rocks

Sedimentary rocks of the Mizunami and the Seto Groups form the cover rocks in the vicinity of the Shobasama Site. The Mizunami Group has been divided into the Toki Lignite-bearing Formation, Akeyo Formation and Oidawara Formation in ascending order.

・Mizunami Group

The group consists mainly of pyroclastic materials and granitic clasts, occasionally yielding silicified wood and organic remains (large fossils of mollusks and plants). It generally decreases in grain-size upward, composed of silty rocks in the uppermost part. While the Toki Lignite-bearing Formation consists of arkosic sandstone and conglomerate containing granite cobbles to boulders unconformably overlying the Toki Granite, the Akeyo Formation is composed mainly of medium-grained tuffaceous sandstone. The Oidawara Formation is composed mainly of fine-grained tuffaceous sandstone and siltstone. Several unconformities occur through the sequence.

・Seto Group

The Seto Group unconformably overlies the Mizunami Group. It is composed mainly of conglomerate containing granules to cobbles, with a few layers (1 to 3 m thick) of clay and sandy clay intercalated in the lower part. Constituent gravels of the conglomerate are composed of granite, chert, rhyolite, mudstone and volcanic rocks, while the matrix is white-colored tuffaceous or arkosic.

Geological structure

The geological structure in the region is complex, as shown by the maps of the known active faults and several detailed studies done near the Shobasama Site to correlate outcrop scale of fracturing with nearby lineaments. The evidence of vertical movements recorded in the sedimentary sequences by the unconformities is indicative of potential reactivation of earlier faults and thus the potential for multiple

deformation/reactivation events. The type of faulting is also complex, with evidence of reverse, normal and strike slip faults. Large porphyry dykes also intrude the Toki Granite; in some instances coincident with linear valleys/rivers.

・Faults

There are a number of known faults in the Shobasama Site. The Yamada Fault and the Shizuki Fault are nearby. Others are shown on the regional geological maps. The Tsukiyoshi Fault is known to occur at the Tono Mine and is thought to occur east and west at surface in the vicinity of the Shobasama Site [12, 20, 21]. It is visible in a gallery of the Tono Mine where fault gouge centimeters thick are recognized. The Tsukiyoshi Fault is a reverse fault with a strike of N80°W, a dip of 70° and an estimated throw of about 30 m. In-depth studies of the fault in the mine indicate it to be a barrier to groundwater flow across the fault.

・Fractures in granite

Fracture investigations in the RHS Project include mapping and photographing of fractures in outcrop as well as measurements of various parameters of the fractures as are shown in Table 4.1 [15].

Table 4.1 Observed characteristics of fractures

Shape of fracture	Planar Fracture, Irregular Fracture, Curved Fracture, Stepped Fracture
Shape of fracture (detail)	Flat Plane, Curved, Undulating, Stepped, Braided
Structure of fracture plane	Smooth, Rough, Slickensided
Visibility of fracture ends	Both/One/Neither end is covered
Structure of the end of fracture	Obscure/Clear/Forked/Horsetail/Braided/Stepped
Spatial relation to other fractures	Not intersected/Intersected/Contacted
Direction of movement	
Dip/Strike	
Length	Distance between both ends or visible length (0 or 1 end)
Width	Distribution width of microcrack along fracture/Average of amplitude of crack
Aperture	
Filling minerals	
Width of alteration in wall	
Spring (artesian condition)	The amount and pH
Others	Remarkable characteristics

It was clear that two trends (NNW-SSE and NE-SW) of fractures are dominant in the Toki Granite. These trends are coincident with lineament trends in this area. Small faults are recognized in outcrops, but large-scale faults in outcrop were not found.

Quartz porphyry dikes (steeply dipping, several tens of meters wide) are known to intrude in the central (Kawai district, Toki City) and southern parts (Dachi district, Toki City) of the Toki Granite. The strikes of those dikes are mostly NS to NNW-SSE. Small-scale dikes are observed as quartz veins (less than 10 cm wide) at the periphery of the granite with NNW-SSE strike. The strikes of those dikes tend to be N-S to NNW-SSE. It is assumed that fractures with this orientation were open (i.e. tensional fractures) when the dykes intruded to the granite. However, some dikes with the same strikes have clearly been sheared .

Therefore, the evidence in the fracturing implies a complex deformation history.

To determine any relationship between lineaments and fractures, the strike of fractures at selected outcrops was compared with that of a corresponding lineament, that is, a lineament near or adjacent to the outcrop. The results show that orientation trends of both often match well. Each of the ten blocks referred to in Section 4.1.2, and Figure 4.1(2) appear to have different prevailing fracture trends as is shown in Table 4.2. It shows that the prevailing fracture trend is consistent with lineament trends in each block.

Table 4.2 Prevailing strikes of fractures and lineaments in each block

Block	Fracture strike	Lineament trend
d	**NE-SW**, NNW-SSE, ENE-WSW	**NE-SW**, NW-SE, EW
e	**EW**, NS	**EW**
f	**NS**, NE-SW, WNW-ESE, **NW-SE**	**NS**, NNW-SSE, **NW-SE**
h	EW, NS, NNW-SSE	NW-SE, NNE-SSW
i	**NW-SE**, NS	**NW-SE**, NNE-SSW, EW
j	**NE-SW**, WNW-ESE, NS	**NE-SW**, NW-SE

It implies that it may be possible to estimate or predict dominant fracture trends using the trend of the lineaments in the respective block.

4.1.2.3 Ground geophysical survey

Regarding ground geophysical surveying, the results of a ground electromagnetic survey in the RHS Project are available. It was carried out to estimate the thickness of the sedimentary cover and depth to the conformity between sedimentary rocks and granite and the location of structures in the granite. Furthermore, the results of reflection/refraction seismic survey, carried out to understand the geology and geological structure in the RHS Project and Shaft Excavation Effect Experiment are also available. Details of those surveys are shown in Tables 4.3 and 4.4. Dynamite as well as small-size hydraulic impactors (Table 4.5) was used as seismic sources.

Table 4.3 Details of ground electromagnetic survey

	Data stations	Dipole length	EM source	Distance from EM source	Data acquisition mode	Radio frequency range	Radio frequency for sampling	Data amount*
CSMT	144	30 m	Artificially induced	200-350 m	HF	750Hz-96kHz	192 kHz	3 counts/radio frequency
MT	144	30 m	Natural induced	—	HF	10Hz-1kHz	12 kHz	30 counts per /measurement point

*** 1count＝4,096 points×3 stacks**

Table 4.4 Details of reflection / refraction seismic survey

Reflection seismic survey (See Figure 4.4)	Line-R-1 (1,700 m)	· Seismic source : dynamite · Seismic source interval : 70 to 160 m · Receiver interval : 10 m
	Line-R-2 (1,900 m)	· Seismic source : dynamite · Seismic source interval : ca.100 m · Receiver interval : 10 m
Refraction seismic survey (See Figure 4.4)	Line-2-1 (500 m) Line-2-2 (500 m) Line-2-3 (500 m)	· Seismic source : dynamite · Seismic source interval : 5m · Sampling rate : 1msec · Data length (Recording time): 1sec
	Line-1 (650 m)	· Seismic source : Impactor · Seismic source interval : 4 m · Sampling rate : 1msec · Data length (Recording time): 1sec

Table 4.5 Details of small oil pressure impactor

Size Length, Width, Height	Weight	Impact energy	Rod weight	Baseplate weight	Impact frequency	Maximum tilt angle
2.5 m, 1.0 m, 2.2 m	1.2 t	2000 J	65 kg	65 kg	10 sec	±30°

Ground electromagnetic surveys (MT and CSMT methods) [15,27]

MT (Magneto-Telluric) method is a way to estimate subsurface resistivity distribution using natural or artificially induced electromagnetic signals (geomagnetism). In this survey, both natural and artificially induced signals are utilized by the MT and CSMT methods, respectively. Data was collected at 144 stations and two components for both electric and magnetic fields were measured. For each point, one-dimensional analysis, assuming a horizontal multi-layered structure is performed. Two-D analysis was carried out for five survey lines, as is shown in Figure 4.2.

A horizontal resistivity distribution map of the one dimension analysis, at an elevation of 200 masl (Figure 4.3) reveals extensive low resistivity areas around the Mizunami sedimentary basin. These occur towards Tono Mine to the west, and towards Shirakura, Hosokute and Shukubora to the north. Another low resistivity area is found in the NW part of study area, from Misano to Tsubashi. According to the results of resistivity logging, it is estimated that resistivity lower than 80 Ωm corresponds to sedimentary rocks of Seto and Mizunami Groups, while areas with higher than 80 Ωm corresponds to granite and other basement rocks. Therefore, low resistivity areas may correspond to an ancient river channel structure on the surface of the granite.

Figure 4.3 shows that low resistivity areas corresponding to the sedimentary rocks do not extend to deeper than 0 masl. It is estimated that the area deeper than 0 masl elevation is occupied by high resistivity basement rocks. This is consistent with the results obtained by borehole investigations. Also it indicates that the depth distribution of the unconformity between granite and sedimentary rocks can be estimated using this resistivity survey method.

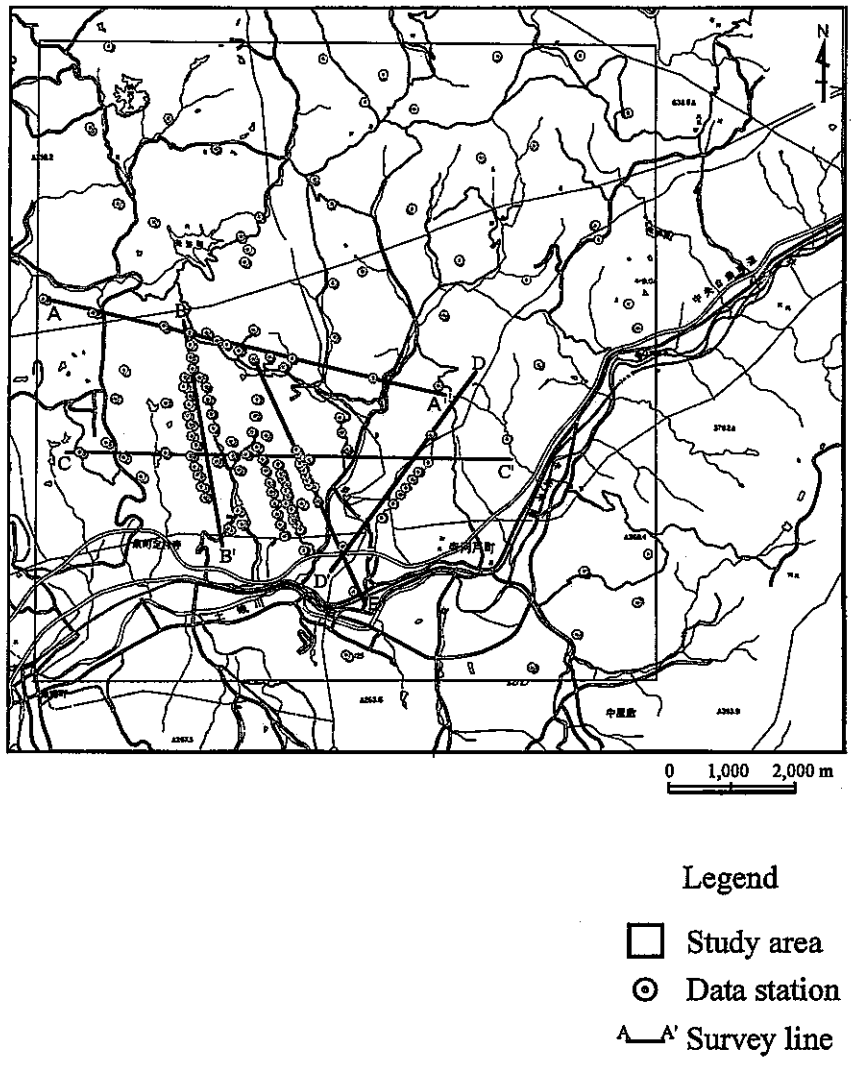

Figure 4.2 Data stations and survey lines of electromagnetic survey

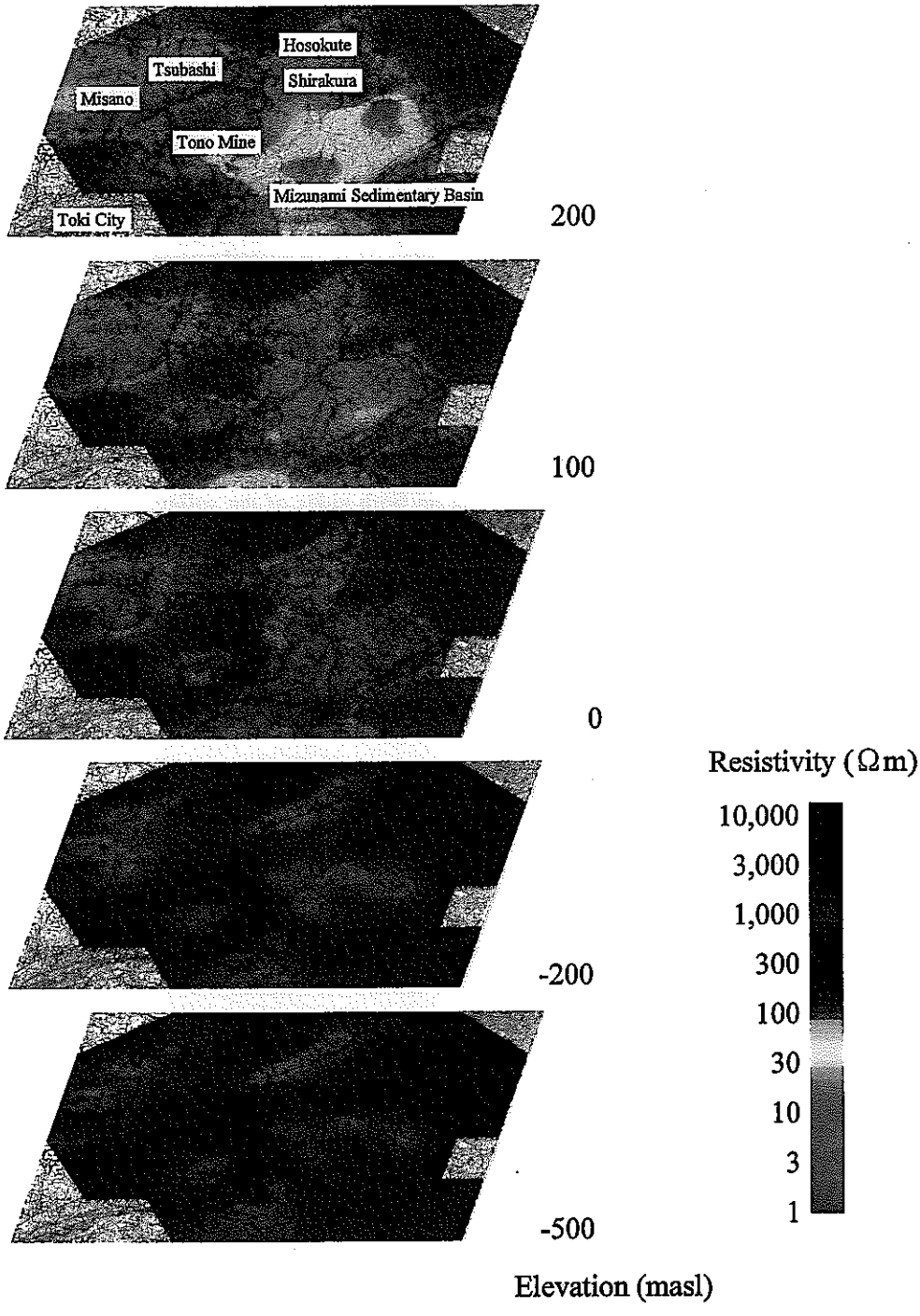

Figure 4.3 Resistivity distribution by elevation based on the result of ground electromagnetic survey

Refraction seismic survey [15,28]

A refraction seismic survey uses seismic waves artificially generated on or under the ground surface. These waves, which refract on bedding planes, are monitored on the ground surface. Using the difference in arrival times of the seismic waves at different measurement points, estimates of seismic wave velocity and the thickness of each layer can be determined. This method has been widely used to determine geological structure and rock condition in the fields of resource exploration and civil engineering.

The length of the survey line was established taking the thickness (up to about 150 m) of Neogene strata into consideration (Table 4.4, Figure 4.4). Receiver interval is 10 m, and source interval is 70 to 160 m.

As is shown in Figure 4.5 (Survey Line-R-1), the Neogene strata are divided into three undulatory but approximately sub-horizontal units based on seismic wave velocity. Also, the depth and shape of the unconformity between Neogene strata and granite are estimated. The results are consistent with the data obtained from the boreholes near the survey line. The seismic wave velocity of the granite is 4 km/s under the valleys, while it is 5 to 6 km/s under the hills on both sides of the valley. It implies that the fractures have developed more under valleys than under hills.

The fracture zone accompanying the Tsukiyoshi Fault may correspond to the low velocity zone (1.2 km/s) at 519 to 568 m on the survey line. The width of the fracture zone is estimated to be about 50 m, much wider than the width of the clay observed along the fault in sedimentary rocks. Also, two other low velocity zones are recognized:

- NE of Tsukiyoshi Fault, 271 to 350 m on the survey line: (velocity: 1.7 km/s) (200 m away from the Tsukiyoshi Fault)
- SW of Tsukiyoshi Fault, 1,333 to 1,362 m on the survey line: (velocity: 0.6 km/s) (800 m away from the Tsukiyoshi Fault)

This implies existence of other faults or possibly secondary faults related to the Tsukiyoshi Fault.

Reflection seismic survey

This survey gives higher resolution than the other geophysical surveys. Also, it can be used to determine geological structures in two dimensions. For these reasons, it is widely used in many kinds of study.

As is shown in Figure 4.6, the geological structures to 200 m depth below surface were estimated [15, 29]. In this cross section, the Tsukiyoshi Fault is represented by discontinuous reflections within the Neogene strata. The result also shows the possibility of previously unknown subordinate faults.

One of the results of the reflection seismic survey carried out in the Shaft Excavation Effect Experiment in Tono Mine is shown in Figure 4.7. Also in Figure 4.7, the cross section of the same kind of survey carried out for Tsukiyoshi Uranium deposit is shown. Nine reflection planes recognized by this survey roughly coincide with the geological strata: the top of the Akeyo Formation, a bedding plane in the Akeyo Formation, the top of the Upper Toki Lignite-bearing Formation, the top of the Lower Toki Lignite-bearing

Formation, two bedding planes in the Lower Toki Lignite-bearing formation and the top of the basement granite.

4.1.2.4 Borehole investigations

Borehole investigations were mainly carried out to study the sedimentary rocks overlying the Toki Granite. For example, surveys were done for the Tsukiyoshi uranium deposit [20,21], the Shaft Excavation Effects Experiment at Tono Mine and other geoscientific research (12 TH-series boreholes [22], 8 AN-series boreholes, 6 SN-series boreholes and 1 HN-series borehole) [30] (Figure 4.8). The borehole investigations confirmed the stratigraphy estimated by the ground geological surveys.

Contour maps [20,21,31] of the basement rock in the Tono area compiled through borehole investigations and surveys on the Tsukiyoshi uranium deposit indicate that there is a paleo-river channel on the erosion surface of the basement granite.

Borehole investigations carried out for the Shaft Excavation Effects Experiment revealed a correlation between the lithofacies (e.g. grain-size) of sedimentary rocks and their apparent resistivity/permeability obtained by electrical logging. These surveys also reveal the high permeability of the conglomerate layers in the Lower Toki Lignite-bearing Formation and that the Oidawara and Upper Toki Lignite-bearing Formations have low permeability [32,33].

Investigations carried out at the Shobasama Site included drilling of the AN-1, 2 and 3 boreholes, core descriptions [34], geophysical logging and BTV surveys to develop methodologies and techniques for rock mass evaluation (Table 4.6). The results of borehole investigations in AN-1 indicate that the granite could be divided into three domains according to shapes of fractures, the varieties/characteristics of fracture fillings and the fracture density [35]. These are Domain I: Ground level (GL) to 300 m depth; Domain II: 300 m to 420 m depth; Domain III: 420 m to bottom of borehole). The results of testing of radar instruments carried out in AN-1 and 3 indicate the presence of a zone characterized by high decay rate (attenuation) of electromagnetic wave amplitude between the ground surface and about 150 m depth [36]. However, there is no more information on the horizontal continuity of these domains and the high decay rate zone. Thus it is not clear whether or not this observation is applicable to the surrounding rock mass nor that it might be representative of the entire Shobasama Site.

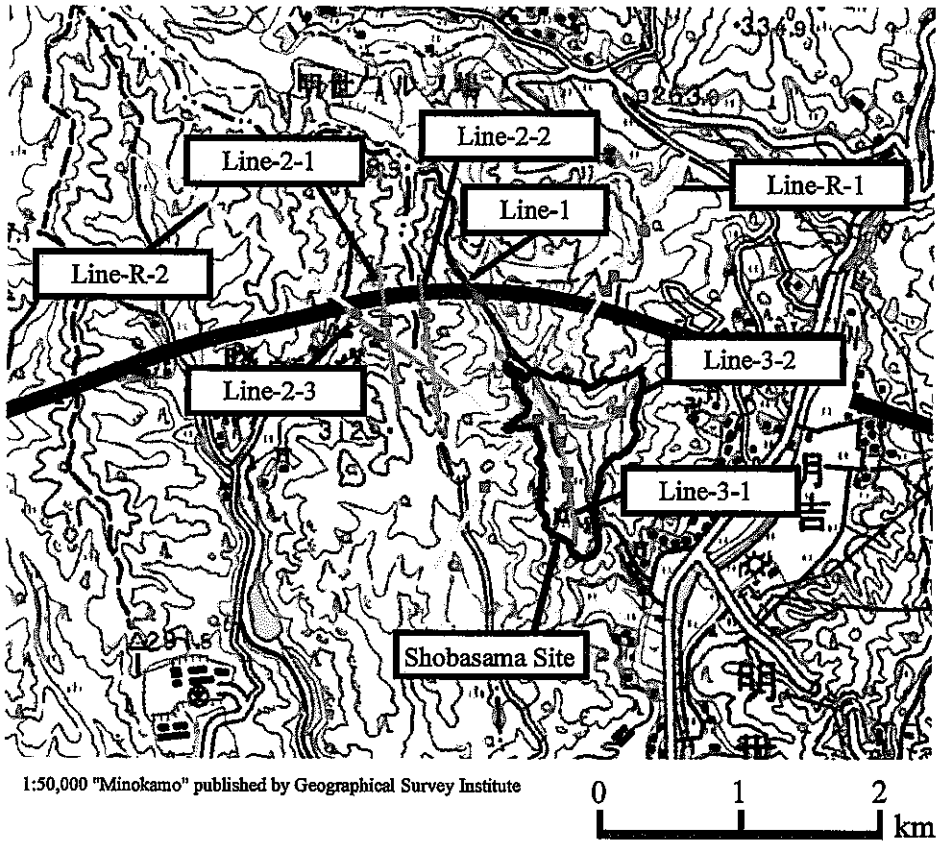

Low-velocity zone

Survey line of refraction seismic survey

Discontinuity zone

Survey line of reflection seismic survey

Tsukiyoshi Fault (Itoigawa, 1980)

Line-1
Line-2-1~3
Line-R-1,R-2

Seismic survey (other geoscientific research)

Line-3-1,3-2

Seismic survey (the MIU Project)

Figure 4.4 Location map of survey lines for seismic survey

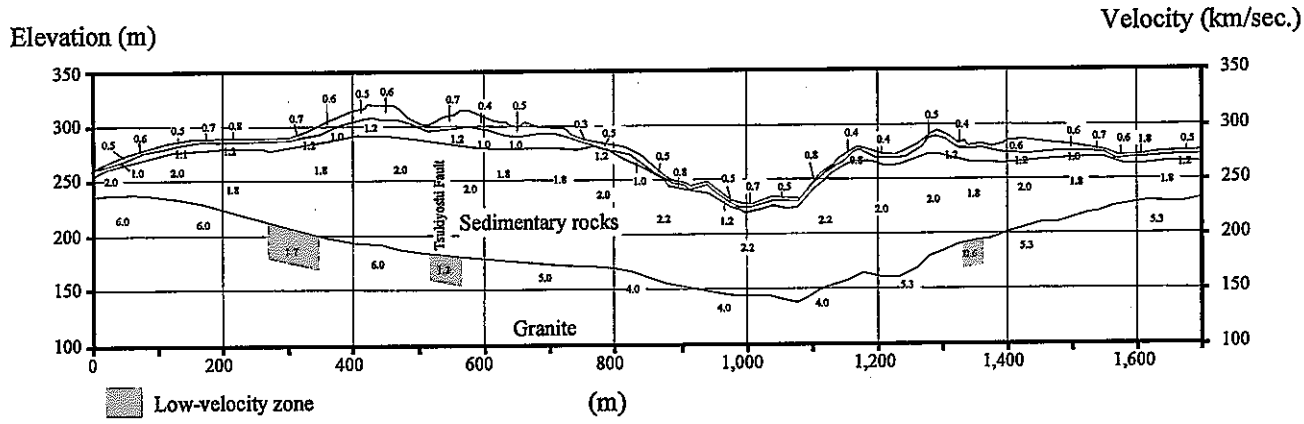

Figure 4.5 Distribution of seismic wave velocity (Line-R-1) [15]

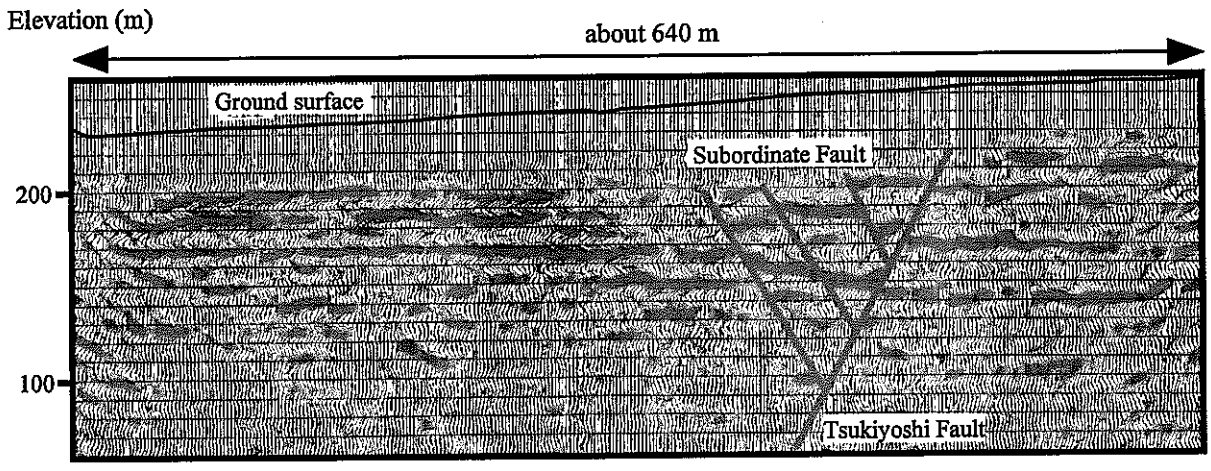

Figure 4.6 Cross section of survey line A-B (Line-1) [15]

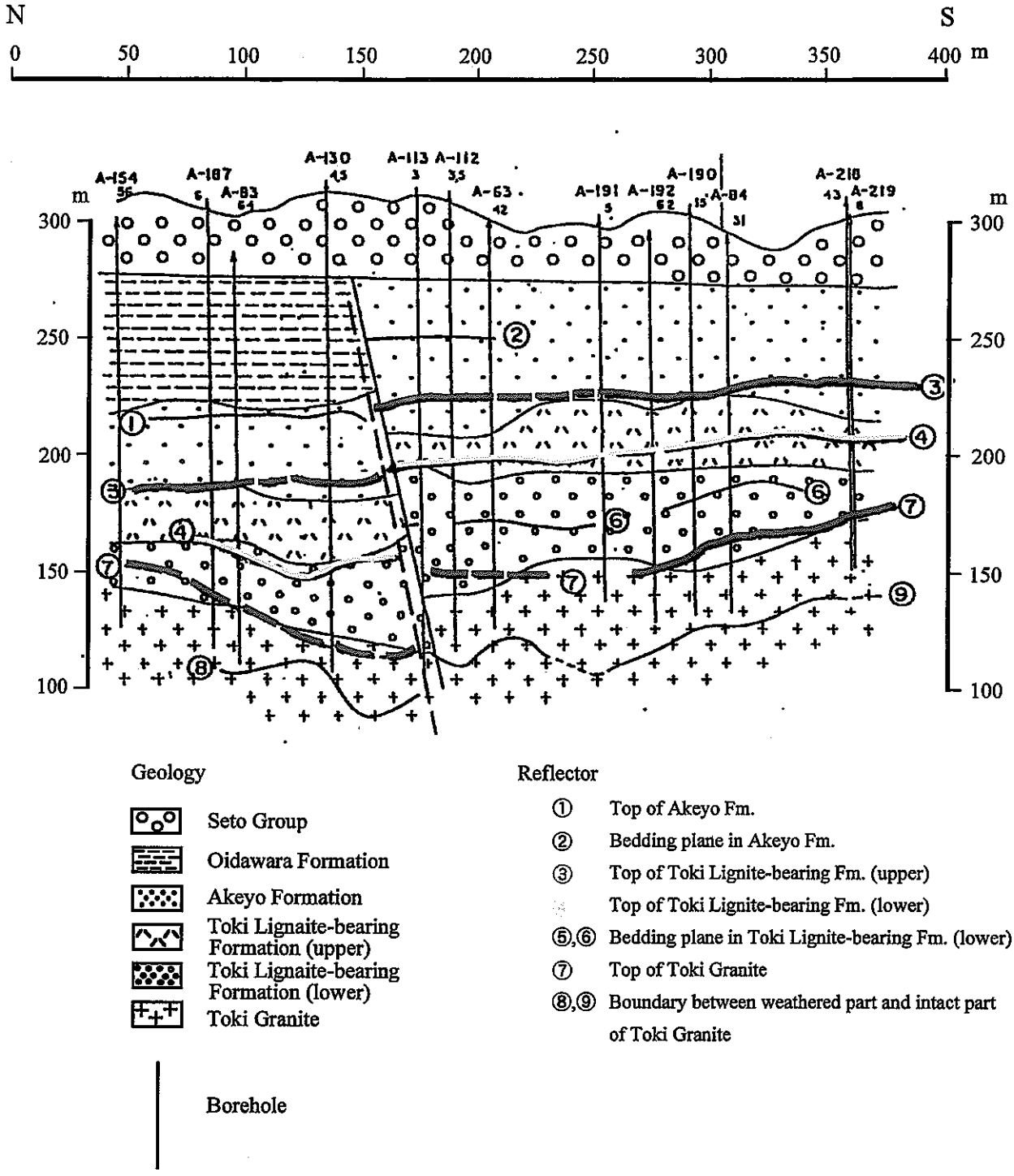

Figure 4.7 Distribution of reflectors obtained by reflection seismic survey

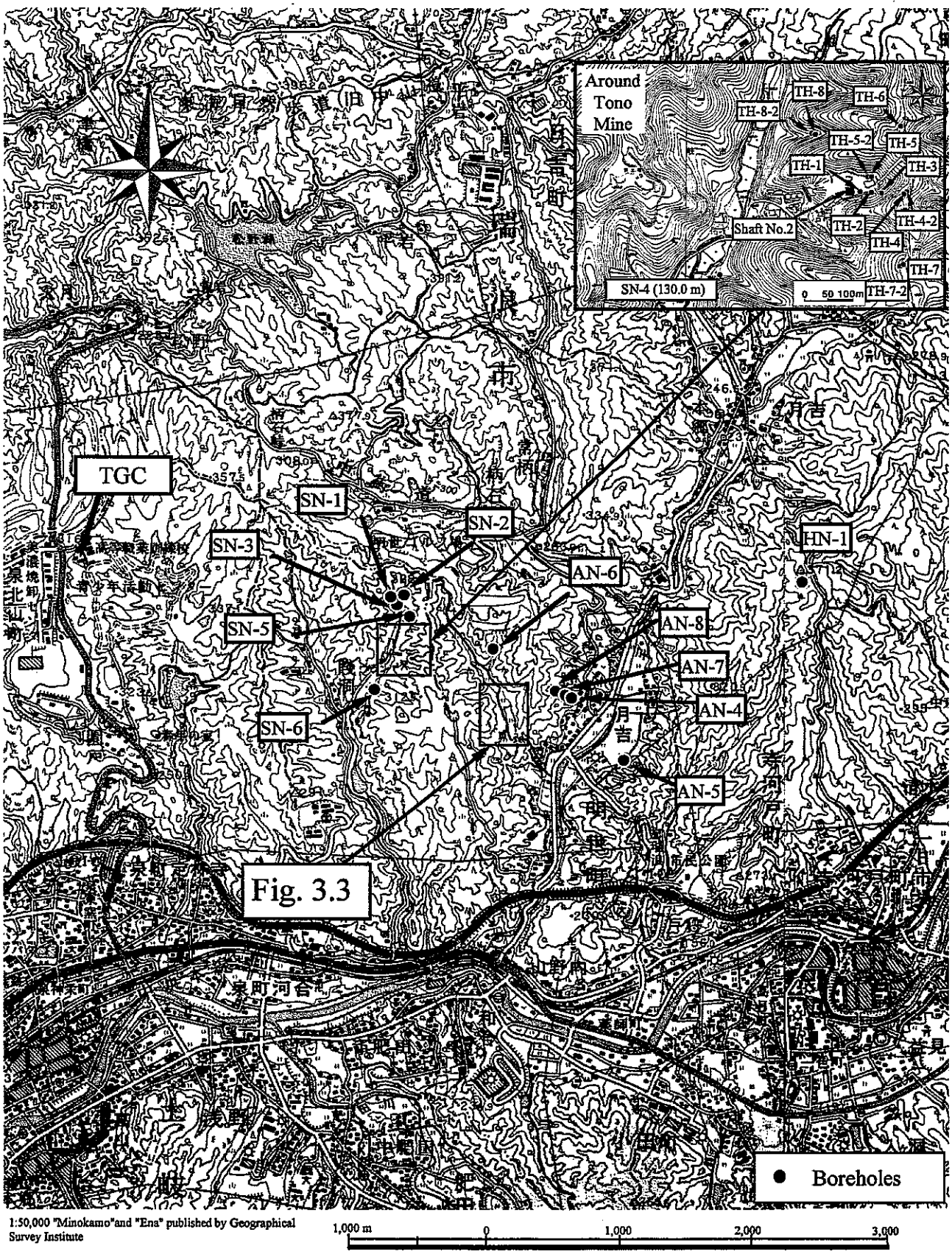

Figure 4.8 Location map of boreholes for the geoscientific research

Table 4.6 Details of borehole investigations (AN-1, 3)

	AN-1	AN-3
Depth (m)	1,000	408
Diameter	HQ (about 100 mm)	HQ (about 100 mm)
Drilling fluid	Fresh water	Fresh water
Geophysical logging*	○	○
BTV investigations	○	○
In-hole hydraulic test	(33 intervals)	(24 intervals)
Laboratory tests using rock specimen	Apparent density (20 samples) Effective porosity (20 samples) Water content (20 samples) Seismic wave velocity (20 samples) Uniaxial compression test (20 samples) Brazilian test (40 samples)	–
Hydraulic fracturing test	(20 samples)	–

* : Electrical, Micro resistivity, Density, Neutron, Gamma-ray, Acoustic, Temperature, Caliper and Deviation

4.1.3 Geological results - results of Phase I-a

Phase I-a includes the work for the MIU Project at the Shobasama Site. This includes the entire borehole drilling at the site in the reporting period (1996-1999), all the multi-disciplinary borehole investigations and any surface investigations such as the geophysical surveying. Lastly, it includes any modeling based on the new information developed in the period.

In Phase I-a, EM magnetotelluric and reflection seismic surveys were done, three boreholes were drilled (MIU-1, 2 and 3, Table 3.2) and multidisciplinary borehole investigations were carried out at the Shobasama Site. Based on the results of these investigations, a revised geological model was constructed. Details of the investigations are as follows.

4.1.3.1 Magnetotelluric survey

A resistivity survey was carried out at the Shobasama Site (survey line: N-S, 200 m, Table 3.1). However, accurate results were not obtained because of the low-resistivity zone in the near-surface part of the site. Also, application testing of a remote-reference method in magneto electric survey (MT) was carried out aiming at understanding the geological structure in deeper parts of the site. The remote- reference method takes advantage of high coherency of MT signal compared with that of regional noise. By comparing the measurement data at two locations, the MT signal can be separated from the regional noise. Unfortunately, reliable data was not obtained because of excessively high noise levels. Thus the results of these surveys are not presented in this report.

4.1.3.2 Reflection seismic survey [37,38]

A reflection seismic survey was carried out to obtain data on geological structures of Mizunami Group and the depth and geometry of unconformity between the basal conglomerate and the Toki granite. Survey lines were run N-S and E-W and are shown in Figures 4.4 and 4.9. These data are used to construct the geological model. Details of the reflection seismic survey are shown in Table 4.7.

Some continuous reflection planes are detected above an elevation of 100 masl throughout both survey lines. The reflectors are consistent with the shape of unconformity between the sedimentary rocks and the basement granite and the internal structures of the sedimentary rocks (Figure 4.10). While partial discontinuities (SF-1-3 in Figure 4.10) are recognized, it was not confirmed whether or not they represent faults.

The reliability of the results below a depth of 200 m was reduced because the survey lines were not long enough and the presence of strong reflections in both the sedimentary rocks and the upper part of the granite.

Table 4.7 Details of reflection seismic survey

Reflection Seismic survey (See Figure 4.4 and 4.9)	Line-3-1 (650 m)	· Seismic source : dynamite · Seismic source interval : 5m · Receiver interval : 5m · Sampling rate : msec · Data length (Recording time): 2s
	Line-3-2 (600 m)	· Seismic source: Dropped weight, vibrator · Seismic source interval : 5m · Receiver interval : 5m · Sampling rate : 1msec · Data length (Recording time): 2s

4.1.3.3 MIU series 1, 2 and 3 borehole investigations [39~41]

Borehole investigations are one of the most important methods to investigate the underground geology and geological structure prior to excavation. These investigations allow collection of core samples, groundwater sampling and measuring the hydrogeological and rock mass properties to depth.

In Phase I-a, geological studies included detailed core logging, borehole geophysics and BTV surveys in the three new 1,000 m-deep boreholes, MIU-1, 2 and 3. Furthermore, petrological and mineralogical studies were carried out using core samples from the boreholes.

Core descriptions include: drilling depth, lithology, rock name, textural description such as grain-size and fabric, mafic mineral content, color, weathering, alteration, RQD, core recovery rate, fracture shape, fracture type and mineral fillings.

Borehole geophysical surveying includes a variety of methods: electrical logging, micro-resistivity logging, density logging, neutron and gamma-ray logging, acoustic logging, temperature logging, caliper logging and borehole deviation surveying. In addition, Borehole TV investigations record images of features, especially structures along a borehole wall. The records include depth, shape, width, fracture aperture, presence of filling and possibly alteration. Orientations are calculated from the geometry of features observed in the boreholes.

For petrological and mineralogical studies, modal and chemical composition analyses are carried out.

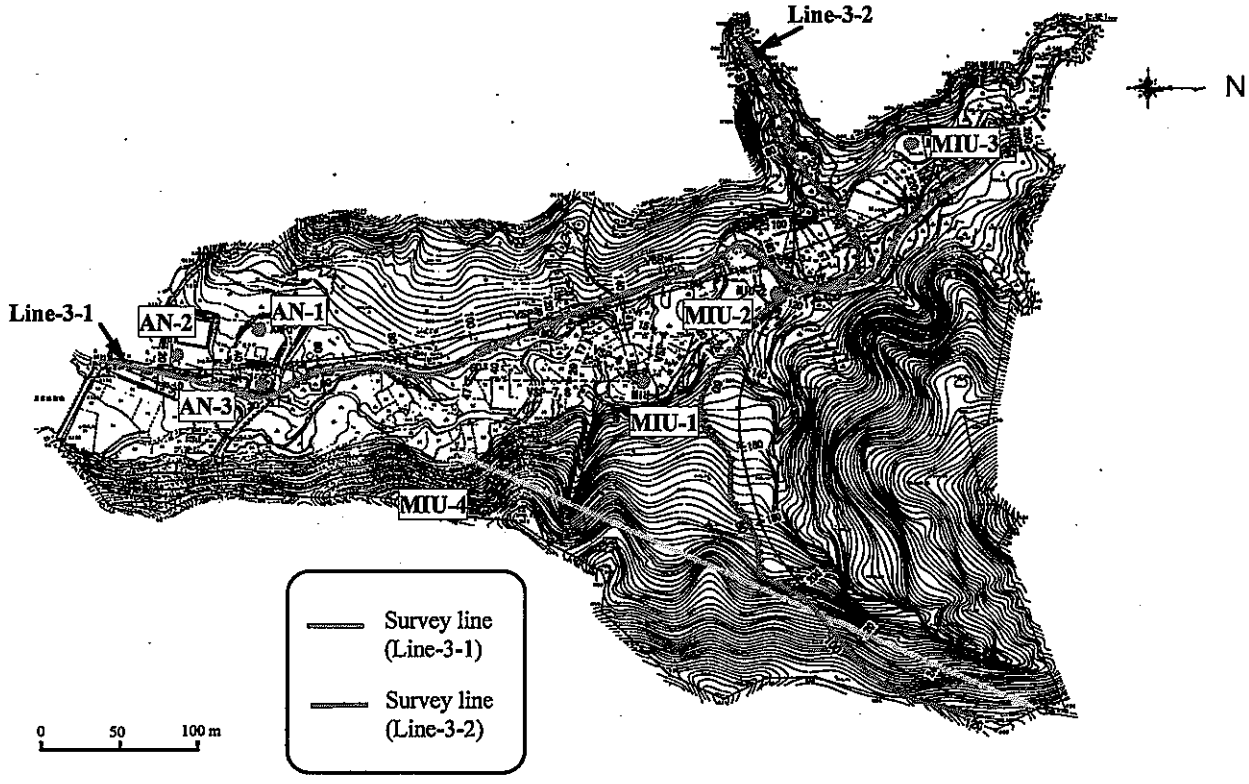

Figure 4.9 Location map of the survey line in Shobasama Site for reflection seismic survey

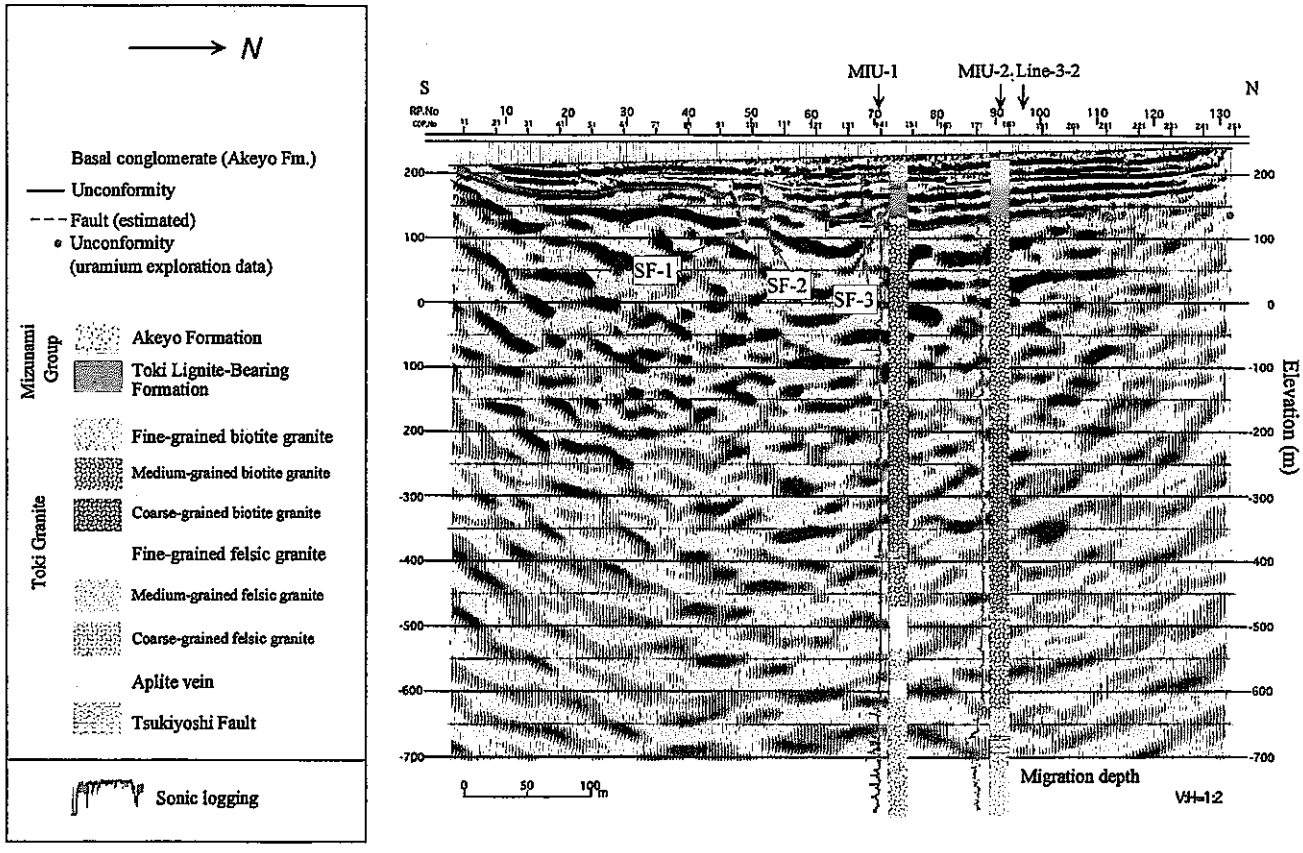

Figure 4.10 Results of reflection seismic survey (Line-3-1)

The results of the above investigations, the core descriptions, geophysical logging, BTV investigations and petrological and mineralogical studies in MIU-1, 2 and 3 are described below. In addition, overviews of the results from these boreholes are shown in Appendices 1, 2 and 3.

Granite lithofacies

Based on the core recovered from the MIU-1, 2 and 3 boreholes, the granite in the Shobasama Site has been classified into 'Biotite granite' and 'Felsic granite' phases. Furthermore, the biotite granite is subdivided into coarse-grained, medium-grained and fine-grained textural types.

The modal analysis of core samples from MIU-1, 2 and 3 indicate the rocks intersected are true granites (Figure 4.11) as classified by the IUGS (1973).

According to the chemical composition analyses, the chemical compositions of the biotite granite and felsic granite phases, in terms of some major oxides are different. An analysis of the variation in major oxide content versus depth, using a least-squares approximation, shows that the trends are different for most oxides in the two rock types. The analyses plot along different lines on the major oxide content-vs. depth diagrams (Figure 4.12).

Characteristics of the fracture distributions in the granite

In MIU-1, 2 and 3, sedimentary rocks were intersected from the surface to approximately 88 to 89 m depth, and these unconformably overly the biotite granite. The uppermost part of the granite is a strongly weathered, approximately 15 m thick zone.

Figure 4.13 shows changes in fracture density, cumulative fracture frequency, and orientation of fractures with depth in the MIU-2. Figure 4.14 shows histograms of fracture frequency distributions related to depth. Based on the variations shown in fracture density and by the cumulative fracture frequency analysis, the granite can be divided into the following three structural domains: "Upper fracture zone", "Moderately fractured zone" and "Fracture zone along the fault" in descending order. Characteristics of each domain are as follows.

· **"Upper fracture zone"**

This zone ranges from the weathered top of the granite down to approximately 300-370 m depth in the three boreholes. The fracture density varies from 3 to 5 fractures per meter (Table 4.8). This zone is characterized by the prevalence of fractures with a shallow inclination (Figure 4.15, Table 4.8).

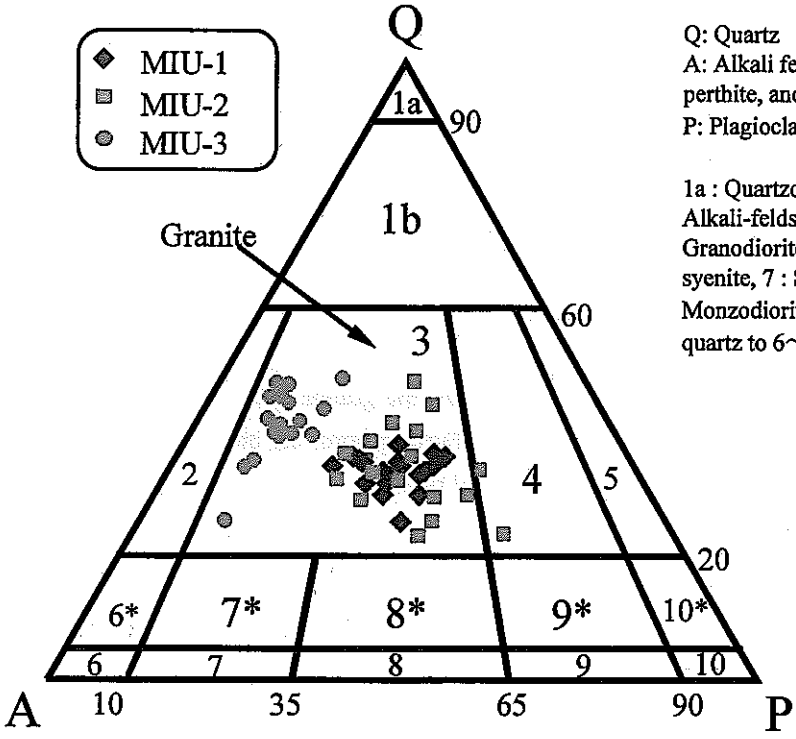

Q: Quartz
A: Alkali feldspers (orthoclase, microcline, perthite, anorthoclase, albite $An_{00\text{-}06}$)
P: Plagioclase $An_{06\text{-}100}$, scapolite

1a : Quartzolite, b : Quartz-rich granitoids, 2: Alkali-feldsper granite, 3 : Granite, 4 : Granodiorite, 5 : Tonalite, 6 : Alkali-feldsper syenite, 7 : Syenite, 8 : Monzonite, 9 : Monzodiorite, 10 : Diorite (6*～10* : Add prefix quartz to 6～10) (IUGS,1973)

Figure 4.11 Modal composition of the Toki Granite

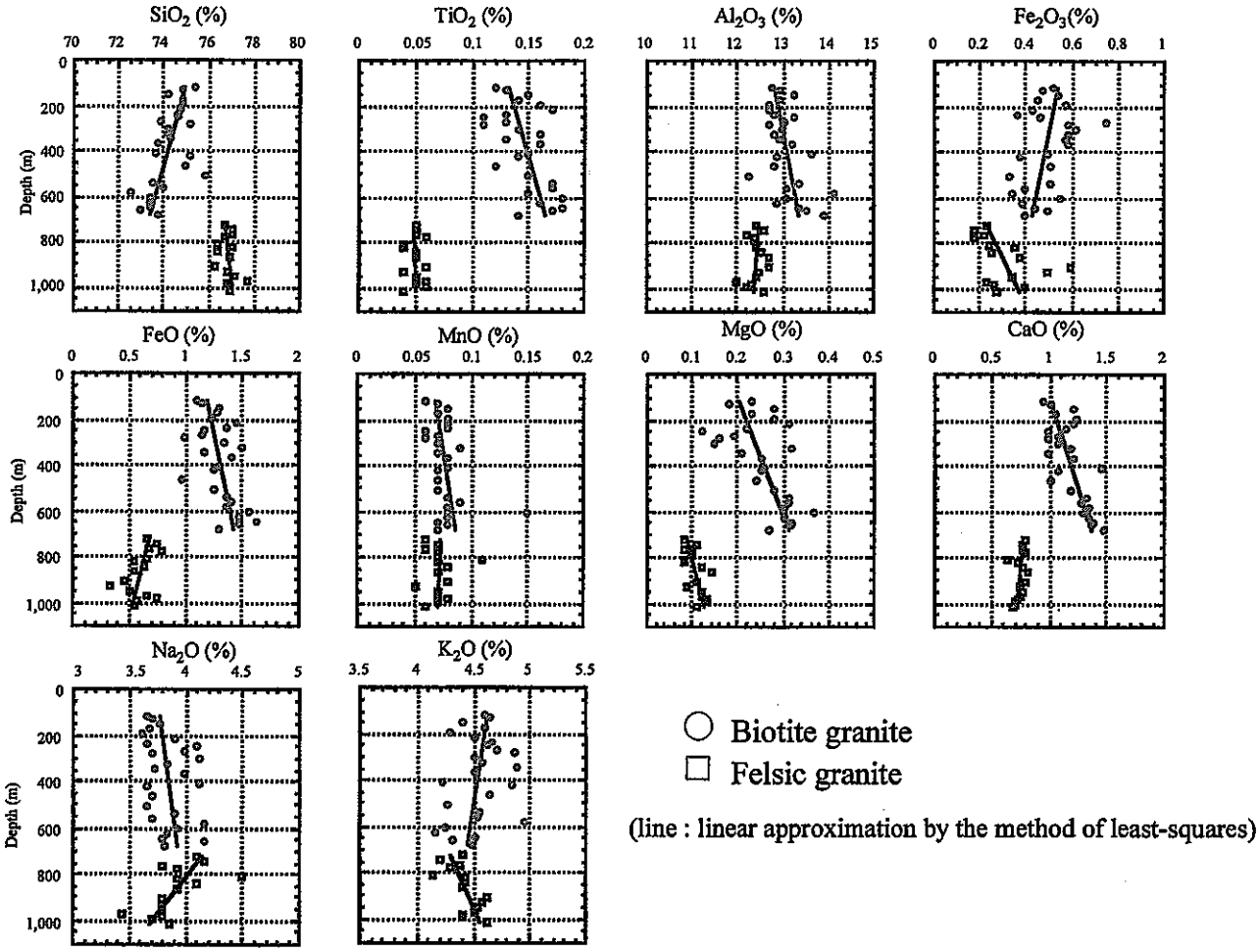

(line : linear approximation by the method of least-squares)

Figure 4.12 Chemical compositions of the Toki Granite

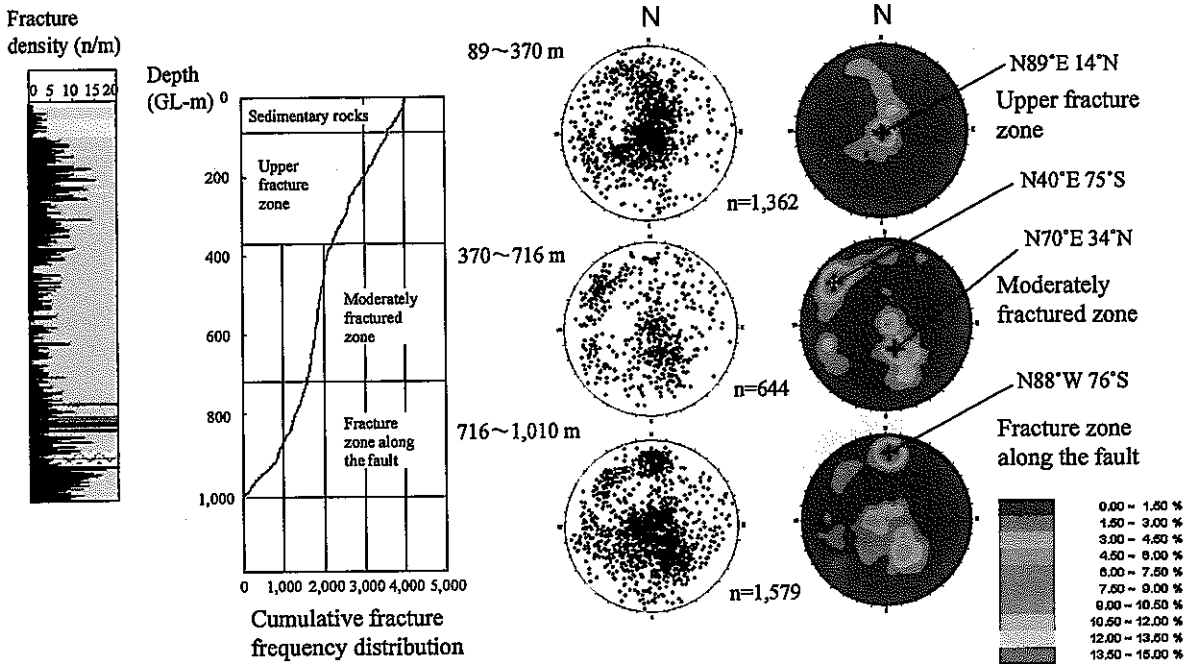

Figure 4.13 Fracture density, cumulative fracture frequency distribution and orientation of fractures vs depth (MIU-2)

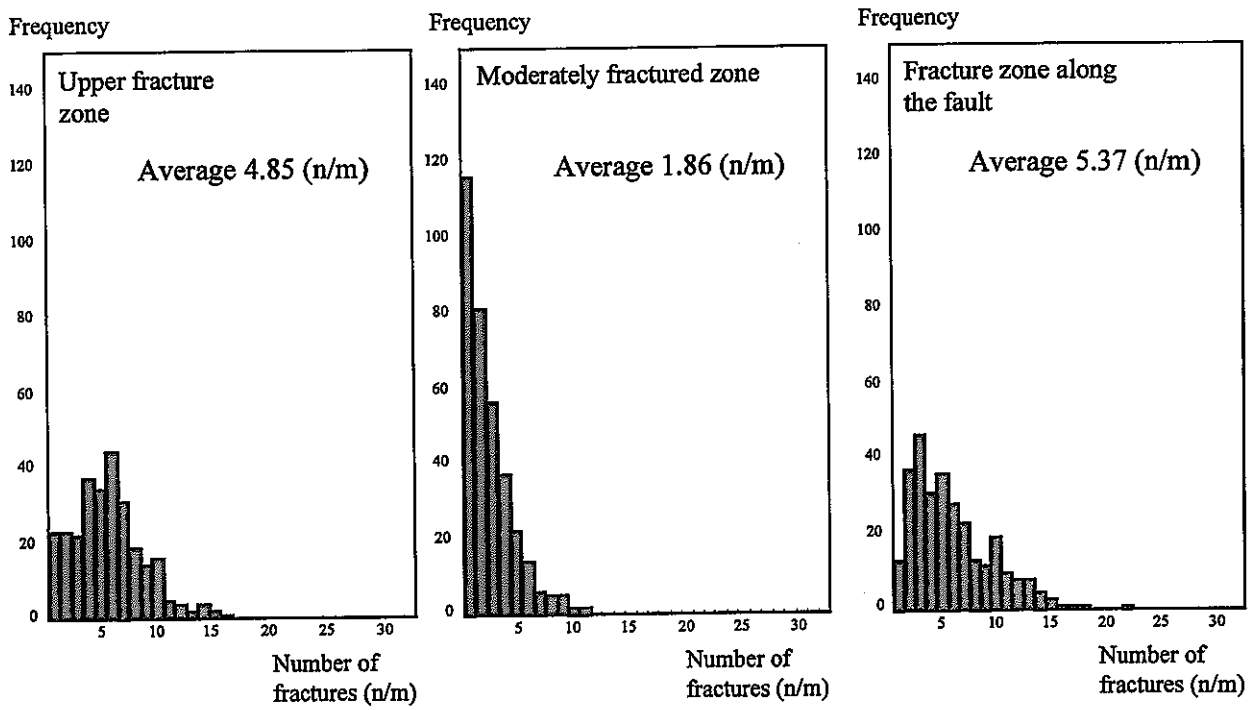

Figure 4.14 Fracture density vs depth (MIU-2)

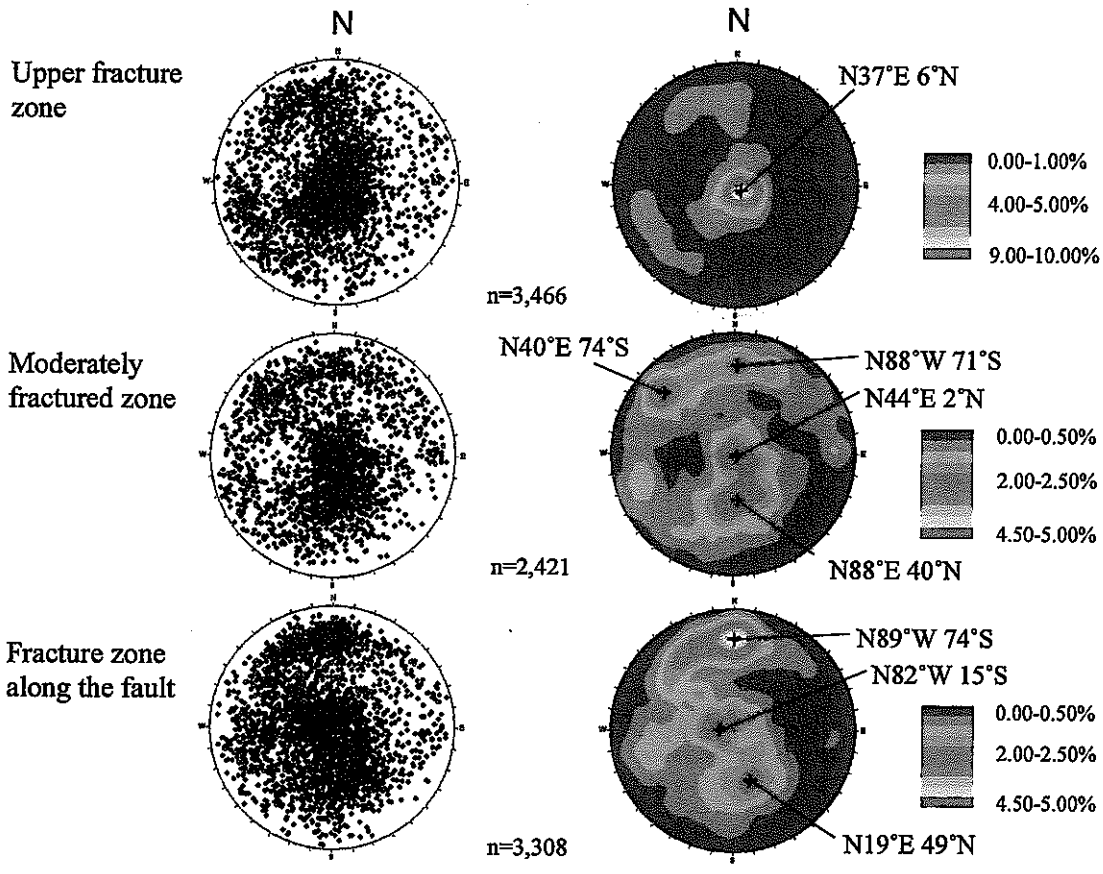

Figure 4.15 Orientation of fractures vs depth (MIU-1~ 3)

· **"Moderately fractured zone"**

This zone occurs between the "Upper fracture zone" and the "Fracture zone along the fault". The fracture frequency ranges, on average, from 1 to 3 fractures per meter in the three boreholes (Table 4.8). Like the underlying "Fracture zone along the fault", this zone is composed of a combination of shallow (0-30°), middle (30-60°) (strike: E-W, dip: N) to high (60-90°) (strike: NE-SW, dip: SE) -inclination fractures as shown in Figure 4.15 and Table 4.8.

· **"Fracture zone along the fault"**

This zone is characterized by the concentration of fractures developed along the Tsukiyoshi Fault, ranging in density from 3-6 fractures per meter in the three boreholes (Table 4.8). This zone is composed of low, middle (strike: NNE-SSW, dip: WNW) and high (strike: E-W, dip: S) -inclination fractures (Figure 4.15, Table 4.8). In particular, the strike of the most common fractures is approximately EW with steep southerly dips, which may be a reflection of the orientation of the Tsukiyoshi Fault.

Table 4.8 Densities and prevailing orientations of fracture in each structural domain

	"Upper fracture zone"	"Moderately fractured zone"	"Fracture zone along the fault"
Average fracture density*	3 to 5 /m	1 to 3 /m	3 to 6 /m
Prevailing orientations, Strike/dip	· Low/	· Low/ · High/EW, S · Medium/ EW, N · High/ NE-SW, SE	· Low/ · High/ EW, S · Medium/ NNE-SSW, WNW

* : Fracture data obtained from the BTV investigations

In general, the "Upper fracture zone" and the "Fracture zone along the fault" are characterized by higher hydraulic conductivity (10^{-7} to 10^{-5} m/s) than the "Moderately fractured zone" with lower conductivities (10^{-7} to 10^{-10} m/s) (Figure 4.16).

Differences in fracture characteristics such as shapes and mineral fillings in the three structural domains are yet to be analyzed.

Physical properties obtained by borehole geophysics in the granite

In the MIU-1, 2 and 3 boreholes, geophysical surveys included:

- electrical logging
- micro-resistivity logging
- density logging
- neutron logging
- gamma-ray logging
- acoustic logging
- temperature logging
- caliper logging
- borehole deviation logging

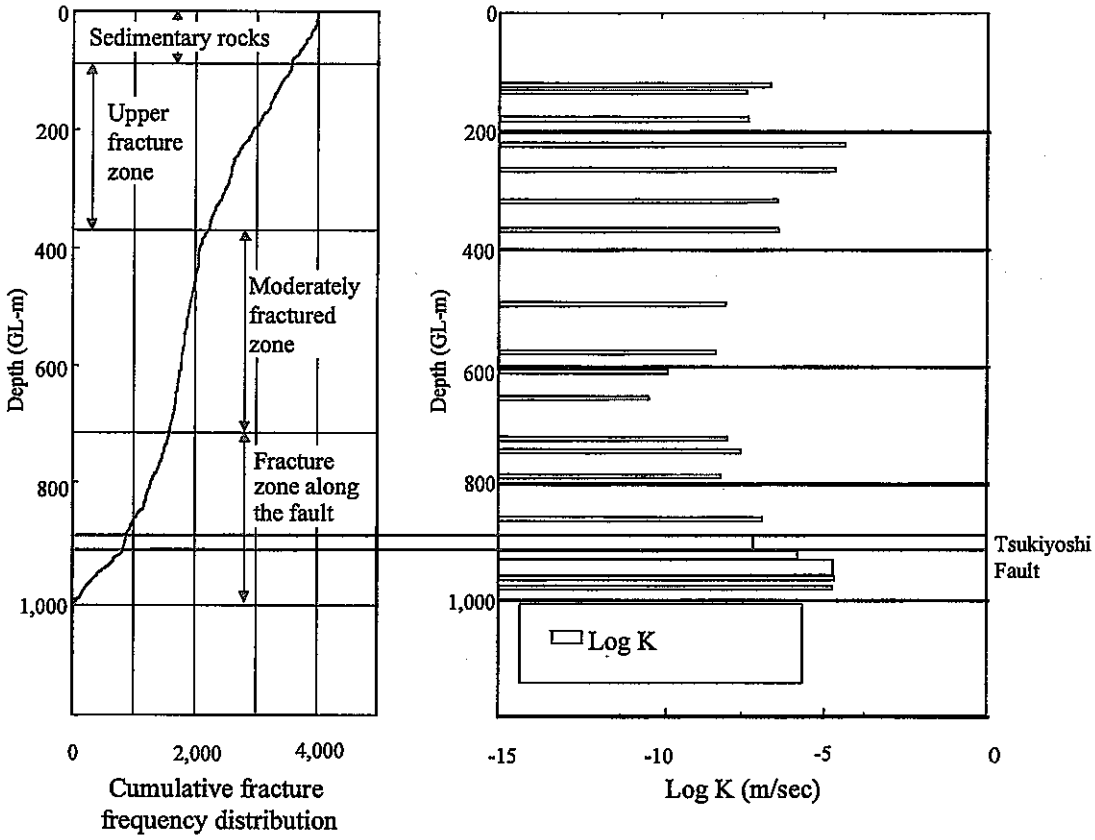

Figure 4.16 Comparison between cumulative fracture frequency distribution and hydraulic conductivity distribution

The results of the apparent resistivity (short and long-normal) obtained from electrical logging, porosity obtained from neutron logging and P-wave velocity obtained from acoustic logging are shown on Figure 4.17. Anomalies in the log profiles of these three methods are considered to provide good indications of increased permeability in the rock mass. Stated very simply, the two former methods give indications of water content and the latter can be an indication of the degree of fracturing of a rock mass. Neutron logging is based on the principal that neutrons are scattered or slowed by collisions with hydrogen atoms and gamma radiation produced. For our purposes, hydrogen is present only in water or in hydrated minerals. Thus an increase in water results in an increase in neutrons captured or moderated. Therefore, saturated rocks with high porosity will have a lower neutron count than low porosity rocks. With respect to electrical resistivity, the rocks and soils of the earth exhibit a wide range. The presence of water increases the ability of earth materials to conduct electricity. Therefore, very simply stated, unsaturated or slightly saturated rocks will normally have a higher resistivity than the same rocks under more saturated conditions. With respect to acoustic logging, the P-wave velocity, which is very dependent on rock type, will be faster in intact rock than in the same rock if it is fractured. As the degree of fracturing increases the P-wave velocity decreases. And as the degree of fracturing increases the permeability will also likely increase.

The results of comparison of porosity, apparent resistivity and P-wave velocity among the three zones of the granite are as follows.

・ Porosity

The range of average porosity of "Upper fracture zone", "Moderately fractured zone" and "Fracture zone along the fault" determined by neutron logging are 4 to 7%, 3 to 5% and 4 to 8%, respectively. Intersections of the Tsukiyoshi Fault (highlighted by yellow in Figure 4.17) show porosities of about 8% and 14% respectively in MIU-2 and 3.

・ Apparent resistivity

The average apparent resistivity is smallest in the "Fracture zone along the fault" and largest in the "Moderately fractured zone". The ranges of average resistivity in Ωm are:

- "Upper fracture zone": short-normal- 800 to 2,000; long-normal 1,800 to 2,800
- "Moderately fractured zone": short normal 1,500 to 2,500; Long normal 2,800 to 3,500
- "Fracture zone along the fault": short normal 400 to 1,500, long normal 700 to 1,600

Local decreases in apparent resistivity occur at shorter intervals in the '"Upper fracture zone" than in the "Moderately fractured zone". The average apparent resistivities of the Tsukiyoshi Fault measured in MIU boreholes are very low:

MIU-2: short normal 400 Ωm, long normal 300 Ωm

MIU-3: short normal 100 Ωm, long normal 200 Ωm

・P-wave velocity

The smallest average P-wave velocity is obtained in the "Fracture zone along the fault" and largest in the "Moderately fractured zone". The ranges are:

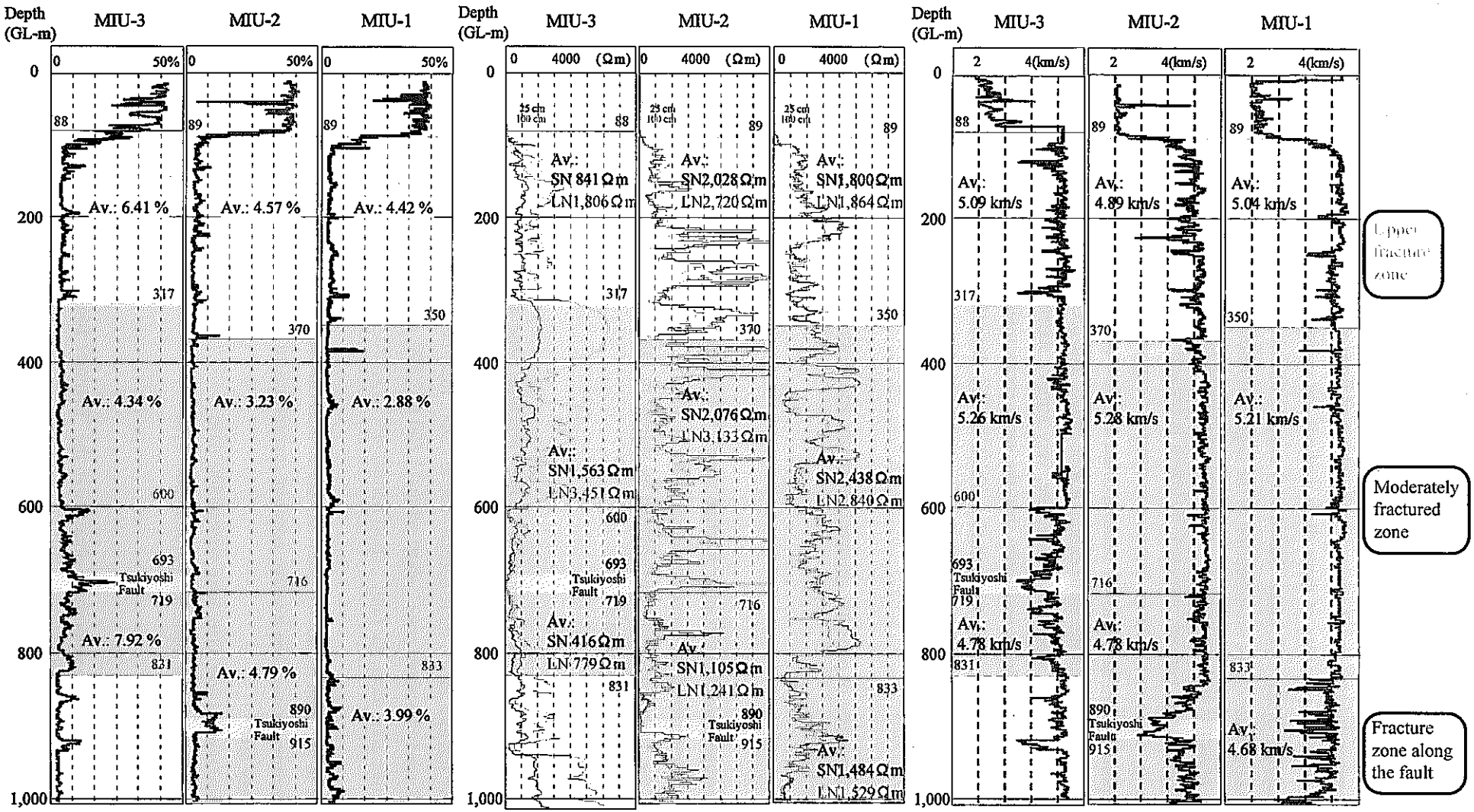

(a) Neutron porosity (b) Apparent resistivity (c) P-wave velocity

SN : short normal (25 cm)
LN : long normal (100 cm)

Figure 4.17 Results of geophysical logging

'Upper fracture zone', 'Moderately fractured zone' and 'Fracture zone along the fault' are defined according to the result of fracture density and geophysical logging.

"Upper fracture zone" 4.8 to 5.1 km/s
"Moderately fractured zone" 5.2 to 5.3 km/s
"Fracture zone along the fault" 4.6 to 4.8 km/s

Local decreases in P-wave velocity (<5.0 km/s) appear more often in the "Upper fracture zone" than in the "Moderately fractured zone". P-wave velocity averages in the Tsukiyoshi Fault are lower than 0.4 km/s in MIU-2, 3.

Characteristics of faults in the granite

The Tsukiyoshi Fault is intersected by MIU-2 at 890 to 915 m depth and by MIU-3 at 693 to 719 m depth. In both intersections the core of the fault is composed of about a 10 to 20 m-wide cataclasite zone around which an approximately100 m-wide fractured zone is developed. In particular the "Fracture zone along the fault" intersected by MIU-2 is much more permeable than the "Moderately fractured zone" (Figure 4.16).

4.1.4 Construction of the geological model for the about 4 km × about 6 km study area

4.1.4.1 Conceptualization of the geological model for the about 4 km × about 6 km study area surrounding the Shobasama Site : data from the literature and "other geoscientific research"

Geological units

The geological model was constructed solely with data from the literature and the "other geoscientific research" for the about 4 km × about 6 km study area (Figure 3.4).

For both sedimentary rocks and granite, lithofacies are considered as primary whereas fractures and faults are secondary features generated after rock formation.

The following sedimentary rocks are treated as individual units in the geological model: the Seto Group, and the Oidawara, Akeyo and Toki Lignite-bearing Formations. For granite, it is divided into only two parts; the upper highly weathered zone is considered as a separate geological component from the rest of the granite below the weathered zone. The Tsukiyoshi Fault is a structural part of the model that crosscuts the lithological units.

Model construction

Using the data from the sources shown in Table 4.9, the geological units and their physical boundaries were defined. Topographical features, each unit's boundary and the shape of the fault plane were estimated using the minimum tension theory [42] (Figure 4.18). The results of borehole investigations in AN-1 and 3 were used to extract the geological units. However, these results were not used when defining the above-mentioned boundaries as the granite was only divided into three parts in these boreholes: weathered

granite, the granite below the weathered zone and the Tsukiyoshi Fault.

Table 4.9 Sources of data used to define geological structural boundaries of the geological model
(Study area: about 4 km × about 6 km)
(MIU Phase I-a sources are excluded)

Boundary	Data Source
Ground surface	Digital elevation data (20 m mesh)*
Upper boundary of Oidawara Fm.	59 boreholes for uranium exploration AN-8, SN-1, 2, 3 and 4, TH-6, 8 Seismic survey in the Shaft Excavation Effect Experiment*
Upper boundary of Akeyo Fm.	53 boreholes for uranium exploration AN-8, SN-1, 2, 3 and 4,TH-6, 8 Geological map (PNC, 1994)
Upper boundary of Toki Lignite-bearing Fm.(Upper)	135 boreholes for uranium exploration AN-6, 8, SN-1, 2, 3, 4 and 6,TH-1, 2, 3, 4, 6, 7 and 8 Seismic survey in the Shaft Excavation Effect Experiment*
Upper boundary of Toki Lignite-bearing Fm.(Lower)	141 boreholes for uranium exploration AN-6, 8,SN-1, 2, 3, 4 and 6,TH-1, 2, 3, 4, 6, 7 and 8 Seismic survey in the Shaft Excavation Effect Experiment*
Upper boundary of weathered granite	120 boreholes for uranium exploration AN-6, 8, SN-2, 3, 4 and 6, TH-1, 2, 3, 5, 7, 8, HN-1 Topographical map of basement rock [20,31] Seismic survey in the Shaft Excavation Effect Experiment*
Upper boundary of intact granite	(Calculated by assuming the thickness of weathered granite is 20 m)
Tsukiyoshi Fault	13 boreholes for uranium exploration TH-1, 2 and 3 Topographical map of basement rock [31] Seismic survey in the Shaft Excavation Effect Experiment*

* : 1:25,000 "Toki" and "Mizunami" topographic maps published by Geophysical Survey Institute

As with most models, there are uncertainties. The main ones are considered to be as follows:

① Data on the heterogeneity of the granite deep underground were scarce. As a result, the granite could only be divided into two units: the weathered zone at the top and the rest of the granite.
② Information on the Tsukiyoshi Fault was not available where it crosscuts the granite. Thus, it was postulated that the fault in the granite has the same properties as it has in the sedimentary rocks.

4.1.4.2 Revision of the geological model with data from MIU Phase I-a

The initial geological model was revised with data from the MIU Phase I-a

Geological units

For the sedimentary rocks, the Seto Group, and the Oidawara, Akeyo and Upper and Lower Toki Lignite-bearing Formations there was no change in these geological units.

For the granite, the weathered zone remained the same. The previously undivided granite could be subdivided on a structural basis into domains, the: "Upper fracture zone", "Moderately fractured zone" and

"Fracture zone along the fault". The Tsukiyoshi Fault was included as before.

Model construction

Using the data from the sources shown in Table 4.10, the boundaries between the above geological units were defined. The drilling results of AN-1 are also included in the data.

Table 4.10 Data sources used to set geological boundaries of the geological model
(Study area : about 4 km×about 6 km)
(MIU Phase I-a sources included)

Boundary	Data Source	
	Data obtained by literature study / geoscientific research prior to the MIU Project	MIU Project data Phase I-a
Ground surface	Digital elevation data (20 m mesh)*	–
Upper boundary of Oidawara Fm.	59 boreholes for uranium exploration AN-8, SN-1, 2, 3 and 4, TH-6, 8 Seismic survey in the Shaft Excavation Effect Experiment*	–
Upper boundary of Akeyo Fm.	53 boreholes for uranium exploration AN-8, SN-1, 2, 3 and 4, TH-6, 8 Geological map (PNC, 1994)	–
Upper boundary of Toki Lignite-bearing Fm. (Upper)	135 boreholes for uranium exploration AN-6, 8, SN-1, 2, 3, 4 and 6,TH-1, 2, 3, 4, 6 and 8 Seismic survey in the Shaft Excavation Effect Experiment*	–
Upper boundary of Toki Lignite-bearing Fm. (Lower)	141 boreholes for uranium exploration AN-6, 8, SN-1, 2, 3, 4 and 6, TH-1, 2, 3, 4, 6 and 8 Seismic survey in the Shaft Excavation Effect Experiment*	–
Upper boundary of weathered granite	120 boreholes for uranium exploration AN-6, 8, SN-2, 3, 4 and 6, TH-1, 2, 3, 4, 5, 7 and 8, HN-1 Topographical map of basement rock[20,31] Seismic survey in the Shaft Excavation Effect Experiment*	–
Upper boundary of "Upper fracture zone"	**AN-1** [34]	**MIU-1, 2 and 3** [39~41]
Upper boundary of "Moderately fracture zone"	**AN-1** [34]	**MIU-1, 2 and 3** [39~41]
Tsukiyoshi Fault	**Geological map** [12]	**MIU-2, 3** [40,41]
Upper and Lower boundary of "Fracture zone along the fault"	–	**MIU-1, 2 and 3** [39~41]

* : 1: 25,000 "Toki" and "Mizunami" topographic maps published by Geophysical Survey Institute

Bolded: Data used to revise the initial, study area geological model

Uncertainties in the geological model are as follows.

① The MIU-1, 2 and 3 boreholes are nearly vertical. Therefore, steeply inclined fractures may be under-sampled.

② The methodology to specify permeable fractures needed to form an equivalent continuum model were not sufficiently established. As a result, the specification was unreliable.

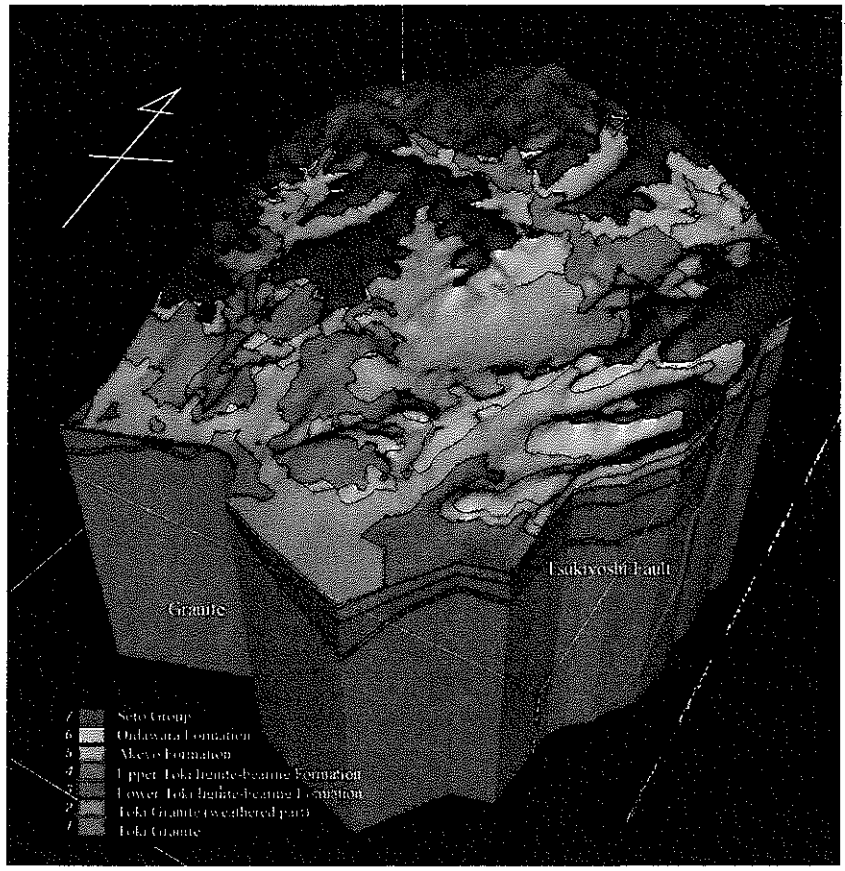

Figure 4.18 Geological model (about 4 km × about 6 km, down to 1,000m in depth) based on literature survey and existing data before the MIU Project

4.1.5 Construction of the geological model for the Shobasama Site

The model referred to here is the Shobasama Site-scale model. As was done for the other models, the procedure followed was to build the model iteratively starting with existing data and systematically adding information and knowledge to the model as new data became available.

4.1.5.1 Conceptualization of the geological model using data from literature survey and from other geoscientific research

The components of the Shobasama Site model may be divided into primary and secondary. In general the granite phases are primary whereas the structures such as fractures and weathered zones are secondary. Other structures such as the sedimentary rock layers are primary but with secondary structures such as crosscutting faults.

For the sedimentary rocks, the Seto Group, and the Oidawara, Akeyo and the Upper and Lower Toki Lignite-bearing Formations are the defined geological units (See Section 2.3). Though different lithofacies were recognized in the granite through the earlier investigations and analyses, enough information was not obtained for a reliable, deterministic modeling of their distribution and continuity. As for faulting, only the Tsukiyoshi Fault is considered to be well enough understood, and only in the sedimentary rocks, for inclusion in the model. Thus, this model is essentially the same as the initial model for the study area and is comprised of the same units in the granite:

① Fractured zone including the weathered zone,
② The granite below the weathered zone,
③ The Tsukiyoshi Fault.

The geological model of the Shobasama Site is shown in Figure 4.19. Three dimensional visualization software was not used because the software had not been introduced at the time and if it had would not likely have contributed meaningfully, as the model was too simple to benefit.

Uncertainties in the geological model are as follows.

① Knowledge of the subsurface distribution of geological units and the granite lithofacies were not well developed with the existing data base prior to 1996. As a result, the granite was only divided into two elements: the fractured zone including the weathered part and the rest of the granite.
② Information on the Tsukiyoshi Fault is not available in the granite. Thus, it is postulated that the fault in the granite has the same properties as that in the sedimentary rocks.

4.1.5.2 Revision of geological model using all data, including the results of MIU Phase I-a

Geological units

The general conceptualization developed for the first model of the sedimentary rocks remained basically

unchanged. The units are divided into Seto Group, Oidawara Formation, Akeyo Formation, the Upper and Lower Toki Lignite-bearing Formation and Tsukiyoshi Fault. The MIU boreholes provided additional details on the layers in terms of thickness stratigraphy and confirmed the earlier findings.

Based on the borehole investigations in MIU-1, 2 and 3, the following improvements were possible.

① The secondary tectonic zones produced after the formation of the granite, the zone of weathering, the "Upper fracture zone", "Moderately fractured zone", the Tsukiyoshi Fault, and the "Fracture zone along the fault" were defined. Since the "Upper fracture zone" is thought to be characterized by a high fracture density and permeability, it could be distinguished from the "Moderately fractured zone" in the Biotite granite and Felsic granite. The Tsukiyoshi Fault has an approximately 100 m-wide fracture zone on both sides.

② Based on these results, the geological units established for the granite are the weathered part, the "Upper fracture zone", the Tsukiyoshi Fault, "Fracture zone along the fault", the Biotite granite and the Felsic granite.

Fracture zone distribution is shown schematically in Figure 4.20.

Model construction

Based on the data from the sources shown in Table 4.11, the boundaries of the geological units and the shape of the main fault plane were estimated using the minimum tension theory [42]. This model construction was carried out for the Shobasama Site, smaller than the above study area covers, and approximately 0.8 km×1.3 km, the "modeling area" (Figure 4.21). This modeling area contains the Tsukiyoshi Fault, which is presumed to greatly affect the hydrogeology of the Shobasama Site (See Section 4.2.4). Data sources used for the modeling are shown in Table 4.11. However, MIU-3 data was available too late for the modeling and therefore was not included in this exercise. Methods to establish the above-mentioned boundaries are as follows.

① Topographical surface:
Digital elevation data (Table 4.11) in 20 m intervals are used.

② Boundary between the Seto Group and the Oidawara Formation:
The Oidawara formation is restricted to the footwall (north side) of the Tsukiyoshi Fault, and therefore was not intersected by the boreholes drilled at the Shobasama Site. For modeling, the digitized contact shown on the geological map of the Toki-Mizunami district was used.

③ Boundary between the Seto Group and the Akeyo Formation:
This boundary is so shallow at the drilling sites in the Shobasama Site that no core was recovered. For the modeling, the digital information of the boundary location drawn on the geological map of the Toki-Mizunami district was used.

④ Boundary between the Akeyo and the Toki Lignite-bearing Formations:
The depth of this boundary was determined from the results of the MIU-1 and 2 borehole investigations. On the other hand, the Toki Lignite-bearing Formation is absent in the southern

part of the site and was not intersected by AN-1 or AN-3 nor is it visible in any surface exposure. Thus, on the knowledge that the unit does not extend to the south, depth information obtained in the MIU-1 and 2 are used for the modeling.

⑤ Boundary between the sedimentary rocks and the weathered part of the granite:

The MIU-1 and 2 and AN-1 and 3 borehole investigations established the depths of the boundary at the site. The upper part of the granite exposed on the ground surface is thought to be weathered. Accordingly, the depth information obtained in the boreholes and the digital database developed from the geological map of the Toki-Mizunami district are used for the modeling.

⑥ Boundary between the weathered granite and "Upper fracture zone" of the granite:

The weathered parts of the granite have the following characteristics.

- Zone with grade C_M or below by the rock mass rating in Japan [43]
- Zone dominated by RQD values of less than 50%
- Zone characterized by low resistivity or density and high porosity from geophysical logging
- Zone in the granite near the boundary with the sedimentary rocks. The matrix in this zone contains limonite and kaolinite [44], common weathering products.

Based on these definitions, the thickness of the weathered zone was estimated using data from MIU-1 and 2 and AN-1 and 3 borehole investigations.

⑦ Boundary between the "Upper fracture zone" and the "Moderately fractured zone" in the Biotite granite:

The "Upper fracture zone" is defined as a zone characterized by higher fracture density, higher porosity in geophysical logging and/or the frequent occurrence of horizontal fractures compared with the "Moderately fractured zone". This boundary is modeled using the information obtained from the MIU-1 and 2 borehole investigations.

⑧ Boundary between the "Moderately fractured zone" in the Felsic granite and the "Upper fracture zone"

This boundary is modeled using the information obtained from AN-1, 3 borehole investigations.

⑨ Boundary the "Moderately fractured zone" of the Biotite granite and the "Moderately fractured zone" of the Felsic granite

These are not distinguished on the existing geological map [12]. As a result, this boundary is modeled using the information obtained from the MIU-1, 2 and AN-1, 3 borehole investigations.

⑩ The Tsukiyoshi Fault

The Tsukiyoshi Fault was intersected by MIU-2, but not by the adjacent, more southerly MIU-1. Therefore, the depth information in MIU-2 and the digitized information of the fault line from the existing geological map [12] are input to the modeling. For modeling, 30 m of displacement by the Tsukiyoshi Fault was used (historic information) for the juxtaposition of units on opposite sides of the fault.

- Boundary between the Akeyo Formation and the Toki Lignite-bearing Formation
- Boundary between the sedimentary rocks and the underlying weathered granite
- Boundary between the weathered granite and the "Upper fracture zone"
- Boundary between the "Moderately fractured zone" in the Biotite and Felsic granites.

However, any genetic relationship between the "Upper fracture zone" and the Tsukiyoshi Fault is

unknown. Therefore, the fault displacement of the boundaries between the "Upper fracture zone" and "Moderately fractured zone" in the Biotite granite and the Felsic granite were not considered.

⑪ Upper boundary of the "Fracture zone along the fault" (hanging wall side):

The information on thickness of the "Fracture zone along the fault" on the hanging wall side could only be obtained from MIU-2. Thus it has been assumed, for modeling, that the thickness of the fracture zone, as indicated by MIU-2, would be uniform all along the fault in the modeling area.

⑫ Lower boundary of the "Fracture zone along the fault" (footwall side):

The presence of the "Fracture zone along the fault" was confirmed on the footwall side of the Tsukiyoshi Fault in MIU-2. However, its lower boundary was not penetrated, so true thickness in unknown. Consequently, for lack of a better reason, the fractured zone on the footwall side of the fault is assigned the same thickness as on the hanging wall side.

Table 4.11 Data sources used to establish geological boundaries in the geological model

Boundary	Data	
	Literature study / geoscientific research except for the MIU Project	The result of MIU Phase I-a
Surface	Digital elevation data (20 m mesh)*	–
Upper boundary of Oidawara Fm.	Geological map [12]	–
Upper boundary of Akeyo Fm.	Geological map [12]	–
Upper boundary of Toki Lignite-bearing Fm. (Upper)	Geological map [12]	MIU-1, 2 [39,40]
Upper boundary of weathered granite	Geological map [12] AN-1, 3 [34]	MIU-1, 2 [39,40]
Upper boundary of "Upper fracture zone"	AN-1, 3 [34]	MIU-1, 2 [39,40]
Upper boundary of "Moderately fractured zone" of the Biotite granite	–	MIU-1, 2 [39,40]
Upper boundary of "Moderately fractured zone" of the Felsic granite	AN-1, 3 [34]	–
Tsukiyoshi Fault	Geological map [12]	MIU-2 [40]
Upper/lower boundary of "Fracture zone along the fault"	–	MIU-2 [40]

* : 1: 25,000"Toki" and "Mizunami" topographic maps published by Geophysical Survey Institute

Uncertainties in the geological model are as follows.

① Data in the northeastern part of the Shobasama Site are lacking.

② Since the MIU-1, 2 and 3 boreholes are all vertical, information on fractures with a steep inclination is insufficient because they are statistically under sampled.

③ Information on the variation in thickness of the "Fracture zone along the fault" is insufficient.

④ Heterogeneity of the individual geological units of the granite are not known.

⑤ Information below 1,000 m depth is not available.

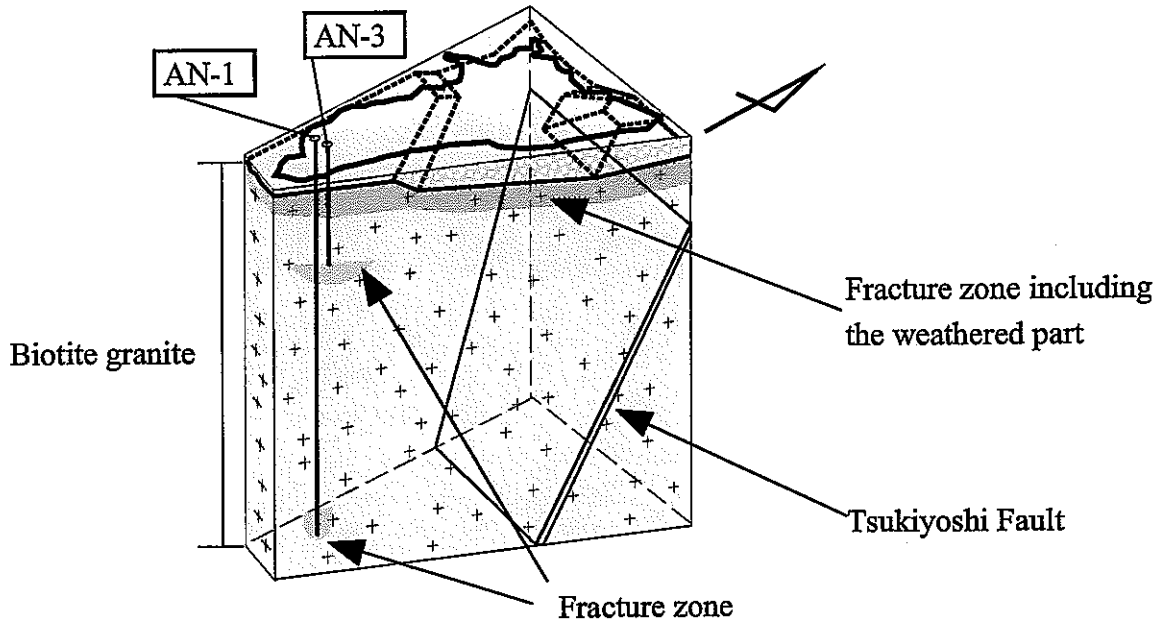

Figure 4.19 Geological model (Shobasama Site) based on literature survey and existing data before the MIU Project

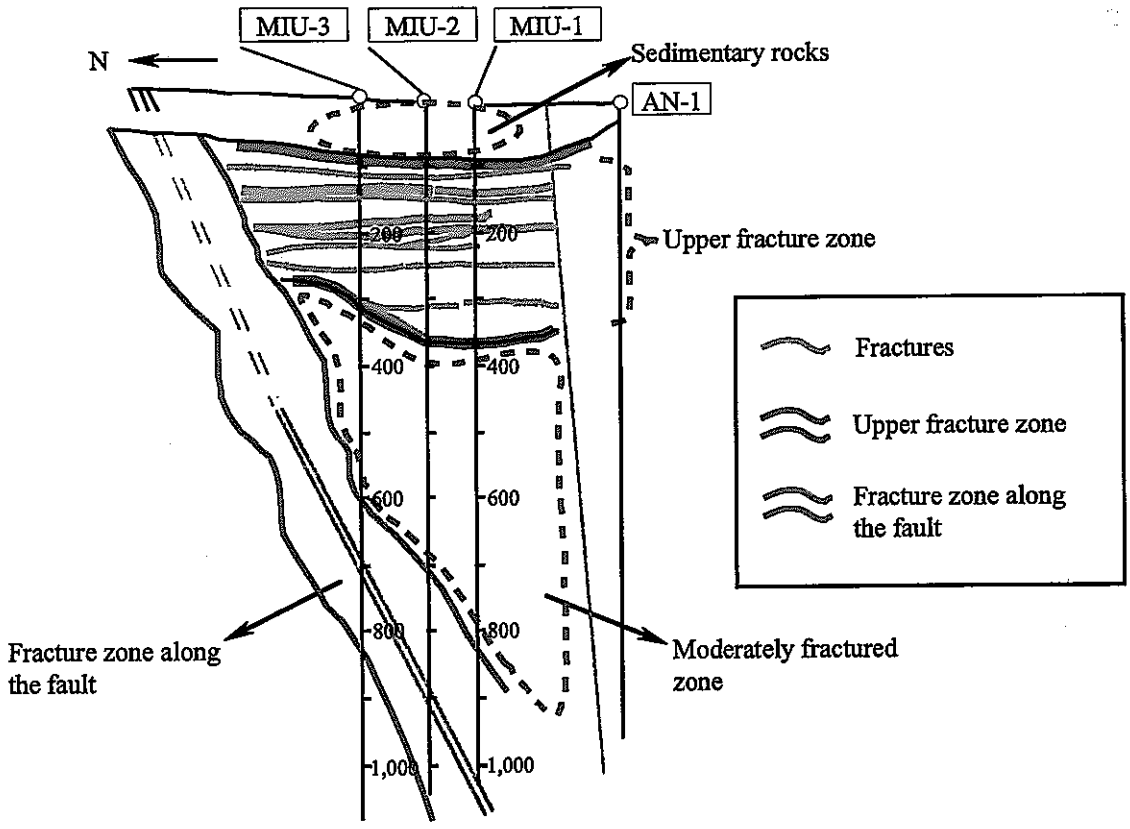

Figure 4.20 Distribution of fracture zone estimated with data from MIU-1~3

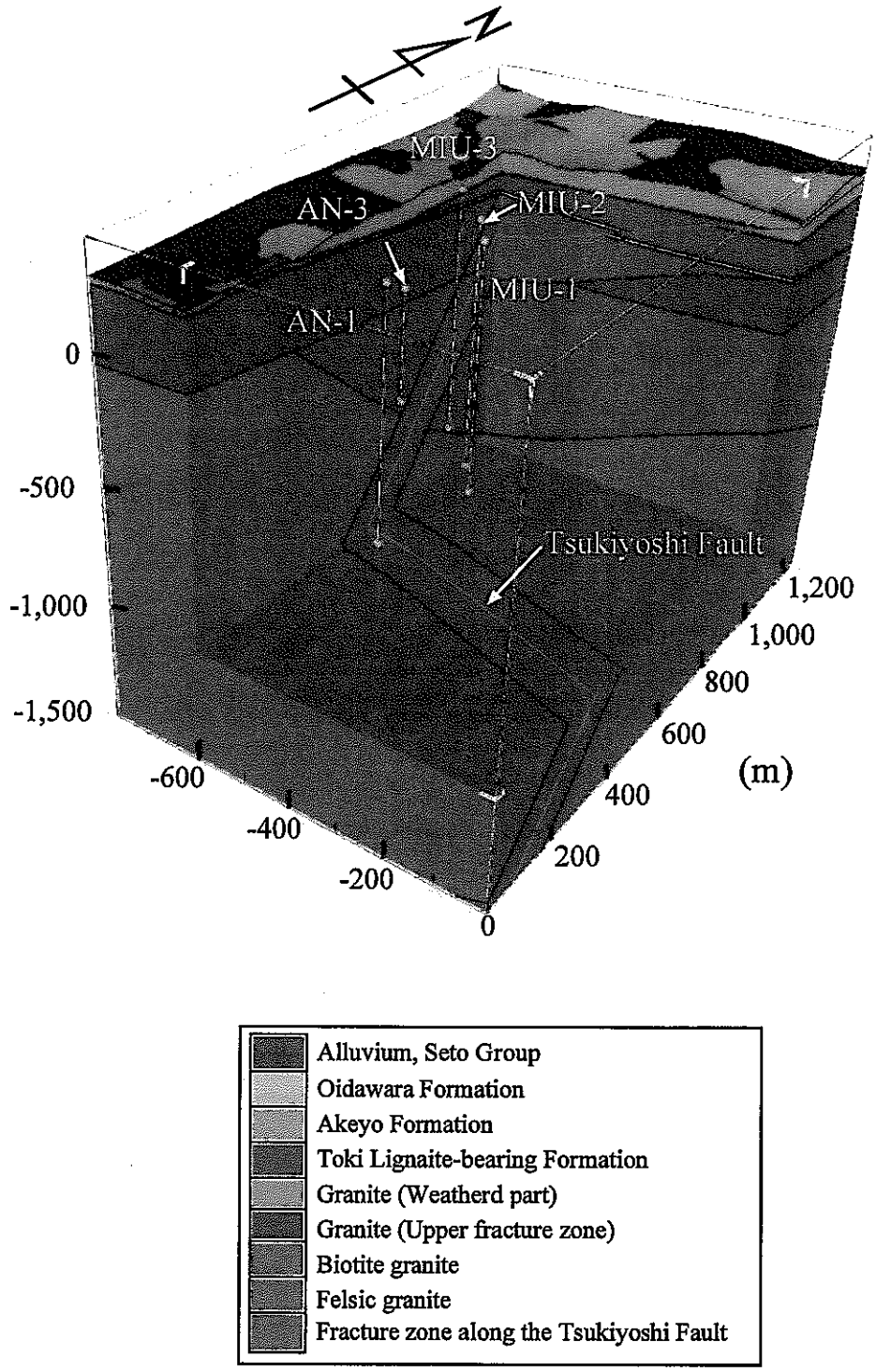

Figure 4.21 Geological model of the Shobasama Site based on the existing data and results of Phase I-a

4.1.6 Summary

The geological models are constructed so that the data requirements and the investigations performed in terms of the type, detail and scope and the analysis/evaluation techniques can be assessed in terms of their quality and accuracy. For each area, the Shobasama Site (0.8 km × 1.3 km) and the more regional study area for groundwater flow simulation (about 4 km×about 6 km), two increasingly detailed models were constructed. The first model for each of the above areas was based on the data from literature surveys and other geoscientific research. The second model was a revision of the first model, with new data from MIU Phase I-a investigations, including MIU-1, 2 and 3 boreholes.

In the first modeling exercise for both areas, the granite could only be divided into two parts, largely because of the lack of information regarding fracture zones in the granite and the possibility of variations in lithology. The two parts are the weathered zone at the top of granite and the remaining rock mass below the weathered zone.

In the second modeling exercise for both areas, new geological units defined in Phase I-a were added to the initial geological models. These units are the biotite granite, felsic granite, "Upper fracture zone", "Moderately fractured zone" and "Fracture zone along the fault". The revised models were utilized for construction of models for the other disciplines, namely the hydrogeological, hydrochemical and rock mechanical models and the numerical, groundwater flow simulation and rock response models. An important consideration in these exercises is knowing the data requirements of the models that build on the geological model.

The uncertainty in the revised geological models include the shortage of information on geological structures in the northeastern part of the Shobasama Site and at depths exceeding 1,000 m, little knowledge on the heterogeneities in the geological units defined and on the distribution of fractures with a steep inclination.

4.1.7 Future tasks

The future tasks are as follows:

① In order to improve the methodology of model construction, the uncertainty in the data and thus in the models should be investigated by comparing the existing models with new data and analysis in Phase I-b and later.

For example, geology and geological structure around the MIU-4 were predicted (Figures 4.22, 4.23) prior to drilling planned in Phase I-b. The predictions shown in Figures 4.22 and 4.23 were developed from the information presented in Figures 4.21 and 4.24 for each. Figure 4.24 [45] is a model constructed using all the available data prior to planning the MIU-4 drilling. Databases used for the construction of the geological models are shown in Table 4.12.

The revised geological models will be subject to evaluation by comparing predictions with the

new information from the MIU-4 borehole investigations.

② The geological model constructed in Phase I-a was based on the assumption that the groundwater flow simulation will adopt a continuum modeling approach. Future groundwater flow simulations will likely adopt other modeling methodologies. It will be necessary to meet the data requirements of these methodologies with appropriate geological models.

③ Regional geological history should be understood as well as possible. If the geological model constructed in Phase I-a is not consistent with the geological history, the model should be revised to make it more reliable.

Table 4.12 Databases used to establish the geological boundaries in the geological model for planning MIU-4 borehole investigations

Boundary	Data source	
	Data obtained by literature study / Geoscientific research prior to MIU Project Phase I-a	The result of the Phase I-a
Ground surface	Digital elevation data (20 m mesh)*	—
Upper boundary of weathered granite	140 boreholes for uranium exploration AN-1, 3, 6 and 8, SN-1, 2, 3, 4 and 6, TH-1, 2, 3, 4, 5, 7 and 8, HN-1 Topographical map of basement rock [20,31] Seismic survey in the Shaft Excavation Effect Experiment	MIU-1, 2 and 3
Upper boundary of "Moderately fractured zone" in Biotite granite	AN-1, 3 [34]	MIU-1, 2 and 3
Upper boundary of "Moderately fractured zone" in Felsic granite	AN-1, 3 [34]	MIU-1, 2 and 3
Tsukiyoshi Fault	12 boreholes for uranium exploration TH-1, 2 and 3 Geological map [12]	MIU-2, 3

* : 1:25,000"Toki" and "Mizunami" topographic map published by Geophysical Survey Institute

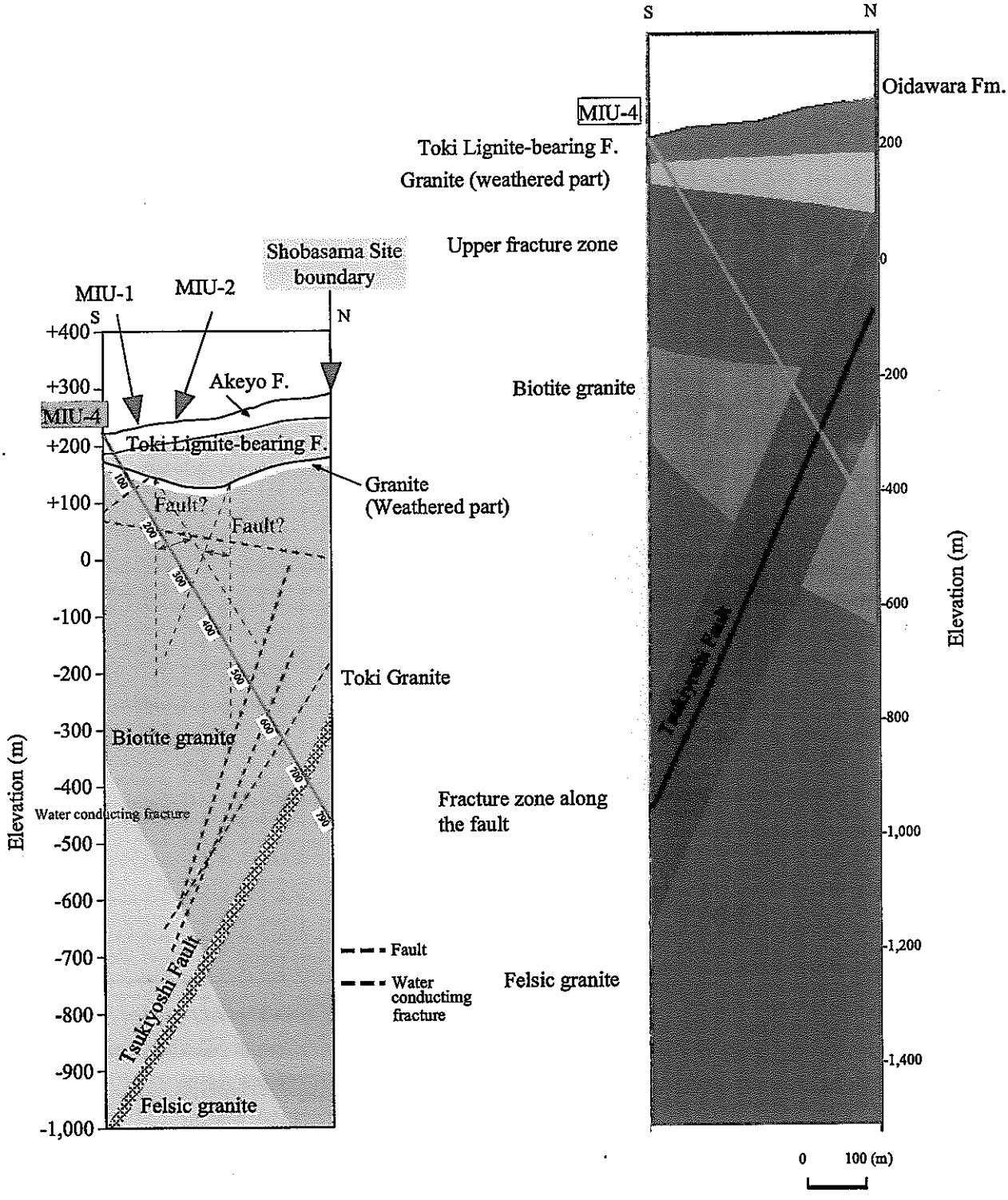

Figure 4.22 Cross section of geological model of the Shobasama Site based on the results of Phase I-a

Figure 4.23 Cross section of geological model of the Shobasama Site (before MIU-4 excavation)

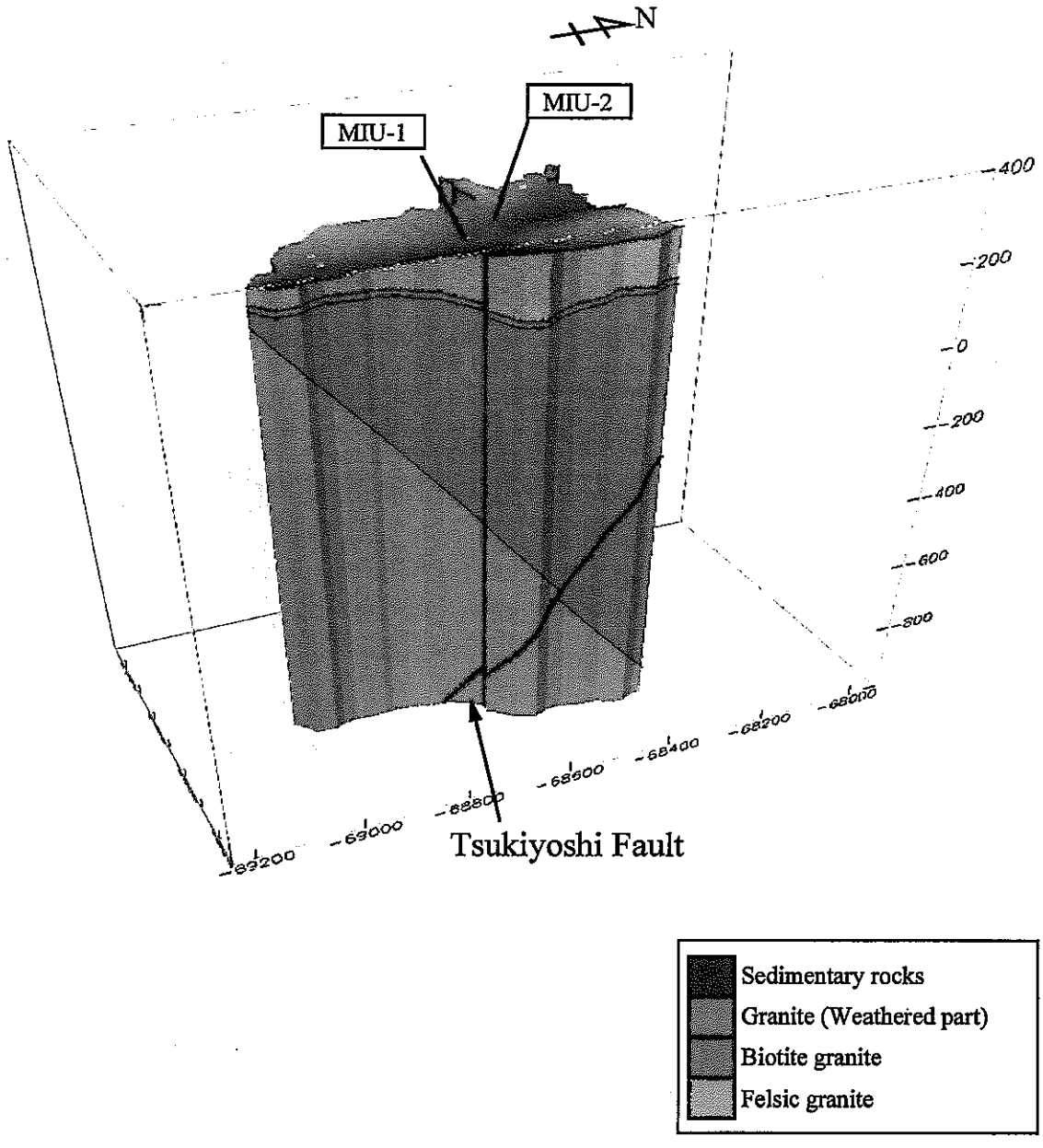

Figure 4.24 Geological model of the Shobasama Site (before MIU-4 excavation)

4.2 Hydrogeological investigations

4.2.1 Overview

4.2.1.1 Objectives

The objectives of the hydrogeological investigations are based on those set for the entire MIU Project and its individual Phases as follows [7].

① Acquisition of the hydrogeological properties of those geological units, features, structures (faults, fractures, etc.) that could be flowpaths for groundwater and determination of the hydraulic heterogeneity of the rock mass due to lithofacies, weathering, alteration, etc.

② Construction of hydrogeological model and testing or assessing its validity

③ Understanding the hydrogeology in the Shobasama Site and prediction of changes to the flow system (drawdown) and of the amount of water inflow into the shafts caused by shaft excavation

④ Development of methodologies for systematic investigations and analyses of hydrogeology

4.2.1.2 Performance and development of the study

It is important to ascertain the following:

- Thorough understanding of the information obtained,
- Understand the uncertainty in data and models,
- Priority of data acquisition for decreasing uncertainty

The study is expected to evaluate and decrease uncertainty by performing an "analysis loop of groundwater hydrology" (Figures 3.1 and 4.25).

4.2.1.3 Development of the conceptual hydrogeological model

In the geological investigations a number of geological models were developed at the regional scale for the about 4 km × about 6 km study area and at the detailed scale for the Shobasama Site (0.8 km × 1.3 km). At both scales the distributions of the geological units were outlined in 3-D space. These conceptual geological models provide the framework for the hydrogeological models investigated.

Hydrogeological models in the rock mass are classified into a continuum model that treats the rock mass as a porous continuous medium and a fracture network model that takes structural discontinuities such as fractures into consideration. In the MIU Project, both porous continuum and fracture network models are to be adopted to examine the applicability of each modeling methodology.

In Phase I-a (1996-1999), the continuum model was adopted for the following reasons:

- Information on the distribution of fractures and their hydrogeological properties were not available in sufficient detail to develop a discrete fracture model
- Time and computation constraints

4.2.1.4 Phase I-a hydrogeological investigations and analyses

During Phase I-a, two analysis loops were implemented. In the 1st analysis loop, only the hydrogeological information obtained from the about 4 km × about 6 km study area and the studies in the Tono Mine were used for construction of the hydrogeological model and performance of the groundwater flow simulation.

In the 2nd analysis loop, the information obtained in Phase I-a of the MIU Project was combined with the data used in the 1st analysis loop to improve the hydrogeological model and groundwater flow simulation. In the 2nd analysis loop, problems identified during the 1st analysis loop were taken into consideration.

4.2.2 Hydrogeological model and groundwater flow simulation (1st analysis loop)

4.2.2.1 Overview

The hydrogeological model used in the 1st analysis loop is constructed from the conceptual geological model for the regional study area, about 4 km × about 6 km encompassing the Shobasama Site.

The purposes of construction of the hydrogeological model and groundwater flow simulations in the 1st analysis loop are as follows:

- Develop an understanding of the general hydrology and hydrogeology in and around the Shobasama Site
- Begin to develop the expertise and methodology needed in future to predict impact on hydrogeology caused by shaft excavations
- Identify problems to be solved in the subsequent investigations and analyses

The study area

The study area (about 4 km×about 6 km, Figure 4.26) encompasses the Shobasama Site. It is surrounded by ridges and streams that are considered to be groundwater flow boundaries. It was selected because it is regional in scale and considered to include a complete regional flow system from recharge to discharge. The results of the RHS Project [46] indicate that mountain ridges generally form hydraulic boundaries. Selecting an area this size is intended to improve the accuracy of groundwater flow simulation.. The depth of this study area is set as GL-3,000 m. This takes the depth of planned shafts for the MIU Project and the scale of the study area into consideration.

Schedule of shaft excavation (developed pre-1998)

For the flow simulation, the planned shaft for the MIU Project is included. The parameters are outlined below.

The planned depth and diameter are 1,000 m and 6 m, respectively. Based on preliminary designs before 1998 FY, it was planned to do the excavation in the following stages (Figure 4.27).

- Excavation from ground surface to 500 m depth
- 6 month investigation stage
- Excavation from 500 m to 900 m depth
- Three-year investigation stage
- Excavation from 900 m to1,000 m depth

The shaft is included in the simulation because it is expected to have the strongest hydraulic impact (sink) on the flow system and on storage in the surrounding rock mass.

Development of the numerical model for the groundwater flow simulation

A finite element method (FEM)-based on the 3-D saturated/unsaturated seepage flow simulation program (TAGSAC) [47] was adopted. TAGSAC was developed for modeling porous media. A steady-state simulation taking the Tono Mine into consideration and a transient simulation for predicting the groundwater hydrology affected by the shaft excavation were carried out.

4.2.2.2 Construction of the hydrogeological model

The 3-D simulation mesh

The about 4 km × about 6 km study area was modeled by generating a 3-D simulation mesh to carry out the FEM-based 3-D saturated/unsaturated seepage flow simulation. The procedures are as follows.

① The surface of the 24 km^2 study area was divided into a grid on a 2-D plane so that the Tsukiyoshi Fault, the boreholes, the planned shafts for the MIU Project and the Tono Mine shafts were represented.. The number of element divisions are 875 (25 EW ×35 NS). Elevations of the individual nodes are calculated from the 20 m-interval digital elevation data to express the topography of the study area (Figure 4.28). The ground surface elevation ranges from 134 to 380 masl.

② The 3-D mesh (FEM model) was prepared by dividing the rock mass from surface to the bottom of the study area into 20 horizontal layers. The bottom of the model was set at -3,000 masl. Also included in the 3-D mesh are the shafts and galleries of the Tono Mine. For the Tsukiyoshi Fault, 1 m-wide platy elements are set stepwise to make the element division easy. The number of nodal points and elements in the 3-D simulation mesh measures 19,656 and 17,500, respectively. The hydrogeological model is shown in Figure 4.29.

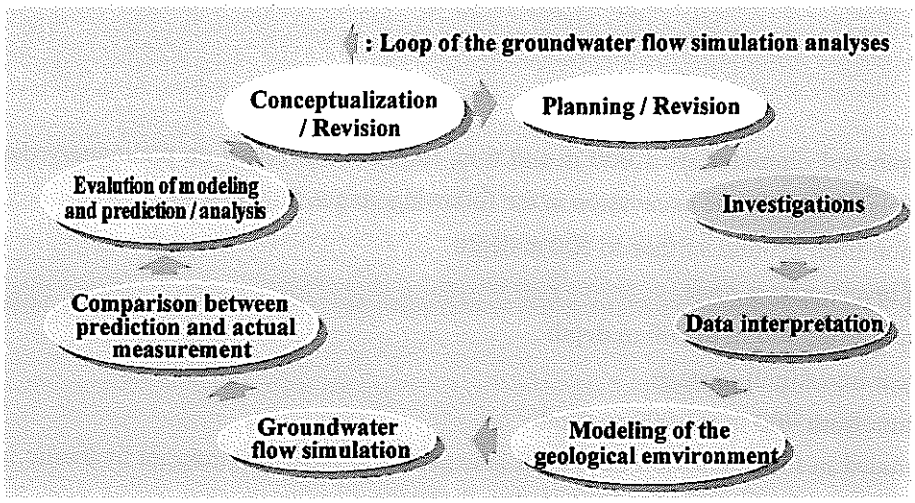

Figure 4.25 Approach to investigations, analysis, modeling and flow simulation

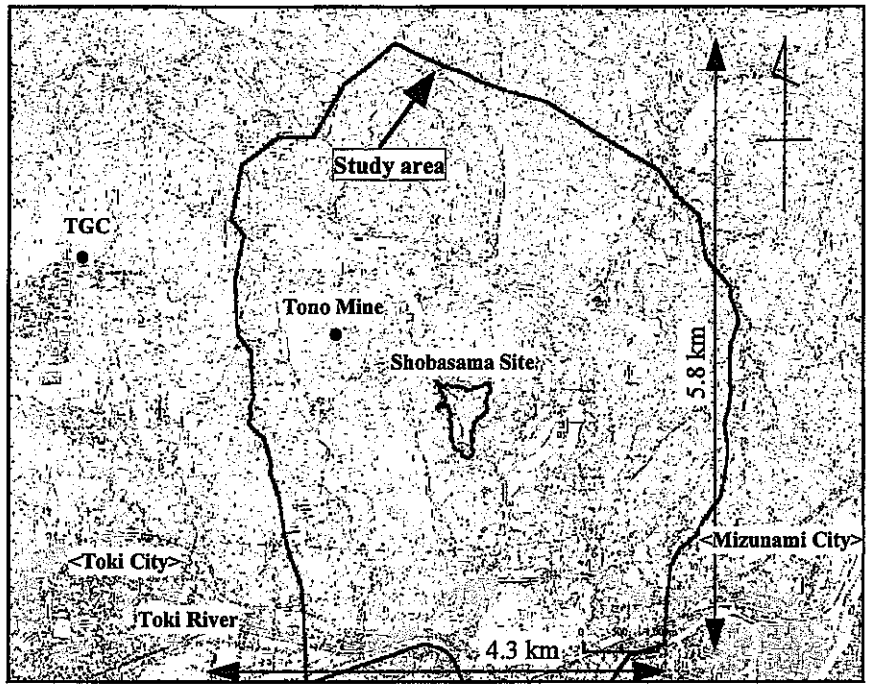

Figure 4.26 Location map of study area and Shobasama Site

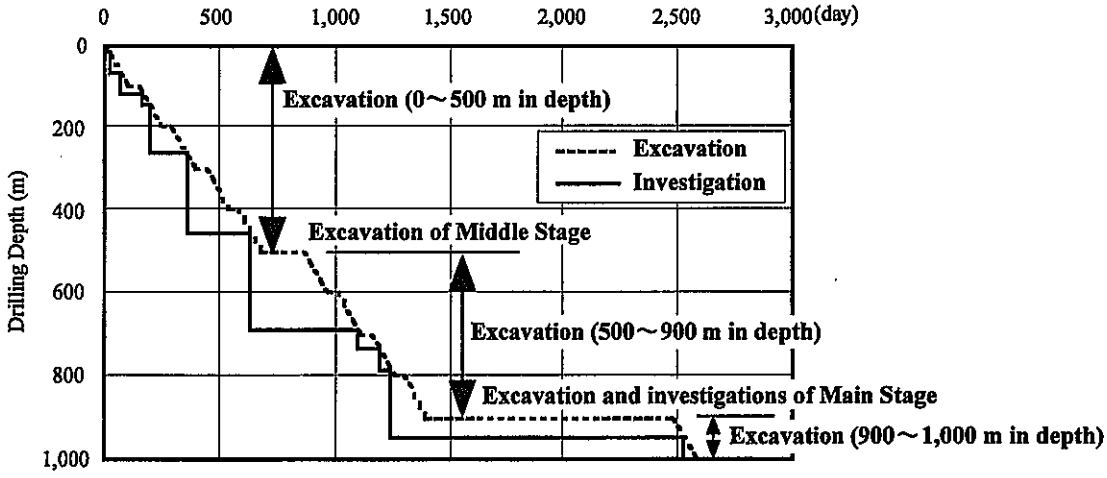

Figure 4.27 Schedule of shaft excavation and investigations as of 1998 FY

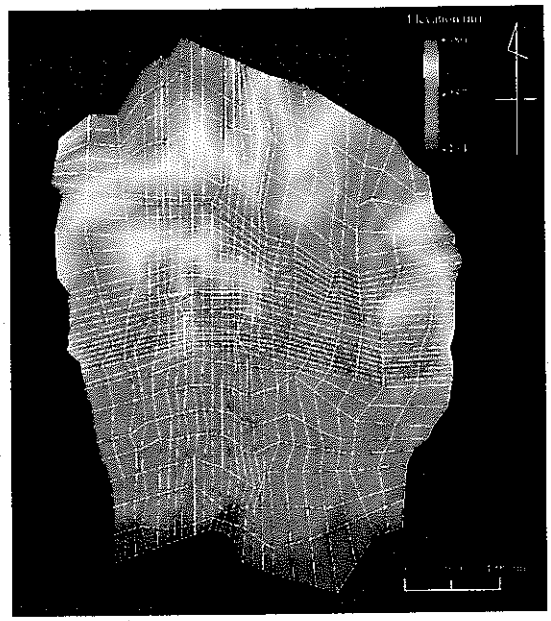

Figure 4.28 Finite element mesh and altitude distribution of model top boundary

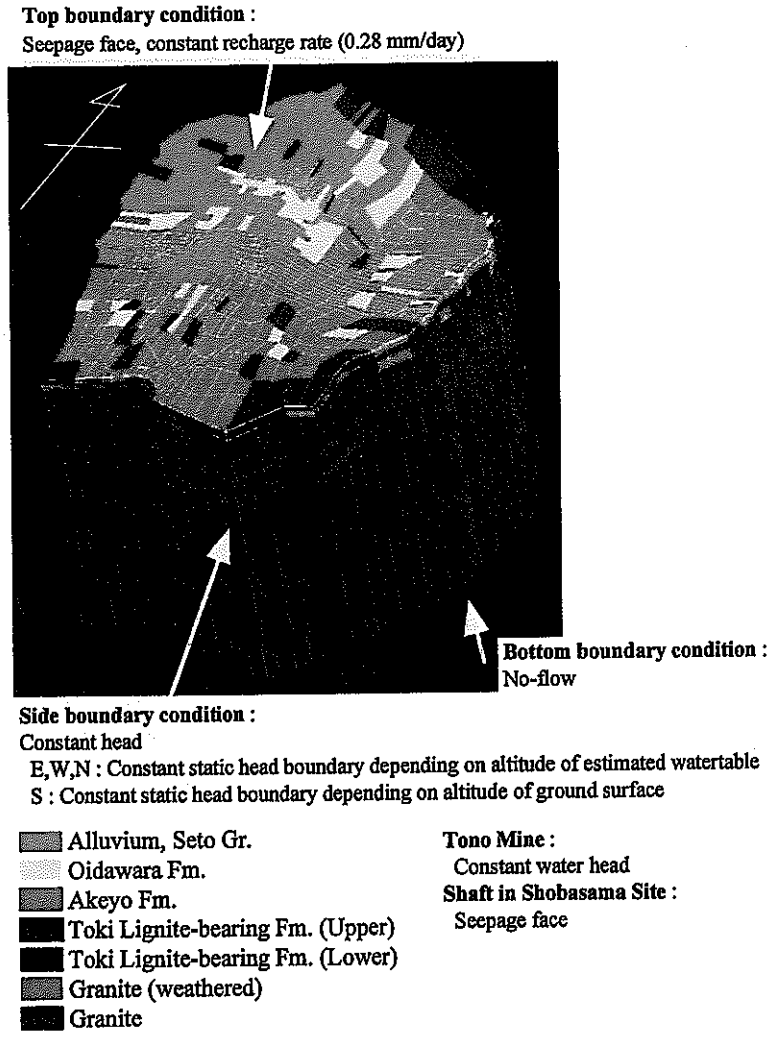

Figure 4.29 Hydrogeological model

Stratigraphy, lithology and hydrogeological properties

The 3-D simulation mesh was fit to the geological model (about 4 km×about 6 km : Section 4.1.4). However, the mesh layers do not always directly corresponds with the thickness of the individual geological units of the geological model. Therefore, any geological units at the center of the mesh are allocated to the 3-D simulation mesh. The hydraulic conductivity values in Table 4.13 are established for each geological unit on the assumption that each geological formation is hydrogeologically homogeneous and behaves as a continuum. These values are based on data from the RHZ and the results [48] of groundwater flow simulations in and around the Tono Mine. Permeability in unsaturated domains was set based on the moisture characteristic curve and relative hydraulic conductivity curve shown in Figure 4.30 [49~51].

Table 4.13 Hydraulic conductivities of the geological units

Geology	Hydraulic conductivity (m/s)
Seto Group	1.0×10^{-7}
Oidawara Fm.	1.0×10^{-9}
Akeyo Fm.	1.0×10^{-9}
Toki Lignite-bearing Fm. (Upper)	5.0×10^{-9}
Toki Lignite-bearing Fm. (Lower)	1.0×10^{-8}
Toki granite (Weathered)	1.0×10^{-7}
"Moderately fractured zone"	1.0×10^{-9}
Tsukiyoshi Fault	1.0×10^{-10}

Establishing boundary conditions

Top boundary condition

The top boundary was based on digitization of the topographic map of the Tono area. Recharge at the top boundary takes precipitation, evaporation and run-off into consideration. The recharge rate of 0.28mm/day, [52] an average rate calculated from observations between 1990 and 1997 in the vicinity of the Tono Mine, was adopted on the assumption that the recharge rate in the larger study area is the same. The ground surface is set as a free seepage face.

Bottom boundary condition

The bottom boundary, at –3,000 masl was set as a no-flow boundary.

Side boundary conditions

The side, groundwater flow boundaries coincide with mountain ridges (the northern, eastern and western boundaries) and the Toki River (the southern boundary). The ridges could be considered as watershed divides; however, some studies point out that these ridges are not always coincident with watershed boundaries because of local geological structures. In addition, the results [53] of groundwater flow simulations for the larger RHS, encompassing the study area, indicates southwestward groundwater flow controlled by regional topography. Accordingly, side boundaries along the ridges are set as permeable, and constant head. The constant heads assigned to the boundaries are determined by the following equation, which formulates the relationship between surface elevations and the water levels observed in boreholes around the study area (Figure 4.31).

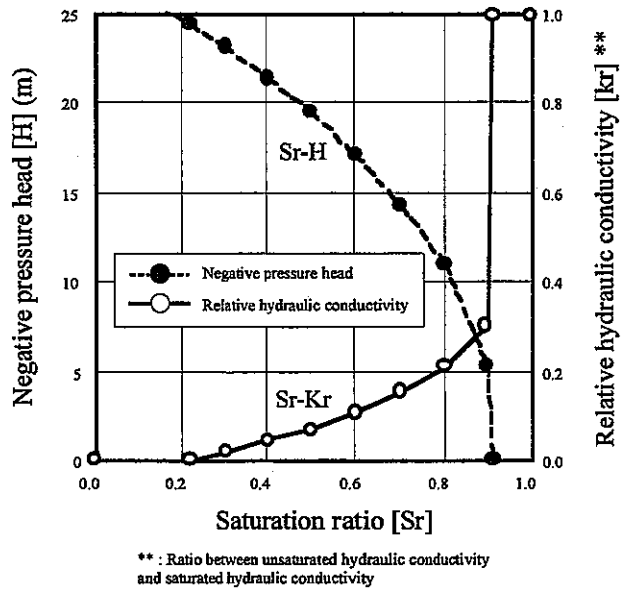

Figure 4.30 Moisture characteristic curve and relative hydraulic conductivity curve

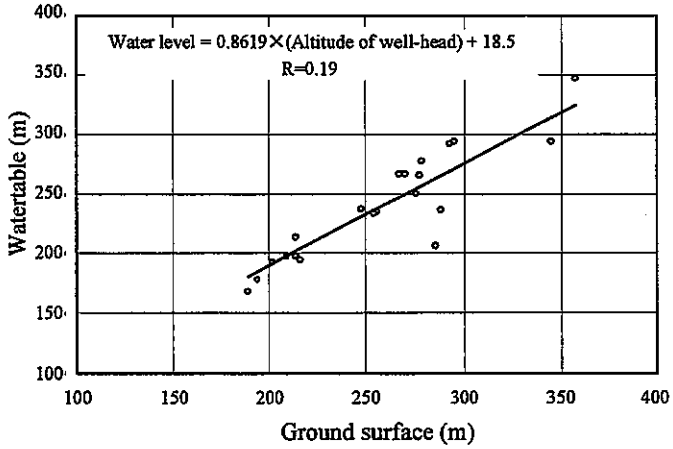

n=21

AN-1	DH-1 [54]	KA-3
AN-3	DH-2 [55]	SN-1
AN-4	DH-3 [56]	SN-2
AN-5	DH-4	SN-3
AN-6	HN-1	SN-4
AN-7	KA-1	SN-5
AN-8	KA-2	SN-6

(Data obtained from these boreholes)

Figure 4.31 Relationship between elevation of ground surface and watertable

Φ (Constant head (masl)) = 0.86×H (elevation of each location in masl) + 18.5

The boundary along the Toki River is also set as permeable, and constant static head. Surface elevation is used as the constant head assigned to the boundary.

Tono Mine and planned shaft for the MIU Project

The galleries in the Tono Mine are assigned a pressure head of 0 m, because the galleries are at atmospheric pressure.

As for the planned shaft in the MIU Project, the geological units are removed from the hydrogeological model one by one in response to the progress of shaft excavation. Nodal points representing the shaft wall are set as free seepage points on the assumption that all the groundwater seeping into the shaft will be pumped to surface.

4.2.2.3 Groundwater flow simulation

Steady-state simulation (simulation of undisturbed groundwater conditions)

Prior to a transient simulation (simulation of the disturbance due to shaft excavation), a steady simulation was carried out. The simulation was intended to develop an understanding of the groundwater hydrogeology but takes the existence of the Tono Mine in the study area into consideration. The validity of the simulation is tested by comparing the simulated results with the head distributions in boreholes in the study area.

Comparison of simulated results with head distribution data

Figure 4.32 shows the comparisons between distributions of the measured hydraulic heads and the simulated results.

The simulation model described above employs coarser meshes than the model used for the groundwater flow simulation carried out around the Tono Mine [48] and gives insufficient consideration to the position of the Tsukiyoshi Fault. Nonetheless, the distributions of groundwater pressure measured in AN-1, 6, 7 and 8, drilled largely in sedimentary rocks around the Tono Mine, are closely matched by the model's simulation of drop in head due to the existence of the Mine. Also, the general trend of head distributions is reproduced well (Figure 4.32 (a), (b), (c) and (d)).

Simulated values for DH-9, drilled largely in granite, (Figure 4.32 (e)) are also coincident with the measured values of trend of head. However, the simulated values are higher than the measured values. This discrepancy of about 30 m is thought to be caused by inaccuracies in the hydrogeological model, as follows:

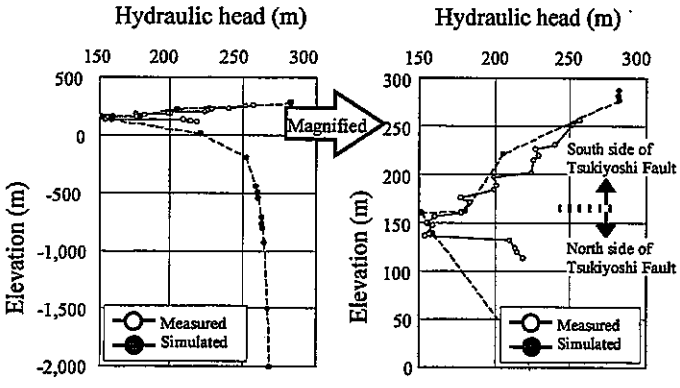

(a) TH-1

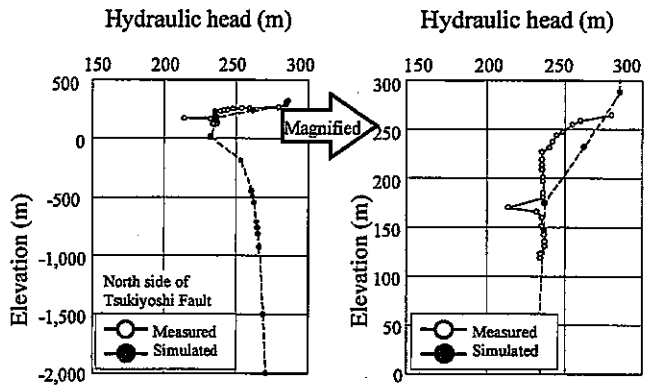

(b) TH-6

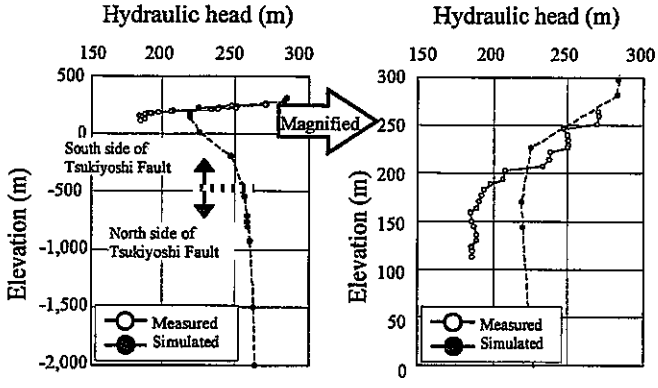

(c) TH-7

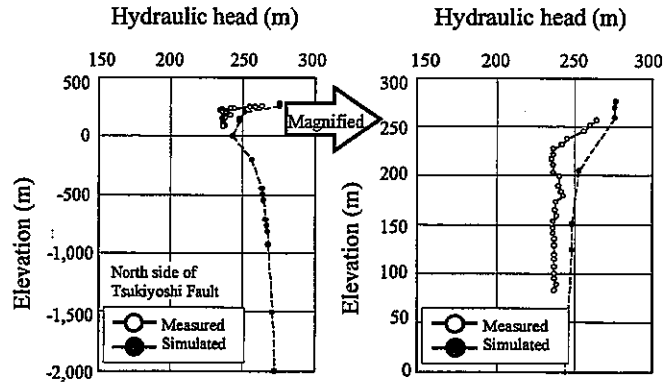

(d) TH-8

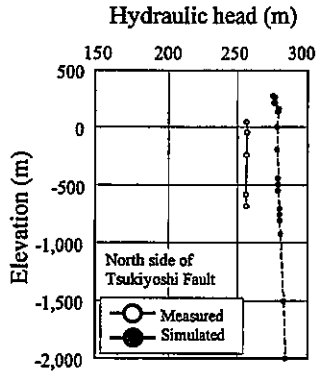

(e) DH-9

Figure 4.32 Head distribution (comparison between measured data and simulated data)

- Permeability contrast generated by the Tsukiyoshi Fault
- Top boundary condition; i.e., recharge rate
- Position/shape of the Tsukiyoshi Fault

Groundwater hydrogeology in the undisturbed state

This steady-state simulation shows the following results on the distribution of heads and Darcy velocity vectors (Figure 4.33). Figure 4.34 shows the cross sections of the simulated results.

① Heads in the study area generally decrease from north to south (Figure 4.33 (1, 2 and 3)) indicating that the groundwater flows generally from north to south as a whole.

② The flow of groundwater above an elevation of 0 masl ("shallower part") is more affected by the topography of the ground surface than is the flow below an elevation of –758masl ("deeper part"). As a result, local variations in head and Darcy velocity vector distributions are generated (a, c in Figure 4.33 (1); d in Figure 4.33 (3); e in Figure 4.33 (4)). The shallower part, being more permeable and sensitive to the top boundary condition than the deeper part, gives rise to larger values of Darcy velocity vectors (Figures 4.33 (3) and (4)). The distribution of Darcy velocity vectors is locally disturbed around the Tono Mine (b in Figure 4.33 (1)).

③ The head distributions in the deeper part gently varies. The Darcy velocity vectors are nearly horizontal from north to south (Figure 4.33 (3)) suggesting that the deeper part is hardly affected by the topography of the ground surface and the local flow systems developed.

④ The groundwater flow simulation based on the current hydrogeological model indicates that the Tsukiyoshi Fault exerts only a small influence on the distribution of heads and Darcy velocity vectors (Figure 4.33 (1), (2), (3) and (4)).

Transient simulation (predictive simulation of disturbance to groundwater flow due to MIU shaft excavation)

The transient simulation was carried out on the assumption that MIU shaft would be excavated on the schedule as shown in Figure 4.27.

Simulation results: effect on heads and Darcy velocities

The results of predictive simulation of groundwater hydrogeology caused by shaft excavation are summarized below and shown in Figure 4.35. The cross sections shown in Figure 4.35 are along the same planes as those in Figure 4.34.

① Heads are lowered around the shaft. The groundwater around the shaft not only flows but also changes the potential or gradient toward the shaft with the result that Darcy velocities toward the shaft increase.

② The groundwater flows upward, into the shaft at depths greater than 1,000 m in the region of the shaft, (Figure 4.35 (2), (3)).

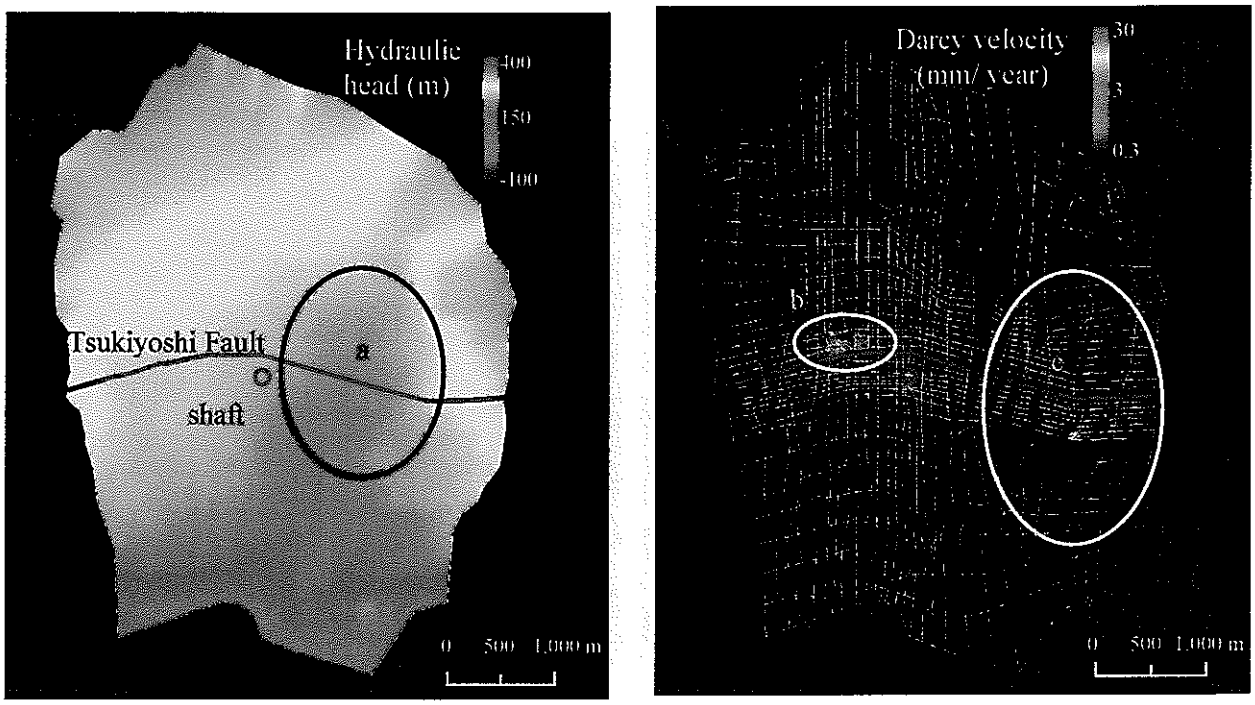

(1) Head and Darcy velocity vector in the horizontal plane at the altitude of 0 m

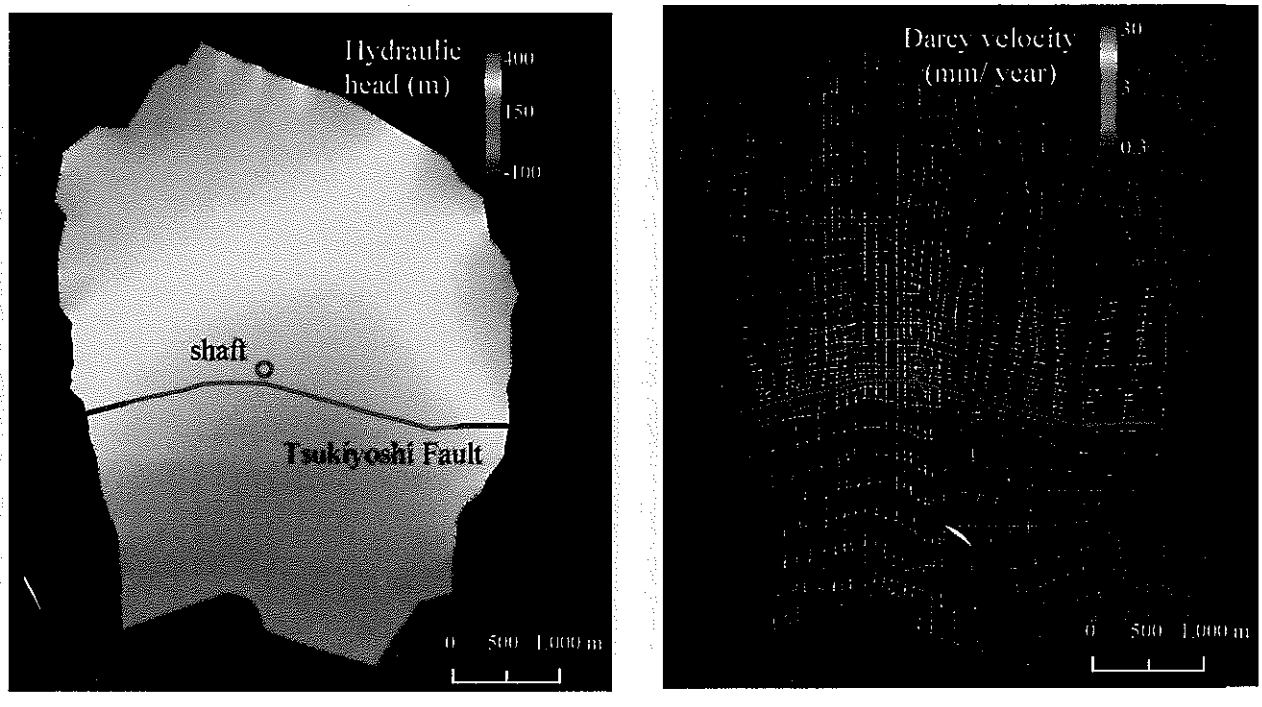

(2) Head and Darcy velocity vector in the horizontal plane at the altitude of -758 m

Figure 4.33 The result of groundwater flow simulation (Steady state) (1/2)

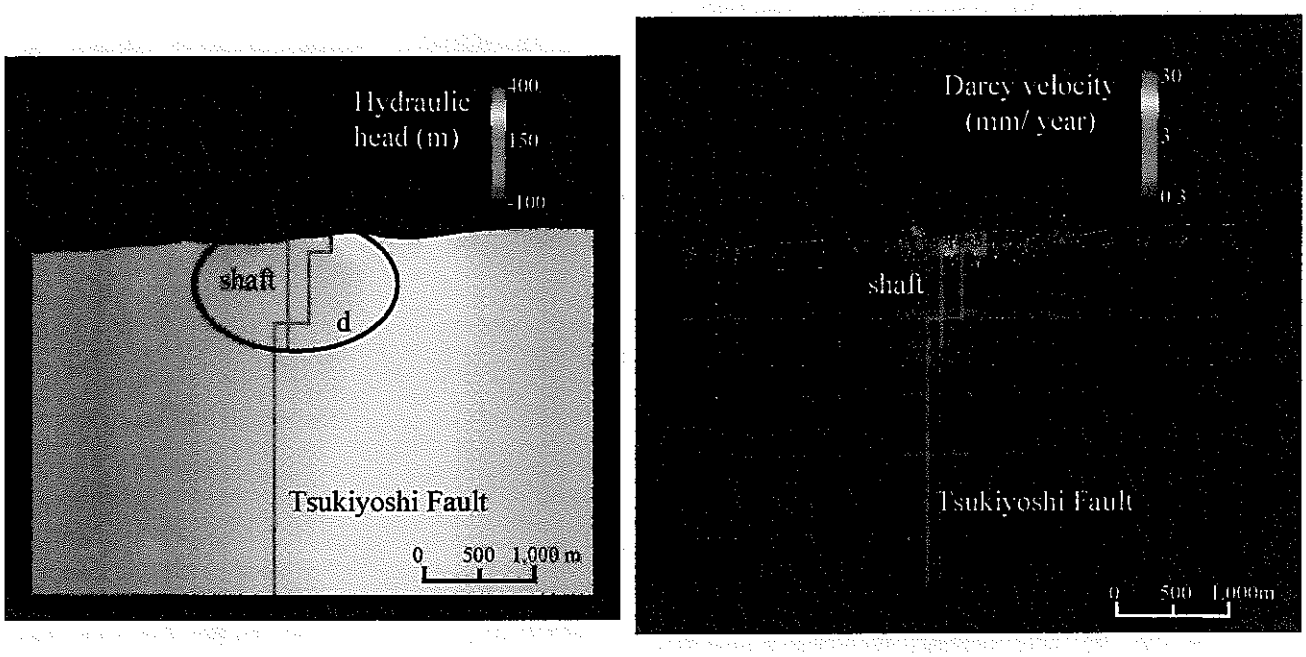

(3) Head and Darcy velocity vector in N-S section passing through the shaft

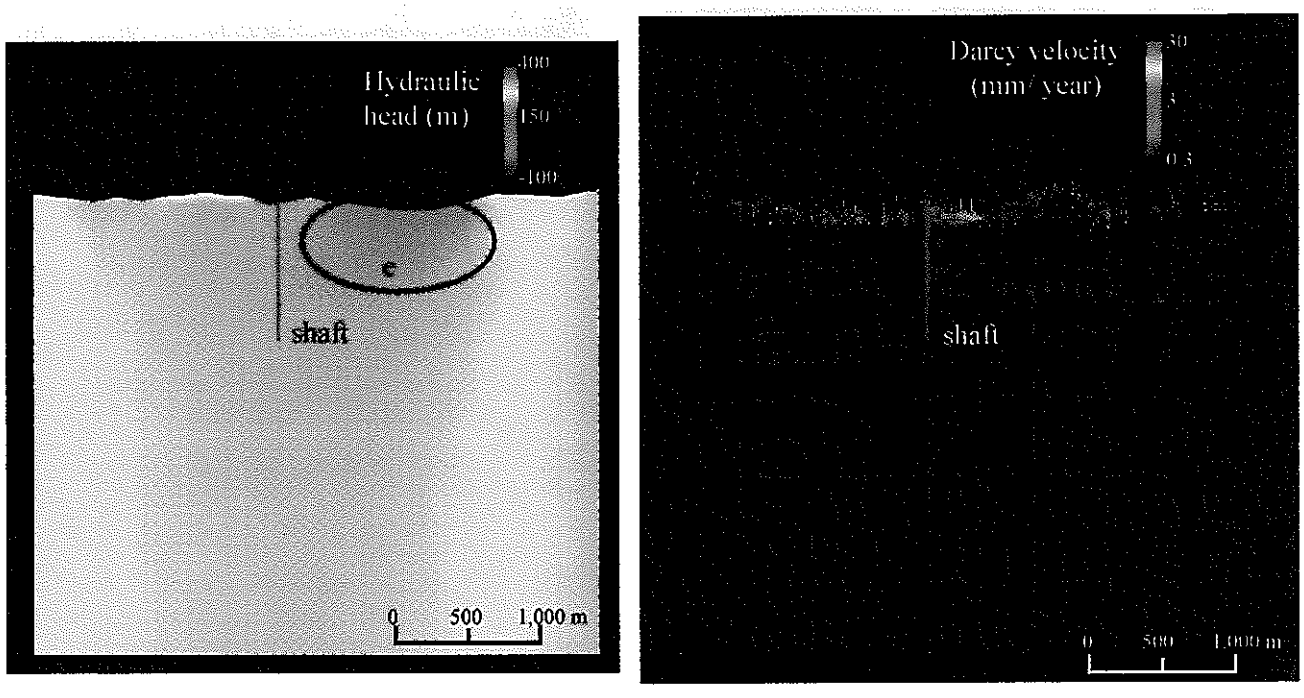

(4) Head and Darcy velocity vector in E-W section passing through the shaft

Figure 4.33 The result of groundwater flow simulation (Steady state) (2/2)

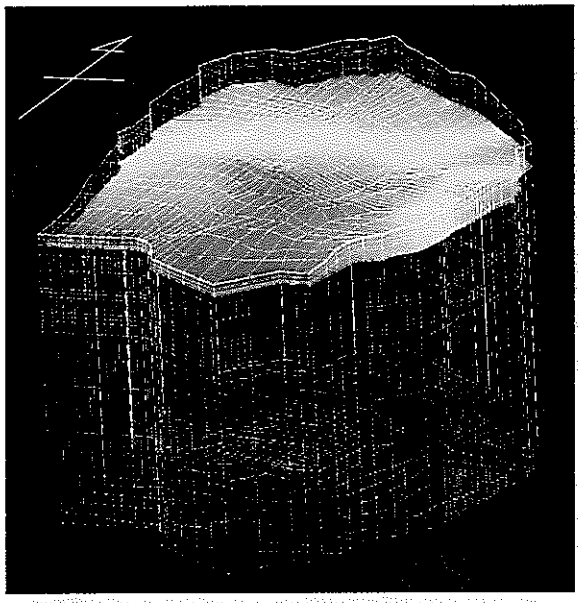

(a) Section 1 : Horizontal plane at the altitude of 0 masl

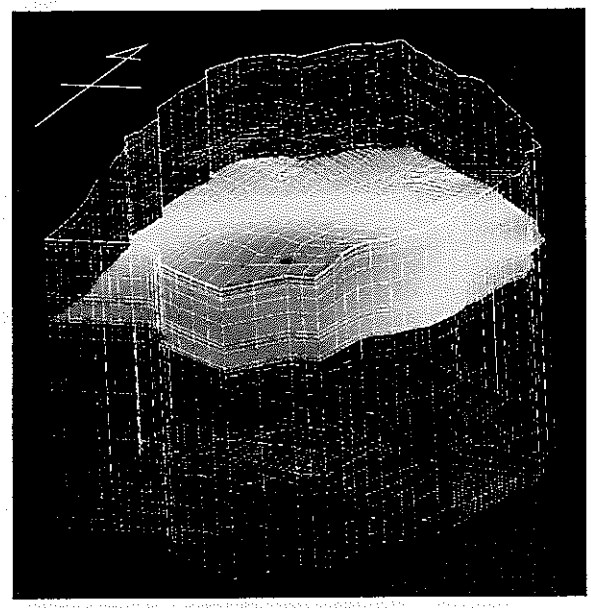

(b) Section 2 : Horizontal plane at the altitude of -758 masl

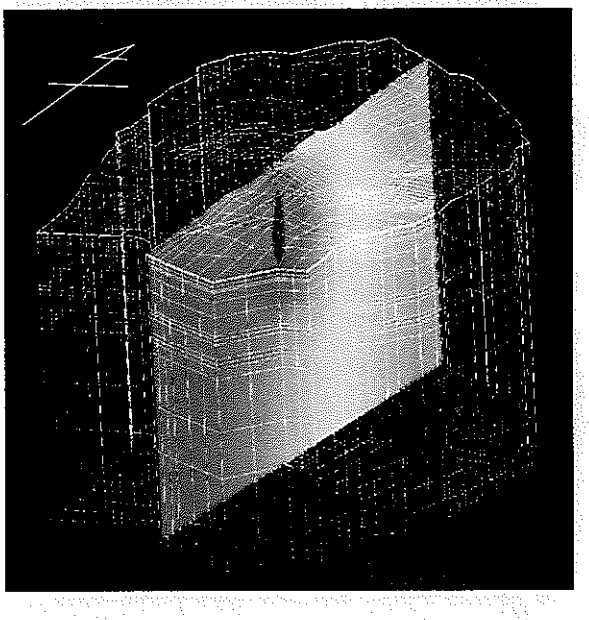

(c) Section 3 : N-S Section passing through the shaft

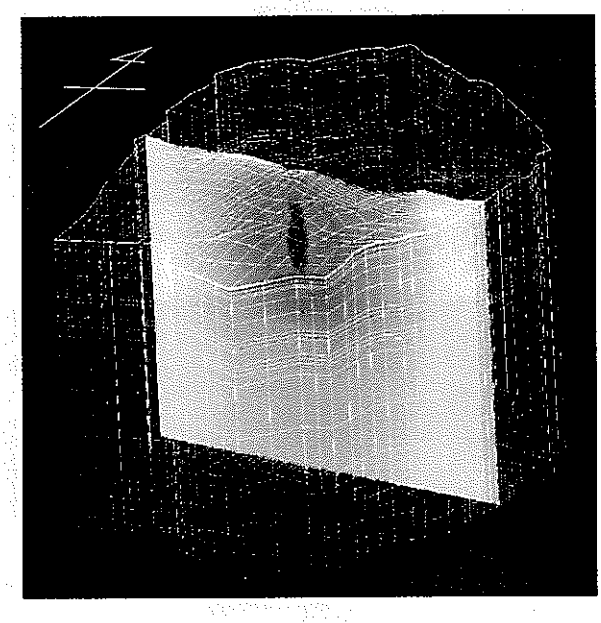

(d) Section 4 : E-W section passing through the shaft

Figure 4.34 The result of groundwater flow simulation (cross section)

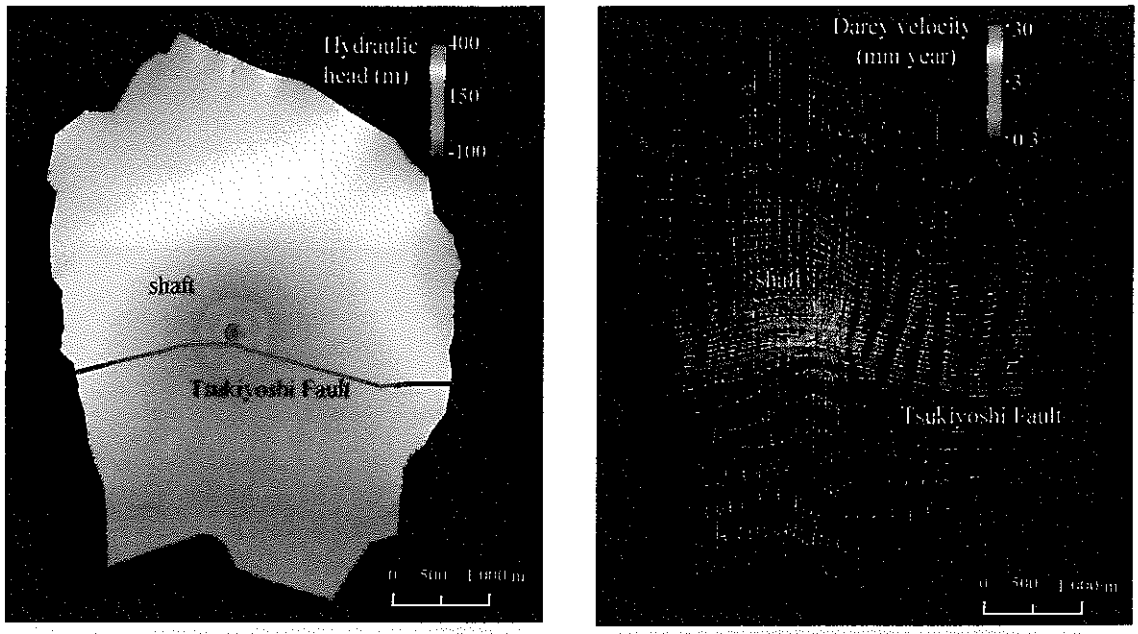

(1) Hydraulic head and Darcy velocity vector at the altitude of -758 m

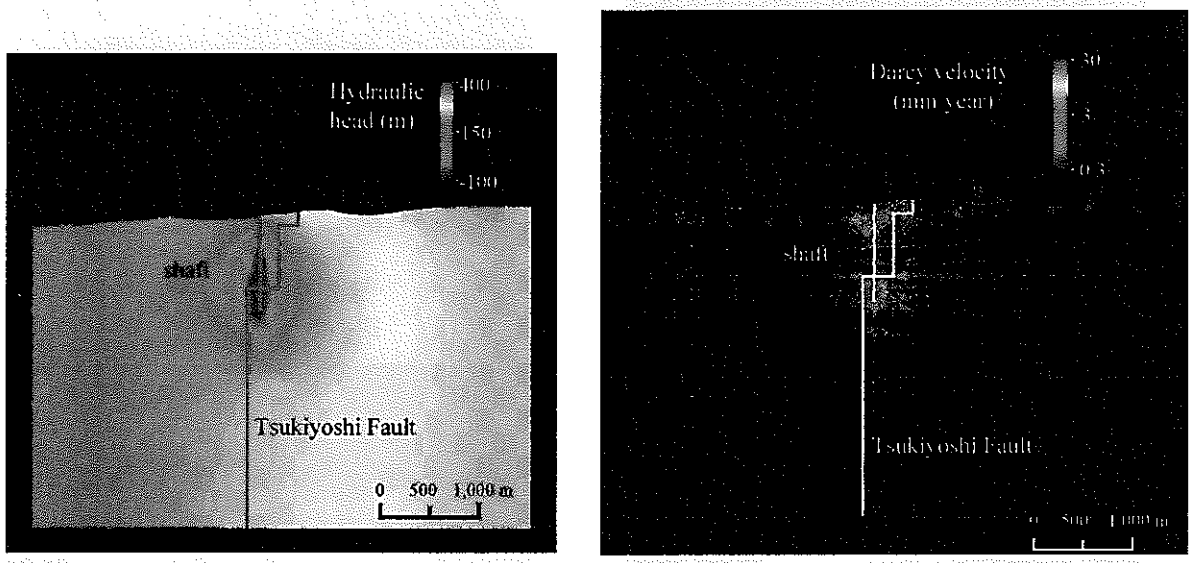

(2) Hydraulic and Darcy velocity vector in N-S section passing through the shaft

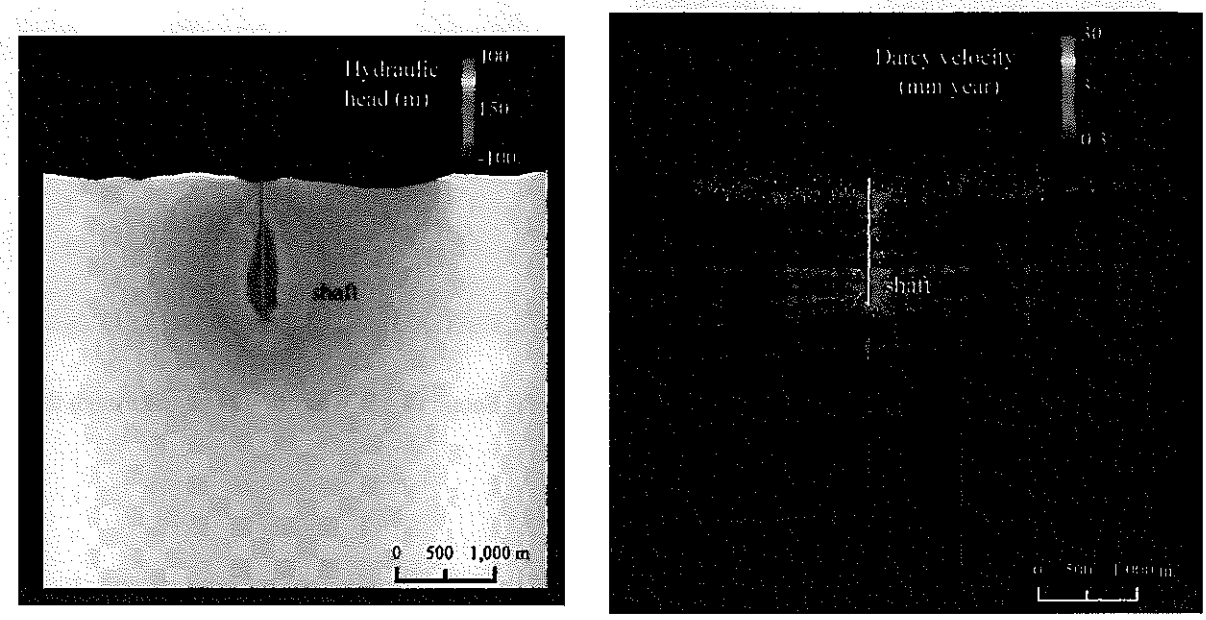

(3) Hydraulic and Darcy velocity vector in E-W section passing through the shaft

Figure 4.35 The results of the predictive simulation

Simulation results: effect on groundwater hydrogeology

Changes in groundwater hydrogeology caused by MIU shaft excavation are as follows (Figure 4.36). The cross sections in Figure 4.36 are along the same planes as in Figure 4.34.

① The drawdown on the horizontal plane at surface shows a nearly concentric pattern of drop in head with the shaft as the center. This indicates that the Tsukiyoshi Fault exerts negligible influence on the groundwater flow in the simulation with the properties currently included in the hydrogeological model.

② The distribution of drawdown in vertical N-S and E-W sections that include the shaft shows an onion-shaped pattern (Figure 4.36 (1), (2)). This suggests that properties assigned to the upper geological units are such that the heads near the surface are prevented from falling.

③ Drawdown effects due to shaft excavation are within the boundaries of the about 4 km× about 6 km study area (Figure 4.36).

4.2.2.4 Evaluation of boundary conditions

Evaluation of the results of the 1st analysis loop has identified the following problems to be solved during the 2nd analysis loop.

① For the steady-state-simulation, the results approximately reproduce the existing groundwater hydrogeology. It suggests that the boundaries as defined are appropriate. However, simulated values are generally a little larger than measured values. This can be caused by the method of establishing the relationship between groundwater level and elevation, on which the hydrostatic pressure assigned to the side boundaries are based (Figure 4.29). Ii is also possible that overestimation of the recharge rate is the cause. Thus, these should be considered in the 2nd analysis loop.

② The transient simulation results show a small drawdown in shallow part of the model, despite the shaft excavation as shown in Figure 4.36. It suggests that perhaps the recharge rate exerts a greater effect on groundwater hydrology in the shallow part than considered previously. Therefore, it may be necessary to assign recharge rates according to the properties of individual areas and the underlying geological formations instead of giving an averaged value to the study area.

③ Effects of the shaft excavation do not extend to the bottom boundary of the study area. This suggests that it is appropriate to define the bottom boundary to be a no-flow boundary at the depth used in this simulation.

4.2.2.5 Summary

Simulation results are as follows.

① The groundwater flows from north to south.

② Drawdowns caused by the shaft excavation are within the boundaries of the about 4 km× about 6 km model area. It suggests that the size of the study area is appropriate for understanding the extent of area affected by the shaft excavation.

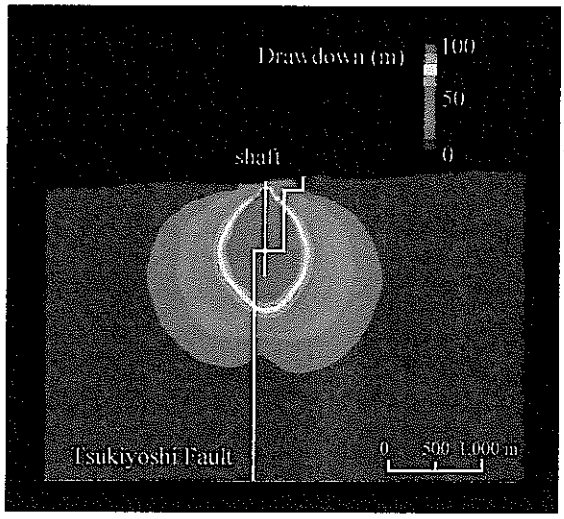

(1) Drawdown in N-S section passing through the shaft

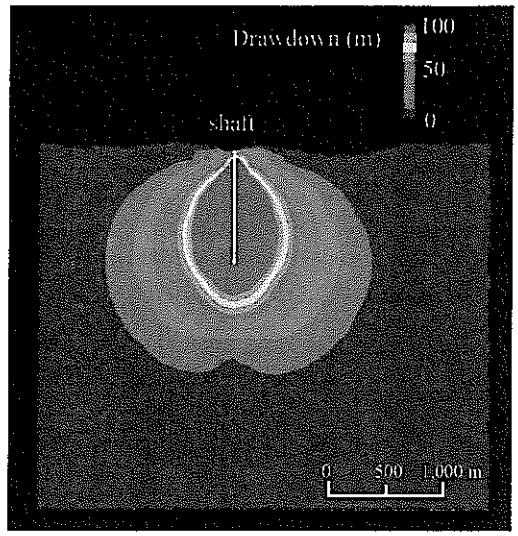

(2) Drawdown in E-W section passing through the shaft

Figure 4.36 Distribution of drawdown immediately after the completion of shaft excavation

③ In the groundwater flow simulation using the hydrogeological model, the horizontal distribution of the drawdown shows a concentric pattern with the shaft as its center. It does not indicate that the Tsukiyoshi Fault forms an impervious zone.

④ The simulation results shows the size of the study area and setting of the boundary conditions used for this simulation could be used for 2nd analysis loop.

4.2.2.6 Future tasks

While the steady-state and transient flow simulations allow understanding the overall groundwater hydrogeology in the study area, none of the investigation results obtained in the area were used for these simulations. The following are extracted as tasks to be dealt with in the future.

① Examine the method of establishing the geological units for the geological model; especially taking the heterogeneity of granite into consideration

② Consider the variety, quantity and quality of information (the data requirements) needed for modeling and groundwater flow simulation

③ Understanding the hydrogeological properties of individual geological units and predict the 3-D distribution of hydraulic conductivity

④ Methodology for construction of the hydrogeological model
Consider the method for estimating 3-D distribution of hydraulic conductivity

⑤ Methodology of groundwater flow simulation
Consider the methods for saturated/unsaturated simulations and the applicability of finite element and finite difference methods.

⑥ Method of setting hydraulic boundary conditions
Consider the method and basis for the top and side boundary conditions, considering the available data

⑦ Assessment of the uncertainty inherent in data obtained, in models and in the groundwater flow simulation
Consider which factors could contribute to reduction of the uncertainty, and, if possible, the prioritization of data acquisition.

4.2.3 Hydrogeological model and groundwater flow simulation (2nd analysis loop)

4.2.3.1 Overview

The groundwater flow simulations carried out for the 2nd analysis loop are based on enhancements to the geological models with data and knowledge from additional hydrological data, borehole investigations in three 1,000 m-deep boreholes (MIU-1, 2 and 3), reflection seismic surveys, and other data to be described below. The borehole investigations consisted of the following:

- Core descriptions and BTV investigations to acquire detailed information on location, orientation and style of fracture zones that are considered to be potential water conducting features (WCF) in the granite

- Hydraulic tests in 100 m-sections (long test intervals) to develop a comprehensive, albeit averaged, database on hydraulic properties from near surface to depth
- Hydraulic tests in sections several metres long (short-test intervals) to establish their hydraulic properties. The specific sections may be potential WCFs, fluid loss zones or major structures.

Based on the results of the above investigations, the geological model for the MIU Project was developed in more detail, with a definition of additional units in the granite (See Section 4.1.4) and their hydrogeological properties were determined for modeling purposes. As a result, the following are made clear.

① The "Upper fracture zone" and "Fracture zone along the fault" have high permeability, whereas the "Moderately fractured zone" has low permeability;

② The piezometric water level in the footwall of the Tsukiyoshi Fault is 20 m higher than that in the hanging wall, suggesting that the fault may be a barrier to flow, which would be a confirmation of earlier work that reached the same conclusion.

Based on the above results, groundwater flow simulations in the 2nd analysis loop for the study area (about 4 km× about 6 km) was carried out with the purpose of understanding changes in hydrogeological properties caused by planned MIU shaft excavation, reassessing the effects of the Tsukiyoshi fault, and examining whether it is necessary to take permeable fractures into consideration.

In the 2nd analysis loop, the following six subjects were to be examined in the development of the hydrogeological model and for the groundwater flow simulation.

① Method of determining the geological units in the geological model

② Data requirements needed for development of the geological and hydrogeological models and the groundwater flow simulation

③ Methodology for construction of the hydrogeological model

④ Groundwater flow simulation methodology

⑤ Method of determining hydraulic boundary conditions

⑥ Assessment of the uncertainty in data, models and the results of groundwater flow simulation

4.2.3.2 Hydrogeological investigations

Hydrogeological investigations are divided into surface hydrological investigations and groundwater hydrogeological survey. The former studies the water budget and infiltration mechanism of the surface water, whereas the latter studies the distribution of hydraulic conductivities and pore pressures in the deep rock mass, flow paths of groundwater and their continuity.

4.2.3.2.1 Surface hydrological investigations

Water balance observations have been carried out in the Shobasama Site to establish the top boundary conditions required for groundwater flow simulation. To evaluate the water balance around the Shobasama Site, results of the meteorological and groundwater observations carried out in the RHS Project can be used.

Results of the subsurface hydrological investigations carried out in both the RHS Project and this project are as follows.

(1) Water budget

The map of the drainage basins identified for water budget determination carried out in the MIU Project and the RHS Project are shown in Figure 4.37. Table 4.14 provides details on watershed characteristics. The drainage basins were established taking their topography, geology, relative location and scale into consideration [57]. Observation devices installed for the RHS Project in the drainage basin of the Shoba River can be used for the water balance calculations for the MIU Project.

Table 4.14 Details of hydrological monitoring network used for the MIU Project

River			Drainage basin		Fluvio Meter	Lithology	Catchment area (ha)	Elevation (m)	Observation period
Toki River	Hiyoshi River	Shoba River	Shoba River	Shoba River	SPD	Toki Gravel, Sedimentary rocks	53.5	(224)	1989.4.21-
				Upper stream	SPU		15.5	(253)	1989.4.21-
				Itadoribora River	IPU		1.2	(267)	1993.3.6-
			Shoba River model*		SPM		1.5	262	1998.12.24-
		Garaishi River	Garaishi River	Garaishi River	GPD	Toki Gravel	23.3	(296)	1999.3.20-
				Minor	GPU	Granite	1.0	(342)	1999.5.26-
	Shizuhora River		Tono Mine		TPU	Toki Gravel, Sedimentary rocks	6.2	(257)	1990.9.18-2000.2.17

* carried out in the MIU Project (all others were carried out in the RHS Project)

Infiltration rates of the rock mass are converted to estimated yearly ranges based on the observation results in the individual drainage basins obtained for the past ten years. These are 0.3 to 1.0 mm/day (0.6 mm/day on average) in the Shoba River drainage basin and 0.1 to 1.8 mm/day (1.0 mm/day on average), in the upper streams of the Shoba River drainage basin. It indicates that there are spatial and temporal variations within individual basins. The infiltration rate in the Garaishi River basin, which is underlain by granite and located to the north of the Shobasama Site, was determined to be 0.2 mm/day according to observations in 1999 FY. It is necessary to establish a methodology for determining the infiltration rates of each basin by examining the correlation of infiltration rates into the rock mass with topography, geology and land utilization.

(2) Groundwater monitoring

Groundwater monitoring is intended to provide data on the fluctuations of water level in unconsolidated layers (Seto Group) and sedimentary rocks (Mizunami Group) with which to directly estimate recharge rates. Locations of groundwater observatories for the MIU Project and the RHS Project are shown in Figure 4.38. Open-air-type water level gauges are used for measuring water level in open boreholes, while soil moisture meters are used in soil and the upper part of the Seto Group.

Groundwater observations of the MIU Project were carried out in the six boreholes shown in Table 4.15 [58, 59]. In this study area, there are also the TH-series-boreholes, the SN-series-boreholes and the AN-6 borehole around Tono Mine, in which continuous observations on water level and water pressure are under way with either open-air-type water gauges or multiple piezometer systems (MP system) [60].

Table 4.15 Details of water level monitoring for the MIU Project

Borehole	Target geology	Location and sensitivity to rainfall
AI-4	Weathered part of granite ~ Lowest part of Toki Lignite-bearing Fm.	· The vicinity of planned shaft in the Shobasama Site · Hardly sensitive to rainfall
97MS-01	Upper part of Akeyo Fm.	· Ridge on the Shoba River drainage basin · Sensitive only to heavy rain
97MS-02	Lower part of Seto Group	· Ridge on the Shoba River drainage basin · Sensitive to rainfall
98MS-03	Middle part of Akeyo Fm.	· Ridge on the Shoba River drainage basin · Not sensitive to rainfall
98MS-04	Lower part of Seto Group	· Slope in the Shoba River drainage basin · Sensitive to rainfall
99MS-05	Lower part of Akeyo Fm.	· Slope in the Shobasama Site, southward from planned shaft · Sensitive to rainfall, if not less sensitive than Seto Group

Soil moisture observations are carried out at two locations [59] in the Shoba River basin (Table 4.16) with the purpose of estimating the water movement through the unsaturated zone layers into the saturated zone. From these observations, local recharge rates can be estimated. Outside the study area, groundwater observations are under way at 12 stations in the Itadori-bora and Tono Mine drainage basins.

Table 4.16 Details of soil moisture monitoring in the MIU Project

Tensiometer	Target geology	Location and sensitivity to rainfall
SmTP	Soil~ Upper part of Seto Group	· Located on ridge · Became saturated 7 months after installation, but inconsistent with groundwater level (>3 m).Since then, become sensitive even to light (4 mm) rainfall (<2) · No response except for heavy rain (>3m)
SmTS	Soil~ Upper part of Seto Group	· Located in slope · Become saturated 3months after installation (>5m). · Sensitive to rainfall (<1.5 m), whereas no response except for heavy rain (>2 m)

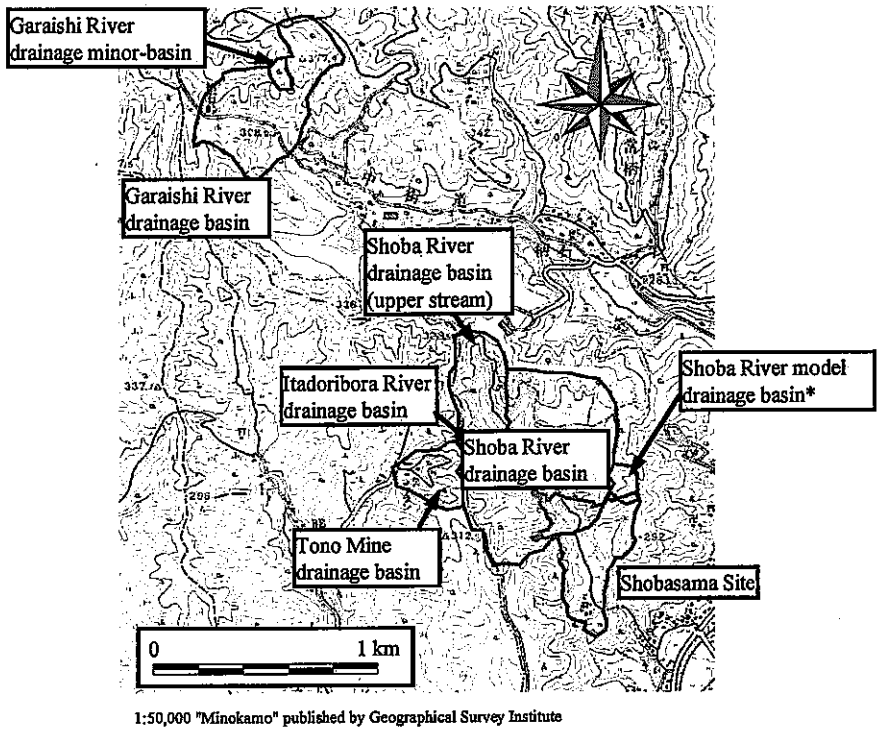

Figure 4.37 Drainage basins for the water budget determination in the MIU Project* and the RHS Project

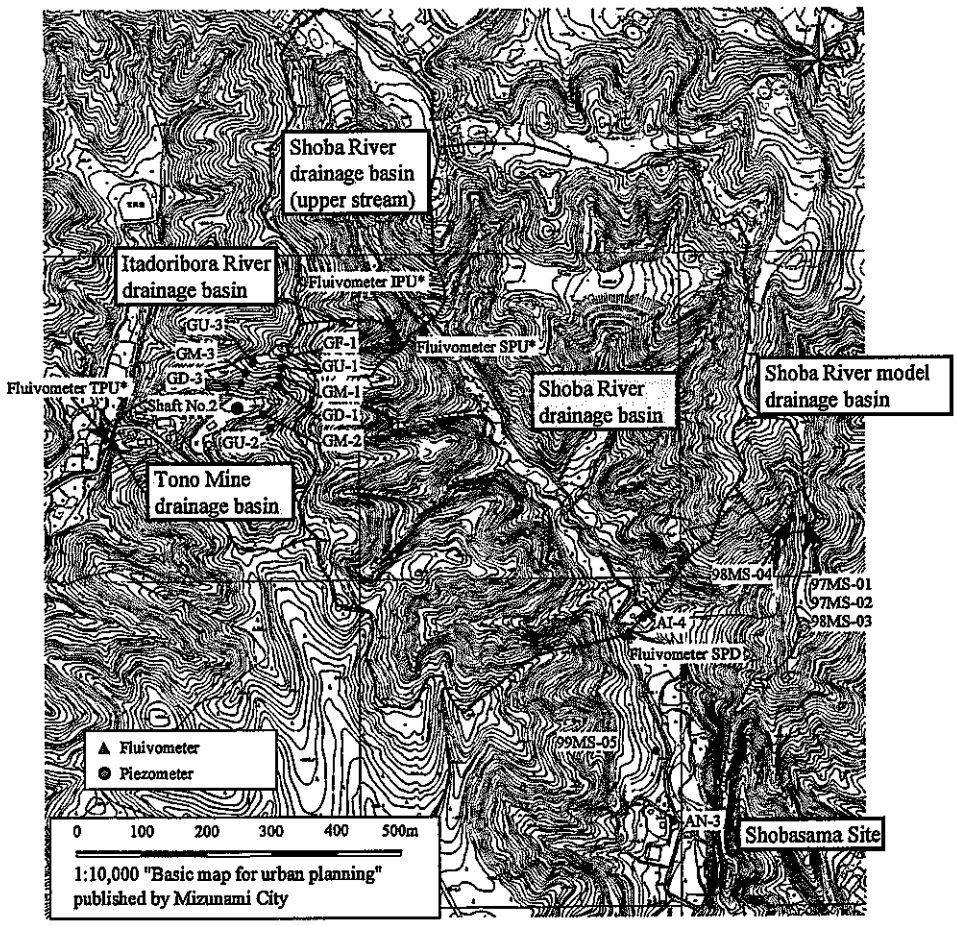

Figure 4.38 Location map of groundwater observatories and the water level monitoring on the MIU Project* and the RHS Project

Infiltration rates of rainfall into the soil and the underlying weathered part of the Seto Group, which cover the surface of hills, have yet to be understood quantitatively due to developmental status of the measuring technique to determine soil moisture. On the other hand, groundwater stored in the Seto Group, which occupies the upper half of hills surrounding the Shobasama Site, is thought to form the base flow of the Shoba River and others [58, 61].

In the Mizunami Group, an unsaturated zone develops, which produces confined groundwater separated from the groundwater in the overlying Seto Group. Furthermore, the heterogeneous distribution of geological formations in the Mizunami Group generates a heterogeneous distribution of water pressures within it [58, 62, 63].

4.2.3.2.2 Groundwater hydrogeological survey

The "Groundwater hydrogeological survey" refers to investigations to understand hydrogeological properties of the rock mass using boreholes exceeding several hundred meters in depth. While the drilling of the MIU-1, 2 and 3 were in progress in the Shobasama Site, hydraulic tests were carried out to determine flow system characteristics such as hydraulic conductivity [39, 40, 41]. The methods used and number of hydraulic tests performed are shown in Table 4.17. Crosshole hydraulic testing between MIU-2 and 3 were carried out to confirm whether the Tsukiyoshi Fault acts as a hydraulic barrier to flow and to obtain data on the continuity and physical properties of the "Fracture zone along the fault" [64].

Table 4.17 Details of hydraulic tests

Borehole		Depth (m)	Details	Tests
MIU Project	MIU-1 [39]	1,011.8	Pulse/slug tests were carried out for both fracture zones and intact rock, with 6.5 m test intervals. Also, pumping tests were carried out continuously in 100 m long test intervals.	Pulse/slug:28 Pumping:9
	MIU-2 [40]	1,012.0	Same as MIU-1. In addition, flow rates in pumping test were carefully controlled. Also, timing for pumping test completion was being improved.	Pulse/slug:30 Pumping:8
	MIU-3 [41]	1,014.0	Pulse/slug tests with several to several tens of meters intervals were carried out to study fractures (zones). Pumping tests with intervals up to 100 m were carried out. The test intervals were set according to fracture distributions. Also, flow rates in pumping test were carefully controlled. Adopting derivative plots of change in water pressure enhanced reliability of analysis data.	Pulse/slug:23 Pumping:11
Other geoscientific research	AN-1	1,010.2	Drilling of these AN-series boreholes was carried out from 1986 to 1988. Test intervals of 2 to 3 m were used to target mainly the fractures (zones).	Pulse/slug:34
	AN-3	408		Pulse/slug:24
	DH-2 [55]	501	Pulse/slug tests were carried out for both fracture zones and intact rock, with 2 to 8 m long test intervals.	Pulse/slug:10
	DH-4	505		Pulse/slug:9
	DH-9 [65]	1,030.0	Pulse/slug tests were carried out in 6.5m test intervals. Pumping test was in an 80 m test interval. Test intervals include fracture (zone), intact granite and anomalies detected by physical logging.	Pulse/slug:5 Pumping:1
	DH-11 [66]	1,012.0	Pulse/slug tests were in 10 m test intervals to target groundwater flowpaths. Pumping tests were carried out in 40 to 116 m long test intervals to cover the entire hole.	Pulse/slug:3 Pumping:8

MP borehole completion systems were installed in boreholes for continuous observation of water pressure and water chemistry after the MIU excavations. In the Shobasama Site, drilling and investigations in the AN-series of boreholes were carried out prior to investigations in the MIU-series boreholes. In addition to using the information obtained by these investigations, the MP systems were installed in the AN-series of boreholes to obtain new data on the pressure and water chemistry. Table 4.18 shows timetable of actual drilling and investigations in the boreholes in the Shobasama Site (MIU-1, 2 and 3, AN-1 and 3) and the DH-series of boreholes drilled for the RHS Project.

Table 4.18 Timetable of drilling and investigations

Borehole		～1997	1998	1999	2000
MIU Project	MIU-1				MP*
	MIU-2				MP*
	MIU-3				Crosshole Hydraulic test
Other Geoscientific research	AN-1	1986.7～1988.4			MP*,**
	AN-3	1987.7～1987.9			MP*,**
	DH-2	1994.12～1994.3			
	DH-4	1994.11～1995.3			
	DH-9				
	DH-11				

* Hydraulic observation using MP system, ** carried out in the MIU Projects

Results of the long-interval pumping tests carried out in the MIU-1, 2 and 3 shown in Figure 4.39 are expressed as vertical distribution of hydraulic conductivity with depth. The basal conglomerate of the Toki Lignite-bearing Formation, the weathered part of the granite, "Upper fracture zone", "Moderately fractured zone", "Fracture zone along the fault" and the Tsukiyoshi Fault are considered the geological features controlling the groundwater hydrogeology. Results of hydraulic tests (pulse/slug tests) and pumping tests indicate that the hydraulic conductivity of the "Moderately fractured zone" is about an order of magnitude lower than the "Upper fracture zone" and "Fracture zone along the fault" (Figure 4.40).

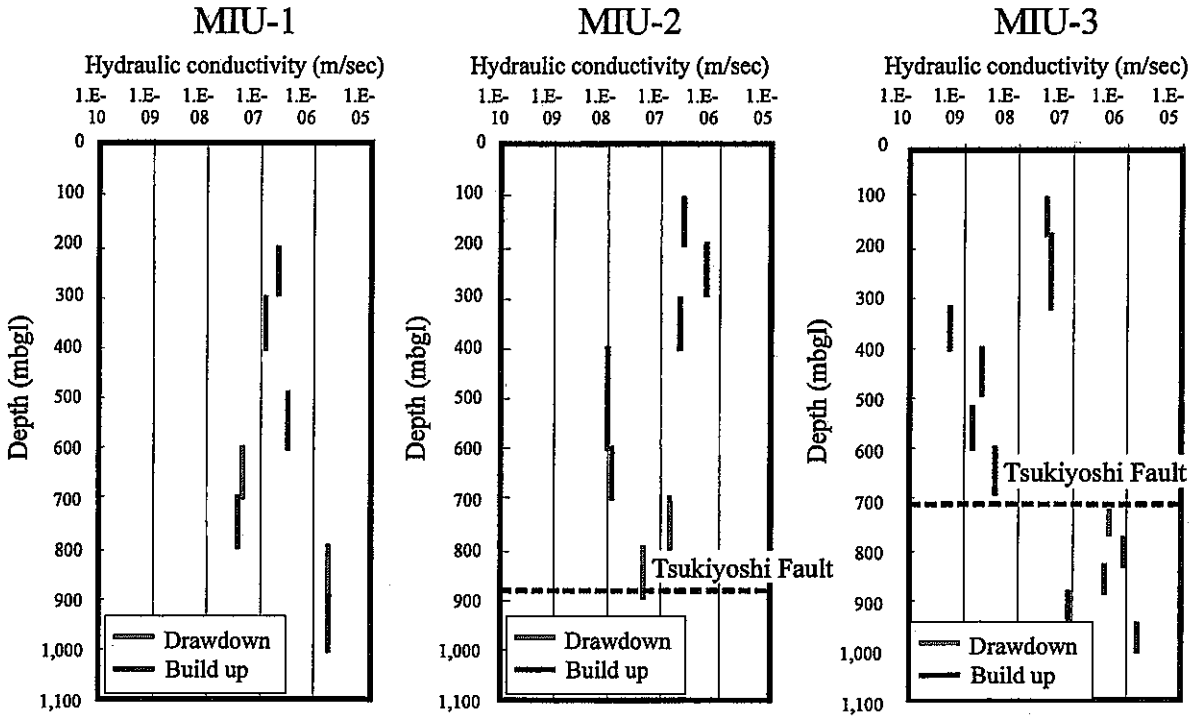

Figure 4.39 Hydraulic conductivity based on the pumping test

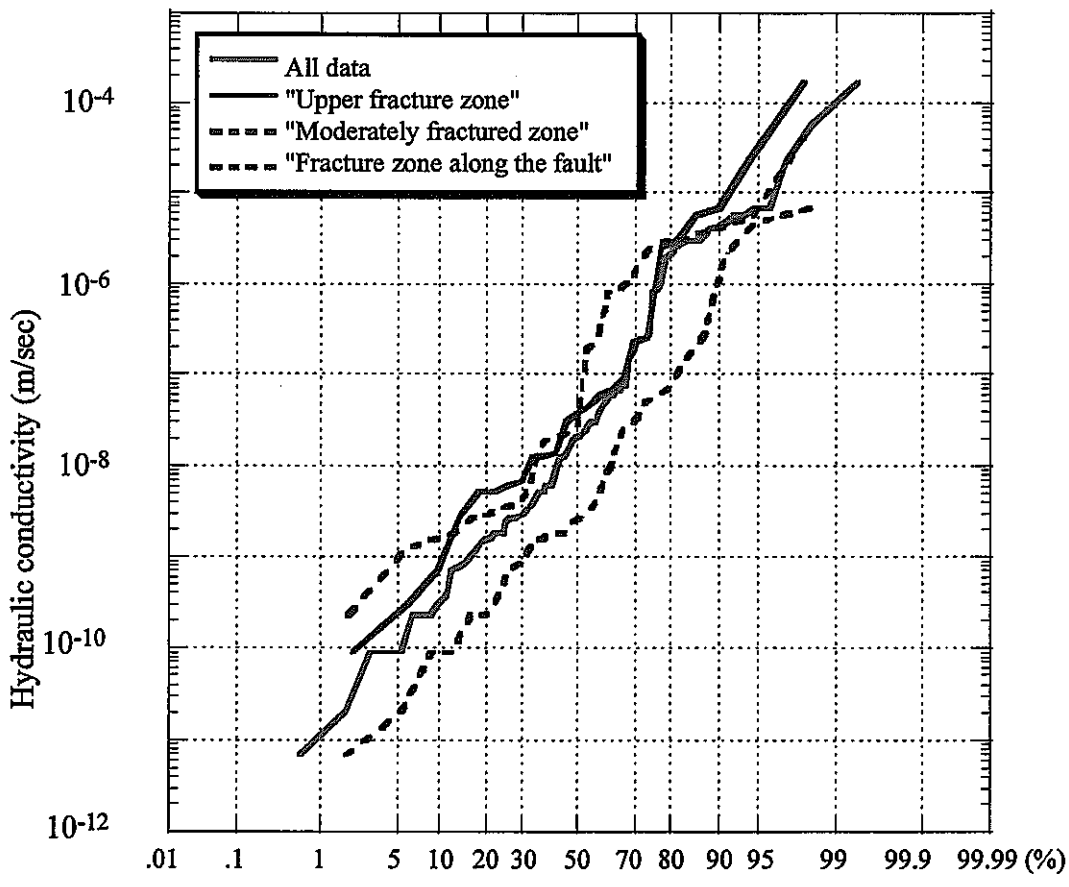

Figure 4.40 Hydraulic conductivity of MIU-1~3

An example of the pore water pressure distribution in the Shobasama Site is shown in Figure 4.41. The pore water pressures are measured in isolated sections in MIU-1, 2 and 3. The largest pressure difference is recognized between the measuring sections on opposite sides of the Tsukiyoshi Fault. The fault is intersected by MIU-2 at an elevation of -650 masl as shown in the correlation graph between elevation and pore pressure and at the No.26 measuring section shown in the water level histogram, respectively. The nos.1 to 3 measuring sections, which are characterized by a high pore pressure decreasing with depth, correspond with the distribution of the Akeyo Formation (consisting of mudstone, sandstone and conglomerate). This suggests that the mudstone and sandstone in the formation are low in permeability and form a hydraulic barrier to flow. The fact that the Akeyo Formation in the Shobasama Site has a higher pore pressure is ascertained in the 99MS-05 borehole drilled for the surface hydrological survey.

In general, the pore pressure in the MIU-2 is higher and more variable with depth than in the MIU-1. As for the pore pressure in the MIU-3, it has a tendency similar to that in the MIU-2 though it is affected by the pressure release of the MIU-2. The clarification of temporal change in pore pressure and the observation on annual/seasonal variations in pore pressure behavior as well as hydrogeological effects of borehole excavations are in progress.

4.2.3.3 Hydrogeological model and groundwater flow simulation (study area)

4.2.3.3.1 Overview

Based on the results of the hydrogeological investigations and the problems to be solved in the 2nd analysis loop, a groundwater flow simulation was carried out [67] using the model described below. The aim was to test the hydrogeological model and methodology for the groundwater flow simulations. This model expresses the heterogeneous distribution of physical properties (due to structural discontinuities) of the rock mass, by an equivalent continuum. This model is called the equivalent continuum model.

4.2.3.3.2 Setting of the study area

The study area is identical with that modeled in the 1st analysis loop (about 4 km× about 6 km encompassing the Shobasama Site at its center).

4.2.3.3.3 "Equivalent Continuum Model"

This model allows expressing discontinuous and heterogeneous hydrogeological properties in the rock mass by dividing the study area into finite elements and by computing permeability tensors of the individual finite elements from the information on fracture distribution. Unlike the fracture network model dealing with each fracture, this model sets an equivalent physical value (permeability, etc.) in response to fracture density in each mesh. Therefore, this model is suitable for groundwater flow simulation of several km square fractured rock masses.

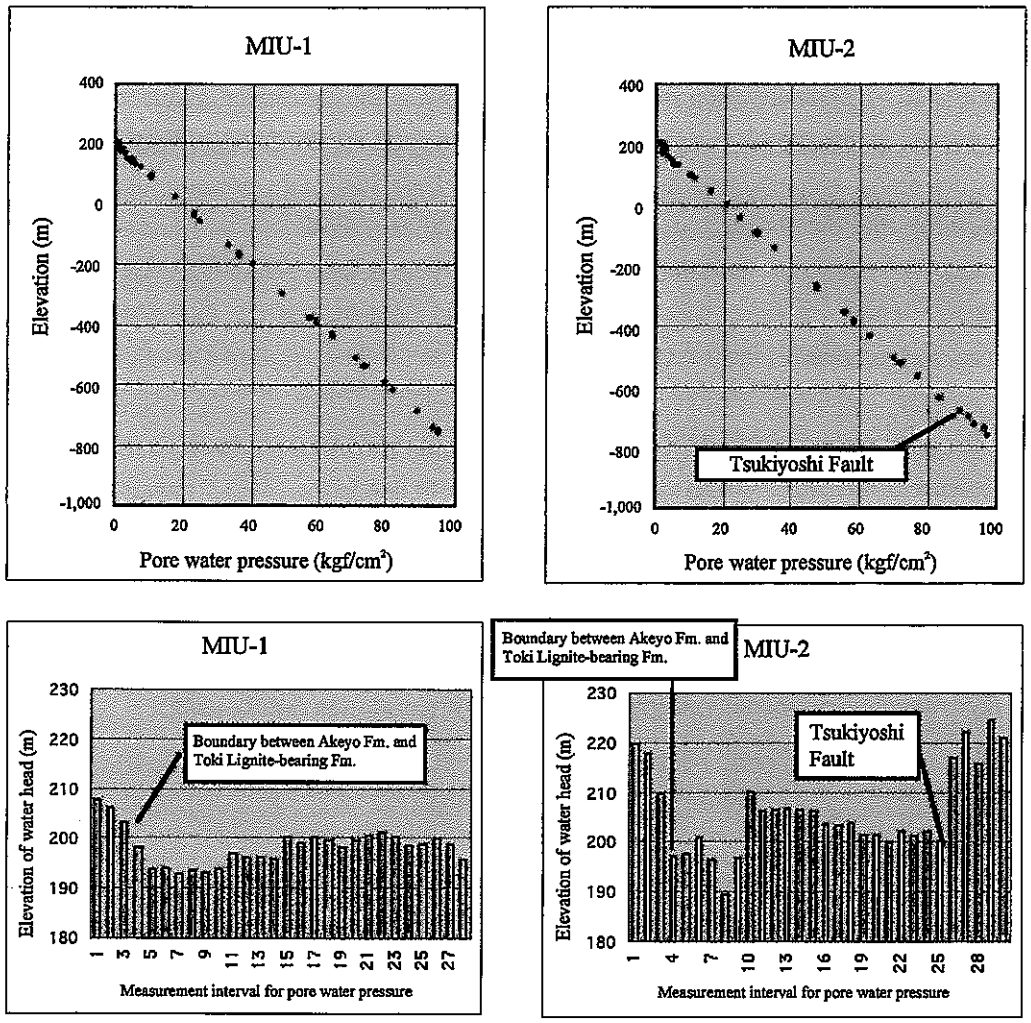

Figure 4.41 Pore water pressure distribution at the MIU-1, MIU-2

4.2.3.3.4 Hydrogeological model

(1) Procedure for model construction

The model development procedure for groundwater flow simulations is shown in Figure 4.42. Based of geological units and the results of hydrogeological investigations (See Section 4.2.3.2), "equivalent continuum model" is constructed for the study area (about 4 km×about 6 km).

A statistical processing of fractures is applied to three units, the "Upper fracture zone", the "Moderately fractured zone" and the "Fracture zone along the fault". As in the 1st analysis loop, a unique physical value is assigned to each of the sedimentary rock formations, the weathered granite and the Tsukiyoshi Fault, thus they are treated as a homogeneous continuum. For the sedimentary rocks and the Tsukiyoshi Fault, statistical treatment is not applied because sufficient detail on the fracture network systems did not exist for them. The deeply weathered part of the granite is not only lacking details on fracturing and hydraulic character but also is so porous due to weathering and alteration that it is treated as a uniform zone with unique physical properties. As a result, it is not included in the statistical processing of fractures.

(2) Generation of fracture network model

The construction of "equivalent continuum model" requires determining the statistical distribution of geometrical azimuth, aperture and radii of fractures. The 3-D fracture density is also required. Particularly, hydraulic apertures must be used instead of geometrical ones observed on the walls of the rock mass or boreholes.

Figure 4.43 shows the process of generation of a fracture network model. The main process is as follows.

- Identify open fractures which are generally presumed highly permeable, based on results of BTV investigations
- Determine their orientations (n), intensities (1-D fracture density) in boreholes (ρ_1) and geometrical apertures (t_g)
- Carry out virtual permeability tests simulating hydraulic tests in boreholes.
- Estimate the averages of radii (r) and hydraulic apertures (t_h) of fractures by comparing simulated and measured values of hydraulic conductivities
- Calculate 3-D densities (ρ_3) by inputting a mean square value of fracture diameter and ρ_1 into a geometrical relational expression of fracture.

Derivation of statistical values of fractures

Orientation (n)

Using a cluster analysis of the orientations of all fractures intersected by the BTV survey, fractures in the "Upper fracture zone" are divided into four sets with the following major attitudes: (1) low angle fractures; (2) N50-70E, dip 70-80SE; (3) N80-90W, dip 60-70N; and (4) N20-50E, dip 70-80SW. Based on the

cluster analysis, fractures are divided into groups on a Schmidt diagram and fracture orientations within the groups are defined by using a Bingham distribution. Parameters of fractures (Figure 4.44) are shown in Table 4.19.

The Fisher distribution (hemispheric normal distribution) has been most popular as a statistical model to express orientations of fractures in the rock mass. The Fisher distribution is characterized by an isotropic distribution around the center of dominant orientation. On the other hand, the Bingham distribution is characterized by an anisotropic distribution and allows modeling an elliptic or belt-shaped distribution. Orientations of fractures intersected by MIU-1, 2 and 3 are not always isotropic, suggesting constraints on the reproduction of data by the Fisher distribution. Thus, the Bingham distribution was employed for modeling orientations of fractures.

Intensities (1-D fracture density) (ρ_1)

The total fracture population detected by BTV surveys in all MIU boreholes is 10,369. However, of the total fracture population, only 188 are clearly open fractures, representing 1.8% of the total. The 1-D densities of total fracture population and the open fractures are shown for the four major orientation sets in the individual zones in Table 4.19.

Table 4.19 Fracture density according to the results of the BTV investigations

	Interval	Frequency	Total Fracture density (n/m)	Open fracture density (n/m)
"Upper fracture zone"	Set-1	1,911	2.479	0.045
	Set-2	341	0.442	0.008
	Set-3	484	0.628	0.011
	Set-4	732	0.949	0.017
	Total	3,468	4.498	0.082
"Moderately fractured zone"	Set-1	839	0.755	0.014
	Set-2	461	0.451	0.008
	Set-3	538	0.484	0.009
	Set-4	583	0.524	0.010
	Total	2,421	2.177	0.039
"Fracture zone along the fault"	Set-1	1,670	1.888	0.034
	Set-2	809	0.915	0.017
	Set-3	1,128	1.275	0.023
	Set-4	873	0.987	0.018
	Total	4,480	5.066	0.092

Geometrical aperture (t_g)

Using the data on aperture of open fractures determined from the BTV investigations, the relationships between apertures and 1-D fracture densities (the total number of open fractures with openings less than a given value) are examined. The results are shown in Table 4.20.

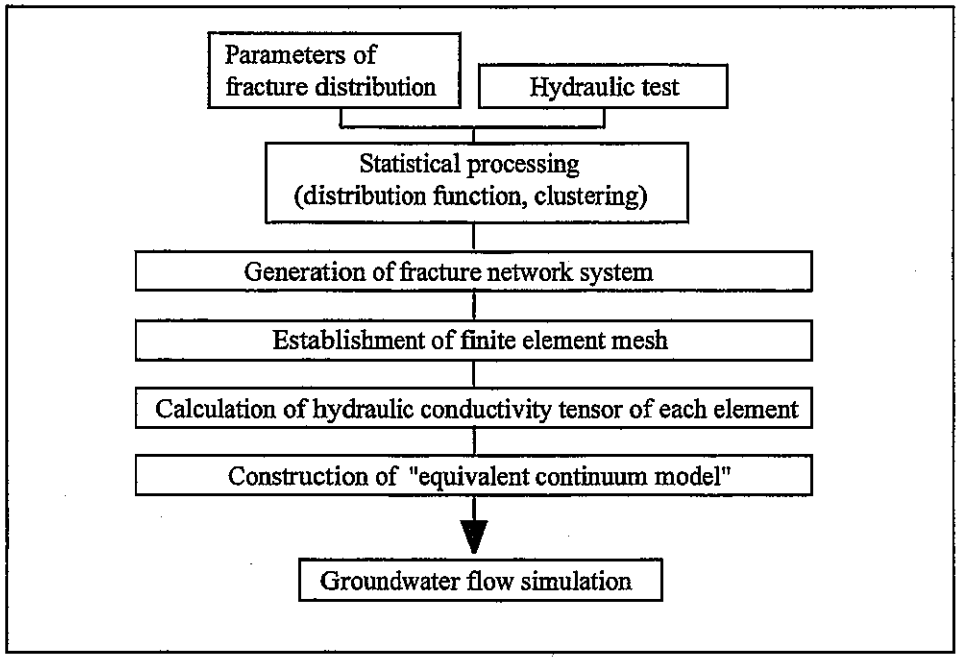

Figure 4.42 Procedure for construction of the "equivalent continuum model"

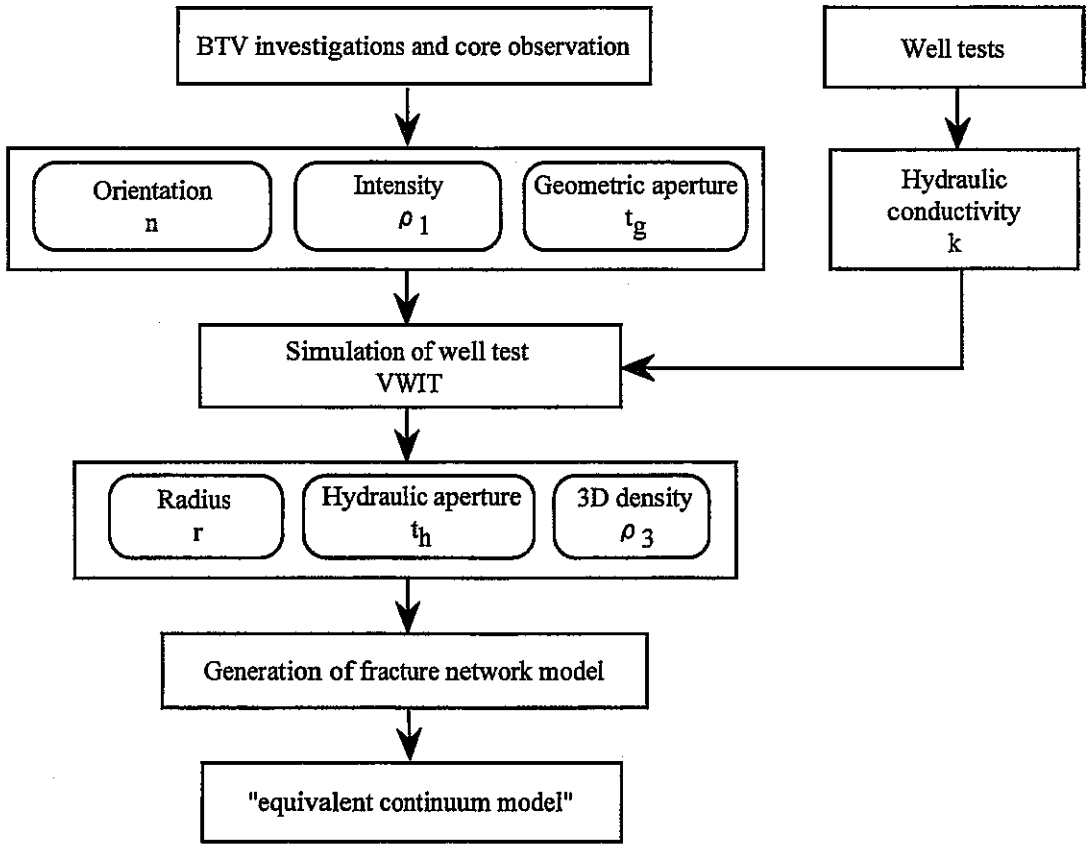

Figure 4.43 Flow diagram for determination of fracture statistics for equivalent heterogeneous continuum modeling

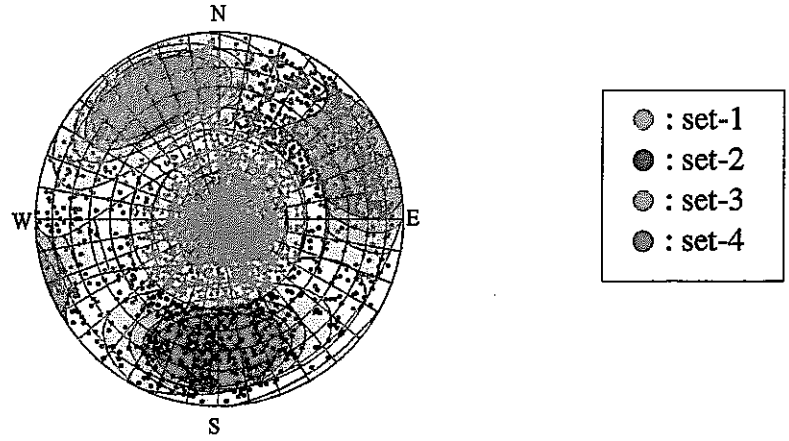

(a) "Upper fracture zone"

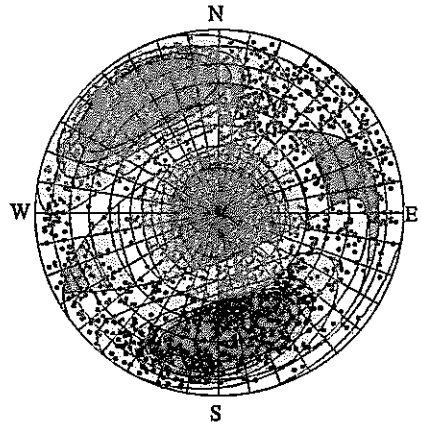

(b) "Moderately fractured zone"

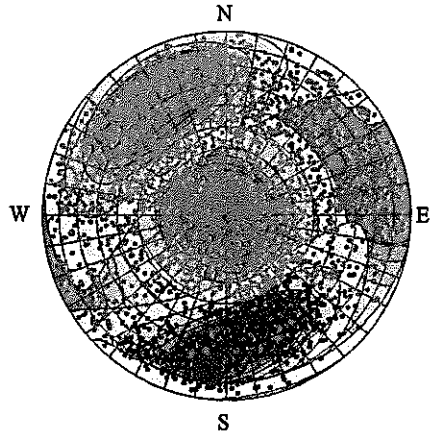

(c) "Fracture zone along the fault"

Figure 4.44 Lower hemisphere stereonet projection for three zones

Table 4.20 Relationship between aperture and fracture density of the MIU-1, 2 and 3

Aperture(mm)	Frequency	Cumulative percentage (%)	Cumulative frequency	Fracture density (n/m)
0.0	60	100.00	188	0.0688
0.5	15	68.09	128	0.0468
1.0	42	60.11	113	0.0413
1.5	21	37.77	71	0.0260
2.0	10	26.60	50	0.0183
2.5	15	21.28	40	0.0146
3.0	4	13.30	25	0.0091
3.5	4	11.17	21	0.0077
4.0	4	9.04	17	0.0062
4.5	4	6.91	13	0.0048
5.0	2	4.79	9	0.0033
5.5	1	3.72	7	0.0026
6.0	2	3.19	6	0.0022
6.5	1	2.13	4	0.0015
7.0	1	1.60	3	0.0011
7.5	0	1.06	2	0.0007
8.0	0	1.06	2	0.0007
8.5	0	1.06	2	0.0007
9.0	0	1.06	2	0.0007
9.5	0	1.06	2	0.0007
10.0	0	1.06	2	0.0007
>10.0	2	1.06	2	0.0007

Generation of fracture network model by virtual permeability tests

Virtual permeability tests

Virtual permeability testing is a trial-and-error method to determine fracture statistics (fracture radius, hydraulic aperture and 3-D fracture densities) through numerical simulations of hydraulic tests. From the fracture statistics, distribution of hydraulic conductivity was calculated as if actual permeability tests were carried out. The method for derivation of fracture radii, hydraulic apertures and 3-D densities used in the computing process is shown in Figure 4.45.

Distribution of hydraulic conductivity

Results from single-borehole permeability tests carried out in MIU-1, 2 and 3 were used for comparison with results of the virtual permeability tests. Figure 4.40 shows distributions of hydraulic conductivities obtained by permeability tests carried out in the granite. The results indicate that measured hydraulic conductivities roughly have a log-normal distribution. These hydraulic conductivities extend over a numerical range exceeding 8 orders of magnitude, indicating an extremely high heterogeneity. Also, the results indicated that the hydraulic conductivity of the "Moderately fractured zone" is nearly an order of magnitude lower than those of the "Upper fracture zone" and "Fracture zone along the fault". The virtual permeability tests (described below) compute the fracture distribution parameters that allow reproducing these tendencies.

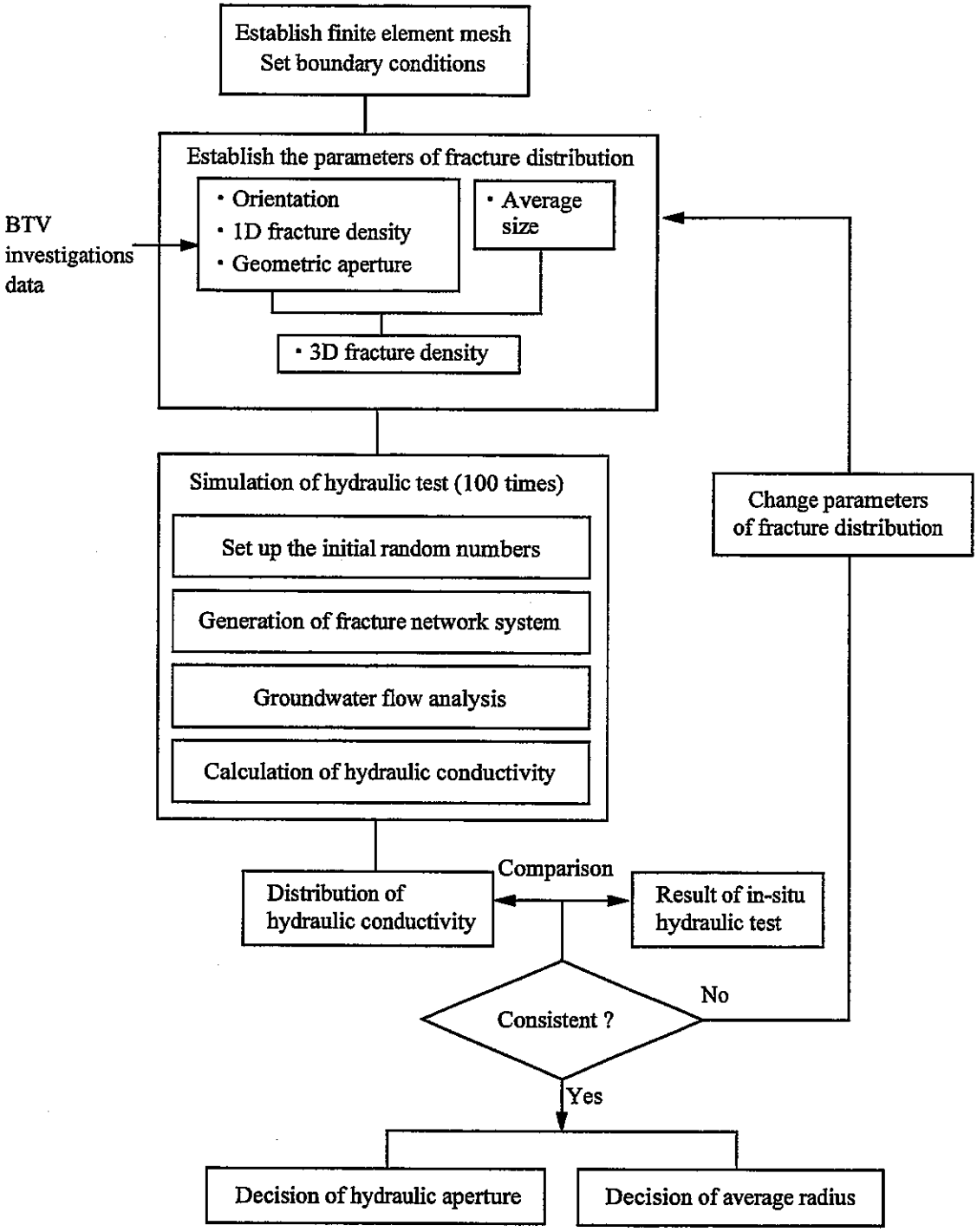

Figure 4.45 Procedure of virtual water injection test (VWIT)

Virtual permeability tests

Given 1-D fracture densities and fracture radii distribution (or diameter distribution), 3-D fracture densities are obtained by the following equation:

$$\rho_3 = \frac{4}{\pi} \cdot \frac{\rho_1}{\langle d^2 \rangle}, \quad (4.2.1)$$

ρ 1: 1-D fracture density, ρ 3 : 3-D fracture density, $\langle d^2 \rangle$: a mean square of fracture diameter

In the identification of parameters by virtual permeability tests, it is confirmed whether or not the tests can express the groundwater hydrogeology, on the following assumptions.

① Only open fractures are employed to determine the 1-D fracture distribution.
Open fractures are generally thought to control groundwater hydrology.

② Aperture of fractures shows a negative exponential distribution. One distribution parameter is applied to all of the fracture sets.
Open fractures in the individual fracture groups are too few to provide meaningful statistical information. Therefore, not only to all open fractures but also to the individual groups of fractures, is a negative exponential distribution of aperture applied.

③ The Bingham distribution is applied to the orientation distribution of the individual fracture groups.
The Bingham distribution is employed to express an anisotropic tendency of the fracture distributions.

④ The following truncated power law distribution and negative exponential distribution are assumed to express the distribution of fracture radii. Irrespective of fracture groups, one distribution parameter is applied to a group.
Power distribution and negative exponential distribution are applied on the basis of the existing studies [68, 69].

$$f(r) = \frac{b-1}{r_{\min}} \cdot \left[\frac{r_{\min}}{r} \right]^b, \quad r \geq r_{\min} \quad (b=3)$$

$$f(r) = \lambda \cdot \exp(-\lambda r), \text{ but } \lambda = 1/\langle r \rangle$$

r : fracture radius, $r_{\min}$: minimum fracture radius, b : power number, $\langle r \rangle$: average of fracture radii

In the modeling of fracture radii by a truncated power law distribution and a negative exponential distribution, the mean square of fracture diameters $\langle d^2 \rangle$ are obtained by the following equations.

· Truncated power law distribution

$$\langle d^2 \rangle = (b-1)(2r_{\min})^2 \{\ln(2r_{\max}) - \ln(2r_{\min})\},$$

· Negative exponential distribution

$$\langle d^2 \rangle = \frac{1}{\lambda}\left\{\exp(-\lambda d_{min})\cdot\left(\lambda^2 {d_{min}}^2 + 2\lambda d_{min} + 2\right) - \exp(-\lambda d_{max})\cdot\left(\lambda^2 {d_{max}}^2 + 2\lambda d_{max} + 2\right)\right\}$$

r_{max} : maximum fracture radius, d_{min} : minimum fracture diameter, d_{max} : maximum fracture diameter

The $<d^2>$ is very dependent on r_{min} in truncated power law distribution and λ in negative exponential distribution, respectively.

⑤ There is a linear proportional correlation between geometrical and hydraulic apertures.

No tracer test was carried out, therefore, hydraulic aperture could not be verified. At the time it was thought to be the most conservative for analytical purposes to assume that geometrical apertures continue without change by neglecting any possible irregularities of fractures.

· Truncated power law model

The prediction of 3-D open fracture density (ρ_3) based on 1-D open fracture density (ρ_1) from Equation (4.2.1) failed to completely reproduce the measured distributions of hydraulic conductivities which have a range of up to 8 orders of magnitude, as shown in Figure 4.46. It is difficult to have the entire measured dataset, with such a wide distribution range, match with the truncated power law model. Therefore, it will be necessary to devise a method (e.g. fit the measured data for the individual geological units with the model). The present simulation adopts the truncated power law model, employing r_{min} = 70 m and r_{max} = 3,000 m, which shows the best match between measured and computed data. In this case, 1-D density of open fractures is taken into consideration, and the linear (log-normal) distribution of measured data is retained.

· Negative exponential model

The main aim of simulation is to reproduce the heterogeneity of measured hydraulic conductivities. The simulation, following the procedure shown in Figure 4.43, and which used open fractures detected by BTV investigations, failed to achieve a good match between measured and computed values. Accordingly, it was attempted to find fracture distribution parameters that allow computed values to approach the measured values by changing 1-D fracture densities. The simulation indicated that the distribution of hydraulic conductivity is hardly affected by the value of r_{ave} under a constant value of $<d^2>$ in the negative exponential model. Thus, the effect of reducing the 1-D fracture density (ρ_1) was examined with a fixed value of r_{ave}=80 m. As a result, it turned out that the effect of a change in ρ_1 on the heterogeneity of hydraulic conductivity distribution is larger than that of the average fracture radius (r_{ave}) in the truncated power law model. However, too small a value of ρ_1 often results in hydraulic conductivity values ranging from 10^{-11} to 10^{-10} m/s. In this case, the distribution of hydraulic conductivity deviates significantly from a log-normal distribution (Figure 4.47). Thus, the comparison with the distribution of measured hydraulic conductivity justifies adopting r_{ave}=80 m and ρ_1=0.0049 for the negative exponential model.

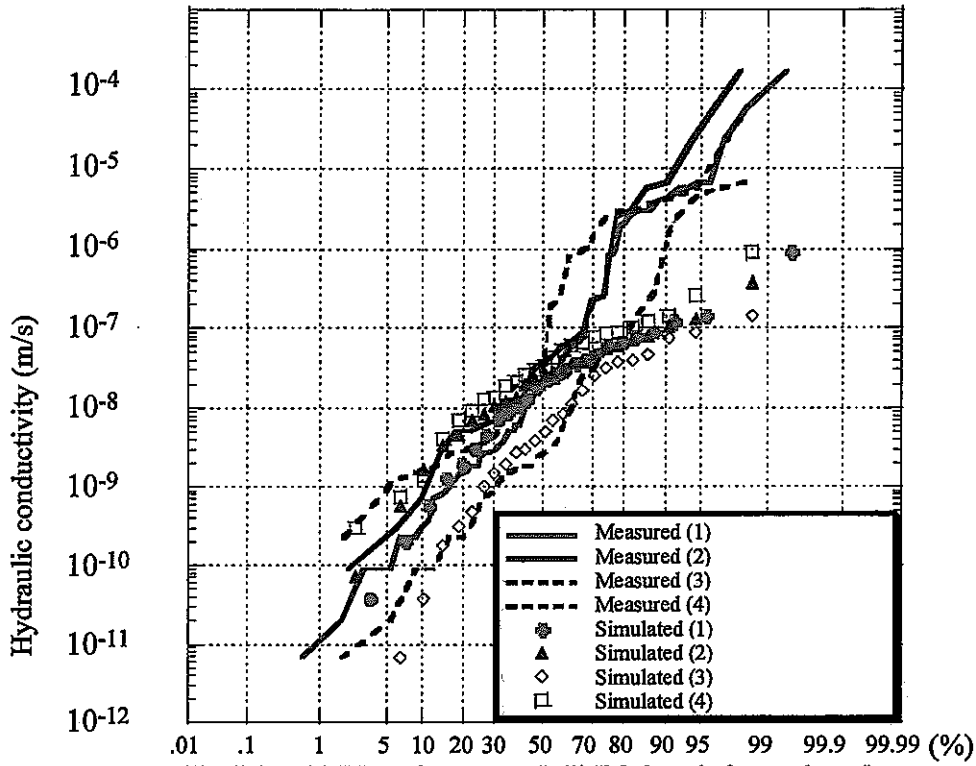

(1) All data, (2) "Upper fracture zone", (3) "Moderately fractured zone",
(4) "Fracture zone along the fault"

Figure 4.46 Cumulative plot of the hydraulic conductivity (MIU-1~3) (Truncated power law model)

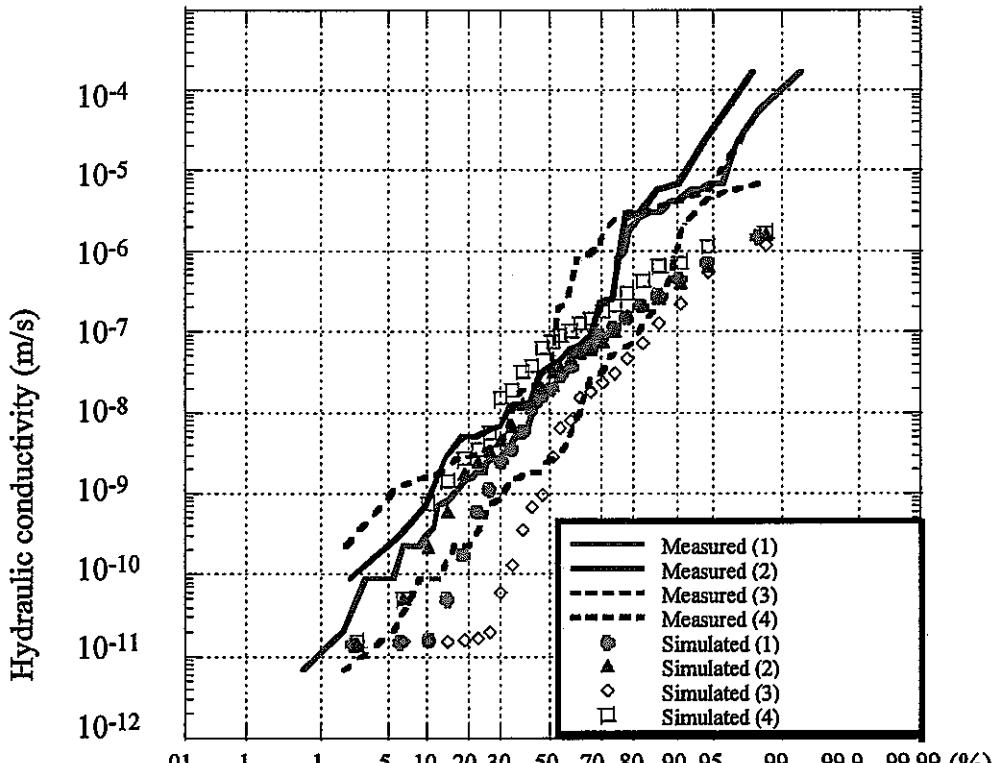

(1) All data, (2) "Upper fracture zone", (3) "Moderately fractured zone",
(4) "Fracture zone along the fault"

Figure 4.47 Cumulative plot of the hydraulic conductivity (MIU-1~3) (Negative exponential model)

These two distribution models are summarized in Table 4.21. Comparing the two models, average fracture diameters and 3-D fracture densities are almost similar. However, Model 1 has a larger distribution range of fracture radii and a higher 1-D fracture density. Thus, the latter is characterized by lower fracture continuity and higher heterogeneity of hydraulic conductivity.

Table 4.21 Details of fracture models

		r_{min}	r_{max}	r_{ave}	<d>	<d^2>	ρ_1	ρ_2
Model 1	Truncated power law	70 m	3,000 m	—	137m	1.47×10^{5} m^2	6.79×10^{-2}	5.87×10^{-7}
Model 2	Negative exponential	—	—	80 m	160 m	1.28×10^{4} m^2	4.9×10^{-3}	4.91×10^{-7}

Summary

Fracture distribution parameters determined by the above statistical derivations are listed in Tables 4.22 and 4.23. Fracture densities (ρ_1, ρ_3) in the individual zones are calculated using whole fracture densities simulated for the above models and the fracture ratio in the sets shown in Table 4.19. On the assumption that hydraulic aperture is proportional to geometrical aperture, a proportionality constant is set so that logarithmic means of both in-situ permeability tests and virtual permeability tests become equal.

Figures 4.46, 4.47 show comparison between simulated distributions of hydraulic conductivity and the measured values in the each model.

Table 4.22 Parameter of statistical fracture distribution
(Truncated power law model)

	Set	Fracture density ρ_1 (n/m)	Mean geometrical aperture t_g(m)	Mean hydraulic aperture t_h(m)	Mean fracture radius r_{ave}(m)	Volumetric fracture density ρ_3($1/m^3$)
"Upper fracture zone"	1	4.49×10^{-2}	1.70×10^{-3}	7.91×10^{-5}	70	3.88×10^{-7}
	2	8.02×10^{-3}				6.39×10^{-8}
	3	1.14×10^{-2}				9.84×10^{-8}
	4	1.72×10^{-2}				1.49×10^{-7}
"Moderately fractured zone"	1	1.37×10^{-2}	1.70×10^{-3}	7.91×10^{-5}	70	1.18×10^{-7}
	2	7.52×10^{-3}				6.50×10^{-8}
	3	8.77×10^{-3}				7.58×10^{-8}
	4	9.51×10^{-3}				8.22×10^{-8}
"Fracture zone along the fault"	1	3.42×10^{-2}	1.70×10^{-3}	7.91×10^{-5}	70	2.96×10^{-7}
	2	1.66×10^{-2}				1.43×10^{-7}
	3	2.31×10^{-2}				2.00×10^{-7}
	4	1.79×10^{-2}				1.55×10^{-7}
PDFs		Bingham	Negative exponential	Negative exponential	Negative exponential	Truncated power law

Table 4.23 Parameter of statistical fracture distribution
(Negative exponential model)

	Set	Fracture density ρ_1 (n/m)	Mean geometrical aperture t_g(m)	Mean hydraulic aperture t_h(m)	Mean fracture radius r_{ave}(m)	Volumetric fracture density ρ_3(1/m^3)
"Upper fracture zone"	1	3.26×10^{-3}	1.70×10^{-3}	1.70×10^{-4}	80	3.25×10^{-7}
	2	5.82×10^{-4}				5.79×10^{-8}
	3	8.26×10^{-4}				8.22×10^{-8}
	4	1.25×10^{-3}				1.24×10^{-7}
"Moderately fractured zone"	1	9.93×10^{-4}	1.70×10^{-3}	1.70×10^{-4}	80	9.88×10^{-8}
	2	5.46×10^{-4}				5.43×10^{-8}
	3	6.37×10^{-4}				6.33×10^{-8}
	4	6.90×10^{-4}				6.86×10^{-8}
"Fracture zone along the fault"	1	2.49×10^{-3}	1.70×10^{-3}	1.70×10^{-4}	80	2.47×10^{-7}
	2	1.20×10^{-3}				1.20×10^{-7}
	3	1.68×10^{-3}				1.67×10^{-7}
	4	1.30×10^{-3}				1.29×10^{-7}
PDFs		Bingham	Negative exponential	Negative exponential	Negative exponential	Truncated power law

In the truncated power law model, the simulated distributions of hydraulic conductivity in the low to intermediate range (cumulative probabilities: 0 to 50%) reproduce the measured data well. However, the simulation does not reproduce the higher permeable parts (hydraulic conductivity > 10^{-7}cm/s) well. That is, simulations with the truncated power law model underestimate frequency of high permeabilities in the rock mass at the Shobasama Site. The reverse is true for the negative exponential distributions. The comparison indicates that the truncated power law model and the negative exponential model successfully reproduce the lower permeability part and higher permeable parts, respectively.

For both models, simulated hydraulic conductivities decrease from the "Fracture zone along the fault" to the "Upper fracture zone", and decrease further in the "Moderately fractured zone". This tendency is the same as that of the measured values. Based on the fracture distribution parameters shown in Tables 4.22 and 4.23, the hydrogeological model was constructed using an equivalent continuum which takes the hydrogeological heterogeneity of the Shobasama Site into consideration.

(3) Construction of hydrogeological model

3-D finite element meshes were developed for the groundwater flow simulation, based on the geological units in the geological model and the 3-D distribution of permeable fractures described in the previous section. The following are taken into consideration.

① The topography is expressed by plane meshes.
② Geological formations and faults expressed in the geological model are expressed by 3-D meshes.
③ The shaft and galleries in the Tono Mine are expressed by nodal points or elements.
④ Locations of major boreholes are arranged to coincide with lattice points of the plane mesh.
⑤ Large-scale fracture zones are expressed by 3-D meshes, if necessary.

3-D meshes are formed, taking boundaries of the geological units shown in Table 4.24 into consideration. The 3-D meshes are shown in Figure 4.48. The number of elements and nodal points total 99,293 and 61,395, respectively.

Table 4.24 Geological units and hydraulic conductivities used for the homogeneous model

Geological units	Hydraulic conductivity (m/s)
Seto Group	1.0×10^{-7}
Oidawara Fm.	1.0×10^{-9}
Akeyo Fm.	1.0×10^{-8}
Toki Lignite-bearing Fm. (Upper)	5.0×10^{-9}
Toki Lignite-bearing Fm. (Basal conglomerate)	1.0×10^{-7}
Toki Granite (Weathered)	1.0×10^{-7}
"Moderately fractured zone"	1.0×10^{-9}
"Upper fracture zone"	2.0×10^{-8}
Tsukiyoshi Fault	1.0×10^{-10}
"Fracture zone along the fault"	1.0×10^{-7}

Using these meshes, the 3-D distribution of permeable fractures described in the previous section is statistically developed in the granite to construct an "equivalent continuum model". For each of the two fracture distribution models (truncated power law model and negative exponential model), a database of fracture distributions was developed. Figure 4.49 shows the 3-D comparison between the two models. Each block in the Figure is a cube with sides 60 m-long. It turns out that the truncated power law model develops more continuous fractures than the negative exponential model.

Figure 4.50 shows a homogeneous model, truncated power law model and negative exponential model. These three models are used for groundwater flow simulations. Here, "homogeneous model" refers to a model where a definite hydrogeological property is given to each of the geological formations without taking any heterogeneous permeability generated by fracture distributions into consideration.

In the homogeneous model (Figure 4.50(a)), hydraulic conductivity listed in Table 4.24 is applied to the finite element meshes shown in Figure 4.28. Most of the hydraulic conductivities applied to each geological unit are identical with those set for the 1st analysis loop (Table 4.13). However, hydraulic conductivities of the Akeyo Formation and the lower part of the Toki Lignite-bearing Formation were changed so that they would represent each element more precisely, with attention paid to contrasts in the geological units. Specifically, the Akeyo Formation is assigned a hydraulic conductivity of 1.0×10^{-8} m/s to represent its typical lithofacies of fine- to medium-grained sandstone. The Lower Toki Lignite-bearing Formation is assigned a hydraulic conductivity of 1.0×10^{-7} m/s because its highly permeable basal conglomerate has the same hydraulic conductivity as the weathered zone of the granite, i.e., 1.0×10^{-7}m/s. The hydraulic conductivities of the "Upper fracture zone", "Moderately fractured zone" and "Fracture zone along the fault" were based on the results of hydraulic tests carried out in MIU-1, 2 and 3.

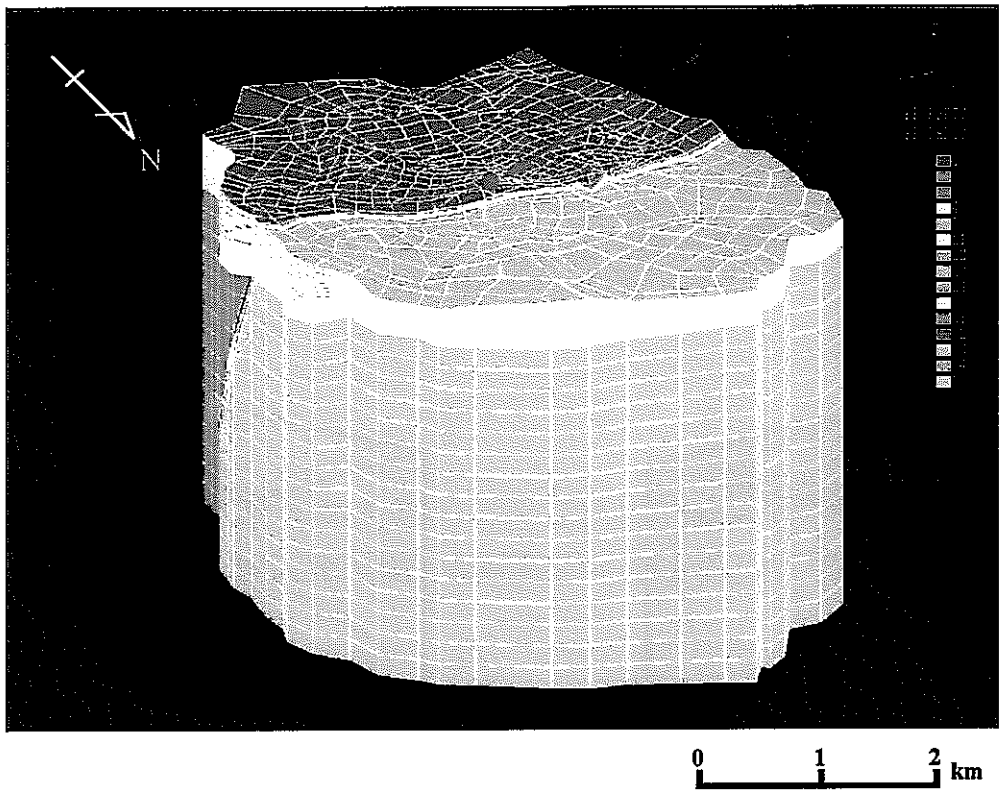

Figure 4.48 3D finite element mesh

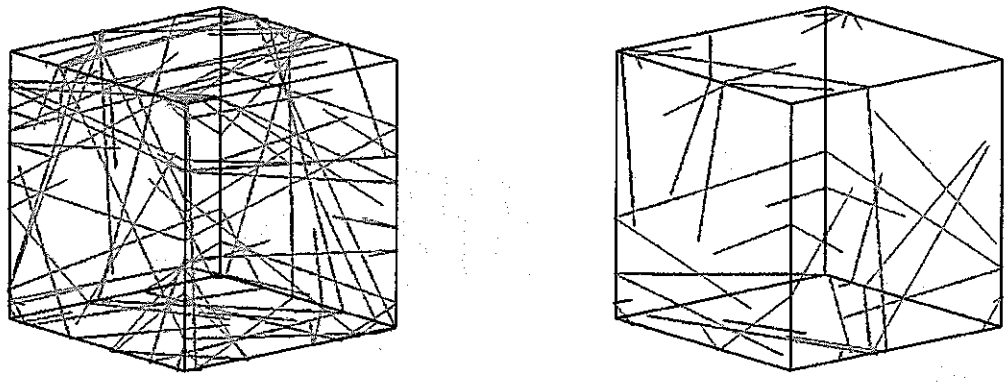

"Upper fracture zone"

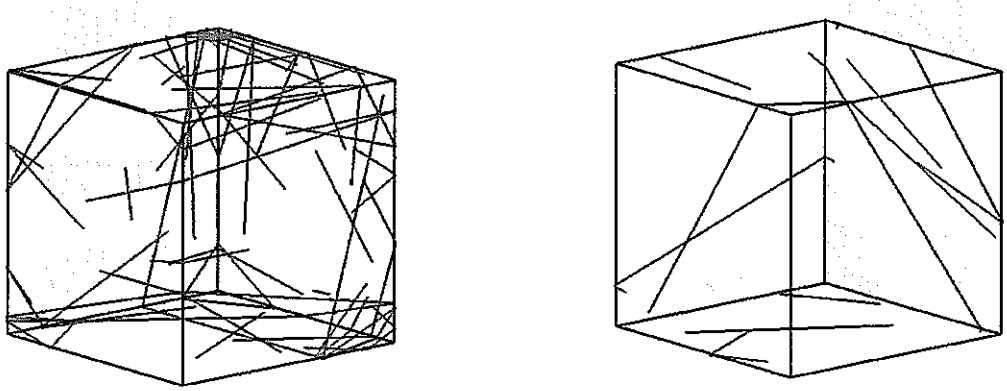

"Moderately fractured zone"

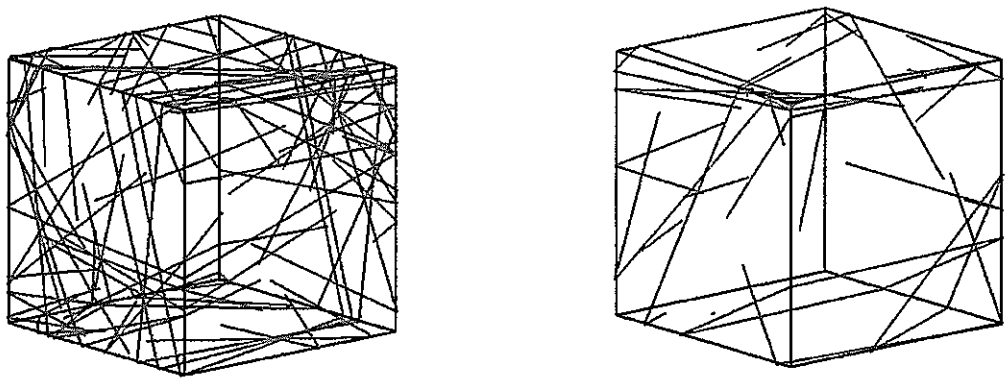

"Fracture zone along the fault"

(a) Truncated power law model (b) Negative exponential model

Figure 4.49 Comparison of fracture distribution between two models

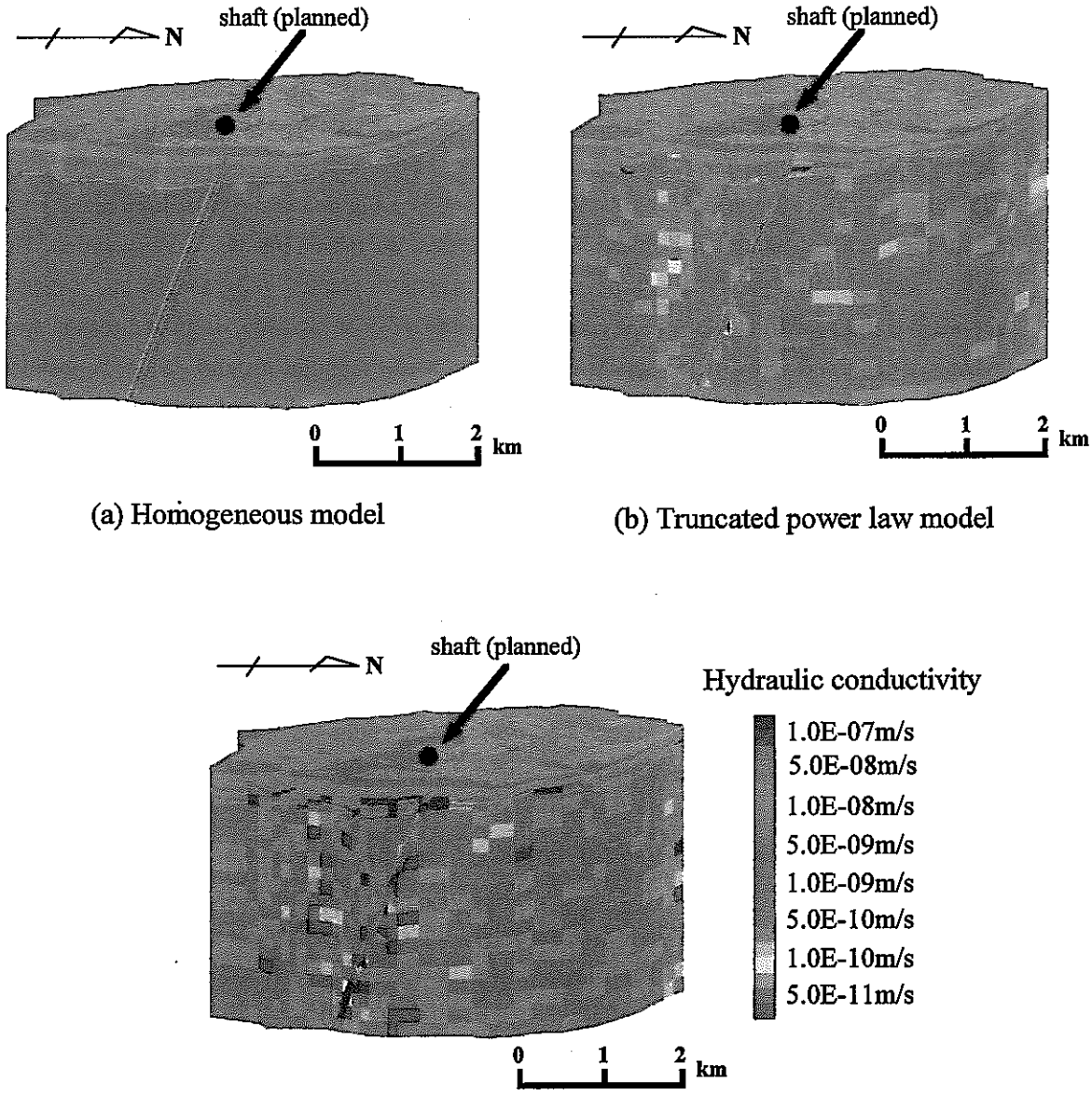

(a) Homogeneous model

(b) Truncated power law model

(c) Negative exponential model

Figure 4.50 Hydraulic conductivity distribution (a bird's-eye view)

Hydraulic boundary conditions for simulation are set as follows:

① Top boundary condition (Ground surface)

Based on the investigations and analyses described in Section 4.2.2.2 **Establishing boundary conditions,** the recharge rate at ground surface was established for the top boundary. The recharge rate of 0.28mm/day, the mean calculated from observations carried out from 1990 to 1997 in the vicinity of the Tono Mine, and employed for the RHS Project was applied to a groundwater simulation (steady-state). The results are compared with the data from groundwater monitoring in boreholes. The results show head distribution derived by the simulation has higher values than the actual observations. While this is presumably due to the calculated recharge rate and/or the head values assigned to the side boundaries, the reason has yet to be specified. Thus, on the assumption that the recharge rate used exerts a greater influence on the results of simulation, the recharge rate was amended to 0.14mm/day so that the simulated results would match the observed data. Taking spring water into consideration, the ground surface is postulated as a free seepage surface with unrestricted inflow and outflow of water possible. The determination of the recharge rate will be examined in more detail in future studies.

② Bottom boundary condition

The bottom boundary is set as a no-flow boundary.

③ Side boundary conditions

The side boundaries are considered to be groundwater flow divides. Three coincide with mountain ridges, the northern, eastern and western boundaries and are assigned constant head values to depth, as a permeable boundary. The constant head values assigned to the side boundaries are calculated by the following formula between the water level data in boreholes and elevations of the ground surface:

$$\Phi \text{ (constant head value)} = 0.86 \times H \text{ (elevation of each location)} + 18.5.$$

The boundary along the Toki River (southern boundary) is also assigned a definite hydrostatic head as a permeable boundary. The elevation of the river surface is used as the constant head values assigned to the southern boundary.

④ Galleries of the Tono Mine and the MIU shafts

Since the Tono Mine's galleries are modeled using nodal points exposed to atmospheric pressure, the constant head value is set as the pressure head of 0 m. As for the MIU shafts modeled using elements, corresponding elements are deleted from the hydrogeological model with the advance of planned shaft excavation. Nodal points corresponding with the shaft wall after excavation are regarded as free seepage points.

4.2.3.3.5 Groundwater flow simulation

The groundwater flow simulation adopts the saturated/unsaturated seepage flow analysis code (EQUIV-FLO) for an equivalent heterogeneous continuum (heterogeneous porous media). This code has governing equations including Darcy's law taking unsaturated domains and saturated flow conditions into consideration using the continuity equation for groundwater flow in porous media (conservation of mass

law) [70]. The 3-D steady-state/transient groundwater flow simulation was carried out from the viewpoint of the known hydrology with existing galleries of the Tono Mine and the predicted hydrology affected by the excavation of the MIU shafts.

(1) Simulation cases

Simulation cases were set as follows.

- Case 1 : steady-state homogeneous model
- Case 2 : steady-state truncated power law model
- Case 3 : steady-state negative exponential model
- Case 4 : transient homogeneous model
- Case 5 : transient truncated power law model
- Case 6 : transient negative exponential model

The excavation schedule of the shaft, which was used for the above transient simulations, was set as shown in Table 4.25. This schedule not only respects the work schedule [71] planned in 1998 FY but also takes the mesh structure of the hydrogeological model into consideration.

Table 4.25 Assumed schedule of shaft excavation

Stage	Depth (m)	Elevation (m)	Cumulative time (days)
2	21.8	209.635	39.1
3	41.0	190.435	73.5
4	60.2	171.235	108.0
5	79.4	152.035	142.4
6	101.8	129.635	182.6
7	145.3	86.135	260.8
8	205.9	25.535	369.4
9	266.4	-34.965	478.1
10	306.8	-75.365	550.1
11	327.0	-95.565	586.7
12	508.5	-277.065	912.5
13	508.5	-277.065	1,460.0
14	690.0	-458.565	1,638.0
15	871.5	-640.065	2,099.0
16	1,001.4	-769.965	2,250.0

(2) Results of the steady-state simulations

Steady-state simulations were carried out with the purpose of understanding the current groundwater hydrogeology in the study area and investigating initial conditions to predict effects of the shaft excavation. The results of simulations using the three models are shown in Figures 4.51, 4.52, 4.53 and 4.54. These show water pressure distribution from several perspectives, including a bird's-eye view, pressure distribution in horizontal sections, the pressure distribution in different vertical sections and the comparison between simulated and measured data of head and water pressure, respectively. The major results are as follows.

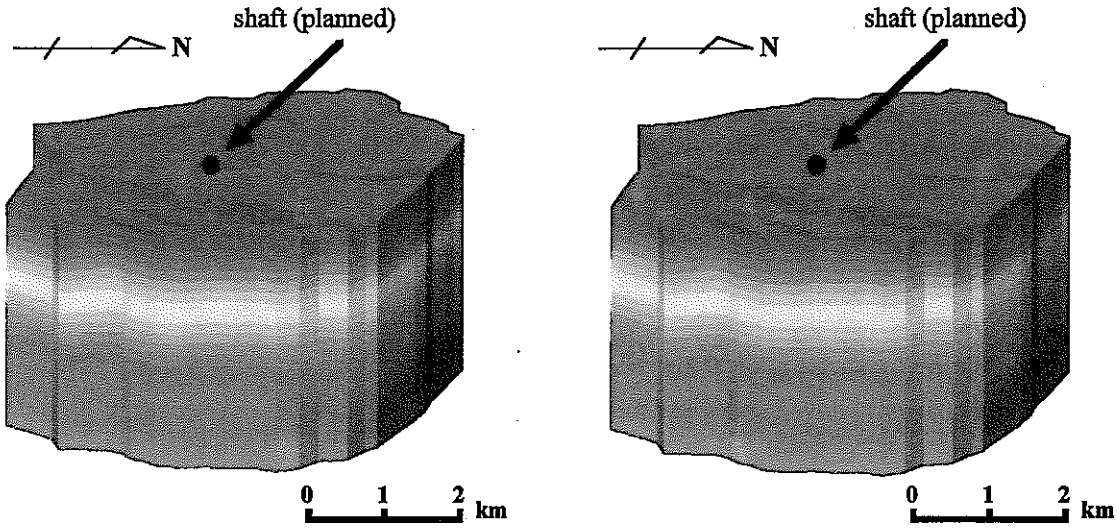

(a) Homogeneous model

(b) Truncated power law model

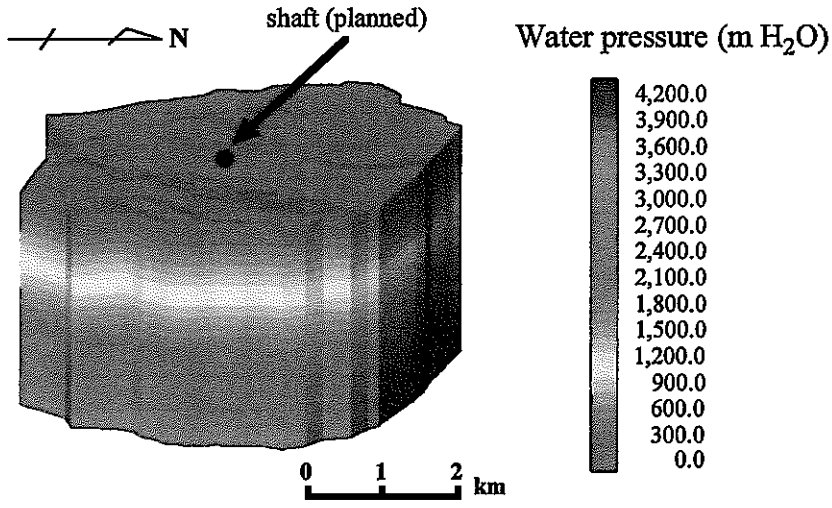

(c) Negative exponential model

Figure 4.51 Water pressure distribution (a bird's-eye view)

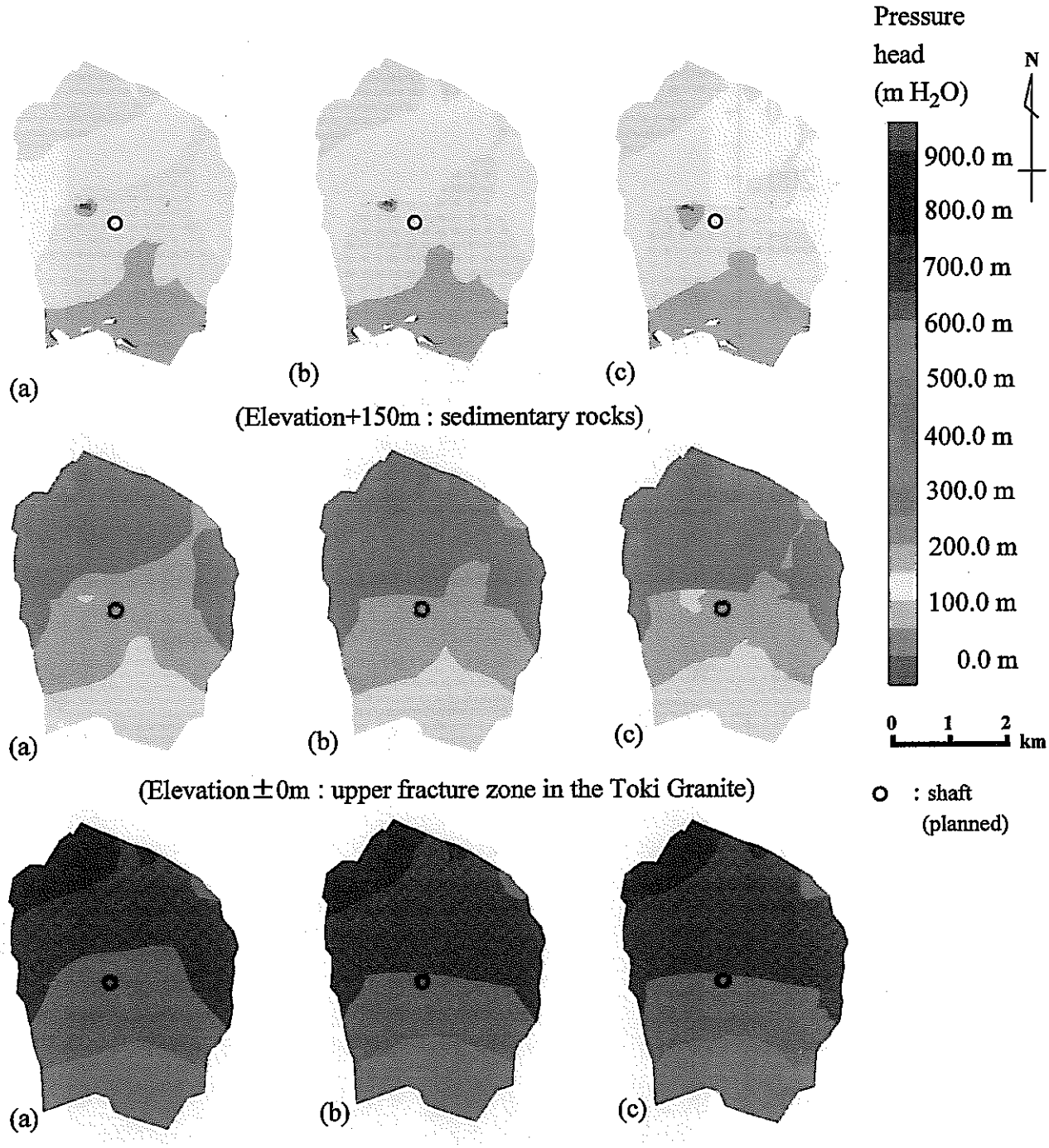

((a) Homogeneous model, (b) Truncated power law model, (c) Negative exponential model)

Figure 4.52 Pressure head distribution in horizontal plane

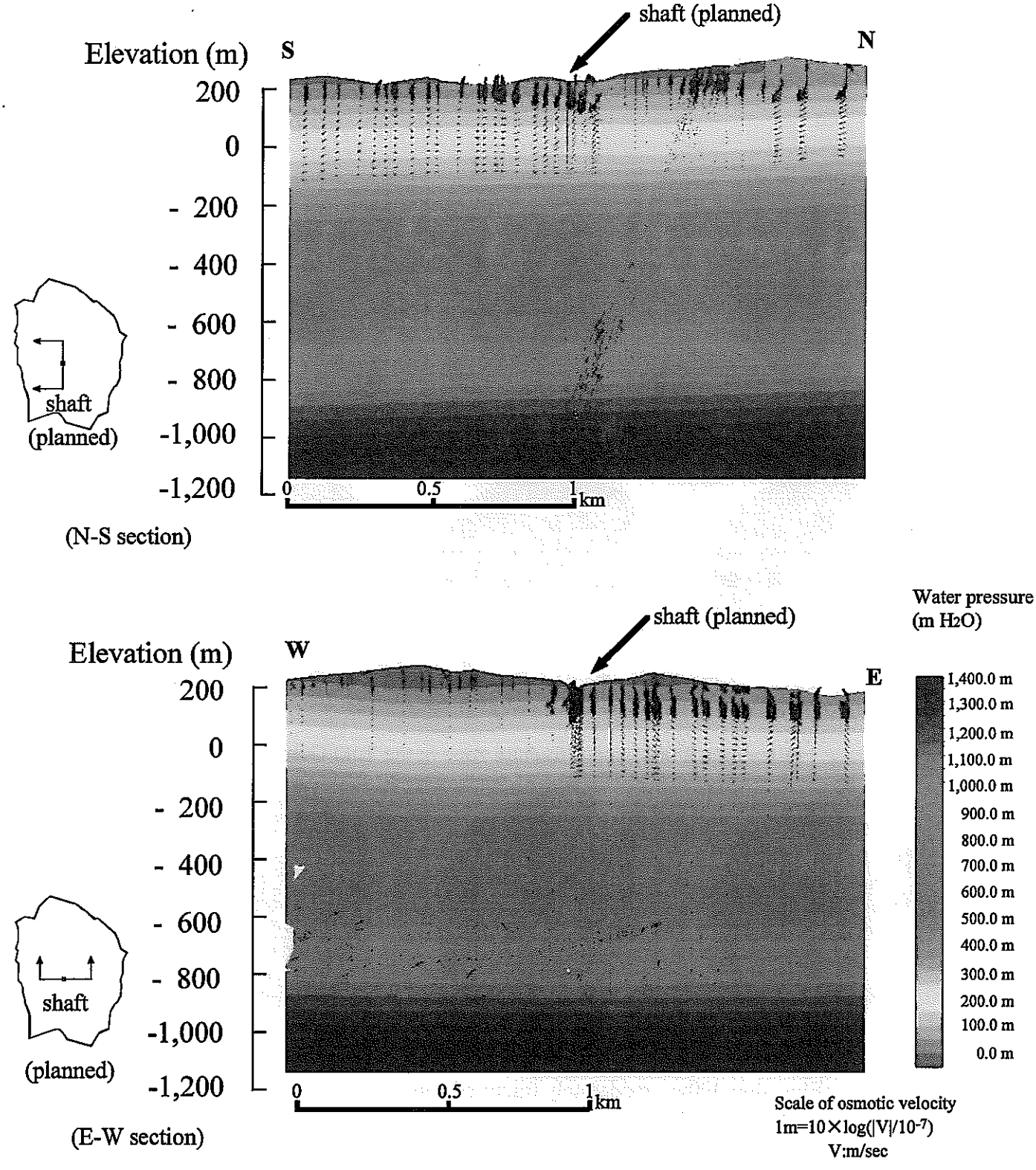

(a) Homogeneous model

Figure 4.53 Water pressure distribution in vertical section (1)

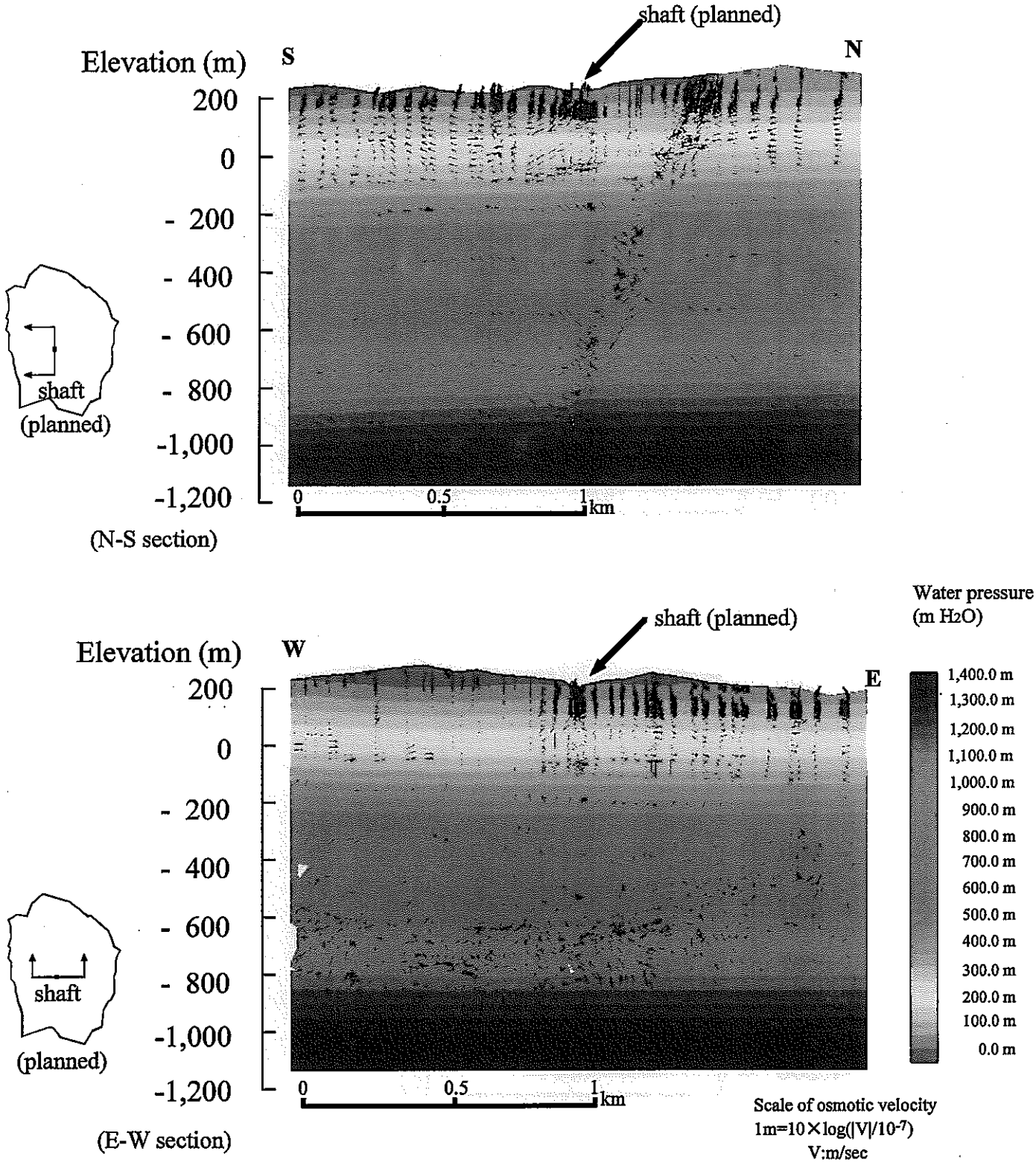

(b) Truncated power law model

Figure 4.53 Water pressure distribution in vertical section (2)

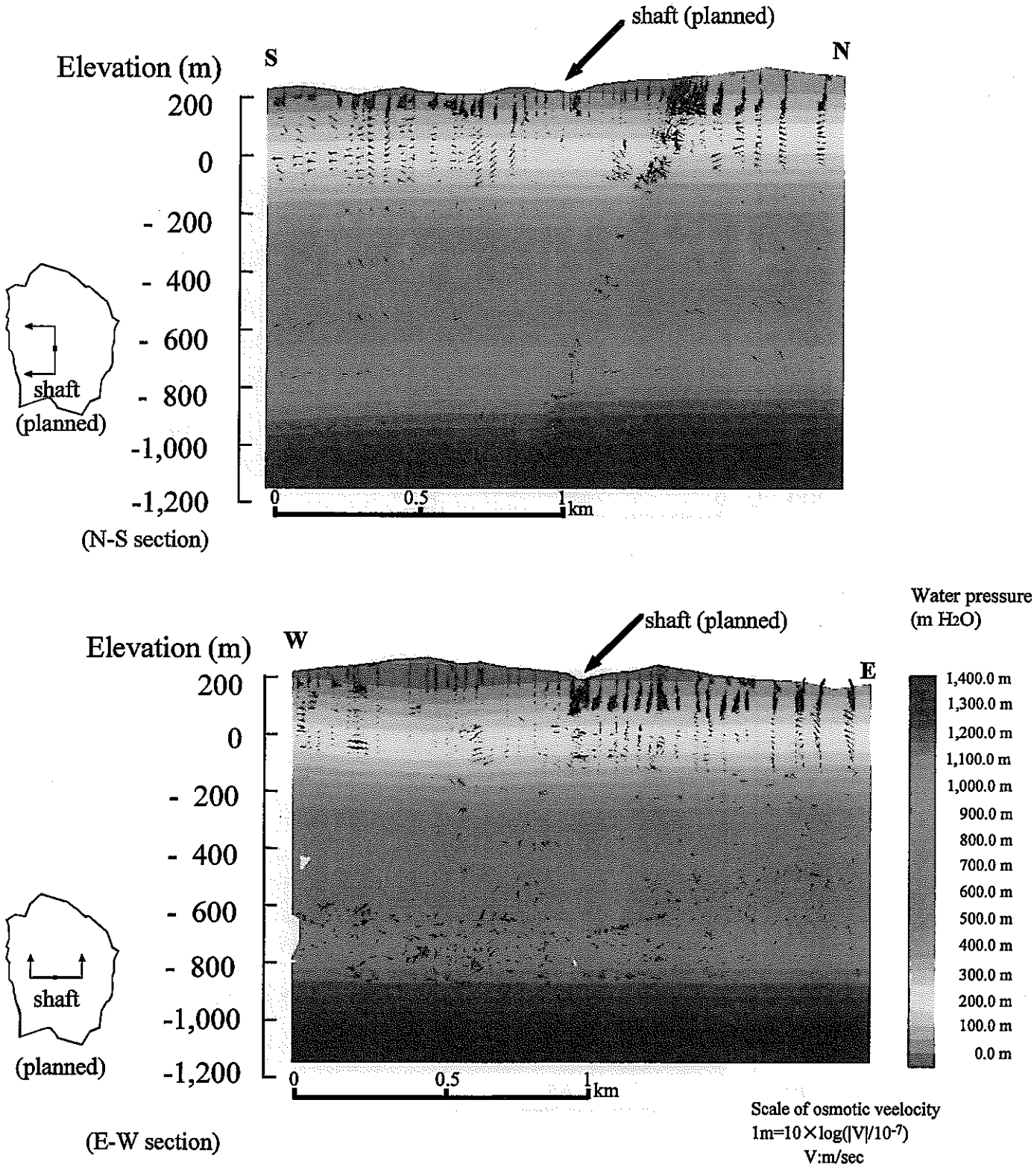

(c) Negative exponential model

Figure 4.53 Pressure head distribution in vertical section (3)

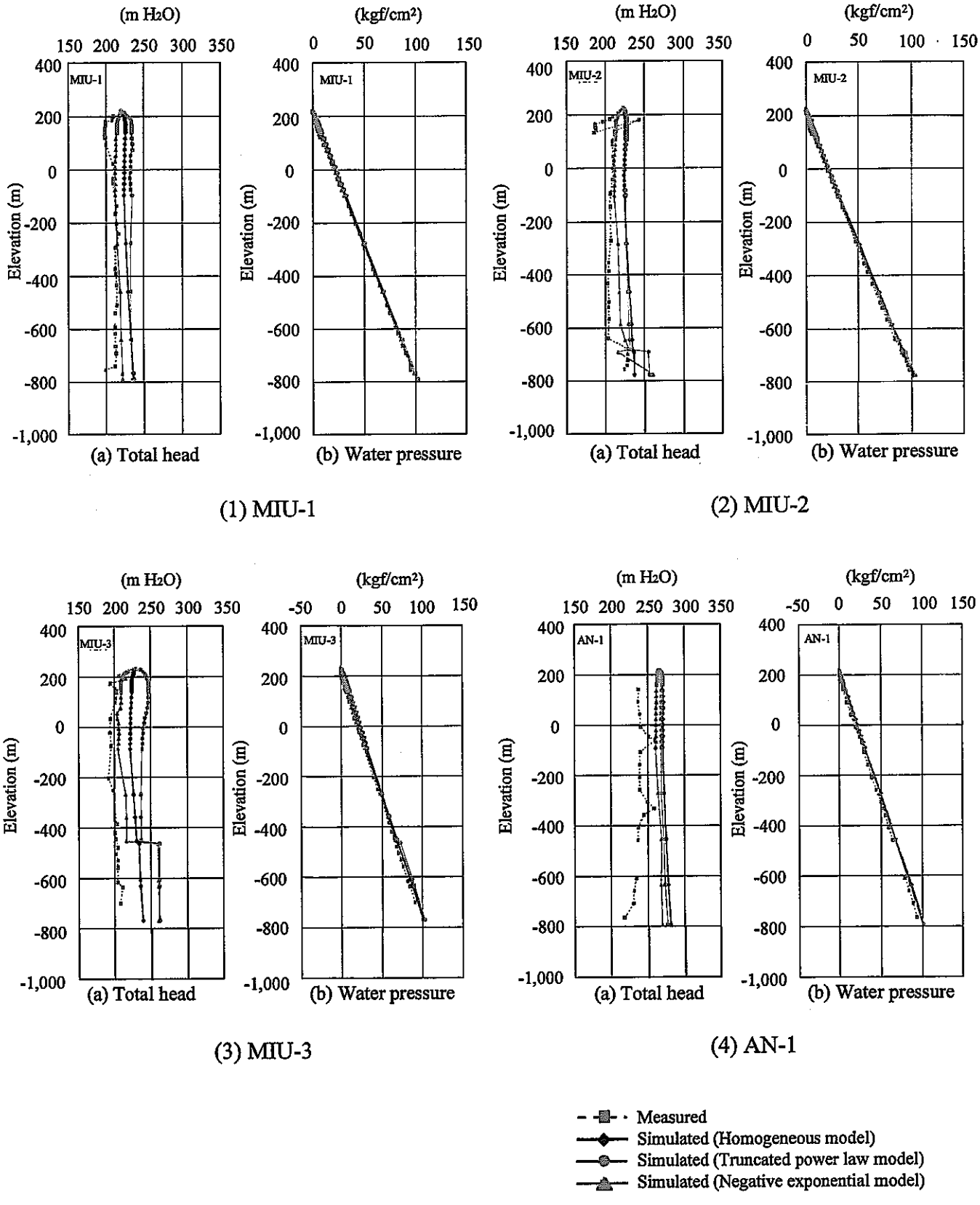

Figure 4.54 Comparison between simulated data and measured data of total head and water pressure

① Head. distributions in all the models indicate that the groundwater flow potential is from the northern side (mountain area) to the southern side (the Toki River) of the study area.

② In shallow parts, local topographical effects are seen; exemplified by a groundwater flow along the Hiyoshi River running from north to south on the east side of the study area (Figures 4.52, 4.53). Topographical effects on the pressure distribution reduce with depth, resulting in a dominant flow from north to south.

③ The groundwater flow simulation using the hydrogeological model in the 1st analysis loop fails to reproduce a barrier to flow effect across the Tsukiyoshi Fault. However, the hydrogeological model (homogeneous model) in the 2nd analysis loop does reproduce the barrier to flow effect.

④ All of the models used in the 2nd analysis loop more or less show a barrier-to-flow effect of the Tsukiyoshi Fault on the southward groundwater flow. Especially, the barrier-to-flow effect of the fault in the sedimentary rocks and the "Upper fracture zone" of the granite are shown in Figure 4.52. In the "Moderately fractured zone" remarkable barrier-to-flow effects of the fault were recognized in the truncated power law model and the negative exponential model, whereas it is less distinct in the homogeneous model. It is presumed to be due to a small difference in hydraulic conductivity in the model between the fault (10^{-10} m/s) and the "Moderately fractured zone" (10^{-9} m/s). On the other hand, the logarithmic mean of hydraulic conductivities of the "Moderately fractured zone" is set at 10^{-9} m/s. in both of the truncated power law model and negative exponential model. However, the hydraulic conductivity varies so widely that it can be as high as 10^{-6}m/s. in parts where fractures are concentrated or fractures with large opening widths occur. Thus, the barrier-to-flow effect of the fault probably appears more distinctly in the truncated power law model and negative exponential model than in the homogeneous model.

⑤ Flow rate in the granite varies in a narrow range in the homogeneous model, whereas highly permeable fractures generate locally fast groundwater flow in the truncated power law model and the negative exponential model (Figure 4.53).

⑥ Heads (measured) in the MIU-1, 2 and 3 are basically equal to hydrostatic pressures. On the other hand, heads in MIU-2 and 3, where the Tsukiyoshi Fault is intersected, change abruptly on opposite sides of the fault (Figure 4.54). Especially in MIU-2, the head on the footwall side of the fault is some 30 m higher than that on the hanging wall side, when converted to water level. While simulated values are generally higher than the measured ones, generally they are more conformable in the negative exponential model than in the other models. Also, pressure rise on the footwall side of the fault in MIU-3 was not measured. This is presumed to be due to a drop in water pressure caused by the penetration of the fault by MIU-2. Head values obtained by the homogeneous model are intermediate between those obtained by the truncated power law model and the negative exponential model (Figure 4.54).

⑦ The water pressure distributions in AN-1 and 3 in the southern part of the Shobasama Site are nearly hydrostatic. In AN-1, sections with locally high and locally low measured heads occur at depth. However, the simulations fail to reproduce these local variations in measured values. Furthermore, simulated heads are generally higher than measured ones.

(3) Results of the transient simulations

Results of the simulations in the following two stages out of the 16 shown in Table 4.25 are discussed below.

① Stage-13 : Left to stabilize for about one and half years after excavation to 508.5 m in depth

② Stage-16 : Shaft excavation is completed to 1,001.4 m depth after penetrating the Tsukiyoshi Fault

Effects of the shaft excavation on water pressure distribution in Stage-13 (shaft 508.5 m)

Stage-13 represents the point when the shaft is excavated to about half its total depth. Vertical profiles of the water pressure distribution shown in Figure 4.55 indicate that the shaft excavation causes a drop in the adjacent water pressure in all models. Furthermore, a lowering of water level around the shaft is wider than the stage prior to the excavation (Figure 4.53).

A cone-shaped drop in water pressure develops around the shaft in the homogeneous model (Figure 4.55 (a)). On the other hand, an asymmetric shape in the drop forms in both the truncated power law model and the negative exponential model (Figures 4.55 (b), (c)). These are created by the excavation effects propagated along permeable fractures intersected by the shaft. Especially, in the truncated power law model containing fractures with a large diameter (Figure 4.55(b)), extensive pressure drops are formed by fractures in the "Upper fracture zone" intersected by the shaft. The pressure drop also develops along fractures in the negative exponential law model (Figure 4.25(c)). However, the frequency of large fractures in this model is lower than the frequency in the truncated power law model, resulting in smaller pressure drops.

Effects of the shaft excavation, which is done entirely in the hanging wall to this point, do not extend beyond the Tsukiyoshi Fault in any models, hardly extend to the north side of the fault (Figures 4.55, 4.56). On the other hand, the pressure drop zone extends east and west, forming a striking contrast to the pressure distributions along the north-south profiles that feature an abrupt change at the fault (Figures 4.55, 4.56). The distribution of flow velocity vectors of groundwater in the north-south profiles indicates that water is supplied into the shaft from the ground surface and at depth through fractured zones around the fault. The truncated power law model and negative exponential model occasionally develop concentrated flows through fractures from the fractured zones around the fault toward the shaft.

Pressure distributions in the horizontal sections at elevations of +150 m and ±0 m above the shaft bottom (GL-508.5m; at an elevation of -277.0 masl) show a pressure drop around the shaft (Figure 4.56). The pressure drop area at an elevation of +150 m forms a concentric circle around the shaft in the homogeneous model (Figures 4.55, 4.56). However, the extent is too limited to exert an influence on the initial pressure distribution of the Tono Mine. The pressure drop in the truncated power law model affects the largest area among the three models, extending to the Tono Mine and the Shobasama Site. It is probably because the pressure drop along fractures in the granite has a large effect on the groundwater flow in the shallow part. The pressure drop area in the negative exponential model is not as large as in the truncated power law model. However, it extends to the pressure drop area of the Tono Mine. Excavation effects of the shaft are

found at an elevation of ±0 masl, too. The pressure drop area around the shaft in the homogeneous model is also linked with the pressure drop area around the Tono Mine. The effect, however, scarcely extends onto the north side of the fault. The affected area in the truncated power law model is the largest among the three models, partially extending to the north side of the fault, too. It is probably because parts of the fractures extend northward across the fault. Though fractures across the fault have yet to be ascertained, this gives a suggestion on the extent of potential excavation effects of the shaft when such fractures are actually verified. No effect of the pressure drop at an elevation of ±0 masl extends to the north across the fault in the negative exponential model. It is probably because there are fewer fractures with a large diameter in the negative exponential model than in the truncated power law model. Effects of the shaft excavation gradually lessen beneath the borehole bottom, scarcely found at an elevation of -600 masl except in the truncated power law model. In the truncated power law model, however, a small pressure drop area occurs even at an elevation of –700 masl, extending northward across the fault. This indicates that large fractures in the "Upper fracture zone" in the granite exert an extensive influence on pressure drop horizontally as well as vertically.

Effects of the shaft excavation on water pressure distribution in Stage-16 (shaft bottom 1001.4 m)

Stage-16 represents the point when the shaft excavation is completed after penetrating the Tsukiyoshi Fault. In this stage changes in water pressure extend into the footwall, the north side of the fault in all of the models (Figures 4.57, 4.58). In the homogeneous model, above all, a conical pressure drop domain extends on the both north and south sides of the fault to show a radial symmetry (N-S, E-W). This is thought to be caused by penetration of the fault by the shaft (Figure 4.58).

The water level distribution at excavation levels shallower than –300 masl on both the north and the south sides of the fault does not show a big change after the excavation extends below 508 m depth (Stage-13), (Figures 4.55, 4.57). This indicates that the shaft excavation influence on the water level in the shallow parts is reduced above an elevation of -300 m, as soon as the shaft passes through the sedimentary rocks and the "Upper fracture zone" of the granite. The water flows along the "Fracture zone along the fault" are more remarkable in Stage 16 than in Stage-13, directly pouring into the shaft.

The horizontal sections of pressure distribution show pressure drops on the north side of the fault in the truncated power law model and negative exponential model, which can be attributed to penetration of the fault by the shaft. However, they are not as extensive as in the homogeneous model (Figure 4.58). This indicates that the barrier-to-flow effect of the fault in the rock mass with homogeneous permeability differs from that in the rock mass with heterogeneous permeability. That is, it is presumable that effects of a pressure drop due to shaft excavation selectively propagate through highly permeable fractures in the heterogeneous model, whereas they almost concentrically (radially) spread in the homogeneous model. The magnitude of pressure drop area around the shaft, at an elevation of -600 masl (831.5 m depth), decreases in sequence from the homogeneous model to the truncated power law model and last to the negative exponential model. The order is the same as that of the fracture continuity.

There is little change in patterns of pressure distribution at an elevation of ±0 masl (231.44 m depth) between Stage-13 and Stage-16. Pressure drop areas develop around the shaft below an elevation of -400 m. The difference in pressure distribution among the three models is not as large as in the shallow part. It is probably because this section is in the "Moderately fractured zone", has fewer fractures and especially fewer fractures with large diameters.

(4) Summary

Results of the construction of the hydrogeological model and groundwater flow simulation are summarized as follows.

① In the 2nd analysis loop, homogeneous, truncated power law and negative exponential models were constructed. They were constructed on the basis of the data on fracture distribution and hydraulic conductivity obtained in the 1,000 m-deep MIU-1, 2 and 3 boreholes drilled inside the Shobasama Site. The truncated power law model is more dispersed in fracture diameter than the negative exponential model, that is, it contains fractures with larger diameter. The negative exponential model is aimed at a better reproduction of the heterogeneity in measured hydraulic conductivity and is characterized by a lower 1-D fracture density.

② No remarkable difference is found in groundwater flow prior to the shaft excavation between the homogeneous model (no fractures taken into consideration) and truncated power law model and negative exponential model (taking fractures into consideration).

③ The shaft excavation generates a conical pressure drop field around the shaft in the homogeneous model. On the other hand, it generates irregular pressure drop fields along the fractures in the other models. There is no large difference in effects of the shaft excavation in the "Moderately fractured zone" between the homogeneous model and the other models.

④ No effect of shaft excavation extends to the north side of the fault until the shaft penetrates the fault. After penetration, a pressure drop forms on the footwall side (north side) of the fault. The extent of the effect depends on the distribution of fractures. The present simulation indicates that an "equivalent continuum model" (model which takes the heterogeneities into consideration) has a more restricted extent of pressure drop. It probably results from the heterogeneities of hydraulic conductivity.

⑤ The "equivalent continuum model" allows representation of the fracture distribution (direction, density, size and permeability) in the hydrogeological model. Therefore, the "equivalent continuum model" can reproduce the low permeability of the Tsukiyoshi Fault, and is applicable as a methodology for evaluating the groundwater hydrogeology of a several km^2 area.

4.2.4 Future tasks

The results of the 1st analysis loop allow overall understanding of groundwater flow. However, their comparison with the measured values obtained through the subsequent borehole investigations indicated a large discrepancy in the head distribution in the granite. Furthermore, an important task recognized was to determine the cause of the discrepancy and the prioritization of data acquisition in order to reduce the uncertainty of the simulated results.

The 2nd analysis loop, including a groundwater flow simulation supplemented with data obtained by three borehole investigations, produced excellent results by application of an "equivalent continuum model". It makes the prospects better for more realistic hydrogeological models and groundwater flow simulations. It indicates that the study approach toward the systematization of methodologies and techniques for investigation, analysis and assessment are coming along well. Results of the past hydrogeological investigations indicated that sufficient data allowing a statistical processing can be obtained to advance model construction and groundwater flow simulation more effectively in the future. However, the present state is not yet satisfactory. Thus, planning the future investigations requires dealing with and resolving the uncertainties.

At the end of the reporting period, the 3rd analysis loop is to begin. In this loop, construction of the hydrogeological model is in progress on the both continuum and discontinuum, using a methodology of comparative analysis. The results of these investigations are planned to be evaluated through comparison with results of long-term pumping tests scheduled in 2001 FY and the subsequent observation on effects of the shaft excavation.

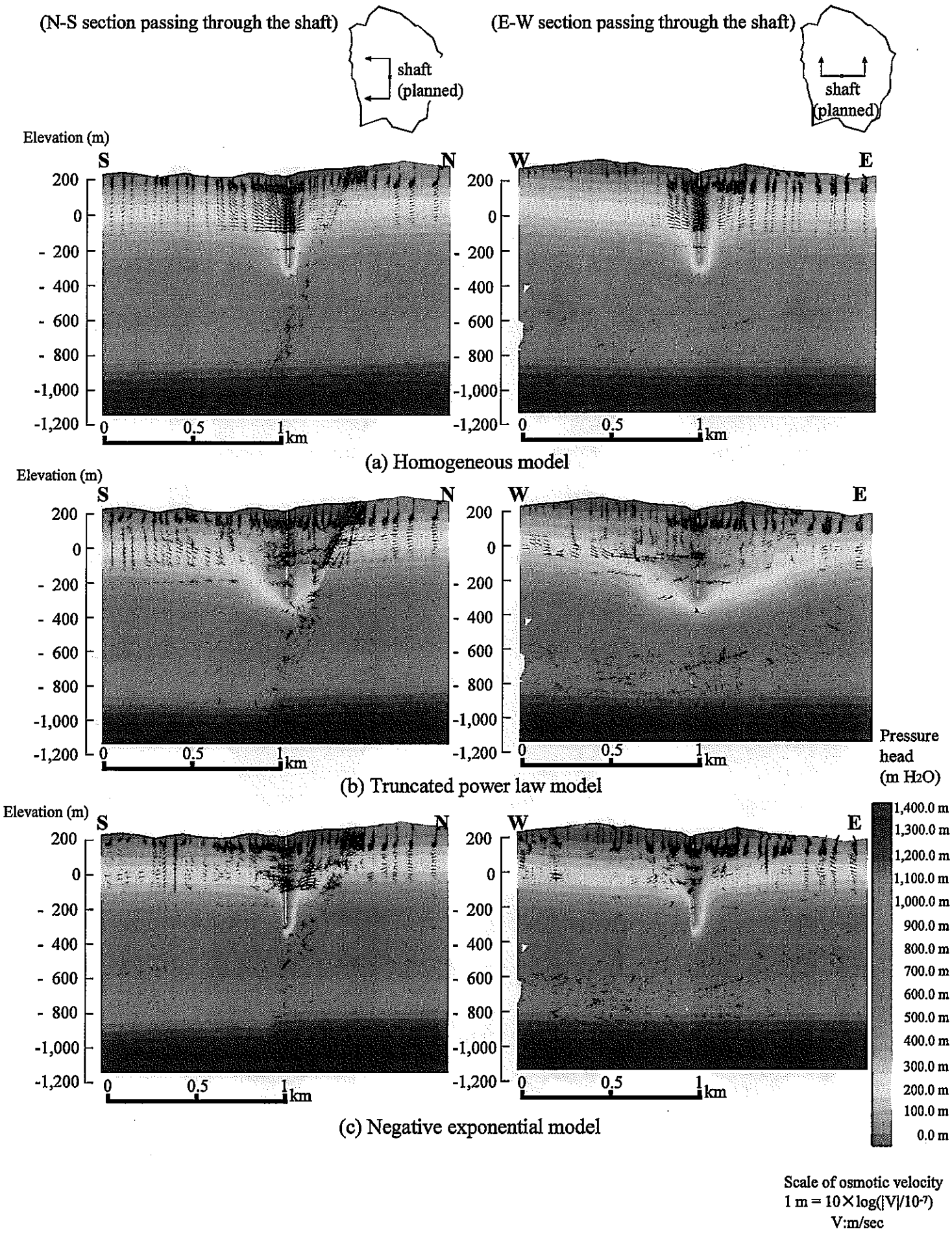

Figure 4.55 Pressure head in vertical section during stage-13 (508.5 mbgl in depth)

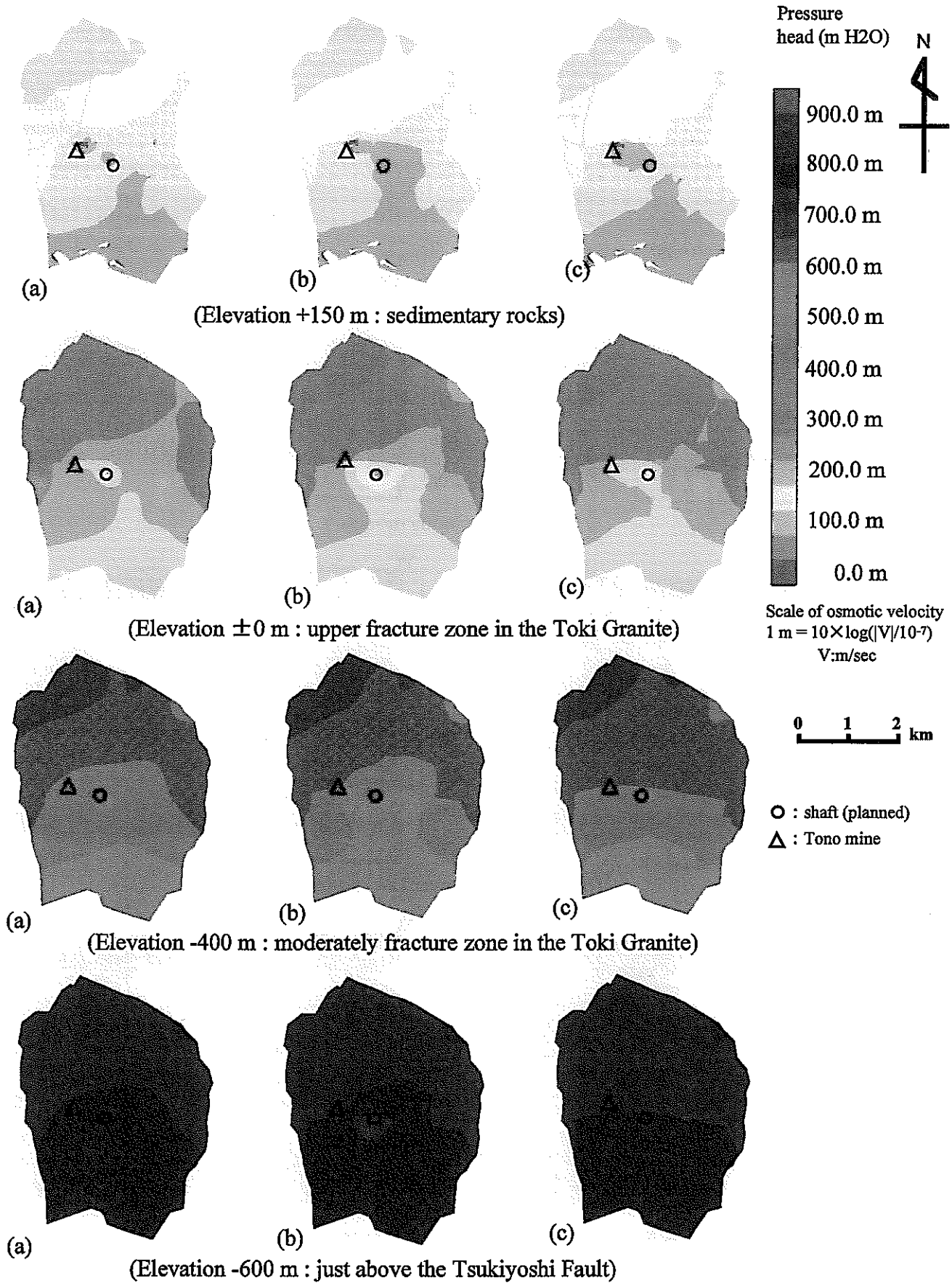

((a) Homogeneous model, (b) Truncated power law model, (c) Negative exponential model)

Figure 4.56 Pressure head in horizontal section during stage-13 (508.5 mbgl in depth)

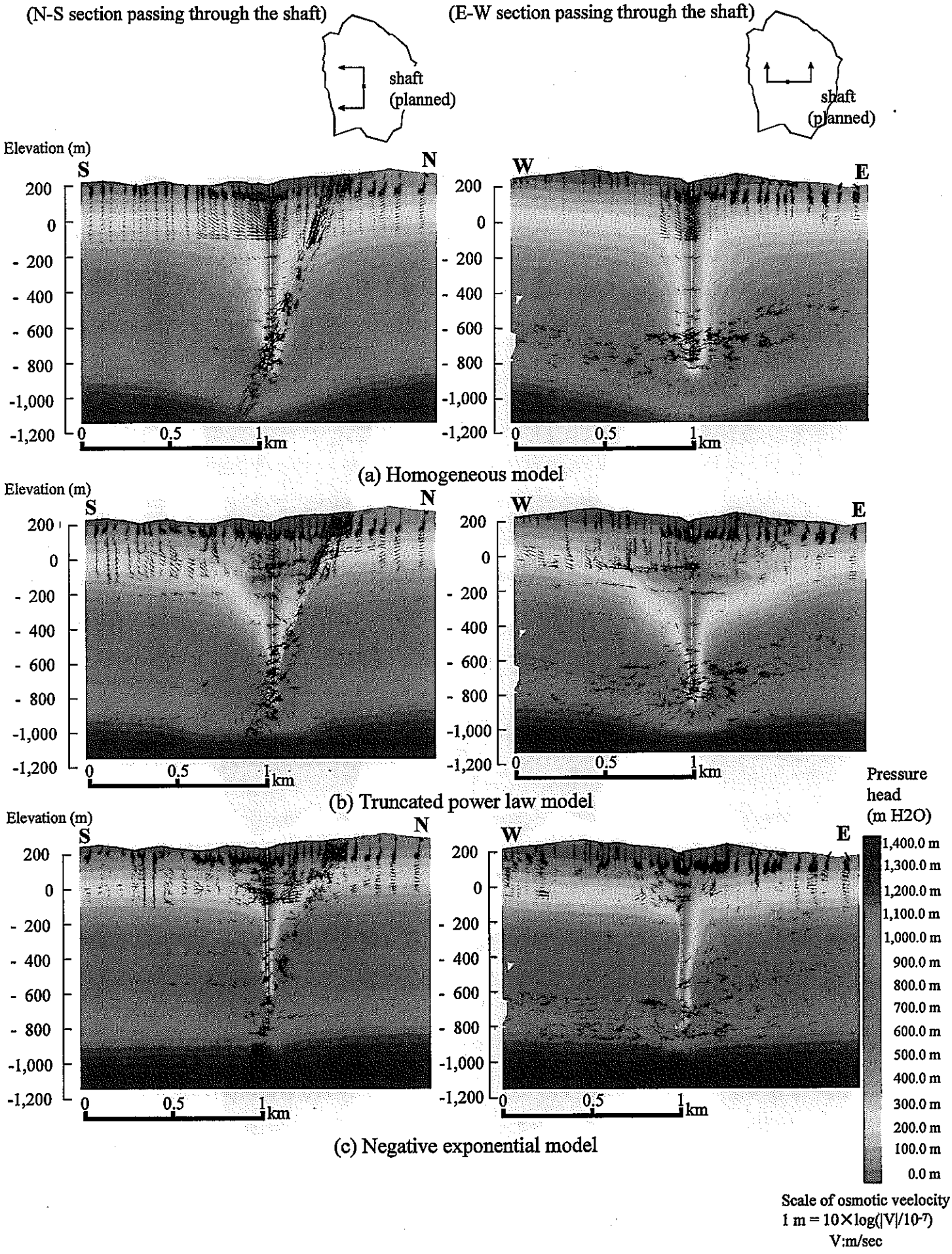

Figure 4.57 Pressure head distribution in vertical section during stage-16 (1,001.4 mbgl in depth)

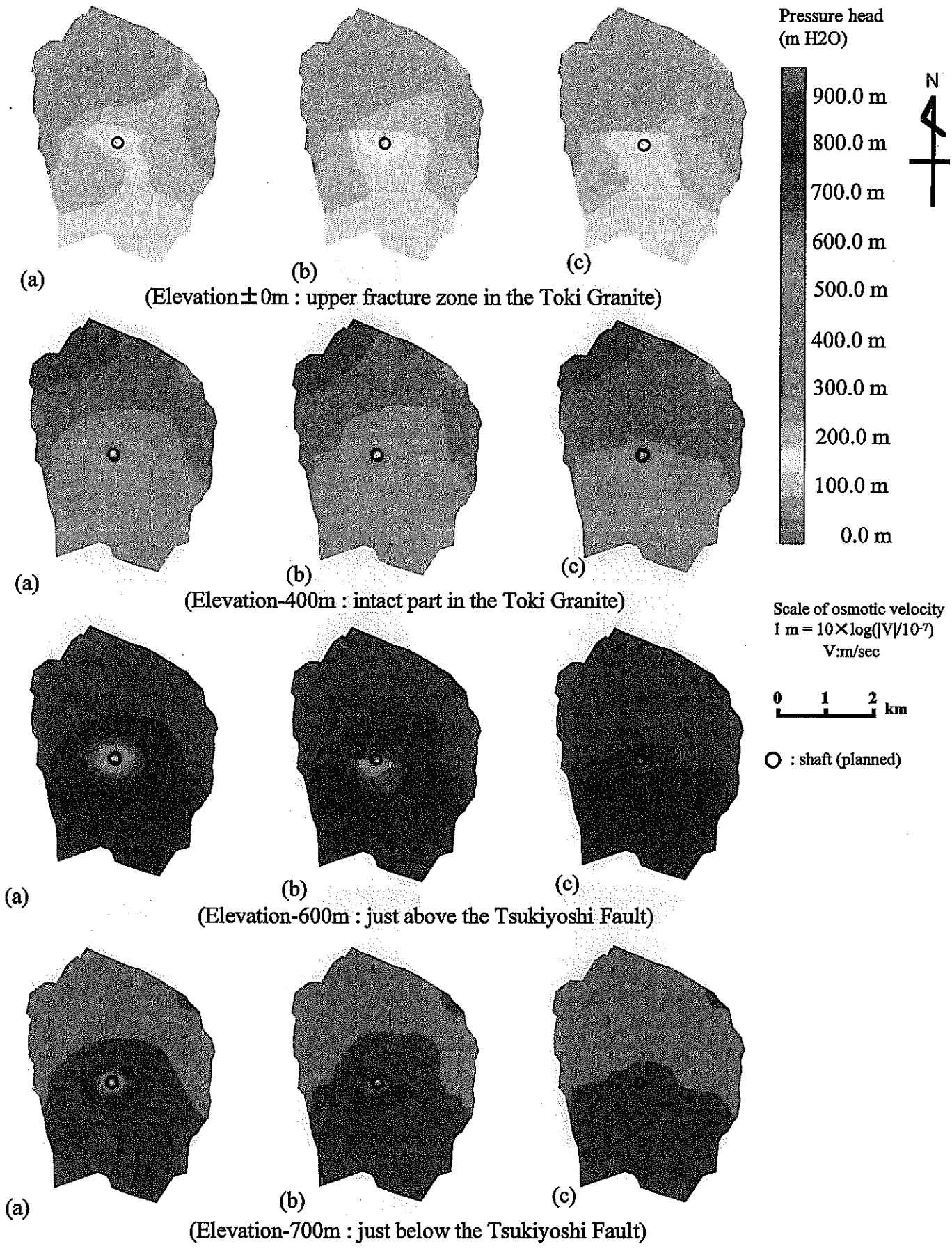

((a) Homogeneous model, (b) Truncated power law model, (c) Negative exponential model)

Figure 4.58 Pressure head distribution in horizontal section during stage-16 (1,001.4 mbgl in depth)

4.3 Hydrochemical investigations

4.3.1 Overview

4.3.1.1 Objectives

The objectives of the hydrochemical investigations, based on the goals set for the entire MIU Project and its Phases, are set as follows [7].

① Data acquisition on hydrochemical properties of groundwater in the individual geological formations and geological units (faults, fracture zones, etc.) between the surface and depth at the Shobasama Site

② Clarification of the mechanism(s) that control the evolution of groundwater chemistry, construction of a hydrochemical model and testing its accuracy by comparison with data

③ Prediction of change in hydrochemical properties of groundwater with the advance of the shaft excavation

④ Development of methodologies for systematic investigations and analyses of hydrochemical properties of groundwater

4.3.1.2 Performance of the study

It is important for hydrochemical investigations to know whether the data on hydrochemical properties of groundwater obtained by investigations at the Shobasama Site are representative of the chemistry of the groundwater widely distributed there. This necessitates specifying the evolution of groundwater chemistry (reaction between water and rock) by investigating geological structures, and chemical and mineralogical compositions of rocks. Furthermore, it requires the knowledge reaction time between rock and water. Consequently, it becomes important to know the residence time of groundwater. In addition, it is thought that the residence time of groundwater could provide data to support groundwater flow simulation results [72]. In addition, examination of the evolution of groundwater chemistry and the residence time necessitate hydrochemical data on rainwater and river water as indicators of initial conditions.

4.3.2 Current status

4.3.2.1 Knowledge obtained from the RHS Project

The following is a synopsis of the knowledge obtained during the RHS Project carried out in the area including the Shobasama Site.

① River water collected at 29 locations has been classified as Ca^{+2}-Na^{+}-$HCO3^{-}$-type [61]. This fact indicates that this type of groundwater is one of the candidate water chemistry types expected in the Seto and Mizunami Groups and the shallow part of the Toki Granite. It suggests that the groundwater of the RHS Project area is of meteoric-type [61].

② Chemical analyses of groundwater collected at 20 points in 6 boreholes and measurements of physicochemical parameters were carried out. The results indicate that groundwater in the

shallow part (< 300 m in depth) of the granite is also of Ca^{+2}-Na^{+}-$HCO3^{-}$-type, neutral (pH 7) and oxidizing (Eh>0 mV). On the other hand, the groundwater in the deeper part (> 300 m in depth) is Na^{+}-$HCO3^{-}$-type, alkalic (pH 9) and reducing (Eh<-300 mV) (Figures 4.59, 4.60) [60].

③ The following knowledge on microbes in groundwater is obtained by determining the total bacteria population and analysis of specific bacteria types (sulfate reducing bacteria, iron oxidizing bacteria) in groundwater in the Toki Granite and Mizunami Group.

- The total number of bacteria ranges from 10^6 to 10^7 cell/ml, regardless of rock type or depth.
- There are depth ranges that lack sulfate reducing bacteria and some with as little as 10^3CFU (Colony Forming Unit)/m.
- The number of iron oxidizing bacteria ranges from 10^4 to 10^5 cell/ml throughout the entire range of depths sampled.

④ Chemistry of groundwater in the Toki Granite is formed by dissolution of pyrite and calcite, argillization of feldspars, and ion exchange between groundwater and clay minerals [60].

⑤ Results of measurement of hydrogen-oxygen isotope ratios indicate that groundwater in the Toki Granite is of meteoric water origin. However, the measurement of ^{14}C suggests that the residence time is some ten thousand years for groundwater around 1,000 m depth [15].

4.3.2.2 Current status of investigations in the MIU Project

Simultaneous data acquisition from the various study fields in the same borehole is not only time-saving but advantageous for comparative examinations of the data from different perspectives. In borehole investigations in the initial stage of the RHS Project, physical logging, hydraulic tests and pumping tests were carried out in this order after borehole drilling using fresh water. However, incidents such as borehole collapse at large-scale fracture zones and loss of drilling fluid into the rock mass, rendered it difficult to collect representative groundwater.

Based on this experience, groundwater sampling in MIU-1, 2 and 3 was planned to be carried out after geophysical logging, hydraulic tests, installation of the MP system in the boreholes and long-term pumping. Thus, MP systems were installed in MIU-1 and 2 in the reporting period; it was also planned that this system be installed in MIU-3 in 2000 FY. However, groundwater sampling in MIU-1 and 2 could interfere with other simultaneous borehole investigations (including hydraulic tests, etc.). Therefore sampling has yet to be carried out. The timing of water collection will be decided based on the progress of borehole investigations.

Based on the failure to efficiently collect water in MIU-1, 2 and 3, a change in investigation procedure was planned for MIU-4 investigations (planned in 2000 FY). According to this change, water collection would be carried out in combination with pumping tests subsequent to immediate suspension of drilling, if drilling fluid loss occurred [45]. In addition, a known concentration of dye would be added to drilling fluid to identify residual drilling fluid in the groundwater lost during pumping. This would be to ensure that samples representative of in situ groundwater are obtained and also, that data quality in the determination of the hydrochemistry of the groundwater would be maintained. Also, different dyes would be used in the sedimentary rocks, in the hanging wall and in the footwall of the Tsukiyoshi Fault on the assumption that

these zones might have different hydrochemical properties and to check on possible interconnectivity of the rock units Pumping tests carried out as part of hydraulic tests are utilized to prepare for groundwater sampling by removal of drilling fluid. The pumping would stop when the concentrations of dye added to the drilling fluid has been reduced to a predetermined value and also, in consideration of the physicochemical parameters obtained by continuous monitoring of groundwater.

Furthermore, hydrochemical data is obtained as part of the study on the evolution of groundwater chemistry using rock core. Measurements of the ratio between Fe^{3+} and Fe^{2+} in the granite indicate that Fe^{3+}/Fe^{2+} is higher at shallow levels (< 300 m depth), but decreases with depth (> 300 m in depth). This indicates that oxidation-reduction environment in the granite probably changes at around 300 m in depth.

4.3.3 Future tasks

In the reporting period, no data on hydrochemical properties of groundwater were obtained in the MIU Project. Therefore, the collection and analysis of groundwater are the priority tasks of future investigations. Based on an improved plan of borehole investigations of the MIU-4, high quality data is expected to be obtained.

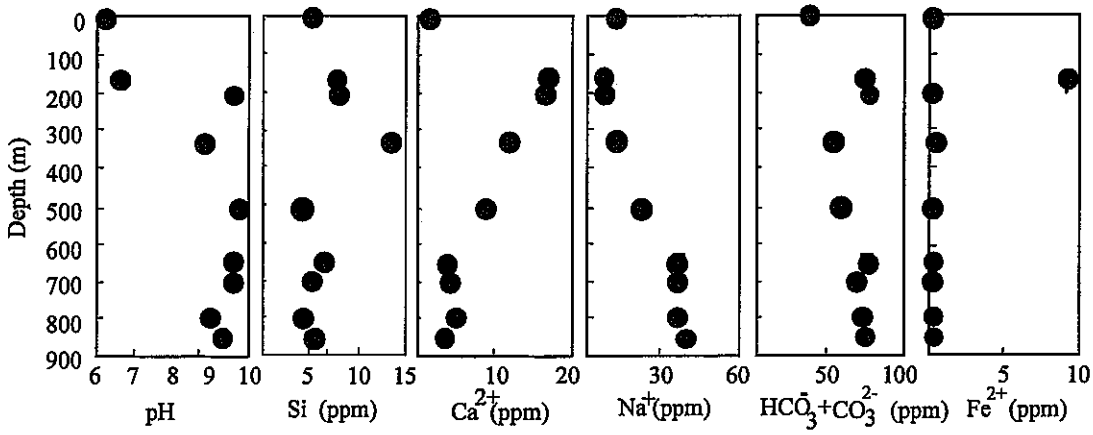

Figure 4.59 Changes in ground water chemistry in granite in the Tono area by depth

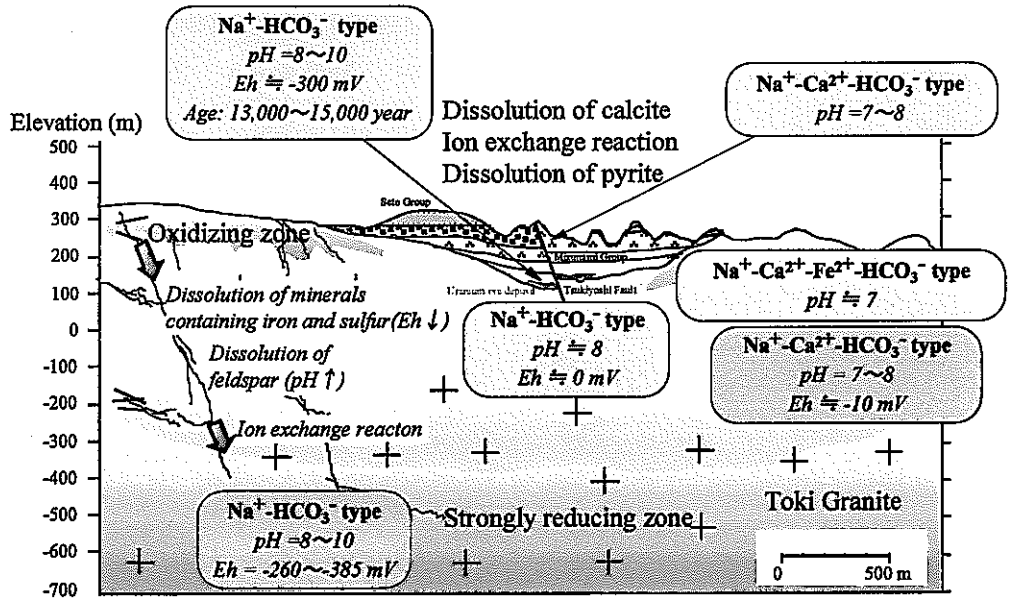

Figure 4.60 Geochemical evolution of the groundwater in the study area [59)]

4.4 Rock mechanical investigations

4.4.1 Overview

4.4.1.1 Objectives

The objectives of the rock mechanical investigations, based on the goals set for the entire MIU Project and its Phases, are as follows [7].

① Acquisition of data on the mechanical properties of the rock mass between the surface and depth at the Shobasama Site

② Determination of the in situ stress state, construction of the rock mechanical model and confirmation of its appropriateness

③ Prediction of changes in the mechanical stability of the rock mass adjacent to the shaft during shaft excavation

④ Development of methodologies for systematic investigation and analyses of rock mechanical properties of the rock mass

4.4.1.2 Performance of the study

This investigation targets the granite. In general, properties of structural discontinuities and their distribution patterns exert a great influence on in-situ mechanical properties of the rock mass. For example, it is assumed that the Tsukiyoshi Fault has a great effect on the stress state of the rock mass distributed in the Shobasama Site. In these investigations, construction and revision of rock mechanics conceptual models were done for the Shobasama Site following analysis of the survey results from AN-1 and MIU-1, 2 and 3. The rock mechanics conceptual model refers to a model in which the rock mass can be divided into several zones according to physical/mechanical properties and in situ stresses. A numerical rock mechanical model was constructed by setting of quantitative physical values based on the rock mechanics conceptual model. With this model, a predictive simulation was carried out to assess the mechanical effects of drift excavation.

The information on rock mechanical data was obtained by a variety of methods, including borehole geophysics, in situ borehole testing such as hydraulic fracturing to determine in situ stress state and a variety of laboratory tests on core to determine rock mass properties and estimates of in situ stress. Based on the results, a rock mechanics conceptual model for the Shobasama Site was constructed. In practice, as each new borehole was drilled to obtain rock mechanical data, the conceptual model would be compared with the new information and revised as necessary. As a result, the conceptual model was revised based on results of the comparative study.

In this report, concepts, contents, results and evaluation of investigations in the AN-1, MIU-1, 2 and 3 are described and the rock mechanics conceptual model is shown.

4.4.1.3 Overview of the investigations

The investigations were divided into two components, determination of physical properties of the rock mass and determination of in situ stress distributions in terms of magnitude and direction.

Physical properties of the rock mass

The distribution of rock mass properties between the surface and a depth of 1,000 m was determined by physical and mechanical property tests of core samples. The physical property tests measure apparent specific gravity, water content, effective porosity and elastic wave (P-wave, S-wave) velocity. The mechanical tests consist of uniaxial compression tests, Brazilian tests and triaxial compression tests. All of the tests were carried out based on ISRM guidelines or JIS standards.

In situ stress

The distribution of in situ stresses between the ground surface and a depth of 1,000 m was investigated by AE/DRA tests on core samples and hydraulic fracturing tests in boreholes. The AE/DRA testing was intended to obtain data on the vertical distribution of in situ stress. The hydraulic fracturing tests were aimed at obtaining data on the distribution of principal stress magnitudes and directions. The hydraulic fracturing tests were employed not only because it was an accepted and best available test at the time to measure the in situ stress state from the ground surface to a depth of 1,000 m, but also because vertical stresses could be one of the principal stresses in this area according to the previous work [73,74].

To ensure the investigation results are comparable, the same types of studies were done in all boreholes. However, the number and depths of testing vary according to the individual boreholes. The tests items carried out in the individual boreholes are shown in Table 4.26. Physical property tests, mechanical property tests, AE/DRA tests and hydraulic fracturing tests number some 20 to 180, 20 to 90, 10 and 10 to 20, in each borehole respectively. As was stated in the geology section, the Shobasama Site is underlain by fractured granite; therefore, results of BTV investigations were used to choose the depths for hydraulic fracturing tests.

Table 4.26 Number of rock mechanical investigations

	Item	AN-1	MIU-1	MIU-2	MIU-3
Physical property	Apparent density	20	180	20	40
	Effective porosity	20	180	20	40
	Water content	20	180	20	40
	Seismic wave velocity (P-wave and S-wave)	20	180	20	40
Mechanical property	Uniaxial compressive test	20	90	20	10
	Brazilian test	40	30	40	10
	Triaxial compressive test	-	90	-	30
In situ stress determination	AE/DRA	-	10	10	10
	Hydraulic fracturing	20	-	20	10

4.4.2 Construction of the rock mechanics conceptual model

4.4.2.1 Overview of the investigations in the AN-1 and the MIU-1 [39, 75~77]

Concept of the investigations

Investigations were carried out in the two 1,000 m-deep boreholes in the early stages of investigations at the Shobasama Site. These are the first investigations carried out using 1,000 m-deep boreholes. Their main aim was to obtain comprehensive data on physical properties and the in situ stresses of the rock mass between the ground surface and 1,000 m in depth.

Scope of the investigations

Based on the objectives and concepts discussed in the above Overview, Section 4.4.1, physical and mechanical property tests and in situ stress measurements were carried out at intervals of about 100 m and 50 to 100 m, respectively. The specifications and quantity of physical/mechanical property tests performed in AN-1 and MIU-1 are shown in Table 4.27. Depths of the in situ stress measurements are shown in Table 4.28.

Table 4.27 Details of physical/mechanical property tests in AN-1 and MIU-1

	Item	Specification	AN-1	MIU-1
Physical property	Apparent density	ISRM method	20	180
	Effective porosity	ISRM method	20	180
	Water ratio	ISRM method	20	180
	Seismic wave velocity (P wave and S wave)	Receiver and transmitter : 200kHz	20	180
Mechanical property	Uniaxial compression test	Loading rate (3kgf/cm^2/s)	20	90
	Brazilian test	Loading rate (3kgf/cm^2/s)	40	30
	Triaxial compression test	ISRM method	-	90

Table 4.28 Measurement depth of in situ stress measurements at the AN-1 and MIU-1

Test	Borehole	Measurement point	Measurement depth (m)
AE/DRA *	MIU-1	10	196.13-196.32; 297.77-298.21; 409.64-409.56; 504.04-504.43; 590.64-592.39; 674.70-674.96; 799.62-799.67; 896.52-896.78; 932.63-932.76; 990.04-990.36
Hydraulic fracturing **	AN-1	20	49.0; 97.0; 156.0; 199.0; 249.0; 309.0; 351.0; 404.0; 439.0; 498.5; 564.0; 600.0; 651.0; 700.0; 749.0; 790.0; 850.0; 900.0; 941.0; 991.0

*: Sampling depth for AE/DRA

**: Mid-point of test interval depth for hydraulic fracturing

Results of the investigations

Results of the physical/mechanical property tests in AN-1 and MIU-1 are shown in Table 4.29 and Figure 4.61. The data varied so widely that results approximated by quartic polynomial expression are also shown in Figure 4.61 to show the relationship between the individual physical property values and depths. Vertical

in situ stress values obtained by AE/DRA tests in the MIU-1 are shown in Figure 4.62. Horizontal in situ stress states obtained by hydraulic fracturing tests in the AN-1 are shown in Figure 4.63. Hydraulic fracturing tests carried out at four depths, 97.0 m, 156.0 m, 439.0 m and 749.0 m, in AN-1 did not produce any longitudinal fracturing needed to satisfy the theoretical assumption. Therefore, the tests at these depths are not used for assessment of stress states and are not shown in the Figure. Also, pore water pressures of the rock mass at depth exert a great influence on values of calculated maximum principal stress. Therefore, both values of maximum principal stress with pore pressures (σH_{min}) taken into consideration and without pore pressure (total stress; σH_{max}) taken into consideration are shown in Figure 4.63. Concerning azimuths of maximum principal stress, the error ranges obtained by a linear approximation using the least squares method for the longitudinal fractures produced by hydraulic fracturing are also shown in Figure 4.63 (b).

Table 4.29 Results of physical/mechanical property tests in AN-1 and MIU-1

	Item	Unit	AN-1	MIU-1
Physical property	Apparent density	-	2.59 to 2.62	2.61 to 2.64
	Effective porosity	%	1.0 to 1.8	1.0 to 1.8
	Water content	%	0.15 to 0.30	0.30 to 0.70
	Seismic wave velocity (V_p)	km/s	4.0 to 4.5	5.0～5.8
	Seismic wave velocity (V_s)	km/s	2.2～2.7	2.8～3.0
Mechanical property	Uniaxial compression test	MPa	120～240	130～250
	Young's modulus (E_{50})	GPa	34～60	45～65
	Poisson's ratio	-	0.30～0.37	0.30～0.37
	Tensile strength (by Brazilian test)	MPa	3～11	4～11
	Cohesion	MPa	-	20～26
	Internal friction angle	Degree	-	50～60

Evaluation of the results

Both physical and mechanical properties of the rock mass in AN-1 show an uneven distribution. The relationships between these properties and depth show different tendencies in the following sections:

- Surface to 300 m in depth
- 300 to 700 m depth
- More than 700 m depth

These relationships in MIU-1 are similar to those in AN-1. Characteristically, values of specific gravity and tensile strength change periodically.

The values of vertical stress obtained by AE tests on core from MIU-1 are thought to be equal to overburden pressure approximated by unit weight and overburden. However, the measured values at 590.64 to 592.39 m, 896.52 to 896.78 m and 990.04 to 990.36 m in depth actually range from a half to a fifth the estimated overburdens. At these depths, fractures are abundant and fracture surfaces are softened. Also, stress discontinuities are found in these depths in the hydraulic fracturing tests. These facts suggest that stresses change locally at these depths. On the other hand, no clear critical point appears in any stress-strain difference curve produced by one to five- repeat loadings. Also, the DRA tests show wide

strain differences in the calculation of vertical stress. These facts suggest that the reliability of the estimated stresses may be low.

Regarding the in situ stress state in horizontal planes determined by hydraulic fracturing tests in AN-1, the maximum principal stress decreases at 300 m and 700 m depth. Furthermore the maximum principal stress does not increase in a uniform linear pattern with depth. Given that vertical stress is equal to calculated overburden pressure, 3-D stress states expected are as follows:

- 0 to 300 m depth - Reverse-fault-type ($\sigma_H > \sigma_h > \sigma_v$),
- 300 to 700 m depth - Transitional-type ($\sigma_H > \sigma_h \fallingdotseq \sigma_v$), and
- 700 to 1,000 m depth - Strike-slip-fault-type ($\sigma_H > \sigma_v > \sigma_h$)

The maximum principal stress orientation changes as follows:

- 0 to 250 m depth - N-S
- 300 to 1,000 m depth - NW to WNW

Thus, the horizontal in situ stresses around AN-1 are divided into three sections: 0 to 300 m, 300 to 700 m and 700 to 1,000 m depth.

Referring to the results of BTV investigations in AN-1 and MIU-1, the characteristics of the fracture distribution in the Shobasama Site were examined. Histograms of fracture frequency distributions observed by BTV investigations in 50 m intervals in these boreholes between the ground surface and 1,000 m in depth are shown in Figure 4.64. These histograms indicate that the degree of fracturing changes at depths of about 300 m and 700 m in AN-1 and 350 m and 750 m in MIU-1, respectively. The results of the BTV investigations affirm the division into three sections based on the results of in situ stress measurement.

4.4.2.2 Construction of rock mechanics conceptual model [78]

As previously stated, the physical and mechanical properties, in situ stress state and fracture distributions change at about 300 m and 700 m in depth. Consequently, a rock mechanics conceptual model can be constructed in which rock mass is divided into three zones with different physical/mechanical properties and stress states at the above depths.

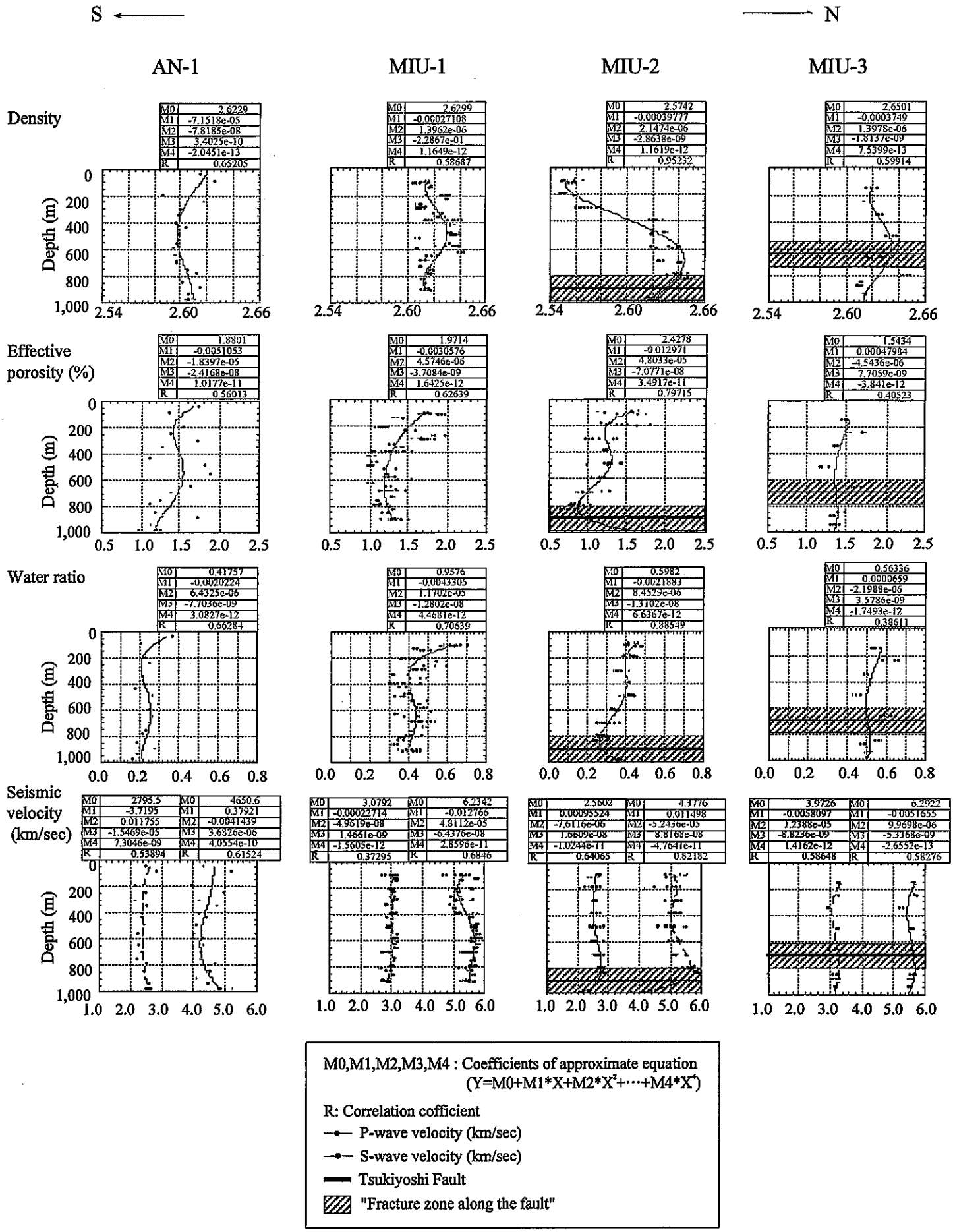

(a) Physical properties

Figure 4.61 Physical and mechanical properties of the Toki Granite

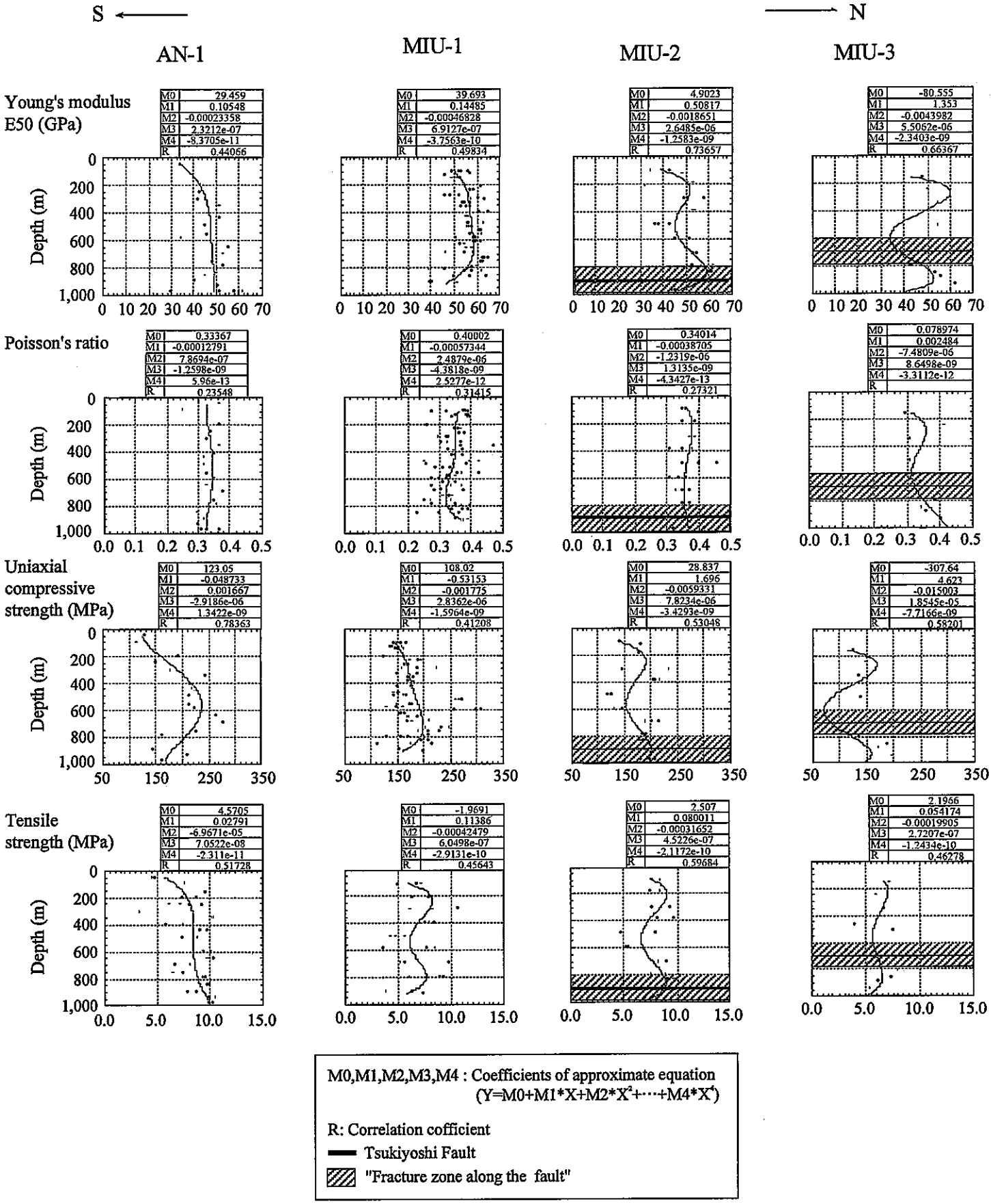

(b) Mechanical properties

Figure 4.61 Physical and mechanical properties of the Toki Granite

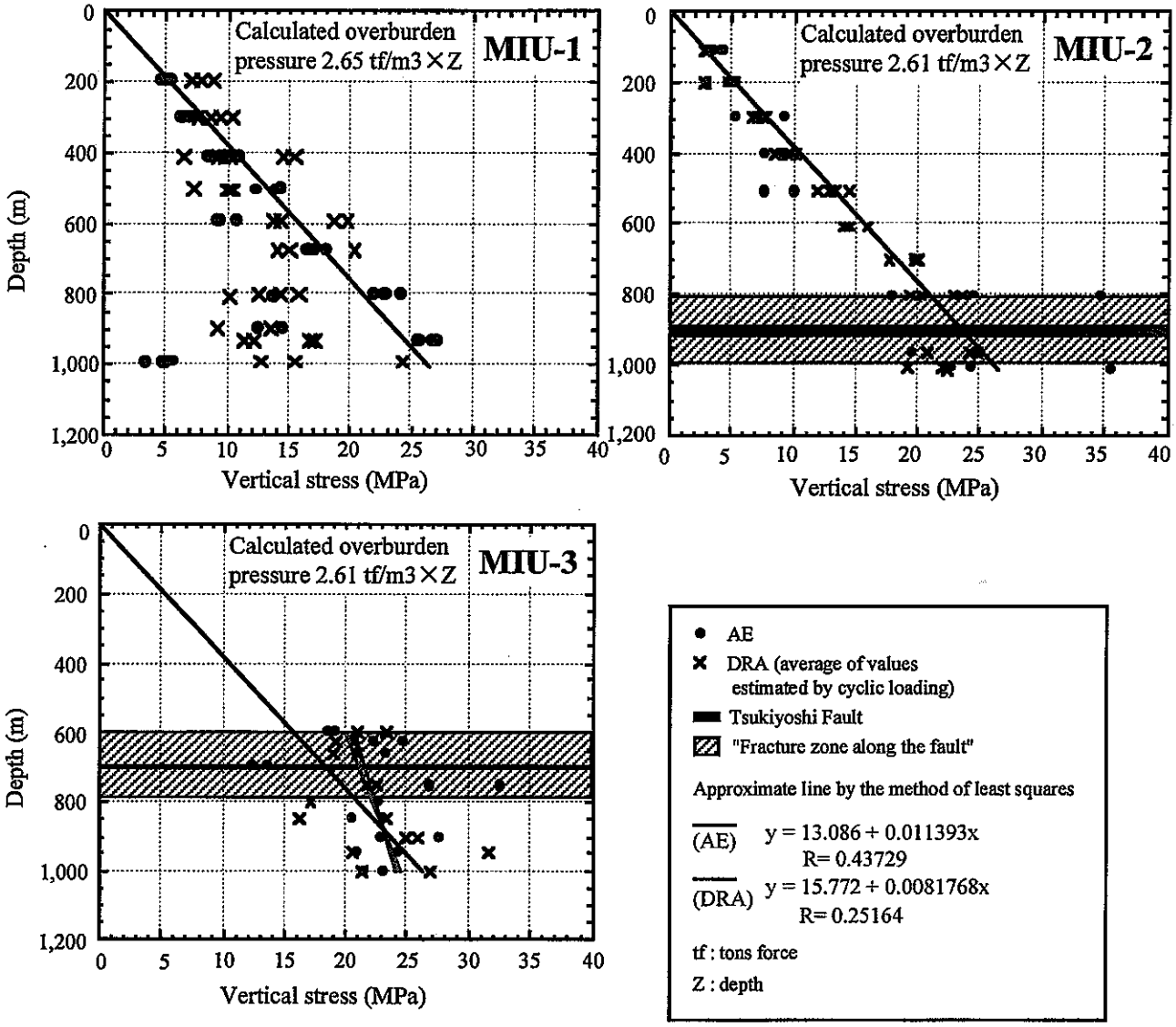

Figure 4.62 Distribution of the vertical stresses vs depth

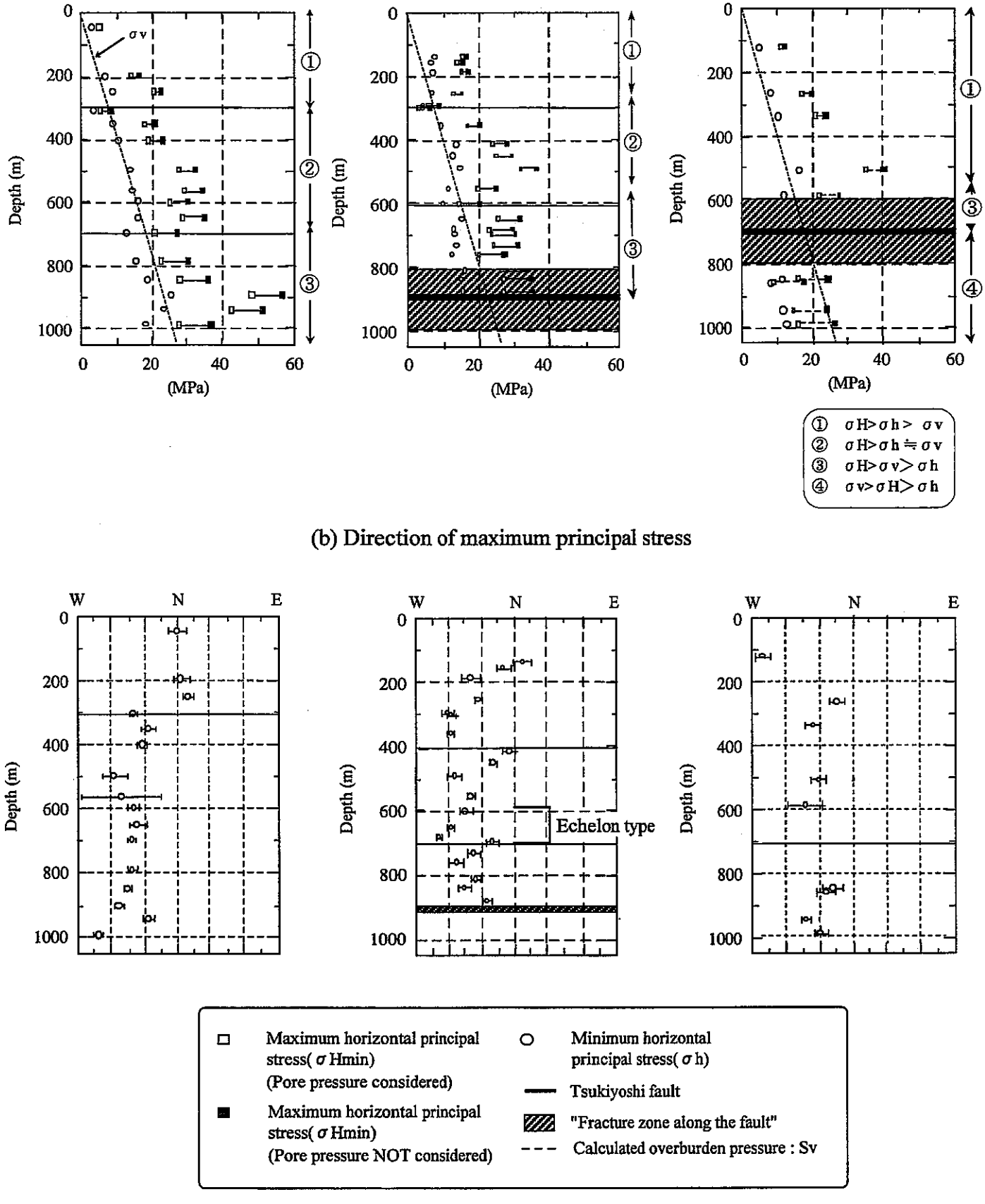

Figure 4.63 Distribution of the horizontal principal stress

4.4.3 Revision of the model based on the results of the MIU-2 investigations

4.4.3.1 Overview of the MIU-2 investigations [40,79]

Concept of the investigations

The main aim is assess and confirm and then build on the above rock mechanics conceptual model.

Scope of the investigations

Tests for physical/mechanical properties, AE/DRA tests and hydraulic fracturing tests were carried out at intervals of 100 m, 100 m and 50 m, respectively, in MIU-2. The intent was to investigate if the distribution of physical properties and in situ stresses are the same or similar in the three depth ranges in MIU-2 and thus confirm the investigation results obtained from AN-1 and MIU-1. However, MIU-2 intersects a major fault, the Tsukiyoshi Fault, in which the footwall has too many fractures for the performance of hydraulic fracturing tests. Thus, the hydraulic fracturing tests were only carried out in the hanging wall of the fault. Details of tests for physical/mechanical properties are shown in Table 4.30. The depths for in situ stress measurements are shown in Table 4.31.

Table 4.30 Details of physical/mechanical property tests for MIU-2

	Item	Specification	Point
Physical property	Apparent density	ISRM method	20
	Effective porosity	ISRM method	20
	Water ratio	ISRM method	20
	Seismic wave velocity (P and S wave)	Receiver and transmitter: 200kHz	20
Mechanical property	Uniaxial compression test	Loading rate (3kgf/cm^2/s)	20
	Brazilian test	Loading rate (3kgf/cm^2/s)	40
	Triaxial compression test	ISRM method	-

Table 4.31 Measurement depth of in situ stress measurements at the MIU-2

Test	Measurement point	Measurement depth (m)*
AE/DRA*	10	106.68-107.88; 196.49-199.45; 296.30-296.66; 402.00-402.36; 505.52-565.58; 603.00-603.35; 698.34-698.70; 800.59-801.39; 963.29-964.77; 1002.20-1011.37
Hydraulic fracturing**	20	138.2; 158.0; 187.3; 254.0; 294.7; 301.5; 356.4; 413.4; 452.0; 491.0; 555.0; 604.0; 651.0; 682.0; 698.5; 733.7; 761.3; 811.3; 837.7; 878.1

*: Sampling depth for AE/DRA

**: Mid-point depth of test interval for hydraulic fracturing

Results of the investigations

Results of physical/mechanical property tests in MIU-2 are shown in Table 4.32 and Figure 4.61. Vertical in situ stresses obtained by AE/DRA tests on cores from the MIU-2 and in situ stress states on horizontal planes obtained by hydraulic fracturing tests are shown in Figures 4.62, 4.63, respectively. The hydraulic fracturing tests produced echelon-type fractures at depths of 604.0 m, 651.0 m, 682.0 m and 698.5 m [80], where it is probable that none of the principal stresses is vertical.

Table 4.32 Results of physical/mechanical property tests in MIU-2

	Item	Unit	Result
Physical property	Apparent density	-	2.51～2.65
	Effective porosity	%	0.7～2.0
	Water content	%	0.24～0.50
	Seismic wave velocity (V_p)	km/s	4.0～6.0
	Seismic wave velocity (V_s)	km/s	2.0～3.0
Mechanical property	Uniaxial compression test	MPa	130～240
	Young's modulus (E_{50})	GPa	32～63
	Poisson's ratio	-	0.30～0.46
	Tensile strength (by Brazilian test)	MPa	4～10
	Cohesion	MPa	13～25
	Internal friction angle	Degree	55～63

Evaluation of the results

Both the physical and mechanical properties of the rock mass intersected by MIU-2 are unevenly distributed, as in AN-1 and MIU-1. Comprehensive examination of the distribution of physical/mechanical properties in MIU-2 indicate that the rock mass can be divided into four zones based on the different trends of the properties: 0 to 400 m, 400 to 600 m, 600 to 900 m depth (the depth of the Tsukiyoshi Fault) and deeper than 900 m. These four zones have the following characteristics.

Zone 1: ground surface to 400 m depth

Apparent density is small, but water content and effective porosity are large. Physical properties tend to vary a little with depth. Young's modulus, uniaxial compressive strength and tensile strength (Brazilian tests) increase slightly with increase in depth.

Zone 2: 400 m to 600 m depth

Variations in average physical properties within this depth range are relatively small. Physical properties abruptly change around the upper and lower boundaries of this zone. All the physical properties but for Poisson's ratio are considerably lower than those in the rock above and below the Zones.

Zone 3: 600 m to 900 m depth (the Tsukiyoshi Fault)

Physical properties tend to change with increased depth. Apparent density and seismic wave velocity, Young's modulus and Poisson's ratio increase with depth, whereas water content and effective porosity decrease.

Zone 4: deeper than 900 m (footwall of the Tsukiyoshi Fault)

Physical properties at this depth and structural position change somewhat from those in the hanging wall; Young's modulus and tensile strength drop abruptly, all the other properties do not change.

The MIU-2 intersects the Tsukiyoshi Fault at 890 to 915m depths. It is known that the hanging wall and

footwall differ in lithofacies from each other (hanging wall: Biotite granite, footwall: Felsic granite). Nevertheless, no meaningful correlation between the facies change and the difference in physical properties has been found yet. Consequently, it is presumed that the discontinuous change in physical/mechanical properties deeper than 900 m is due to damage associated with formation of the fault.

Results of AE tests on the MIU-2 core vary more widely than results from the DRA tests. While sensors for AE tests are usually set in the central part of a test specimen, the sensors are set at both ends of the specimen in this measurement. Presumable this could result in differences in the AE values. Therefore, the distribution of vertical in situ stresses is assessed mainly by the results of DRA tests. The values of vertical stress obtained by DRA tests are approximately equal to the estimated overburden pressure based on unit weight and overburden between the surface and 800 m depth. However, they are a little smaller than the estimated overburden pressures below 900 m in depth.

The in situ stress states in horizontal planes were assessed only in the hanging wall of the fault by hydraulic fracturing tests because these tests could not be carried out below 900 m depth due to the degree of fracturing. The results indicate that stress magnitudes overall tend to increase with depth, but the maximum principal stress magnitude drops at about 300 m and 600 m depth.

Assuming that vertical stress is equal to overburden pressure, the 3-D stress states expected were:

- 0 to 300 m: Reverse-fault-type ($\sigma_H > \sigma_h > \sigma_v$),
- 300 to 600 m :Transitional-type ($\sigma_H > \sigma_h \fallingdotseq \sigma_v$),
- 600 to 900 m: Strike slip-fault-type ($\sigma_H > \sigma_v > \sigma_h$)..

The direction of the maximum principal stress tends to rotate as follows:

- 0 to 400 m: N-S to WNW-ESE,
- 400 to 700 m: N-S to WNW-ESE,
- 700 to 900 m: NNW to WNW and returns to NNW.

Specifically, the azimuth of the maximum principal stress rotates about 60° in the two sections ranging in depth from 0 to 400 m and 400 to 700 m. Furthermore, it rotates from NNW to WNW and back to NNW in the section between 700 and 900 m in depth.

Accordingly, the in situ stress states in the hanging wall of the Tsukiyoshi Fault around MIU-2 are divided into three sections ranging in depth from 0 to 300/400 m, 300/400 m to 600/700 m and 600/700 m to 900 m.

Histograms of fractures distributions sampled by BTV investigations in MIU-2 are shown in Figure 4.64. These histograms indicate that not only do the fracture numbers in MIU-2 change abruptly at 400 m and 700 m depth but also the trend in distributions of the fracture numbers is nearly identical with that of MIU-1.

Thus, physical/mechanical properties, in situ stress states, and fracture distributions abruptly change at 300

to 400 m, 600 to 700 m and about 900 m depth. It indicates that the hanging wall of the Tsukiyoshi Fault is composed of three Zones with different physical/mechanical properties and in situ stress states. Also, it is probable that the footwall of the Tsukiyoshi Fault has different properties from the hanging wall.

4.4.3.2 Comparison between the results of the MIU-2 investigations and the rock mechanics conceptual model based on AN-1 and MIU-1 data. (See Section 4.4.2)

The mean values of the results obtained by physical/mechanical property tests carried out in the AN-1 and MIU-1 and 2 are shown in Table 4.33.

Table 4.33 Results of physical/mechanical property tests in the AN-1, MIU-1 and MIU-2

		AN-1	MIU-1	MIU-2
Physical properties				
Apparent density (—)	Average	2.61	2.62	2.61
	Standard deviation	0.01	0.01	0.03
Effective porosity (%)	Average	1.40	1.33	1.19
	Standard deviation	0.26	0.25	0.27
Water ratio (%)	Average	0.23	0.44	0.36
	Standard deviation	0.05	0.08	0.07
Seismic wave velocity (P wave) (km/s)	Average	4.51	5.48	5.12
	Standard deviation	0.37	0.27	0.52
Mechanical properties				
Young's modulus (E50) (GPa)	Average	47.28	55.95	49.97
	Standard deviation	8.05	5.94	7.45
Uniaxial compressive strength (MPa)	Average	197.16	180.11	165.92
	Standard deviation	44.70	38.30	34.53
Poisson's ratio (—)	Average	0.34	0.32	0.37
	Standard deviation	0.03	0.04	0.04
Tensile strength (by Brazilian test) (MPa)	Average	8.47	7.18	7.92
	Standard deviation	1.82	1.83	1.42
Cohesion (MPa)	Average	—	39.04	22.79
	Standard deviation	—	8.91	4.89
Angle of Internal friction (degree)	Average	—	52.60	57.72
	Standard deviation	—	4.58	2.50

Average values of physical properties in MIU-2 are on average, comparable with the results obtained by the previous investigations. They are close to the values obtained in AN-1 but tend to be slightly lower than those obtained in MIU-1, as a whole. With the exception of values for cohesion, the averages for each of the MIU-2 properties ranges up to 15 % from the averages in other boreholes but most are within 10%. Specifically, values of physical properties, such as unit weight, effective porosity, water cotent and seismic wave velocity are smaller than those of MIU-1. With respect to mechanical properties, all but for angle of internal friction and Poisson's ratio of MIU-2 are less than those same properties in MIU-1. The variation of physical properties with depth tends to increase from AN-1 to MIU-2; that is, from south to north the range in values increases. Though the vertical distribution of Young's modulus shows a similar tendency, none of the other properties shows a clear tendency. Based on these facts, it is presumed that greater mechanical damage has been induced during fault formation in the hanging wall of the Tsukiyoshi Fault, as proximity to the fault increases.

It is presumed that the values of vertical in situ stress in the hanging wall of the Tsukiyoshi Fault are nearly equal to the estimated overburden pressures. The values of principal stresses in horizontal planes tend to increase with depth in the sections between 0 to 300 m and deeper than 600/700 m in AN-1. However, in MIU-2 only slight variation in the principal stress values occurs with depth. Though AN-1 and the MIU-2 are similar to each other in distribution of stresses in the section 300 to 600/700 m depth, stresses in the MIU-2 are larger than those in the AN-1. The azimuth of principal stress shows rotation of as much as 45° at the 300 m depth in AN-1. On the other hand, it rotates from N-S to WNW-ESE with an increase in depth in the sections 0 to 400 m and 400 to 700 m in depth in the MIU-2. However, it changes erratically below 700 m depth in MIU-2. These facts suggest that the existence of the fault might exert a great influence on the present day in-situ stress field.

4.4.3.3 Revision of the rock mechanics conceptual model [81]

Based on the investigation results from the three 1,000 m-deep boreholes (AN-1, MIU-1 and 2), it was shown that the rock mass on the hanging wall side of the fault can be divided into three zones having different geological and mechanical properties down to 1,000 m in depth. Specifically, the ranges of the first, second and third zones are changed slightly from the earlier model with the inclusion of observations from MIU-2. The new ranges are, in themselves, indicative of the heterogeneity of rock mass properties and in situ stress at the site. The new ranges are

- 0 to 300/400 m
- 300/400 to 600/700 m
- Deeper than 600/700 m

Based on the investigation results for the three boreholes, the rock mechanics conceptual model of the rock mass on the hanging wall side of the fault in the Shobasama Site was constructed as shown in Figure 4.65. The rock mechanics conceptual model was constructed on the following assumptions.

① The vertical distribution of in situ stress values in the MIU-2 is complicated due to proximity to and effects of the fault. Thus, attention was paid mainly to the variation in azimuth of principal stresses, which correspond well with the variation in the vertical frequency distribution of fractures.

② The maximum principal stresses in AN-1, which is located farthest from the fault, show a consistent NW-SE trend below 300 m depth. This is coincident with the regional compressive axis [82]. Consequently, it is assumed that the influence of the fault on the stress axes at this location is minimal.

③ The results of BTV investigations in AN-1 show almost the same trend of fracture frequency distribution as those in MIU-1 and 2. Therefore, the structural zone divisions of the rock mass are extended nearly horizontally from MIU-2 to AN-1. However, it is assumed for simplification that stress values at locations distant from the fault increase linearly with depth in each structural zone or domain.

This rock mechanics conceptual model leads to the following interpretation. The current tectonic stress in

the rock mass on the hanging wall side of the Tsukiyoshi Fault is NW oriented, producing oblique compression against the fault. This would be an explanation for the observation that vertical stress in the footwall of the fault is smaller than the estimated overburden pressure and less than horizontal stresses in the hanging wall. Also, a reason for the rotation in azimuths of principal stresses in the individual structural zones could be explained. It is thought that the validity of this hypothesis may be indirectly verified by determining the in situ stress state on the footwall side of the fault in MIU-3.

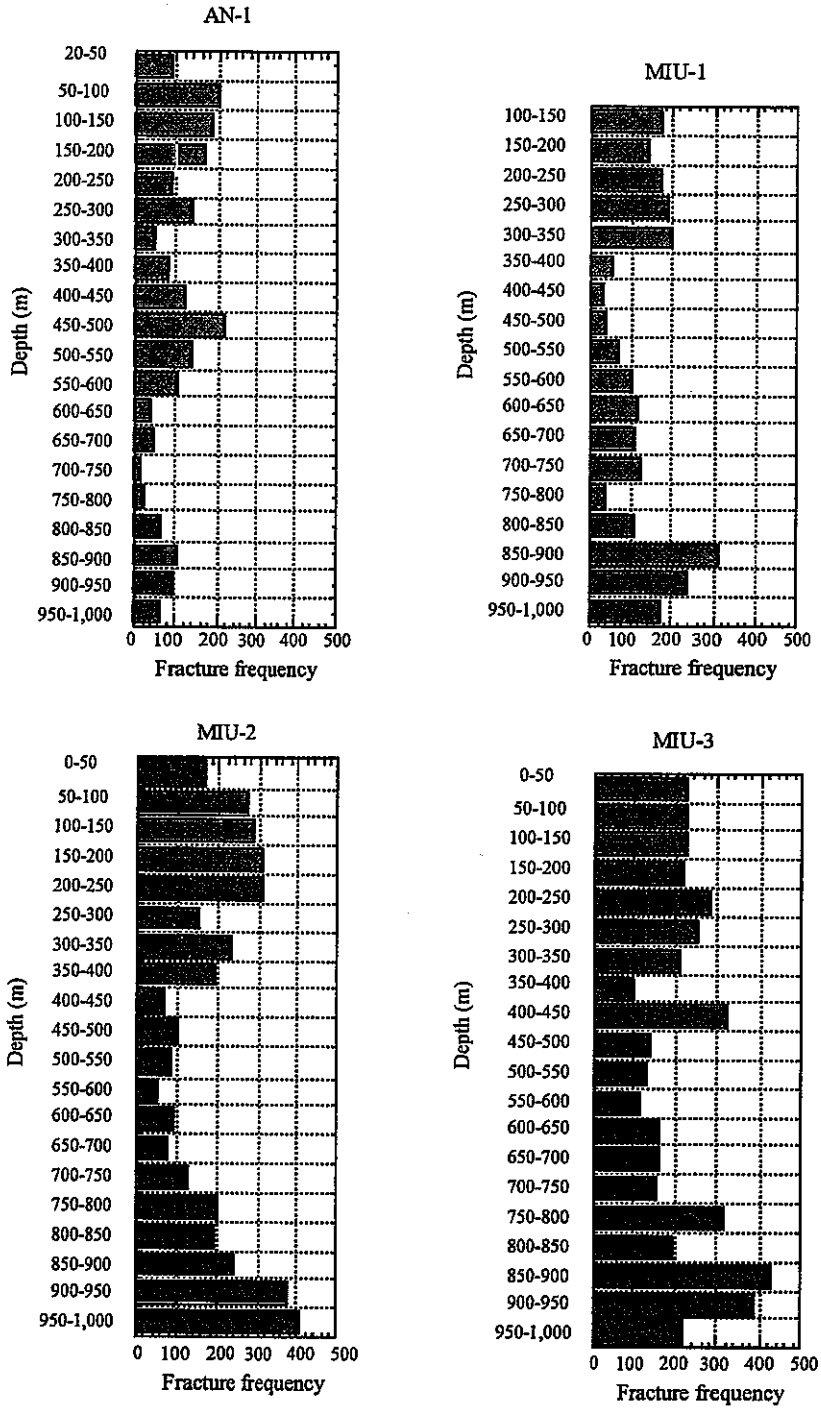

Figure 4.64 Fracture frequency detected by BTV investigations

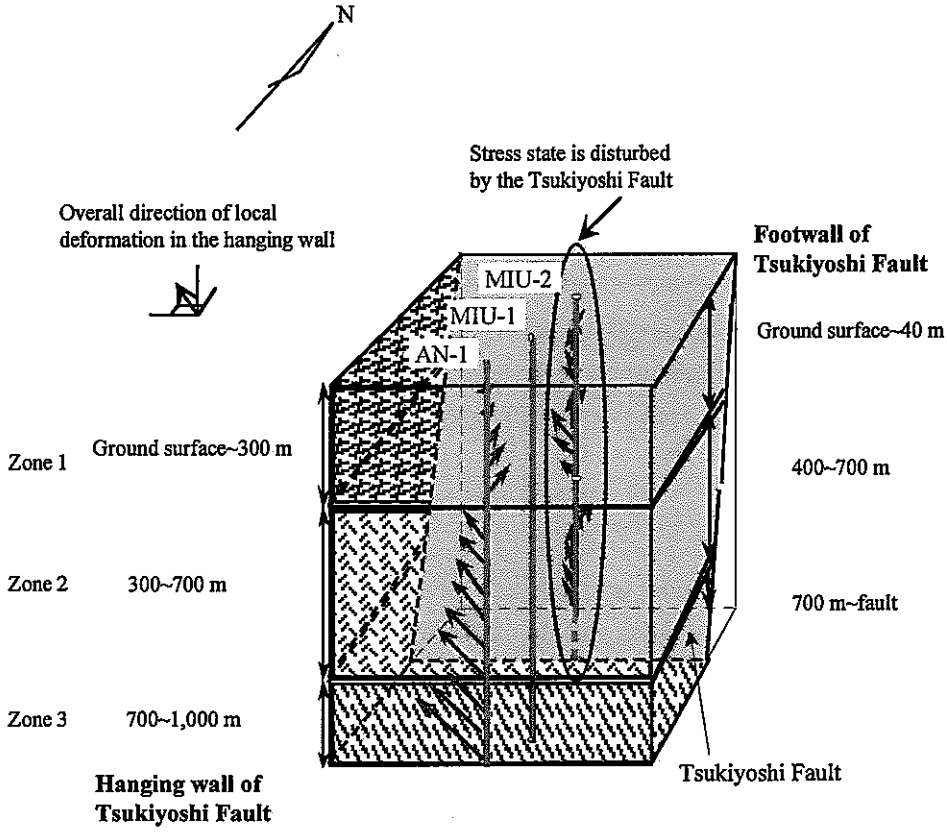

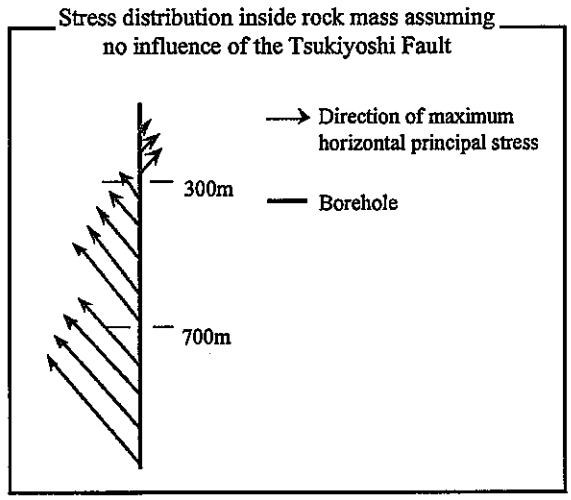

Characteristics of each zone

	Zone 1	Zone 2	Zone 3
• Fracture frequency	High (subhorizontal - horizontal)	Low	High (subvertical)
• Deformability of matrix	Relatively small	Relatively large	Relatively small
• Anisotropy of mechanical properties of rock matrix	Relatively small	Relatively large	Relatively small

Figure 4.65 Rock mechanics conceptual model of hanging wall of Tsukiyoshi Fault

4.4.4 Revision of the model based on the results of the MIU-3 investigations

4.4.4.1 Overview of the MIU-3 investigations [41,83]

Concept of the investigations

The main aim was to provide data to assess and confirm the existing rock mechanics conceptual model and to expand the conceptual model of the rock mass to include the footwall side of the Tsukiyoshi Fault.

Scope of the investigations

With the existing rock mechanical model in mind, test locations were established in order to facilitate acquisition of data on mechanical properties, mainly on the footwall side of the Tsukiyoshi Fault. On the hanging wall of the Tsukiyoshi Fault, samples in the structural zones defined in the rock mechanics conceptual model (See Section 4.4.3) were also required. From the footwall of the Tsukiyoshi Fault, as many samples as possible at equal intervals (some 100 m) were expected. MIU-3 intersects the Tsukiyoshi Fault at 693 to 709 m depth. Details of physical/mechanical property tests and measurement depths of the in situ stress measurements are shown in Tables.4.34 and 4.35, respectively.

Table 4.34 Details of physical/mechanical property tests for MIU-3

	Item	Specification	Number of tests
Physical property	Apparent density	ISRM method	40
	Effective porosity	ISRM method	40
	Water ratio	ISRM method	40
	Seismic wave velocity (P and S waves)	Receiver and transmitter: 100kHz	40
Mechanical property	Uniaxial compression test	Strain rate (0.1%/min.)	10
	Brazilian test	JIS M0303	10
	Triaxial compression test	ISRM method	30

Table 4.35 Measurement depth of in situ stress measurements at the MIU-3

Test	Point	Measurement depth (m)
AE/DRA	10	602.15-602.29; 626.00-626.12; 661.62-661.88; 697.54-698.45; 754.45-754.67; 799.00-799.12; 850.70-850.82; 905.43-905.55; 949.00-949.12; 1,002.60-1,002.72
Hydraulic fracturing	10	122.0; 266.0; 338.0; 462.0; 509.0; 589.0; 847.0; 858.0; 946.0; 988.0

Results of the investigations

Results of the physical and mechanical property tests in MIU-3 are shown in Table 4.36 and Figure 4.61. Vertical in situ stresses obtained by AE/DRA tests on cores from MIU-3 and in situ stress states on horizontal planes obtained by hydraulic fracturing tests are shown in Figures 4.62 and 4.63, respectively. However, hydraulic fracturing tests carried out at two depths (338 m and 462 m) in MIU-3 did not produce longitudinal fractures, in order to satisfy the theoretical assumption.

Table 4.36 Results of physical/mechanical property tests for MIU-3

	Item	Unit	
Physical property	Apparent density	-	2.61 to 2.65
	Effective porosity	%	1.2 to 1.7
	Water ratio	%	0.45 to 0.65
	Seismic wave velocity (V_p)	km/s	5.4 to 6.0
	Seismic wave velocity (V_s)	km/s	3.0 to 3.5
Mechanical property	Uniaxial compression test	Mpa	50 to 200
	Young's modulus (E_{50})	Gpa	20 to 62
	Poisson's ratio	-	0.30 to 0.40
	Tensile strength (by Brazilian test)	Mpa	3 to 8
	Cohesion	Mpa	20 to 50
	Internal friction angle	Degree	48 to 60

Evaluation of results

It is known from the previous investigations that the Tsukiyoshi Fault is associated with an approximately 100 m-wide fracture zone on each side. Accordingly, it is assumed that 100 m-wide areas on the both sides of the main part of the Tsukiyoshi Fault (693.2 to 719.3 m depth) are affected by the fault. Comprehensive examination of the distributions of physical/mechanical properties and this assumption suggests that the granite intersected by MIU-3 could be divided into the following three zones. These vary with depth: that is, approximately 0 to 300 m, 300 to 600 m and 600 to 800 m depth. Each of these has the following characteristics.

Zone 1: 0 to 300 m in depth

Although there were a small number of tests, water content and effective porosity have a tendency to increase slightly with depth. No change was found in apparent density and seismic wave velocity. Young's modulus, uniaxial compressive strength and Poisson's ratio tend to increase slightly with depth, whereas tensile strength (by Brazilian test) decreases.

Zone 2: 300 to 600 m in depth

Apparent density tends to increase with depth, whereas effective porosity and water content tend to decrease. Seismic wave velocity shows no change with depth. Erratic changes were recognized in Young's modulus, uniaxial compressive strength and Poisson's ratio, whereas only tensile strength shows a slight increase with depth.

Zone 3: 600 to 800 m in depth

Individual physical properties vary discontinuously compared with those in Zones 1 and 2. As a whole, effective porosity and water content increase and seismic wave velocity decreases with depth, but the variations are small. Values of mechanical properties show remarkable changes with depth. Young's modulus, uniaxial compressive strength and Poisson's ratio increase, whereas tensile strength decreases.

The dispersion of AE test results is smaller than that of DRA tests at the same depths. Therefore, the distribution of vertical in situ stresses was assessed mainly by the AE test results. Values of vertical stresses

obtained by AE tests are a little larger than the overburden pressures estimated in the hanging wall of the Tsukiyoshi Fault but smaller than those in the footwall of the fault. They vary abruptly around the Tsukiyoshi Fault.

In situ stress states in horizontal planes obtained by hydraulic fracturing tests tend to increase with depth. The values of the maximum stress drop at about 600 m and below 700 m depth in the footwall of the Tsukiyoshi Fault.

Assuming that vertical stress is equal to overburden pressure, 3-D stress states expected are:

- surface to 550 m: Reverse-fault-type ($\sigma_H > \sigma_h > \sigma_v$),
- about 600 m: Strike-slip-fault-type ($\sigma_H > \sigma_v > \sigma_h$)
- deeper than 700 m: Normal-fault-type ($\sigma_v > \sigma_H > \sigma_h$)

The maximum principal stress trends:

- N-S at about 100 m in depth and
- NNW-SSE deeper than 300 m.

Thus, the rock mass around MIU-3 was divided into three sections: 0 to 550 m, around 600 m and deeper than 700 m in depth.

Vertical variations in the number of fractures in MIU-3 are shown in Figure 4.64. While they show a trend somewhat similar to the trends in MIU-1 and 2, the vertical variations in the number of fractures is not as distinct. However, the vertical distribution of the fracture numbers change abruptly at similar depths to those of the physical property changes in MIU-3. These results are conformable with the structure predicted by the rock mechanics conceptual model based on the investigation results of MIU-2.

4.4.4.2 Comparison between the results of the MIU-3 investigations and the rock mechanics conceptual model (See Section 4.4.3)

The mean values of results obtained by physical/mechanical property tests carried out in AN-1 and MIU-1, 2 and 3 are shown in Table 4.37.

Specifically, physical properties in MIU-3, such as apparent density, effective porosity, water content and seismic wave velocity, are all larger than those of AN-1 and MIU-2. Mechanical properties, such as Young's modulus, uniaxial compressive strength, and tensile strength, are the smallest of the four boreholes. Values of cohesion, internal friction angle and Poisson's ratio are almost the same as those of MIU-1.

Table 4.37 Results of physical/mechanical property tests in AN-1, MIU-1, 2 and 3

		AN-1	MIU-1	MIU-2	MIU-3
Physical property					
Apparent density (—)	Average	2.61	2.62	2.61	2.62
	Standard deviation	0.01	0.01	0.03	0.01
Effective porosity (%)	Average	1.40	1.33	1.19	1.41
	Standard deviation	0.26	0.25	0.27	0.14
Water ratio (%)	Average	0.23	0.44	0.36	0.52
	Standard deviation	0.05	0.08	0.07	0.06
Seismic wave velocity (P wave) (km/s)	Average	4.51	5.48	5.12	5.60
	Standard deviation	0.37	0.27	0.52	0.15
Mechanical property					
Young's modulus (E50) (GPa)	Average	47.28	55.95	49.97	47.15
	Standard deviation	8.05	5.94	7.45	12.76
Uniaxial compressive strength (MPa)	Average	197.16	180.11	165.92	131.21
	Standard deviation	44.70	38.30	34.53	50.97
Poisson's ratio (—)	Average	0.34	0.32	0.37	0.36
	Standard deviation	0.03	0.04	0.04	0.05
Tensile strength (by Brazilian test) (MPa)	Average	8.47	7.18	7.92	6.25
	Standard deviation	1.82	1.83	1.42	1.47
Cohesion (MPa)	Average	—	39.04	22.79	35.07
	Standard deviation	—	8.91	4.89	8.92
Internal friction angle (degree)	Average	—	52.60	57.72	53.07
	Standard deviation	—	4.58	2.50	3.34

The vertical distributions of all the physical properties in the four boreholes (Figure 4.61) are dissimilar, to varying degrees. Though variations in vertical distribution of physical properties tend to increase from AN-1 toward MIU-2 (from south to north), the variations in MIU-3 are almost the same as those in MIU-1. This indicates that there is no effect of fault formation on the variations. Vertical distributions of mechanical properties are also uneven. The extent of variations in MIU-2 and 3 are larger than those in the AN-1 and MIU-1. While physical properties in the MIU-3 change non-systematically immediately above the Tsukiyoshi Fault, they start to change about 400 m above the fault in MIU-2. These results indicate that physical/mechanical properties of the rock mass in the Shobasama Site are different enough vertically to allow dividing the rock into zones. The changes in physical/ mechanical properties are probably generated by not only mechanical damage by the formation of the Tsukiyoshi Fault but other factors.

Vertical in situ stresses in the hanging wall of the Tsukiyoshi Fault vary widely but are nearly equal to the estimated overburden pressures (Figure 4.62). On the other hand, vertical stresses are smaller than the estimated overburden pressures in the footwall of the fault. It suggests that vertical stresses are released or decoupled or that there are stress conditions that would cause stress redistribution around and below the fault.

Principal stresses on horizontal planes tend to increase with depth (Figure 4.63) to allow dividing the rock mass down to 1,000 m in depth into zones with different stress states. Based on the investigation results, the rock on the hanging wall side of the Tsukiyoshi Fault is divided into three zones: 0 to 300 m, 300 to 600/700 m and deeper than 600/700 m in depth; on the other hand, although based on a limited database, the footwall seems to form a single zone. In AN-1 the azimuths of principal stresses measured rotate about

45° at 300 m depth, while in MIU-2 it rotates from N-S to WNW-ESE in the sections from 0 to 400 m and 400 m to 700 m. The maximum compressive stress axis in the regional stress field in the Shobasama Site also trends WNW-ESE. Therefore, the maximum principal stress is thought to generally trend WNW-ESE at 300 to 1,000 m in depth in the Shobasama Site.

4.4.4.3 Revision of the previous rock mechanics conceptual model [84]

The validity of the previous rock mechanics conceptual model for the hanging wall of the Tsukiyoshi Fault was confirmed by the investigation results in MIU-3. Also, with the acquisition of rock mechanical data from the footwall in MIU-3, the rock mechanics conceptual model of the footwall was developed. However, the rock mechanical data of the rock mass on the footwall side is restricted to the depth below 900 m in MIU-2 and 700 m in MIU-3. To compensate for this information shortage, the rock mechanics conceptual model of the footwall was examined using the data on the basement granite obtained by rock mechanical investigations [84, 85] in the Tono Mine and the measurement results [65] in the DH-9 borehole drilled for the RHS Project [86]. DH-9 is a 1,000 m-deep borehole drilled about 1 km north of the northern border of the Shobasama Site and on the footwall side of the Tsukiyoshi Fault. Results of mechanical tests of the rocks on the footwall side in MIU-3 and the borehole 99SE-02 (200 m-deep) are shown in Figure 4.66 [85]. Though the upper 50 m-thick part of the basement granite in 99SE-02 is too intensely weathered to collect cores, values of mechanical properties below the weathered part tend to increase with depth. Accordingly, none of the mechanical properties obtained in this borehole probably represent the sound granite with the exception of the data in the deepest part. Rocks in the lowermost part of the borehole (207m in depth) have rock mechanical properties, such as apparent density of 2.62 t/m^3, E_{50} of 50GPa, and uniaxial compressive strength of about 150 MPa. They are almost the same as the physical/mechanical properties on the footwall side in MIU-3 and similar to the mean values obtained on the hanging wall side.

The information on the stress states on the footwall side of the fault was provided by hydraulic fracturing tests carried out deeper than 900 m in MIU-2, deeper than 700 m in the MIU-3, and in four boreholes drilled in the Tono Mine (TM-1, 2, 98SE-01 and 99SE-02). The measurement results are shown in Figure 4.67. The four boreholes in the Tono Mine intersect the Tsukiyoshi Fault and the basement granite at different depths. Therefore, the measurement results of the individual boreholes are arranged from south (hanging wall side) to north (footwall side). Values of principal stresses on horizontal planes measured in the basement granite tend to clearly decrease from the hanging wall side to the footwall side. The minimum principal stresses are nearly equal to the overburden pressures in the northernmost borehole, 99SE-02 and the maximum principal stresses are 1.4 to 1.7 times the values of the minimum principal stresses. On the other hand, stresses on the footwall side in MIU-3 are much lower than those on the hanging wall side. The maximum principal stresses in the Tono Mine trend NNW-SSE to NW-SE, except near the boundary between granite and sedimentary rock.

The investigation results [65] in DH-9 were used for geological structure investigations of the rock mass on the footwall side of the fault. Results of BTV investigations, seismic wave velocity logging and density logging in the individual boreholes (MIU-1, 3 and DH-9) are shown in Figure 4.68. This figure shows that the number of fractures in DH-9 is much smaller than those in the rock mass on the hanging wall side in

MIU-2 and 3. Seismic wave velocity and density drastically drop in highly fractured parts in MIU-2 and 3 and DH-9. As for the rest of the rock mass, seismic wave velocity changes a little where the fracture numbers abruptly change. Sections with more fractures show larger velocity variations, and vice versa. There is little change in seismic wave velocity in DH-9 except for the highly fractured parts. Results of density logging seem to show a similar trend, though their trend is not as clear as the results of seismic wave velocity logging.

Based on the investigation results from MIU-3, the RHS Project and the studies in the Tono Mine, the rock mechanics conceptual model was revised. The revised models for the hanging wall and the footwall of the Tsukiyoshi Fault are shown in Figure 4.69. Furthermore, the following hypotheses were proposed on mechanical properties and stress states of the rock mass on the footwall side.

① According to the results of laboratory tests on cores obtained from the boreholes in the Tono Mine and MIU-3, it is extremely unlikely that mechanical properties of the intact rock or matrix in the "Moderately fractured zone" differ a great deal from those on the hanging wall side.

② According to the results of in situ stress measurements by hydraulic fracturing tests in the Tono Mine and on the footwall side in MIU-3, stress in the footwall side is thought to be considerably lower than that in the hanging wall side. This is supported by the fact that there are a small number of fractures but a highly weathered fracture zone develops deeper than 600 m depth. In general, the apertures of fractures are closely related to stress states. It is presumable that a small number of fractures, which develop under weak stresses in the footwall, cause larger apertures to facilitate infiltration of groundwater near the ground surface. Also, on the footwall side in DH-9, quite a few vertical stress variations are expected to occur, taking the development of considerably thick, highly fractured zones into consideration. However, the extent of the variations would not be as remarkable as in the hanging wall due to the weak stresses. The measurement data in the boreholes in the Tono Mine and MIU-3 suggest that the maximum principal stresses in horizontal planes generally trend NNW-SSE to NW-SE like in the hanging wall of the fault, though there is no data at intermediate depths.

The rock mechanics conceptual model of the footwall of the Tsukiyoshi Fault has the following characteristics.

① Physical/mechanical properties of the rock matrix in the footwall are almost the same as those in the hanging wall. Their vertical variations are not large.

② Fractures are so few in the footwall that mechanical properties of the in-situ rock mass are better than those on the hanging wall side.

③ The minimum principal stresses are equal to the estimated overburden pressures or smaller. The difference between the maximum and minimum principal stresses is small. The maximum principal stresses trend WNW-ESE to NW-SE and don't change vertically a great deal.

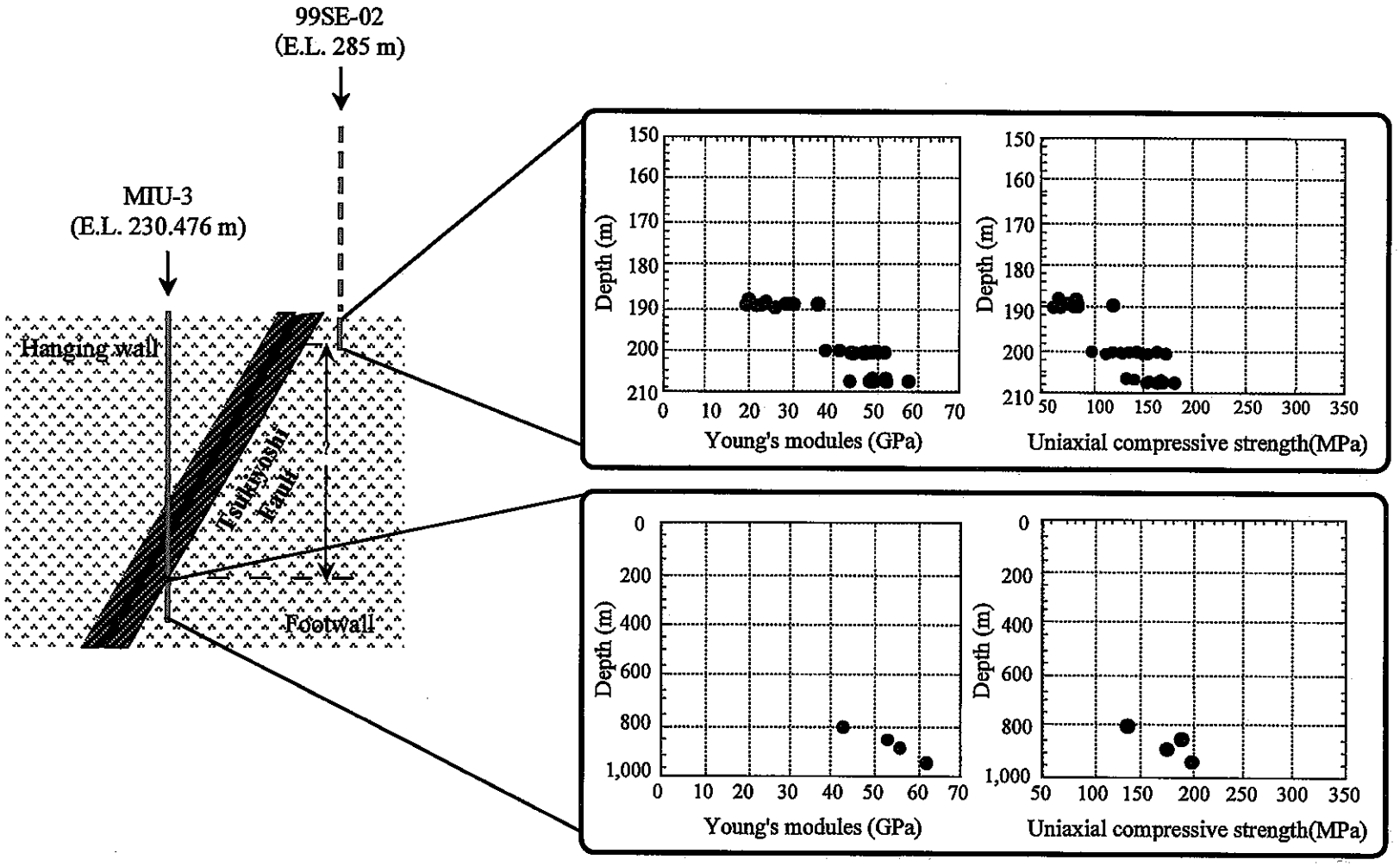

Figure 4.66 Mechanical properties of the Toki Granite in footwall of the Tsukiyoshi Fault

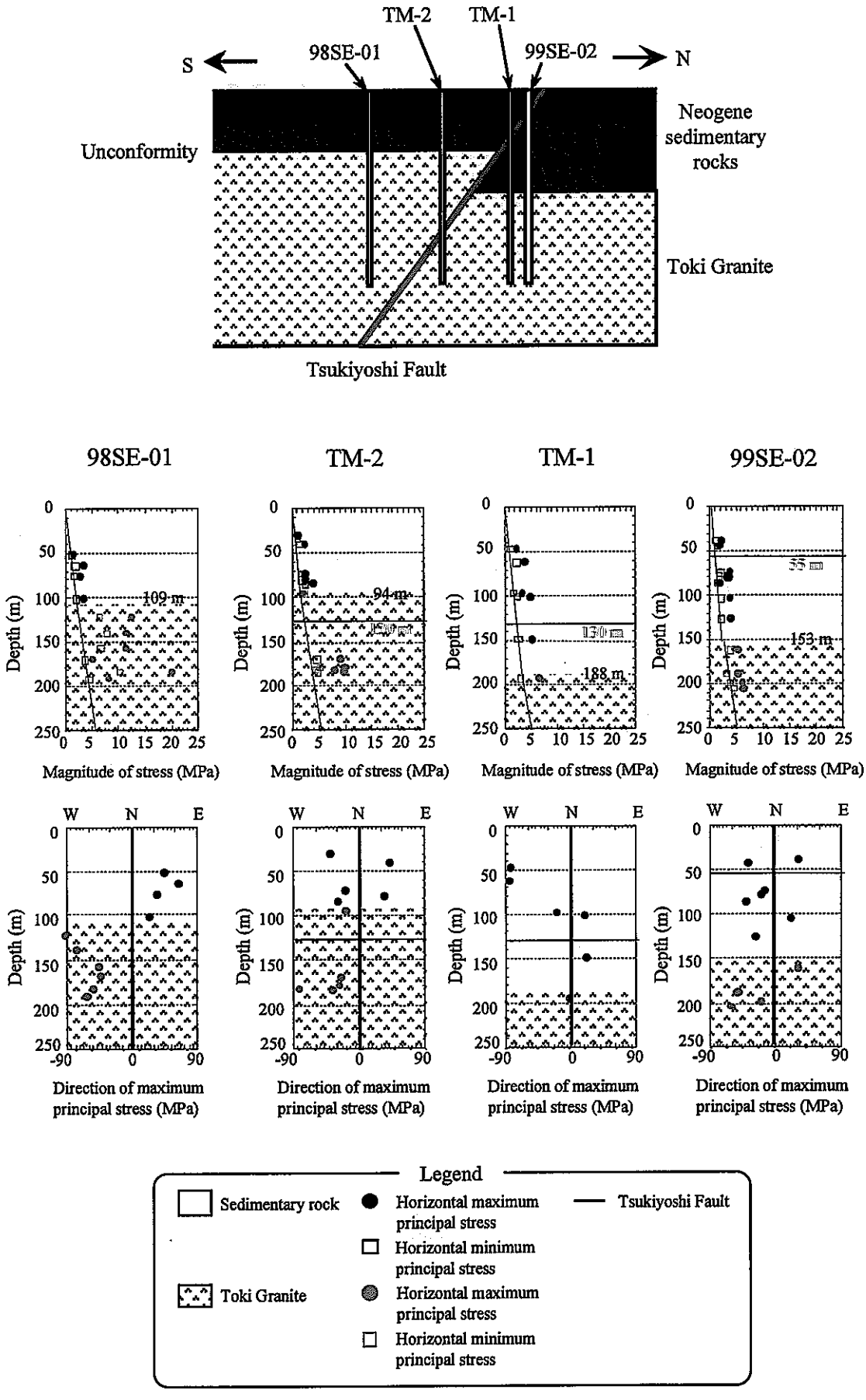

Figure 4.67 Results of the stress measurements with hydraulic fracturing in the Tono Mine [84]

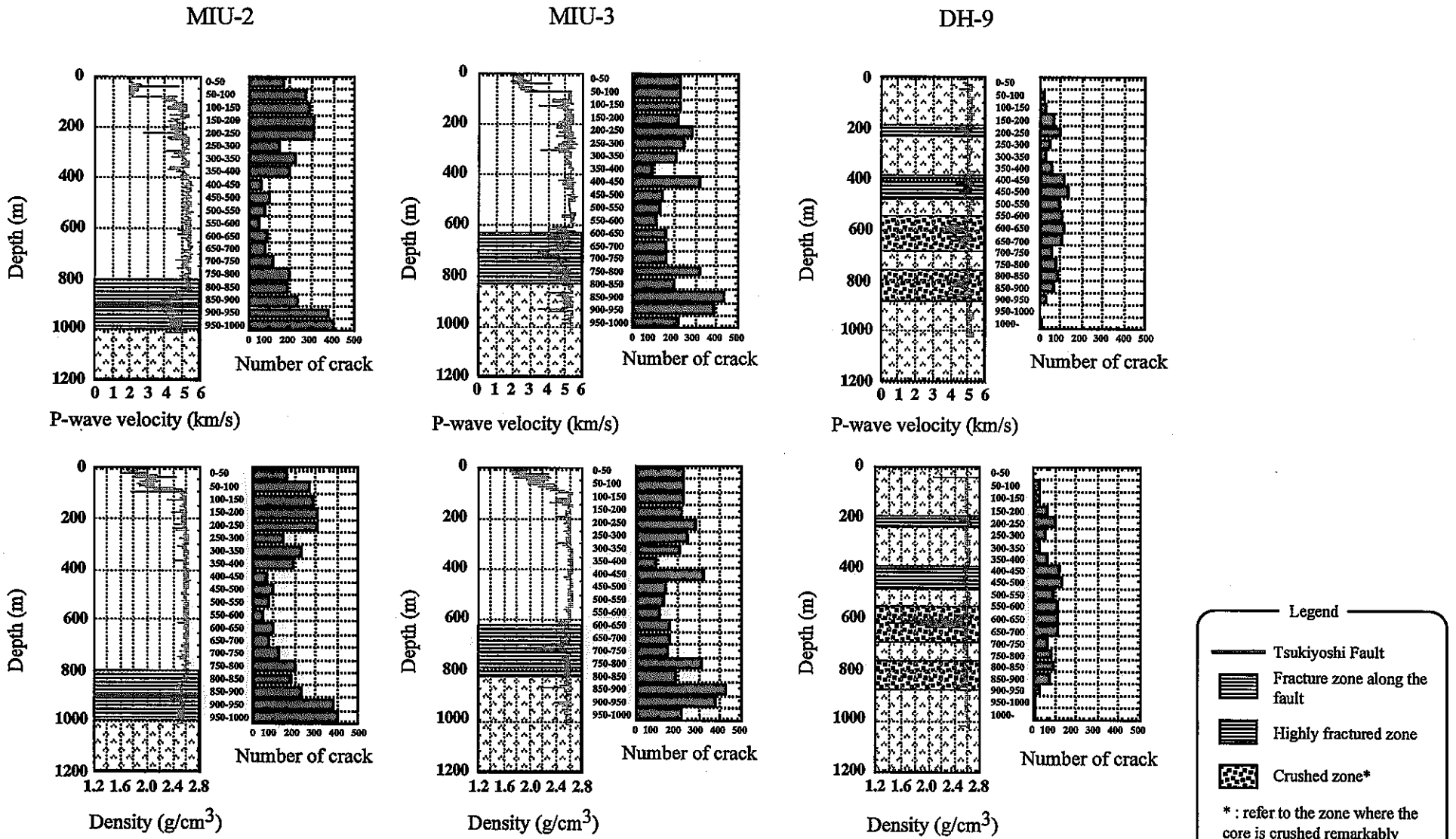

Figure 4.68 Results of BTV investigations, seismic wave velocity logging and density logging

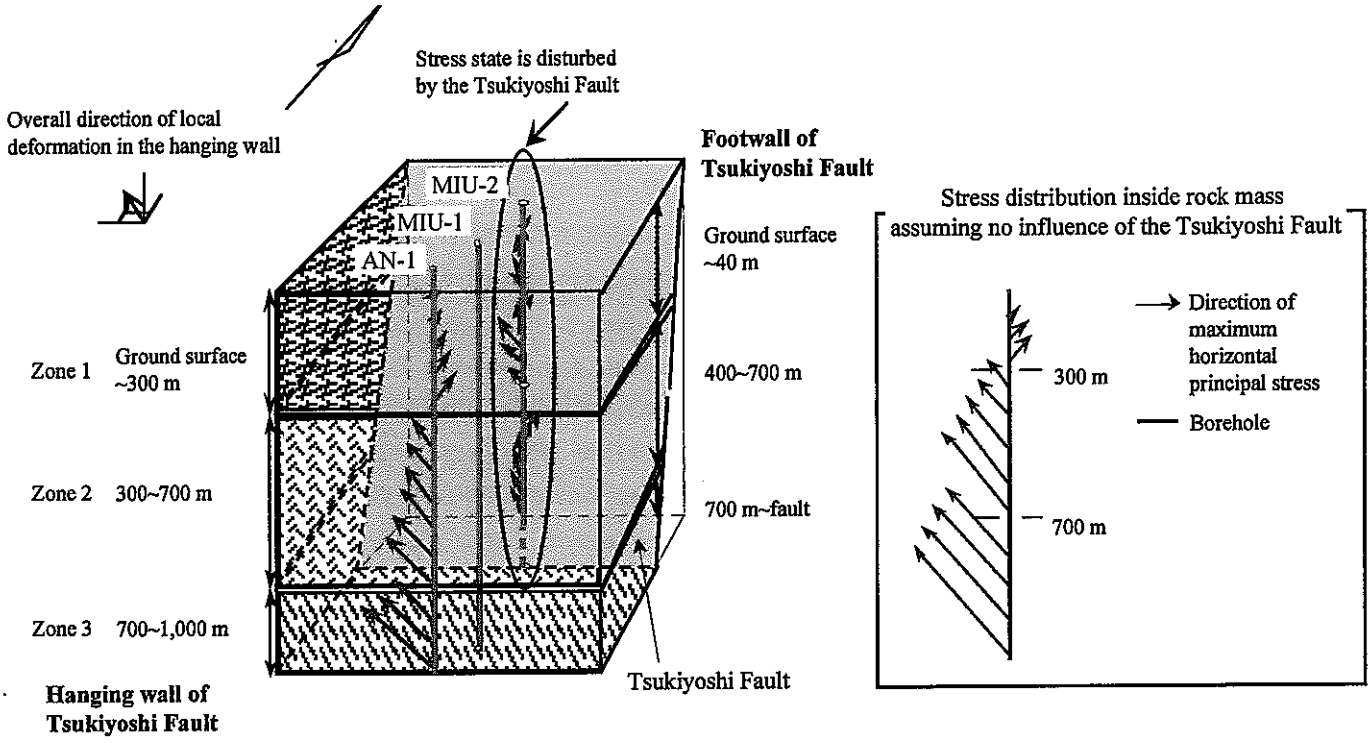

Characteristics of each zone

	Zone 1	Zone 2	Zone 3
• Fracture frequency	High (subhorizontal - horizontal)	Low	High (subvertical)
• Deformability of matrix	Relatively small	Relatively large	Relatively small
• Anisotropy of mechanical properties of rock matrix	Relatively small	Relatively large	Relatively small

(a) Rock mechanics conceptual model of hanging wall of the Tsukiyoshi Fault [77)80)]

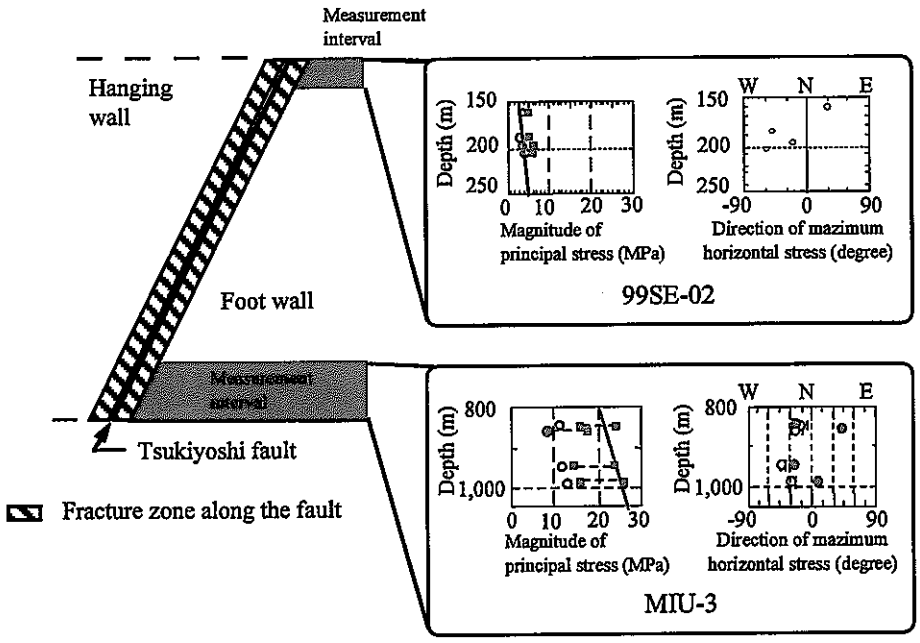

(b) Rock mechanics conceptual model of footwall of the Tsukiyoshi Fault

Figure 4.69 Rock mechanics conceptual model of hanging wall and footwall of the Tsukiyoshi Fault

4.4.5 Summary

Based on a comprehensive assessment of the results of physical/mechanical property tests and in situ stress measurements in AN-1 and MIU-1, 2 and 3, a rock mechanics conceptual model from the ground surface to 1,000 m in depth was developed. The model is shown in Figure 4.70. Its characteristics are as follows.

① The rock mass on the hanging wall side of the fault is divided into three zones characterized by different physical/mechanical properties and stress states. Specifically, Zones-1, 2 and 3 range in 0 to 300/400 m, 300/400 to 700 m and 700 to 1,000 m depth, respectively.

② The investigation results on the footwall side are restricted to 150 to 200 m and 800 to 1,000 m in depth. Therefore, the entire footwall side is assumed, for present purposes, to consist of a homogeneous rock mass. It is difficult to estimate the position and extension of fault-related and fracture-concentrated zones such as those recognized in DH-9. Therefore, the whole section is postulated to consist only of sound rock, without the zones described above.

Though the rock mechanics conceptual model is revised by adding the data on mechanical properties of the footwall, the basic concept of the model was unchanged. In this concept, the rock masses on the footwall side and the hanging wall side show mechanically discontinuous behavior. Furthermore, the hanging wall side of the Tsukiyoshi Fault is considered to be obliquely compressed against the footwall side by the regional tectonic stress. This hypothesis requires that the rock mass on the hanging wall side be divided into large-scale blocks bordered by N-S trending faults, besides the E-W trending Tsukiyoshi Fault. The presence of N-S trending lineaments identified by lineament surveys carried out in and around the Shobasama Site for the RHS Project is thought to support the above hypothesis.

4.4.6 Future tasks

Based on the results of mechanical property tests in MIU-4 (drilling started in 2000 FY), mechanical properties of the Tsukiyoshi Fault and the associated fractured zones are expected to be further understood. Also, the validity of the rock mechanics conceptual model will be tested in the application of numerical analyses. Furthermore, mechanical properties of discontinuity planes should be assessed by joint shear tests. Physical properties of the in-situ rock mass should be evaluated taking the effects of fractures into consideration to quantify the rock mechanics conceptual model.

Stress state

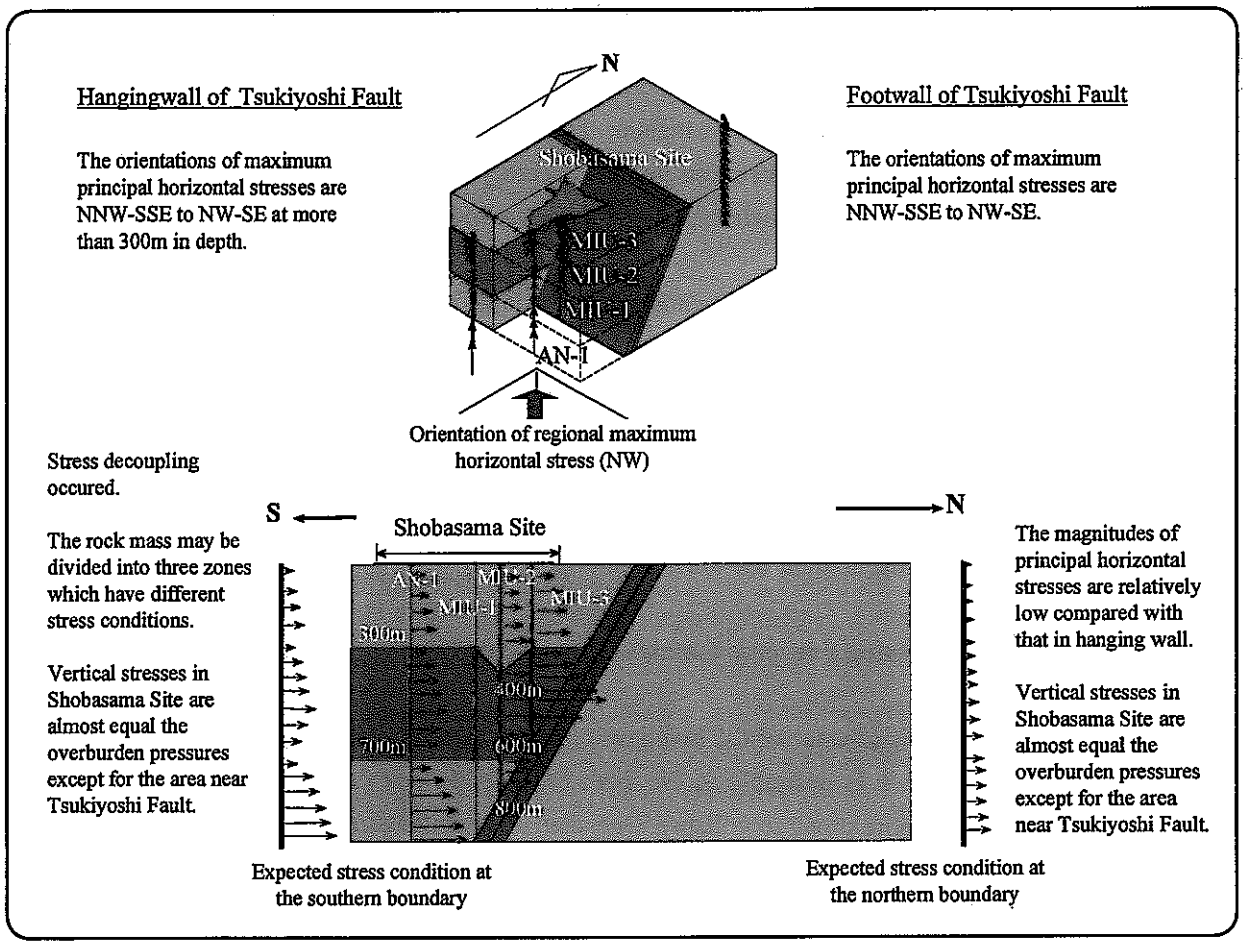

Rock properties

		Hanging wall			Footwall	Near Tsukiyoshi Fault
		Zone 1	Zone 2	Zone 3	Zone 4	Hanging wall / Footwall
Mechanical properties of matrix	Deformability	Low	High	Low	Low	Lowest in Shobasama site
	Anisotropy	?	Large	Small	Very small	?
Fracture distribution		· High fracture frequency · Horizontal~ Sub-horizontal	· Low fracture frequency	· High fracture frequency · Sub-vertical	· Very low fracture frequency compared with hanging wall	· High fracture frequency · Frequency in hanging wall is higher
Expected mechanical properties of in-situ rock mass	Deformability	Lower than Zone 2	Highest in Shobasama site	Lower than Zone 2	Same as hanging wall	Lowest in Shobasama site (about 60 % of other zones)
	Local variation	Large	Small	Large	Small (except for damaged zone)	

Figure 4.70 Rock mechanics conceptual model

4.5 Investigation techniques and equipment

The MIU Project also has the role of testing new investigation techniques and equipment that may be useful for all phases of the investigations. Some techniques and equipment have been or are in the process of being developed by TGC. If the equipment trials or the investigation results do not meet expectations or needs of the individual study field (for example data accuracy or instrument precision and reliability of equipment), the techniques and equipment may be modified to improve performance.

4.5.1 Techniques and equipment for borehole investigations

The MIU Project has adopted an operating guideline to use only fresh water as drilling fluid. Additives such as drilling mud are avoided so that initial permeability of the rock mass and the hydrochemical properties of groundwater are disturbed as little as possible. However, boreholes are less stable and potentially prone to collapse when fresh water alone is used. Therefore, drilling techniques to minimize and prevent collapse and expertise in their use are being developed.

4.5.1.1 Drilling system using a reverse aeration, wire-line method

In order to minimize the disturbance of the hydrogeological properties of the rock mass and hydrochemical properties of groundwater, it is desirable to use fresh water as drilling fluid. However, boreholes drilled without drilling mud are more prone to collapse. One alternative drilling method investigated is the reverse aerated, wire-line method. The method allows use of fresh water for drilling and removal of drilling fluids/rock chips/rock flower by directing fluids into the center of drill rods, which prevents contact with the borehole wall and minimizes collapse of the wall and plugging of open zones (Figure 4.71).

This method was designed in 1997 FY [87] and the overall drilling system in 1999 FY [88].

4.5.1.2 Partial casing insertion equipment

Partial casing insertion equipment was developed to cope with partial collapse of boreholes. This equipment consists of a partial reaming bit, a casing insertion unit and the partial casing [89]. It can be used for drilling of new boreholes as well as maintaining and reaming existing boreholes (Figure 4.72).

The partial reaming bit was manufactured in 1996 FY [90]. An application test was carried out [87] and the casing insertion unit was manufactured in 1997 FY. Also in 1997, the required equipment was assembled and an operational application test on the ground was carried out [87]. In 1999 FY, an overall, trail application test was carried out using the partial reaming bit, the casing insertion unit and the partial casing. Problems with insertion were found by BTV investigation to be at that the lower end of the partial casing set, which was bent to the inside of the borehole and thus prevented the casing from fitting the rock mass adequately. In the future, a method to cut off the bent casing is expected to be developed [88].

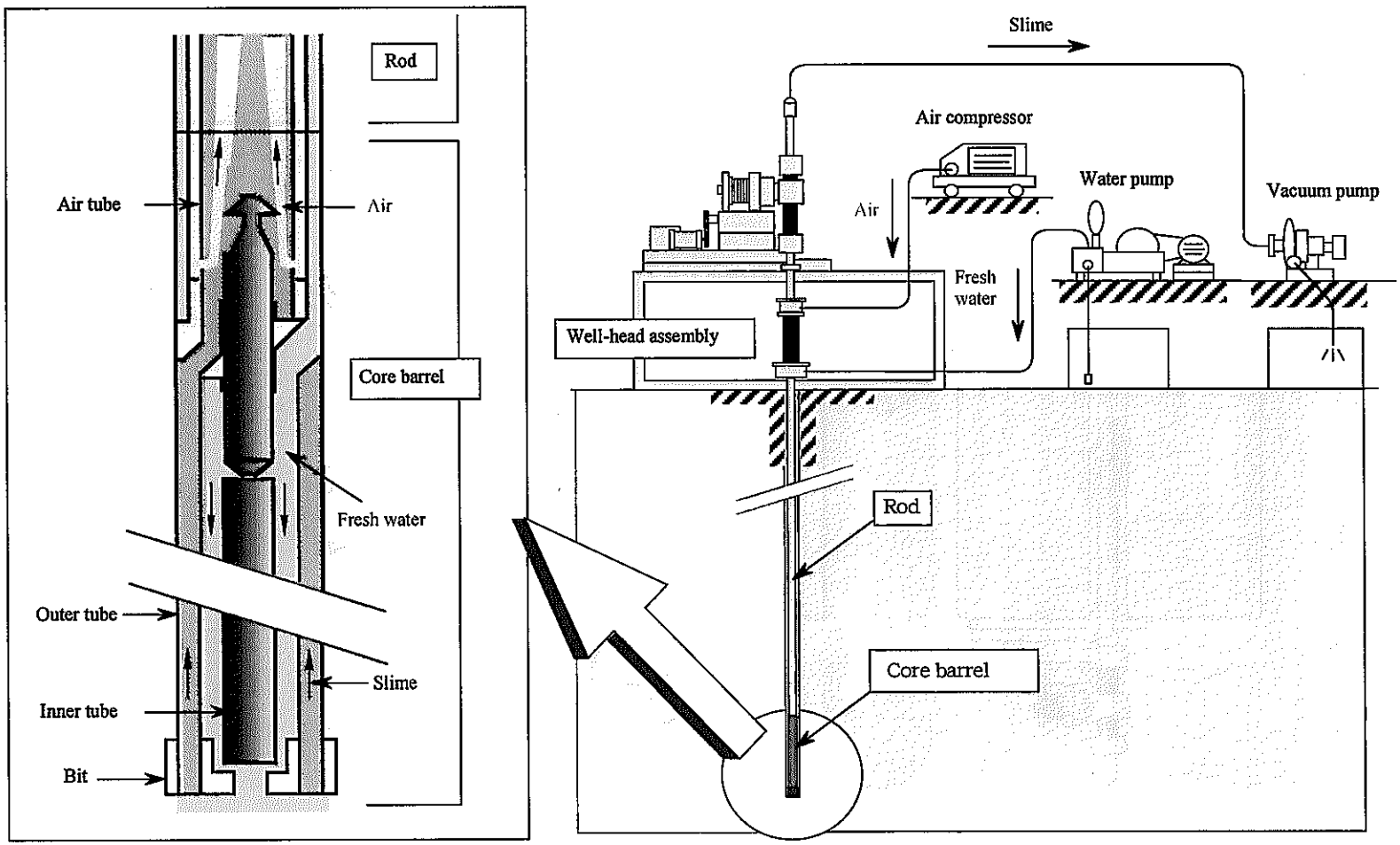

Figure 4.71 Drilling system using reverse aerated wire-line method

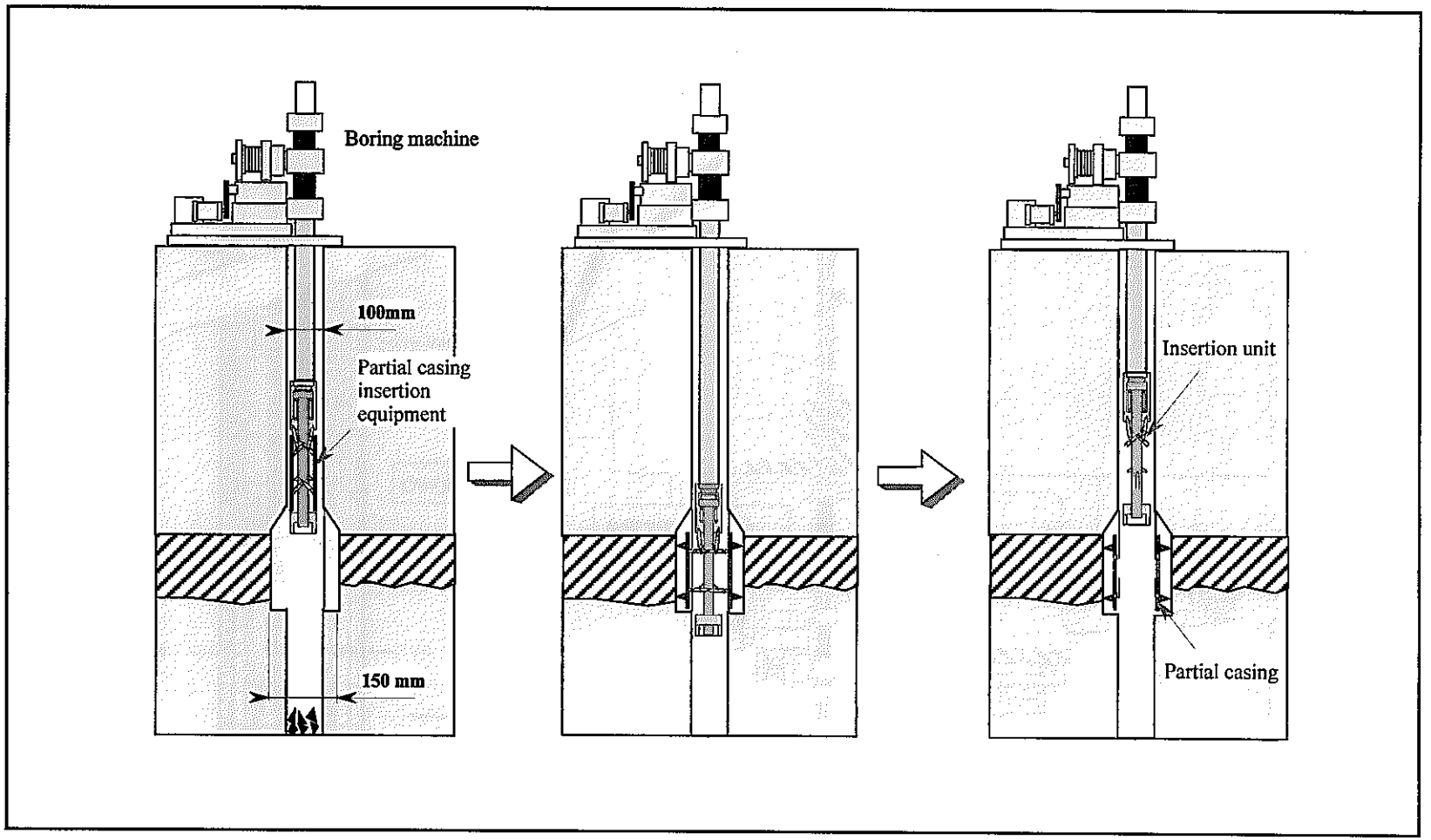

Figure 4.72 Partial casing insertion equipment

4.5.2 Techniques and equipment for geological investigations

4.5.2.1 Seismic tomography

The development of seismic tomography for use in 1,000 m-deep boreholes was in progress to understand the extent of discontinuity planes deep underground. The work in the reporting period consists of the development of an in-hole nondestructive seismic source (sparker) that would work without enducing any damage to the surrounding borehole wall and the development of data analysis techniques.

The in-borehole sparker was designed and assembled in 1997 FY. An application test of the assembled equipment was carried out in 1998 FY [89, 91]. Subsequently, application tests were carried out in MIU-1 and 2 to the depth of 1,000 m in 1999 FY [88]. In addition, the development of a data analysis technique called "full-wave form inversion" was carried out to improve the resolution of signals.

Details of data acquisition in the application tests are shown in Table 4.38. Results of the application tests in the Toki Granite are as follows.

- Using the sparker, tomographic data were obtained with cross-hole intervals of about 100 m and with a target depth of 1,000 m.
- Based on the application test carried out in 1998FY, it was estimated that the maximum distance that allows distinguishing the P-wave generated by the sparker from noise was about 260 m. However, the distance was reduced to about 150 m, due to excessive noise during the test carried out in 1999.
- In order to improve the maximum distance that a P-wave can be recognized, a stacking test with several oscillations was carried out. This test resulted in an improvement of signal to noise (S/N) ratio. For example, Figure 4.73 illustrates an initial P-wave made recognizable by a 32-times stacking test. The maximum distance between the sparker and the receiver was some 240 m.

An initial travel time tomographic analysis was carried out by determining the arrival time of the initial P-wave. Figure 4.74 shows the result of a P-wave velocity structural analysis. The grid size for analysis was 2.5 m (horizontal)×3 m (vertical). The tomographic section was divided into shallow areas with higher velocity (5.3 km/s.) and deeper areas with lower velocity (4.9 km/s.) at about the 850 m depth. This shows a trend coincident with the results of seismic wave velocity logging. The Tsukiyoshi Fault intersected by MIU-2 at around 900 m depth was not recognized as a structure with a sharp velocity contrast against the surrounding rock mass.

As part of the development of analytical techniques for producing seismic tomographic data, an applicability study of full-wave form inversion analysis to actual data was carried out. The data (Table 4.38) obtained by sparker application tests in 1999 FY was used for this study.

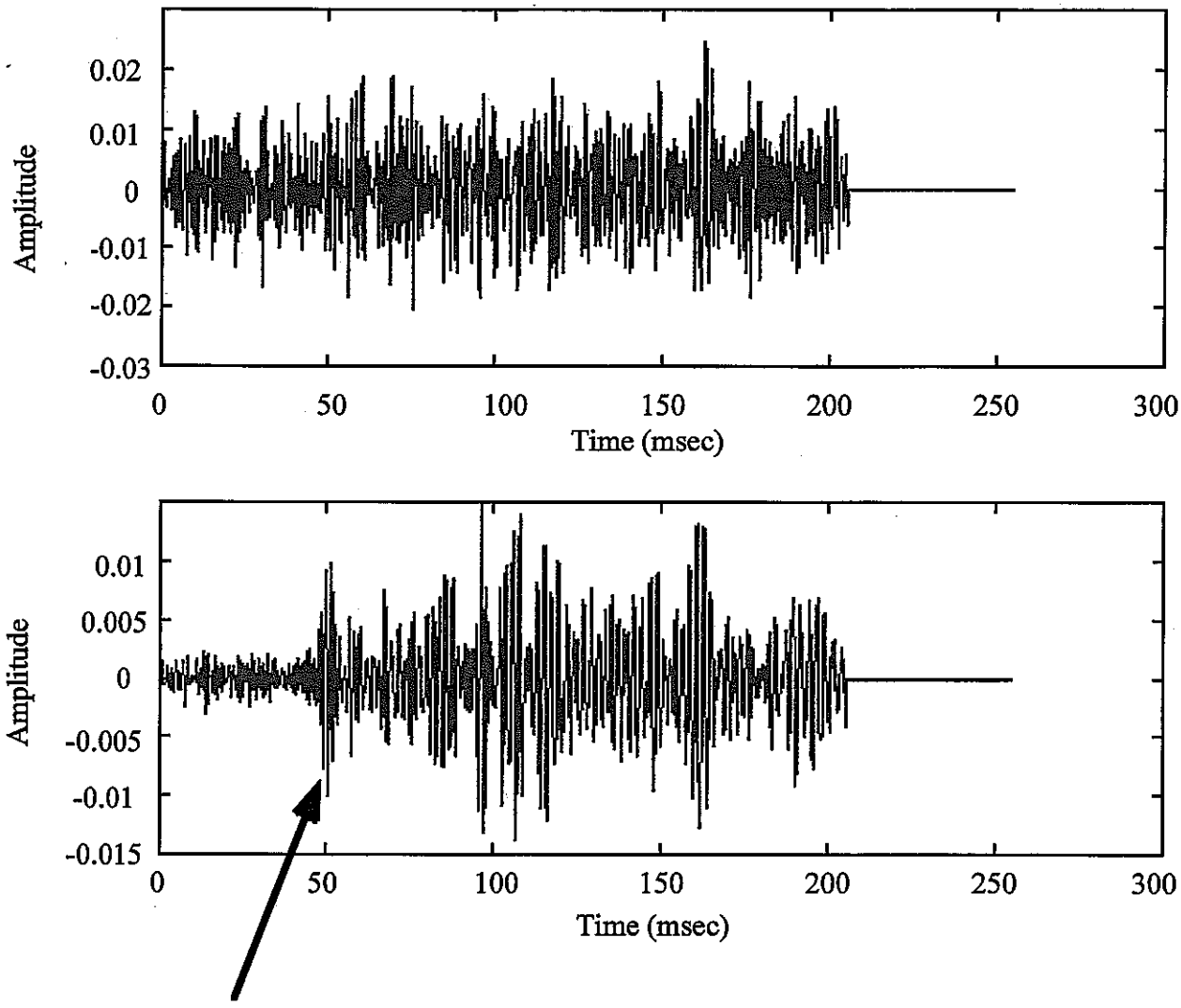

Figure 4.73 Results of stacking test (example)
(depth of sparker : 450 m, depth of receiver : 230 m)

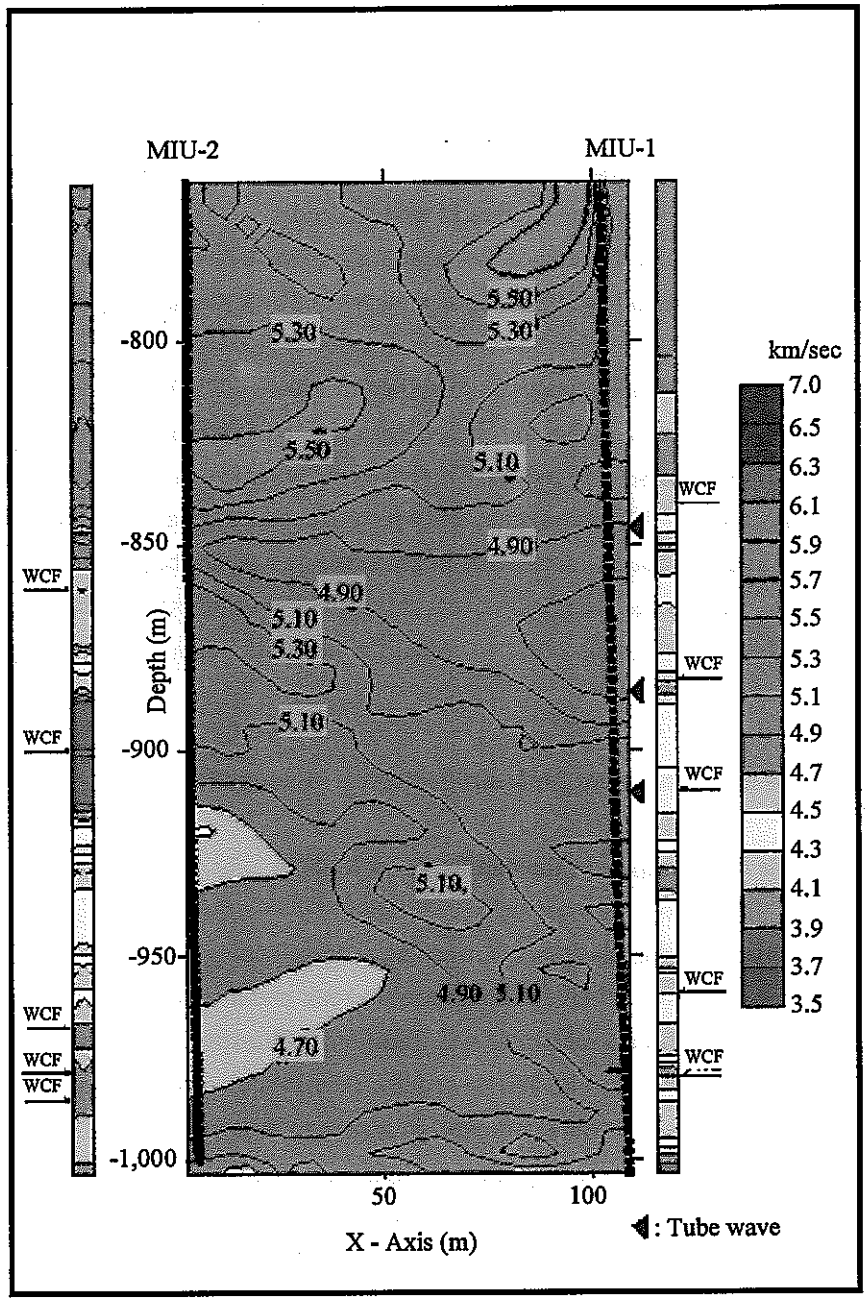

Figure 4.74 The result of P-wave velocity distribution analysis

Table 4.38 Details of seismic tomography

	1998 FY (AN-1, 3)	1999 FY (MIU-1, 2)
Borehole interval	about 36 m	about 95 m
Data acquisition depth	30 m to 364 m	762 m to 1,000 m (Signal) 762.5 m to 1,000 m (Receiver)
Sparker interval/number	1 m/335 points (AN-1)	2 m/120 points (MIU-2)
Receiver interval/number	2 m/168 points (AN-3)	2.5 m/96 points (MIU-1)
Data acquisition number	56,280 (335×168)	11,520 (120×96)
Data length (Recording time)	192 msec	256 msec
Sampling rate	0.125 msec	0.125 msec

Scope of the analysis is as follows.

- Digital simulation for verifying a series of analysis codes
- Study the preliminary processing of data used for full-wave inversion analysis
- Implementation of the full-wave inversion analysis and determination of future tasks

The results of full-wave inversion analysis are shown in Figure 4.75. The grid size for analysis measured 25-cm×25 cm and featured a higher resolution than the conventional initial travel time tomographic analysis with a resolution of several meters. Though vertical variations in velocity show a similar trend to the results of seismic wave velocity logging, only results obtained by a nearly horizontal sparker-receiver pair are usable for analysis due to excessively large noise. As a result, horizontal structures are most likely to be detected. In the future, examination of the application limitation with respect to noise in the full-waveform inversion analysis is expected. Also, the possibility of improvement in the analysis method is needed.

4.5.3 Techniques and equipment for hydrogeological investigations

4.5.3.1 Hydraulic test equipment for depths up to 1,000 m

In order to understand groundwater hydrogeology deep underground, the ability to determine the hydrogeological properties of relatively impermeable rock masses, with hydraulic conductivities of less than 10^{-8} m/s is necessary. Such a rock mass was traditionally classified as impermeable in civil engineering practice. Also, the equipment must be able to acquire accurate data under potentially high temperature and pressure conditions because the target depths exceed hundreds of meters. TGC has been developing equipment allowing in-situ permeability tests on highly impermeable rock masses down to 1,000 m depth (Figure 4.76) [92,93]. This equipment was assembled in 1997 FY, and is being used in the MIU Project and the RHS Project.

The hydrogeological test equipment consists of a downhole unit suspended from stainless steel rods and the surface equipment with cable reels and data acquisition and processor control units. The downhole unit consists of a multi-packer measurement unit with sensors, a pumping unit and a BTV camera. An inner probe can be lowered on an umbilical cable inside the stainless steel suspension rods into the measuring intervals. Use of the stainless-steel pipe provides high tensile strength to the downhole unit and can improve recovery potential in event of borehole wall stability problems. This equipment is useful for the

following permeability tests:

(a) A transient slug test method

(b) A pulse method developed for testing of very low permeability rocks

(c) A pumping test under steady state conditions

By combined use of these methods, a wide range of hydraulic conductivities from 10^{-6} to 10^{-12} m/s can be measured.

The most prominent feature of this equipment is the five multipackers and the BTV at the tip of the equipment string. With five multipackers, it is possible to measure different size test intervals without resetting the equipment. The test intervals can be changed freely by selectively setting the packers between 2 m and 14 m. By measuring pore water pressure and temperature outside of the test interval, it is possible to check if the packers work efficiently. These functions are extremely useful to ensure the quality of the test results. Also, using the BTV, allows the monitoring of the rock conditions in front of and at the sides of the equipment in real time. This enables the confirmation of the rock conditions for packer placement. Furthermore, even when the data has to be collected from a narrow fracture zone, the equipment can be located confidently.

The equipment was improved in 1998 FY [89] for installations in a curved borehole: for example, by adding a centralizer. This improvement is shown in Figure 4.77.

4.5.4 Techniques and equipment for hydrochemical investigations

4.5.4.1 Water sampling equipment for depths of 1,000 m

For fast and precise understanding of hydrochemical properties of groundwater between the ground surface and deep underground, water sampling equipment was being developed [93, 94]. The target depth was 1,000 m and the aim was to minimize further disturbance of the properties of geological environment caused by borehole drilling. This equipment was developed by 1997 FY and has been used for the MIU Project and the RHS Project.

The equipment comprises surface equipment, a connector and underground tools (Figure 4.78). All functions related to water sampling are located in the in-hole section. Installation through drill rods or casing was adopted as the basic procedure, as a precaution against borehole collapse, similar to the above hydraulic test equipment for depths to 1,000 m.

Batch water sampling function was adopted so that sampling in a confined inert state, to ensure maintenance of in situ chemical properties, was possible. Also, the capability for continuous purging of groundwater with a pump was added to enhance the sampling efficiency.

Furthermore, the equipment was improved in 1998 FY [89] for coping with a curved borehole, for example, by adopting flexible joints. The improvement is shown in Figure 4.79.

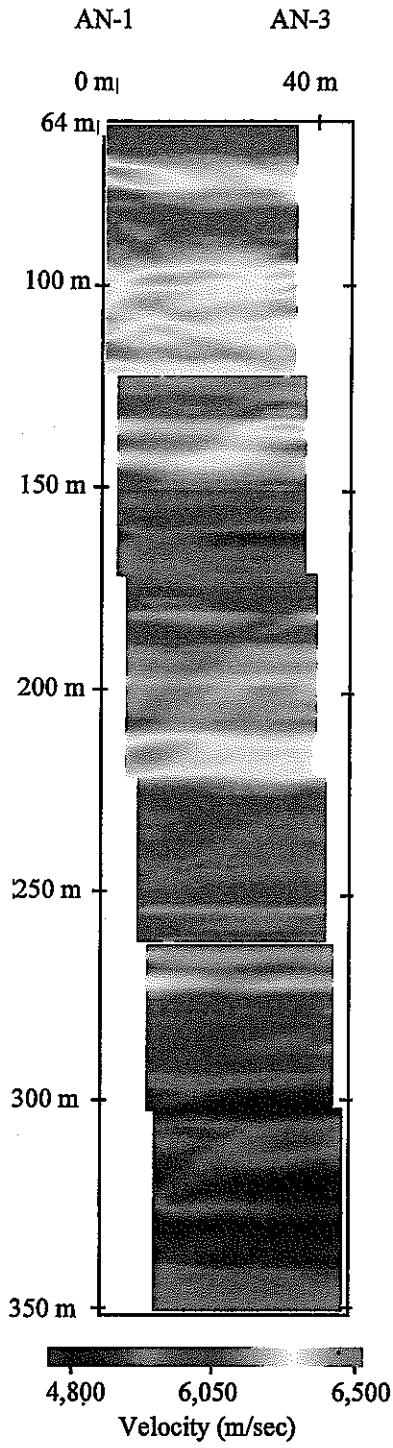

Figure 4.75 The result of full wave-form inversion analysis

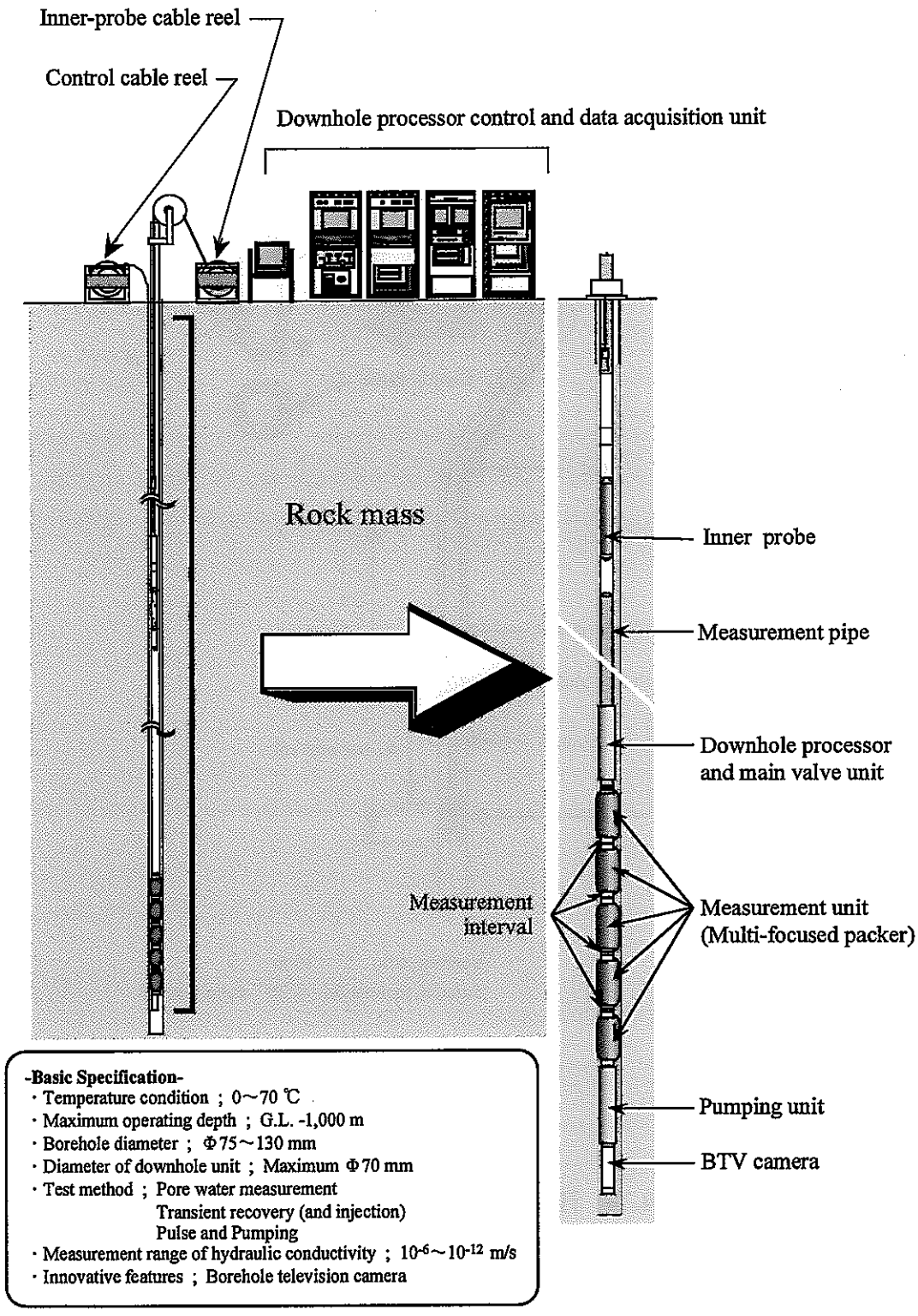

Figure 4.76 Hydraulic test equipment for depths of up to 1,000 m

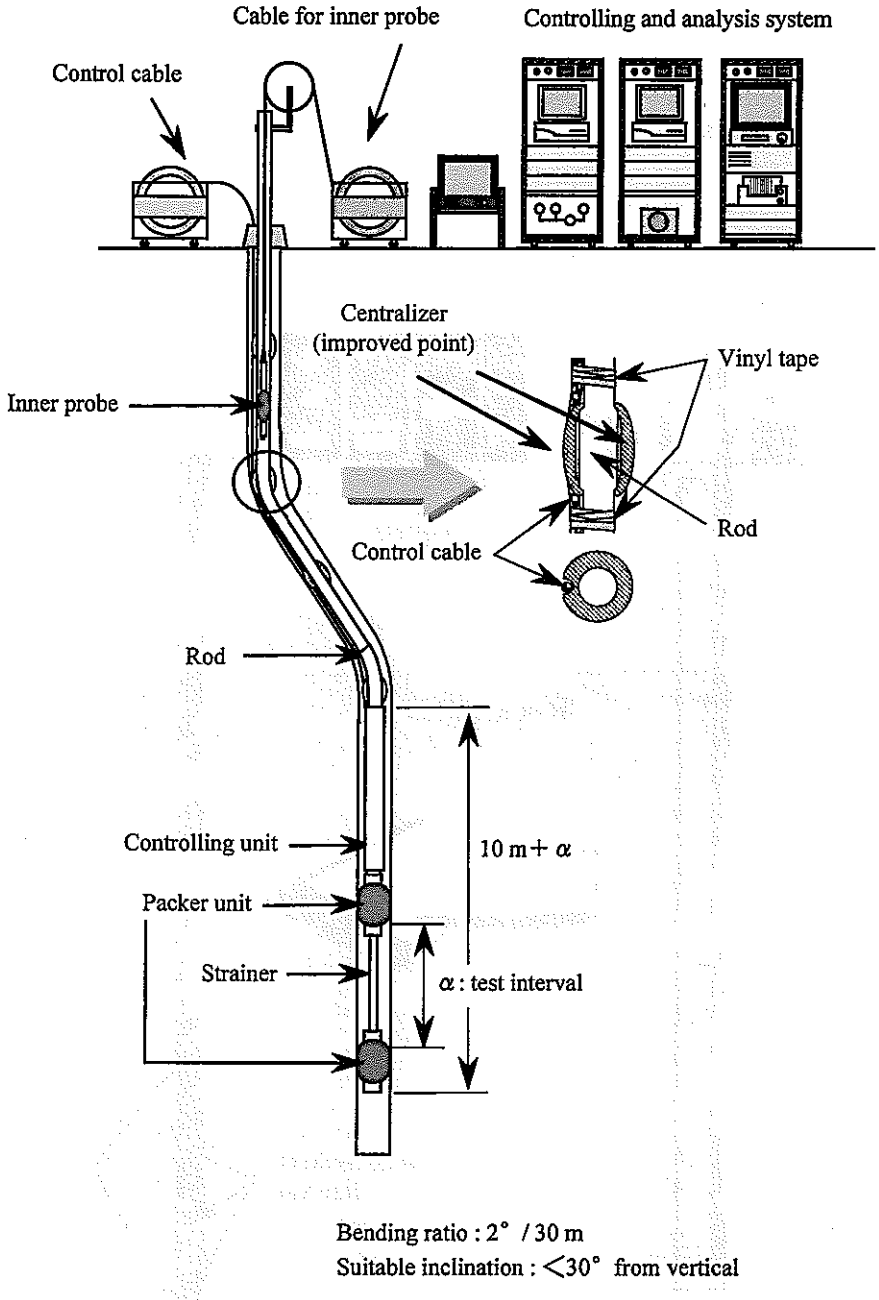

Figure 4.77 Hydraulic test equipment for depths of up to 1,000 m (improved for curved borehole)

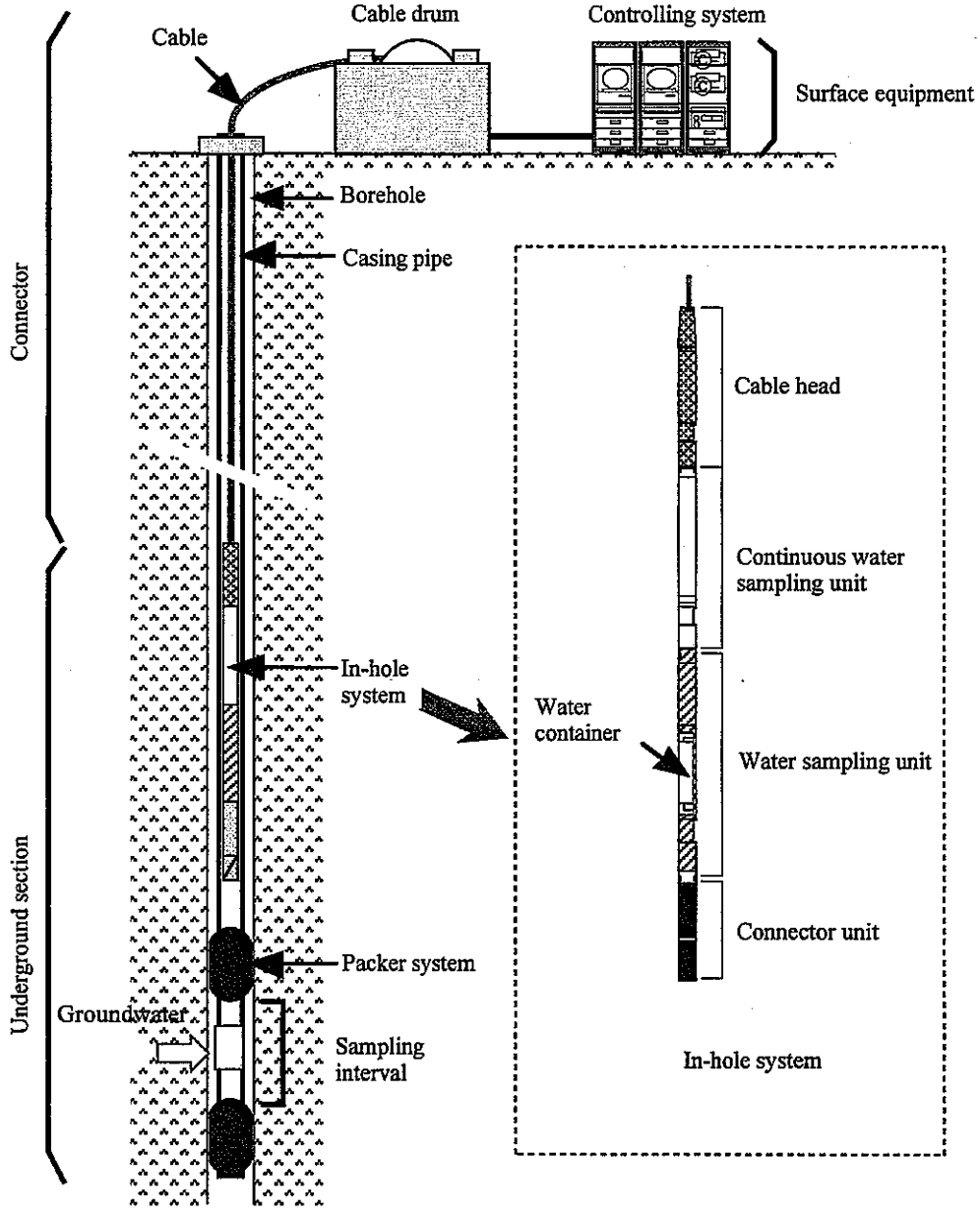

Figure 4.78 Water sampling equipment for depths of up to 1,000 m

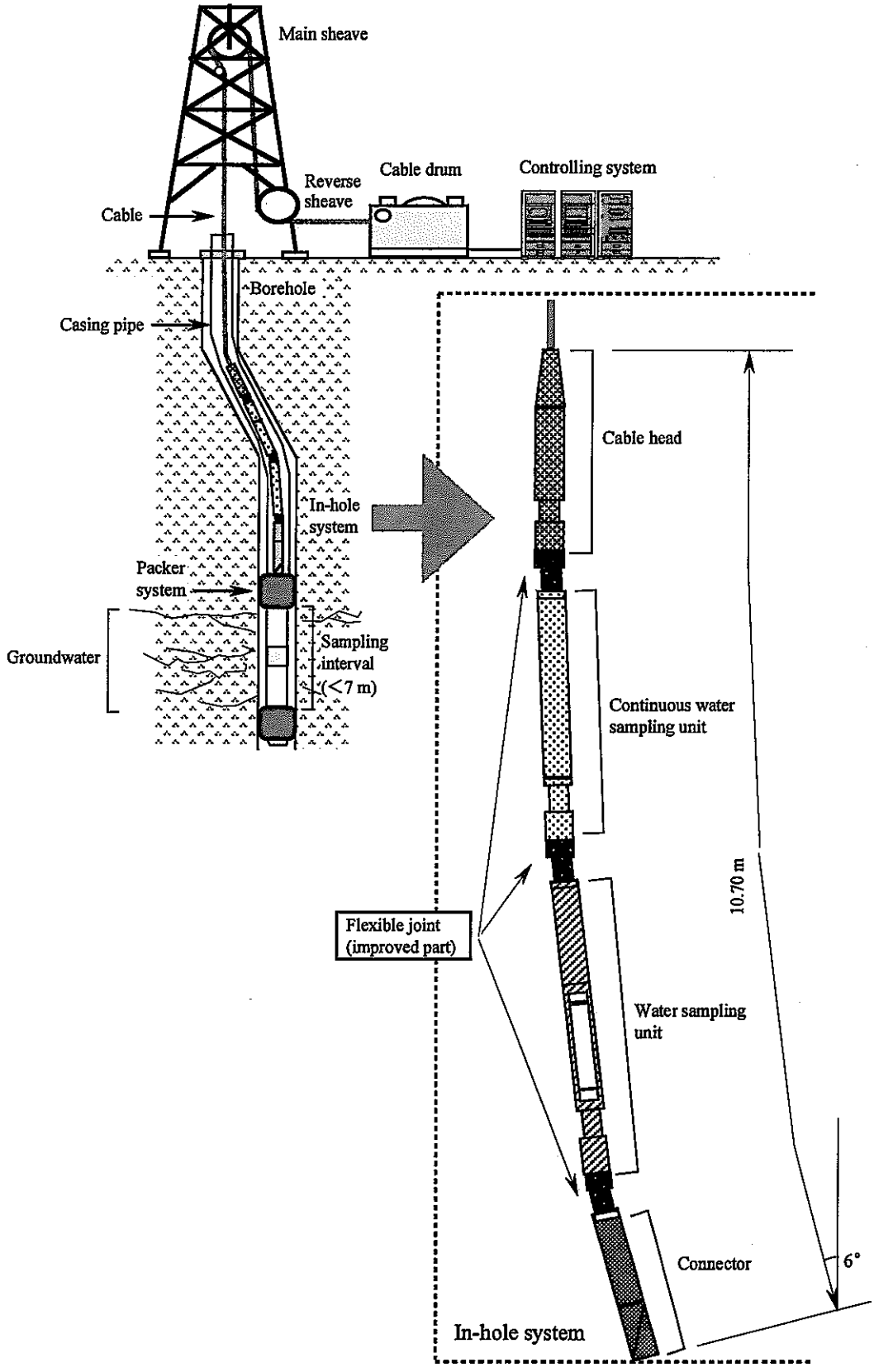

Figure 4.79 Water sampling equipment for depths of up to 1,000 m (improved for curved borehole)

4.5.4.2 Geochemical logging unit

The geochemical logging unit was developed for in-situ acquisition of physico-chemical parameters of groundwater, including pH, redox potential, electrical conductivity, and sulphide ion concentration and water temperature.

This unit was mounted on the water sampling equipment for depths to 1,000 m, allowing real-time data acquisition of the physico-chemical parameters of groundwater during continuous water sampling operations. Thus, it allows confirmation of the in situ chemical condition of groundwater, and in particular, the replacement of drilling fluid in boreholes by groundwater flowing into the sampling interval isolated by double packers. Also, it enables the accurate timing of water sampling [94].

4.5.5 Techniques and equipment for rock mechanical investigations

4.5.5.1 In situ stress measuring equipment for depths to 1,000 m

Determination of in situ stress in the rock mass is necessary because the stress establishes a boundary condition indispensable for optimized designing and stability assessment of the MIU Project's research galleries and for numerical analysis of rock mass response to shaft excavation.

In situ stress determination techniques in general-use are classified into in situ techniques such as borehole methods (e.g. hydraulic fracturing and over-coring techniques) and laboratory techniques using recovered core from boreholes or outcrops (e.g. AE tests and DRA tests, etc.). Techniques are in various stages of development ranging from the proven / practical use stage to the research/development stage. However, limiting conditions are unavoidable for measurement and analysis, including a depth limit for application. Thus, during the reporting period, there was no highly reliable technique for cost-effective and efficient measurement of 3-D in situ stress at 1,000 m depth [95].

Because of this situation, the development of in situ stress measuring equipment for determination of in situ stress at depths up to 1,000 m was required. The equipment to measure in-situ stress by stress relief or strain recovery is based on the over-coring method (Figure 4.80).

Before proceeding with the development of this equipment, literature surveys were carried out on domestic and overseas studies. In 1996 and 1997 FY, recommended techniques and a conceptual design of the equipment were determined. Also, future tasks were determined. [87,90,95]. Based on the results, design of the measuring equipment and manufacturing of parts has been carried out since 1998 FY [89]. The parts are a strain gauge cell (with a thermometer), pressure vessel to house batteries, data recorder and an azimuth-inclination measuring device [89]. The latter components, the azimuth-inclination measuring device and the data recorder, will be manufactured and their function tests will be carried out in and after 2000 FY.

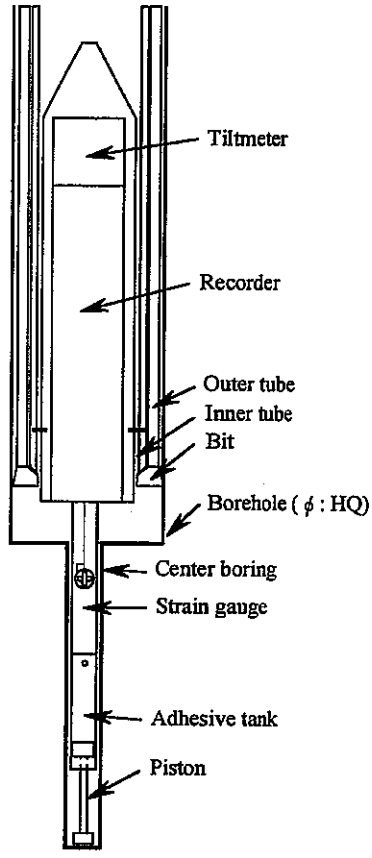

(a) Details of probe

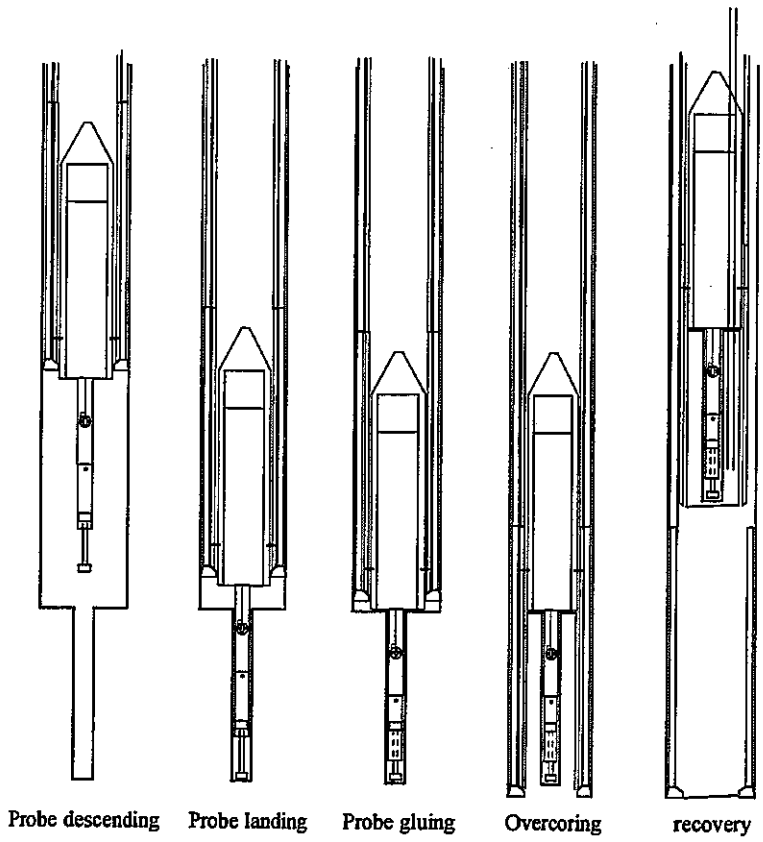

(b) Procedure to measure in-situ stress

Figure 4.80 3-D in-situ stress measurement equipment for depths of up to 1,000 m

4.5.6 Techniques and equipment for use in Phases II and III

4.5.6.1 Continuous-wave radar investigation techniques

Radar tomography can be used for two boreholes with separations of up to several tens of meters. It is presumably possible to expand the distance by employing continuous waves as transmitting-receiving signals, especially, in crystalline rocks such as granite characterized by a large resistivity and a small energy loss (attenuation). An improvement of the borehole radar investigation technique used in the Kamaishi Mine, the continuous wave radar investigation method is being developed. It aims to expand the survey depth and enhance resolution. In the long run, this development aims for higher space resolution and longer survey distance than the current radar capabilities, by putting the ACROSS (accurate regulation of steady signal system) technology [96] to practical use.

In 1998 FY, an experimental device of continuous wave radar was manufactured. In 1999 FY, with the purpose of understanding the heterogeneity near the ground surface and using this technique as a tool for understanding the frequency-dependence of ground electrical permittivity, the input impedance in air and on water were measured using three types of antennas with targeted frequency bands: 1 to 5, 5 to 50, 50 to 200 MHz. As a result, basic data on the resultant impedance of antenna and medium was obtained [88].

4.5.6.2 A long-term monitoring system using boreholes

The MP system described above for observing groundwater pressures does not have the measuring capability to function under a high differential pressure environment that may be caused by shaft excavation in the Phase II and during a large-scale pumping test. Consequently, a long-term monitoring system is being developed to cope with high differential pressure conditions.

Application tests were carried out to 200 m depth using the system manufactured in 1999 FY. As a result, its overall function was ascertained. However, noise (chattering) occurred in the depth sensor, which hindered connection with measuring ports at the correct depths. Oil fouling inside the casing was determined to be the main cause. Cleaning the inner surface of casing with organic solvent solved the problem [88].

4.5.6.3 An investigation system of research gallery walls

The walls of research galleries will be mapped during excavation. The information obtained by the observations will be important to assess the predictions made in Phase I and to understand the geological environments around the research gallery. So far, engineering information on shaft and tunnel face surveying systems has been gathered and the following future tasks determined [89].

- It is important to determine the distribution of discontinuities (e.g. fractures), water inflow conditions and weathering. Determination of fractures requires a high signal / image resolution, whereas extraction of water inflow and weathering requires color capability. Thus, a survey system employing a digital camera was thought to be appropriate.

- When the wall of a 6m-diameter shaft is covered by 4 to 6 photographs using a digital camera, with the highest resolution (six million pixels as of 1998 FY), resolutions as small as some 2mm can be expected.
- Design and cost of the investigation system depend largely on a degree of automation of the photography using digital cameras.
- Extraction of discontinuity planes by image processing was put to practical use. However, automatic extraction of water inflow conditions and weathering has yet to be tested with a practical example.

4.5.7 Data base construction and development of a data analysis/visualization system on geological environments

4.5.7.1 Data base management and construction

The MIU Project will produce a huge amount of data from the investigations. Introduction of database management systems began in 1996 FY for management and utilization of the data [90]. One of them is GEOBASE, an integrated underground resources data base system developed by Geothermal Technology Development Co., which is being improved as follows [87,89].

- Addition of a table for information management to guarantee the data quality, including data acquisition and analysis techniques
- Addition of a table for the management of core descriptions in boreholes and chemical analyses
- Addition of a table for time management of data from boreholes
- Addition of a function to refer to and display the information extracted by BTV investigations
- Development of a PC-based simple reference software
- System innovation so that GEOBASE can be accessible to every researcher using intranet.

The location of boreholes, geophysical logging, hydraulic tests, geological columnar sections and surface water hydrology would be registered in the data base system.

4.5.7.2 Data analysis/visualization system of geological environments

Geological models form the basis of the models for hydrology, hydrochemistry and rock mechanics. Thus, 3-D visualization of the geological model through computer graphics makes it easy to share the necessary information for constructing the other models.

EarthVision, 3-D visualization software developed by Dynamic Graphics Inc., has been used for visualizing the geological model. The software forms a 3-D geological model by estimating shapes of discontinuity planes such as boundaries between geological formations and faults, and integrating the discontinuities by considering their relationships with respect to relative positions and development processes [16,17].. Furthermore, this software has had demonstrated application in overseas projects for geological disposal, such as at Sellafield (Nirex), Wellenberg (Nagra), Äspö HRL (SKB) and Yucca Mountain (USGS, USDOE) [18]. This system was used for the construction of the geological model in the Phase I-a in the MIU Project (See Section 4.1). Minimum tension theory based on spline interpolation, one of the functions of

EarthVision, was applied to estimate the ground surface, geological boundaries and fault planes. The method is an interpolation between adjacent data to find the smoothest curved surface by an n-dimensional polynomial formula using the input data of positions and directions [19].

In addition, this visualization system ensures a close connection with the above-mentioned data management system, GEOBASE and also introduces FRAC-AFFINITY [17], a 3-D saturated/unsaturated seepage flow analysis code using a finite difference method. FRAC-AFFINITY has the following characteristics.

- It can model a hybrid medium that allows simultaneous handling of a porous medium and a fractured medium.
- The fractured medium component can handle both deterministic fractures and stochastically generated fractures.
- Physical properties in a porous medium and a fractured medium (deterministic) can be set either homogeneously for every geological formation/ structure or heterogeneously using statistical techniques based on fractal theory.
- The fractured medium part (stochastically generated) can be set to develop either at random or at fixed positions. Physical properties can be set to develop either homogeneously or stochastically based on a normal distribution.
- Data-interface environments from EarthVision used for the construction of geological models are already systematized. Therefore, it was easy to form input data and differential meshes.

Improvements are expected in and after 2000 FY. For example, a function to take anisotropic permeability of fractures into consideration was expected to be added to the saturated/unsaturated seepage flow analysis code in the existing systems.

4.5.8 Techniques and equipment for information disclosure

4.5.8.1 Virtual reality technology

In order to explain geoscientific studies carried out in the MIU Project to the general public more effectively, virtual reality (VR) technology has been investigated. Also, its applicability to the MIU Project was examined. Specifically, new software has been developed. This software enables users to feel as if they are walking around in the underground facilities; a realistic experience is provided by using a head mounted display (HMD) [97]. In addition, scale models [87] for explaining the MIU Project and the drilling techniques employed are on display in the community plaza at the Shobasama Site.

4.6 Evaluation of predictions

As was described in the Section 2.1, one of the goals of Phase I is "To establish methodologies for evaluating predictions". This goal was set to specify the criteria and detailed methodologies for evaluating predictions made in Phase I by comparison with the data obtained in Phase II.

In order to evaluate prediction properly, it is required to clearly define what to evaluate, how to evaluate, and where and how to obtain data. Aspects to be considered include:

- Was the data used for model development and predictions sufficient?
- Was the data used for predictions accurate?
- Was the conceptual model derived appropriately?
- Was the numerical model derived appropriately?
- Was the data used for evaluations sufficient?
- Was the data used for evaluations accurate?

The ultimate objective is to develop methods and expertise in making accurate conceptual and numerical models for a site. Comparison of actual observations to the predictions made in these models will include an evaluation of the predictions and the degree of accuracy. Evaluations of the predictions will serve as a test of the accuracy and validity of the models and thus provide an assessment of the applicability of the technology and accuracy of the geoscientific data used to build the models. This includes an assessment of the field techniques used to collect the data and an assessment of the analytical methods used to make the predictions.

Thus the evaluation will provide one way to confirm the applicability of the technology for site characterization and selection for waste disposal.

Taking into consideration overseas experience, an approach followed by SKB, Sweden, was examined in Phase I. The outline and possible usefulness, in terms of applicability and lessons learned for the MIU Project, are as follows.

4.6.1 Geological investigations

Predicted geological conditions, the lithologies and structures, will be compared with the geology and geological structures encountered in the shafts, in the stages and in the research galleries excavated in Phase II.

A precedent that established methods for predictions and evaluation was developed by SKB for the HRL project in Sweden [98].

In the HRL Project, geological models with these elements were developed at the following scales:

- Facility-scale (500 to 1,000 m), fracture zones
- Block-scale (50 to 100 m) lithofacies, fracture zones, rock properties, fracture properties

· Detailed-scale (5 to 10 m). Rock properties, fracture properties

For these scales, predictions were made of the following:

- · Lithofacies: ratios of constituent lithofacies, location of facies boundaries, frequency of facies boundaries, mineral composition, and alteration
- · Fracture zone: location, strike, dip, width, RQD (for large fracture zone only)
- · Rock properties: matrix porosity, density
- · Fracture properties: number of fracture systems, general trend, spacing between fractures, trace length and filling minerals

Predicted values included confidence intervals and certainty. Expert opinion played a role in estimating uncertainty. When measured values are within the confidence interval, the prediction is assessed as valid. The validity of the prediction was quantitatively expressed by the following equation.

$$\text{Percent absolute error} = \frac{\text{absolute value of difference between predicted and measured values}}{\text{measured value}}$$

4.6.2 Hydrogeological investigations

Predictions can be evaluated by comparing observations in Phase II with the predictions in the hydrogeological model and the groundwater flow simulations.

Methods of prediction and evaluation used in the HRL project in Sweden, which carried out a groundwater flow simulation based on a hydrogeological model were considered. Major water channels were deterministically integrated into the site model during surface-based investigations [99]. The prediction was evaluated by determining the amount of groundwater inflow. Specifically, total inflow into research galleries, inflow along research galleries (inclined galleries and the spiral ramp) and inflow into weirs. However, the assessment done was qualitative.

For the MIU Project, the following can be used for the evaluation.

- · Volume of groundwater inflow into shafts and research gallery
- · Changes in water pressures in the boreholes (head changes) in response to groundwater drawdown as the shafts and research gallery are excavated.

Concerning inflow, (a) total volume, (b) amount from individual water channels and (c) amount from the sections/locations established in advance for inflow measurement are thought to be predictable. For measurement of inflow, water collection rings or trays can be constructed at selected sections or locations. In fracture zones where significant water inflows are expected, several exploratory boreholes can be drilled for estimating the potential water inflow amounts, if this is possible without disturbing the system.

The drawdown in boreholes due to the advance of research galleries can be measured by the MP monitoring system installed prior to excavation. Intervals for water pressure measurement are determined

from the results of long-term pumping tests carried out prior to shaft excavation and predictive simulations. The predictions can be evaluated by comparing the drawdown with the prediction from the simulation and should be done as quantitatively as possible.

4.6.3 Hydrochemical investigations

The spatial distribution and changes of the hydrochemical properties can be predicted on the basis of observations in Phase I and within the framework of the geological- hydrogeological models. The prediction will be evaluated by comparing the predicted and measured data obtained during the drift excavation. Evolution of the hydrochemistry is more difficult. It is time and rate dependent, responding to groundwater flow system changes and the kinetics of water/rock interaction and microbial activity.

One phenomena expected in the research gallery excavations will be a hydraulic pressure drop due to excavation and resultant drawdown of the groundwater flow system [99]. It is presumed that the distribution of hydrochemical properties of groundwater is closely related to the groundwater flow system. Therefore, a change in groundwater flow system would cause a change in the distribution of hydrochemical properties of groundwater. For example, a drop in water level can allow oxidizing water to penetrate to deeper levels in the rock mass, in turn resulting in a change in redox potential and location of the redox front [100].

To predict changes that originated due to research gallery excavation, it will be necessary to determine items that should and those that could be predicted in Phase I. Based on the 3-D distribution of hydrochemical properties obtained in the Phase I, these items that should be and those that could be are extracted. These items are as follows.

Items that should be predicted:

- All items planned for analysis using boreholes drilled in Phase I

Items that could be predicted:

- Components with no significant difference between surface water and groundwater.
- Components whose analytical quality are not guaranteed.

4.6.4 Rock mechanical investigations

The rock mechanical predictions can be evaluated by determining (a) the response of the surrounding rock mass to excavation and (b) any change in physical properties during the excavation of underground facilities. The distribution of RMR (Rock Mass Rating) was predicted in overseas underground research facilities for predicting the physical properties distribution of the rock mass. However, there was no predictive analysis of the rock mass for the entire facility.

Following predictions are made through modeling and simulation in Phase I.

- 3-D distribution of rock mechanical properties of the rock mass (physical/mechanical properties and in situ stress states)
- Deformational behavior (mode of rock failure) of the rock mass surrounding research galleries in response to their excavation

- Distribution of the damaged zone resulting from stress change/concentration in the rock mass around research gallery

The first prediction was done by construction of the rock mechanics conceptual model. The latter two are predicted from the results of numerical simulations. All of these predictions are evaluated as follows.

4.6.4.1 Data needed for evaluation of the prediction

Data for evaluating the rock mechanics conceptual model

Rock mechanics conceptual model is constructed by interpreting the data obtained from boreholes and rock samples. The following in-situ data obtained during excavation will be necessary.

- Physical properties (physical/mechanical properties of rocks and 3-D in situ stress distribution)

Data for evaluating the results of predictive simulations

The following results of the predictive simulations are necessary.

- Behavior of the rock mass surrounding research galleries (mechanical failure and development of an EDZ, displacement of the rock mass, displacement along fractures and total displacements)
- The extent of stress changes caused by stress redistribution
- The extent of damage (plastic domain) by stress concentration in the rock mass

4.6.4.2 Method of evaluating predictions

Evaluation of rock mechanics conceptual model

The physical properties, the in situ stress distribution (given as a boundary condition) and the division of the rock mass into zones in the conceptual model are to be compared with the measured data. For the in situ stress distribution, it might be greatly affected by the Tsukiyoshi Fault, depending on the location of the research galleries. Therefore, the results of the simulation of the 3-D stress distribution carried out before research gallery excavation will be evaluated. If the conceptual model is determined to be invalid, the numerical model and simulations will likely be incorrect, unless the numeric model is insensitive to the deterministic properties used.

Evaluation of the predictive simulations

When the rock mechanics conceptual model is evaluated as correct, the simulation results described in the above-mentioned "Data for evaluating the results of predictive simulations" in (4.6.4.1) are compared with the measured rock mass response as an assessment of the accuracy of the numerical models. If they are in agreement, the simulations are considered valid.

If the rock mechanics conceptual model is evaluated as incorrect, the rock mechanics conceptual model should be re-constructed with new, better data or interpretations of the deterministic data. As stated above, if the conceptual model is incorrect, the numerical model is also likely to be incorrect.

As well, if the numerical simulations of rock mass response do not agree with the actual rock mass

response, the model must be re-evaluated.

Re-evaluation of the predictive simulations

Two approaches are considered for the re-evaluation. If the conceptual; model developed above is considered appropriate, the numerical simulation is evaluated. If the conceptual model developed above is considered to need revision, this will be done and a new simulation run.

In either case, if there are qualitative discrepancies between the results of the predictive simulations and the measured data, the cause should be examined. If this is the case, the discrepancy is considered to originate in factors that have not been considered in the model. Therefore, the models are adjusted and a re-run of the numerical simulation would be carried out, if possible. When quantitative discrepancies are found, the input parameters for physical or mechanical properties are checked and the model is re-calibrated and re-run.

Following should be possible by the above- process.

- Validation of the process from investigations, model construction to a predictive simulation
- Required data and its accuracy acquired in the Phase I assessed
- Optimization of the investigation methodologies for model construction

4.7 Development of engineering technology for deep underground

In Phase I-a, development of engineering technology was carried out for deep underground application. These are:

- Considered the basic concepts of the MIU Project design, including facilities and science program
- Determine investigation items to be carried out in and after Phase II by referring to domestic and overseas experience and Japanese requirements for an underground research laboratory set out by the Atomic Energy Commission (1994) [1]
- Conceptual design of the research gallery layout.

Regarding the development of the research galleries, the following must be taken into consideration.

① Unlike other underground civil structures, excavation is considered an integral part of the research and therefore, research activities are to be carried out during the excavation.

② Investigations are expected to follow a series of procedures: surveys → simulation → prediction → verification. In case unexpected geological environments are encountered, the facility design and the research plan should be flexible enough to cope with the unexpected geological environments by either avoiding them or incorporating them into the study objectives. This is "Design As You Go" and is considered necessary to ensure excellent results [101].

Geoscientific research carried out in the MIU Project consists of:

① geological investigations
② hydrogeological investigations
③ hydrochemical investigations
④ solute transport
⑤ rock mechanical investigations
⑥ investigation techniques and equipment
⑦ engineering technology for deep underground
⑧ seismological observations, etc.

These investigations are complexly inter-related. Therefore, it was considered important to design an appropriate layout that will allow achieving the goals of the entire project and of each Phase. In designing the layout, the interrelationships of the experimental activities, their requirements in terms of location, access, duration etc must be taken into consideration.

Basic concepts of designs are examined from the above-points of view. In addition, domestic and international experience and Japanese government requirements for underground research laboratories outlined by the Atomic Energy Commission (1994) [1] are examined and investigation items to be carried out in Phases II and III determined [102].

4.7.1 Basic design concept

Basic design concept considered in Phase I-a was as follows (Figure 4.81).

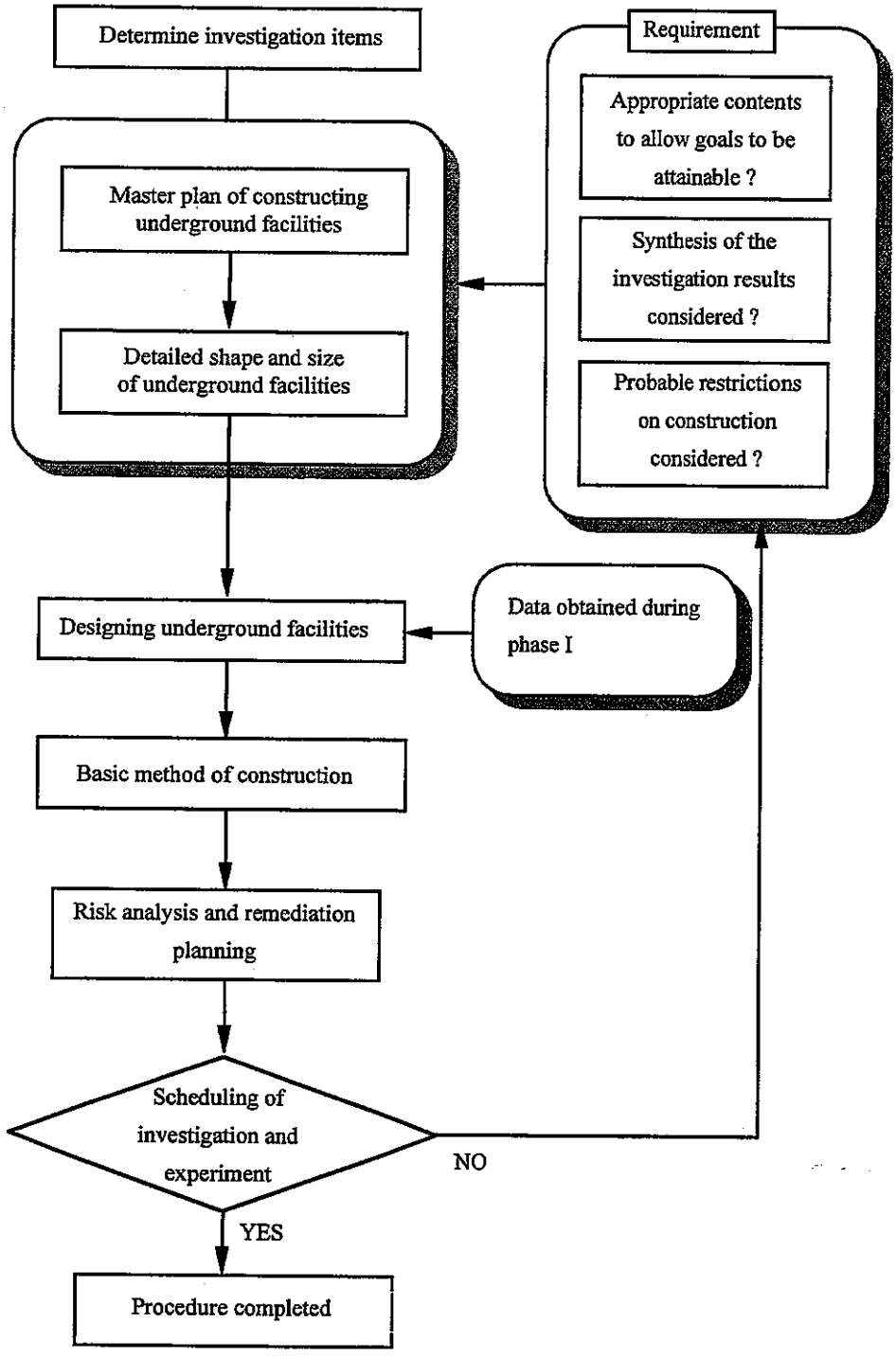

Figure 4.81 Procedure making for overall construction and investigations

First, based on the expected geological conditions in the MIU Project, a range of investigation items is considered. Next, the Master Plan was developed for constructing the underground and surface facilities. Also, detailed size and shape of the facilities were examined. Requirements for these examinations for design of facilities are as follows.

- Investigation items to allow the goals of Phase I to be attainable.
- Synthesis of the investigation results are taken into consideration.
- Probable restrictions on construction are taken into consideration.

Based on the data obtained in the Phase I and the investigation items, the layout of the research galleries takes concrete shape.

Details of the above three requirements are as follows.

Investigation items allow the goals of Phase I to be attainable

This requirement should take the following into consideration.

- Conditions of the geological environment needed for individual investigations

  For example, fracture (zones) serving as water paths and intersections between faults and research galleries are necessary for investigations in and after the Phase II. A major consideration is the hydrogeological flow system. For example any activities at the stages that would impact on hydraulic conditions should be done down gradient of any hydrogeological or tracer test experiments. Location relative to boundary conditions should also be considered.

- The repetition of individual investigations

  The predictions made in Phase I and the investigation methodologies can be re-evaluated by repeating the same experiment or study at both the Middle Stage at 500 m depth and the Main Stage at 1,000 m depth. For depth-dependent investigations, repetition of experiments or studies will be done at as many depths as possible using the above Stages or the Spare Stages. Spare Stages (horizontal, horse-shoe shaped, 3 m×3 m) are to be constructed approximately every 100 m depth, for experiments and studies and to install drainage equipment for maintenance of the research galleries. If unexpected geological are encountered the investigations, with possible reiterations, will be decided in the future.

- Period required for individual investigations

  Approximate schedules and durations must be set properly.

Synthesis of the investigation results are taken into consideration

With the purpose of establishing comprehensive investigation techniques for geological environments, it is important to synthesize the data from various investigations. It is important to construct comprehensive methodologies of "geosynthesis" for a variety of reasons, not least of which is to ensure appropriate and sufficient data is collected for integrated model building and for all concerned end users. For this requirement, objectives for individual investigations (e.g. fractures, fracture zones, faults, etc.), target areas, experiment siting and schedules for performance must be taken into consideration.

Probable restrictions on construction are taken into consideration

It is important to specify various conditions related to the construction schedule, method and facilities required for the investigations. Research galleries will be constructed throughout Phases II and III. Investigations in both Phases will be carried out simultaneously with the related construction work such as excavation and drilling. Therefore, the scheduling of research and construction activities and the timetable exert a great influence on the whole project. Construction itself might need to be suspended so as to perform high priority research investigations, if possible, without having an adverse effect on the overall project. For example when galleries are expected to intersect large or significant fracture zones or faults or when unexpected geological conditions are encountered.

4.7.2 Example of layout of underground facilities

Domestic and overseas experience and the requirements for underground research laboratories outlined by the Atomic Energy Commission (1994) [1] were examined. This exercise is useful in the preliminary planning or scoping of research activities that might be performed during and after Phase II. Complementary to this activity, the conceptual layout of the research galleries was examined. However, investigation activities and facility plans are not finalized yet. They will need to be further developed as the investigations in Phase I progress.

A conceptual layout of the underground facilities is as follows.

The MIU consists of surface facilities, the Main and Ventilation Shafts (each 1,000 m depth), the Main Shaft with a spiral ramp and two principal research locations where most galleries will be excavated, the Middle and Main Stages, for investigations in Phase III. The spiral ramp was designed to avoid premature disturbance of the Tsukiyoshi Fault due to intersection by the Main Shaft at about 950 m depth. The current layout is shown in Figure 4.82.

The Shobasama Site is underlain by rock that has variable structural styles; an uppermost deeply weather zone (~15m deep), a highly fractured 400 m thick structural domain immediately below the weathered rock, a 300 m thick structural domain from about 400 to 700 m depth with a fracture density lower than the rest of the granite. The deepest structural domain, deeper than 800 m, has the highest fracture density. This domain (fracture zone) is considered to be related to deformation due to fault movement. To ensure investigations are done in all the variety of geological settings possible, research galleries are planned at around 500 m and 1,000 m depth. Also, the spiral ramp is constructed to avoid the fault for scientific and operational reasons. One operational reason is to avoid potentially large water inflows from the fracture zones associated with the Tsukiyoshi Fault into the Main Shaft. A scientific reason is to avoid disturbance of the hydrogeological flow field associated with the fault before it can be properly instrumented and studied by boreholes and possibly by Mine-by type experiments. In addition, an operational advantage can be expected for the transportation of construction machinery and drilling of horizontal observation boreholes at several depths can be done more easily.

The surface facilities are composed of research/administration facilities, a sample storage area, an

equipment maintenance facility, a shaft head-frame facility, a muck deposit and a wastewater treatment facility.

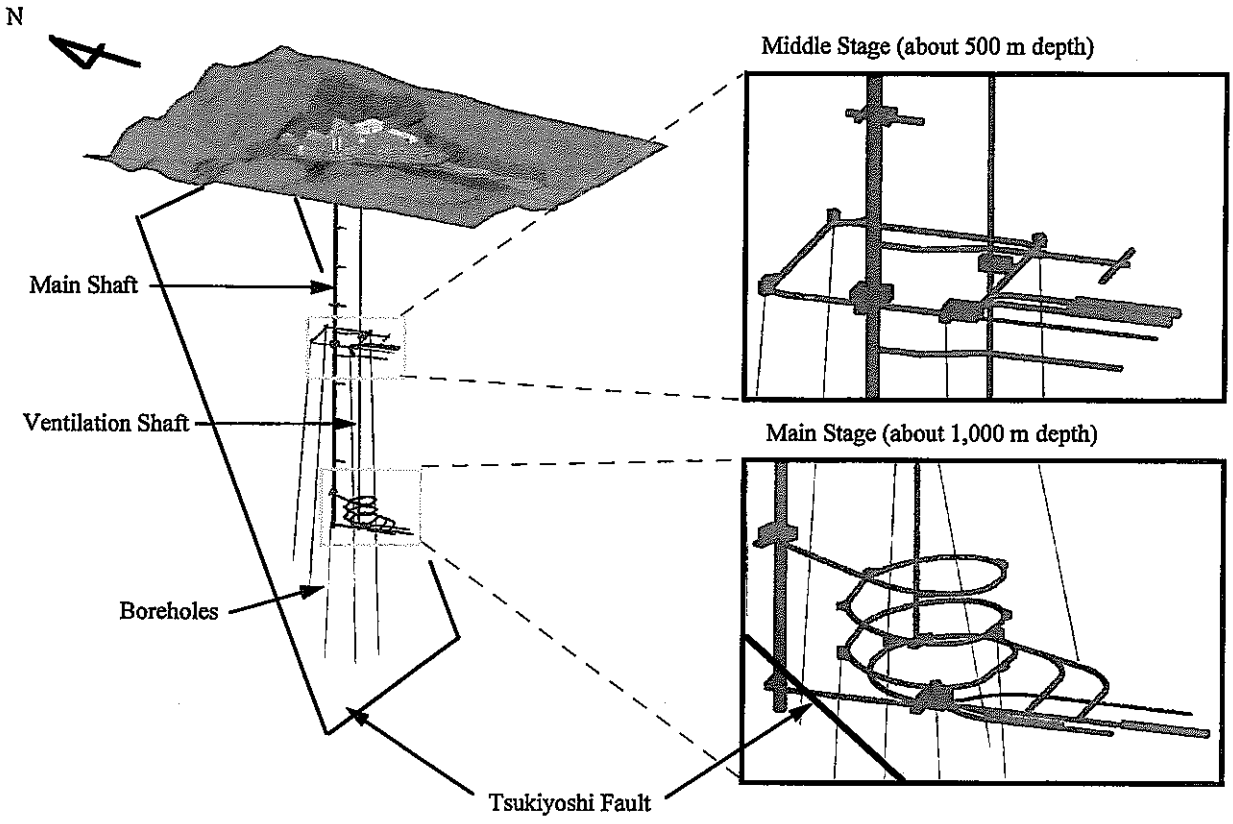

Figure 4.82 MIU conceptual design

5 Summary

5.1 Geological investigations

With respect to an assessment of (a) the amount of data that can or should be acquired, i.e., the data requirements for each of the investigations and the investigations to be performed and the relationship (b) the quality and accuracy of the results needed for analysis and modeling, geological models are constructed. For the Shobasama Site and the larger study area for groundwater flow simulations (about 4 km× about 6 km), two models were constructed. The first model was based on the data from literature surveys and other geoscientific research. The second model was based on this data plus the results from Phase I-a, in the 1996 to 1999 period.

In the first model, the granite could be divided into only two parts, the deeply weathered zone and the remaining rock mass, because of the lack of information of fractured zones or lithological variations in the granite.

The second model, supplemented with investigation results from Phase I-a, new geological units such as biotite granite, felsic granite, "Upper fracture zone", "Moderately fractured zone" and "Fracture zone along the fault" are defined by new geophysical logging and borehole investigations.

However, despite the improvements made, the second model still contains uncertainty related to the lack of information on tectonics in the northeastern part of the Shobasama Site, the deep underground exceeding 1,000 m and the fractures with steep inclination.

5.2 Hydrogeological investigations

In surface hydrological investigations, water balance observations and measurement of meteorological parameters were carried out. The aim is to determine the recharge rate for the top boundary condition needed for groundwater flow simulations and to develop techniques to obtain the evaluation data of the simulation results. As a result, it was estimated that groundwater recharge measures approximately 5 to 10% of the annual precipitation.

Hydraulic tests were carried out using the MIU-1, 2 and 3. As a result, groundwater level and hydraulic conductivity of the rock mass were estimated. In addition, hydrogeological properties of highly permeable fractured zones (presumed to be water channels) and the Tsukiyoshi Fault, presumed to be a hydraulic barrier to flow, were estimated.

As was done for the geological investigations, an assessment of the amount of data that can or should be acquired, i.e., the data requirements and the investigations (type, quantity, detail, scope) to be performed and the relationship to the accuracy of the results needed for analysis and modeling, hydrogeological models were constructed and groundwater flow simulations carried out. Both were carried out based on the following two data sets: a) data from literature survey and other geoscientific researches, b) data including

the results of Phase I-a. A continuum model was applied to the model construction and groundwater flow simulation using the pre-Phase I-a data. Then, an "equivalent continuum model" was developed statistically for the groundwater flow simulations using the earlier data and data from Phase I-a. As a result, it turns out that the "equivalent continuum model" predicts more realistically groundwater flow in the groundwater flow simulation in a medium-sized domain including structural discontinuities, i.e., fractures and faults. Specifically, an irregular hydraulic head drawdown formed along the distribution trend of fractures. Also, the Tsukiyoshi Fault was expressed as a hydraulic barrier to flow by change in hydraulic pressures.

5.3 Hydrochemical investigations

From the results of the RHS Project and other investigations, groundwater was sampled and its physicochemical parameters analyzed. The analysis indicated that the groundwater in the shallow part (shallower than 300 m in depth) in the Shobasama Site is of Ca^{+2}-Na^{+}-HCO_3^{-} type, neutral (pH=7) and oxidizing (Eh>0 mV). It changes to a Na^{+}-HCO_3^{-} type, weakly alkaline (pH=9), and reducing (Eh<-300 mV) at depths greater than 300 m.

To examine the groundwater evolution, the Fe^{3+}/Fe^{2+} ratio in cores (granite) obtained from the boreholes was measured. It indicates predominance of Fe^{3+} over Fe^{2+} at shallower than 300 m in depth. This indicates that oxidation-reduction environment in the granite varies with depth.

In the future, groundwater will be collected and analyzed in MIU-4 drilled in the Phase I-b. Also, using the data from the MIU-4 and the RHS Project, chemical and mineral compositions of rocks and the groundwater evolution will be examined.

5.4 Rock mechanical investigations

On the basis of the data on physical/mechanical properties and in situ stresses obtained in the AN-1 and the MIU-1, 2 and 3, rock mechanics conceptual models were constructed in the following three steps.

a) Construction using the data from the AN-1 and MIU-1,
b) Revision of Model (a) using the data from MIU-2,
c) Revision of Model (b) using the data from MIU-3.

As a result, three zones with unique physical and mechanical properties as well as in situ stress states were identified: ground surface to 300/400 m, 300/400 to 700 m and 700 to 1,000 m in depth.

In the future, mechanical/physical properties of the Tsukiyoshi Fault and associated fractured zones should be understood. Also, the validity of the model should be evaluated by numerical analysis. In addition, mechanical/physical properties of discontinuity planes should be assessed by the results of joint shear tests. As a result, the model is expected to be quantified.

5.5 Investigation techniques and equipment

Existing investigation techniques and equipment are being improved, including those developed by TGC.

In addition, investigation techniques and equipment that would be needed in and after the Phase II are also developed.

(1) Techniques and equipment for borehole investigations
A drilling system using a reverse aeration, wire-line method was designed. As well, the equipment for development of a partial-casing insertion system was assembled and an operational application test was carried out.

(2) Techniques and equipment for geological investigations
The development of seismic tomography using 1000 m deep boreholes was in progress to determine the extent of discontinuity planes deep underground. So far, testing was carried out in the existing boreholes aiming for application down to 1,000 m depth. In addition, the development of a data analysis technique called "full-wave form inversion analysis" was carried out with the purpose of improving data resolution.

(3) Techniques and equipment for hydrogeological and hydrochemical investigations
Hydraulic test equipment and water sampling equipment for depths to 1,000 m, assembled and utilized by 1998 FY, were improved for use in curved boreholes.

(4) Techniques and equipment for rock mechanical investigations
In situ stress measuring equipment for depths 1,000 m was designed and manufacture is underway.

(5) Techniques and equipment for use during and after Phase II
Continuous-wave radar investigation techniques, a long-term monitoring system in boreholes, and an investigation system for survey of research gallery walls were developed.

(6) Data base construction and management and development of a data analysis and visualization system
A data base management system was introduced and improved for management and utilization of the data. The system used for data analysis/visualization of data on geological environments, which is used for the construction of geological environment models and groundwater flow simulation, was also improved to enhance its function and operation.

(7) Techniques and equipment for information disclosure
Virtual reality (VR) technology was introduced, and VR software introducing the MIU Project was developed. Furthermore, the software was improved to allow visitors more realistic experience by using a head mounted display.

5.6 Evaluation of prediction

In order to evaluate predictions appropriately, it was considered necessary to clearly define an evaluation process. Taking this into consideration, international experience was examined.

5.7 Development of the engineering technology for deep underground

Basic design concepts were examined, domestic and overseas precedents considered and the requirements for underground research laboratories outlined by the Atomic Energy Commission (1994) [1] were referred to. According to the examination results, preliminary but conceptual designs of facilities were drawn up.

Reference

(1) Atomic Energy Commission (1994) : Long-term Program for Research, Development and Utilization of Nuclear Energy, Government Printing Office, Ministry of Finance, 41p (in Japanese).

(2) PNC (1996) : Master Plan of Mizunami Underground Research Laboratory, PNC Technical Report, PNC TN7070 96-002 (in Japanese).

(3) PNC (1996): Annual Plan of Geoscientific Researches in the MIU Project (1996), PNC Technical Report, PNC TN7010 97-004 (in Japanese).

(4) PNC (1997): Annual Plan of Geoscientific Researches in the MIU Project (1996), PNC Technical Report, PNC TN7010 97-005 (in Japanese).

(5) PNC (1998): Annual Plan of Geoscientific Researches in the MIU Project (1996), PNC Technical Report, PNC TN7410 98-002 (in Japanese).

(6) JNC (1999): Annual Plan of Geoscientific Researches in the MIU Project (1996), JNC Technical Report, JNC TN7410 2001-004 (in Japanese).

(7) JNC (1998): Mizunami Underground Research Laboratory Project - plan for the surface-based investigation (Phase I : 1999~2000 FY) -, JNC TN7410 99-004 (in Japanese).

(8) JNC Evaluation Committee for Research and Development (1999) : 1999 FY pre-research evaluation report - Research in the deep underground research facilities - (in Japanese).

(9) Wakita, K.(1988): Origin of chaotically mixed rock bodies in the Early Jurassic to Early Cretaceous and sedimentary complex of the Mino terrace, central Japan, Bull. Geol. Surv. Japan, 39(11), 675-757.

(10) Ryoke Research Group (1972): The Mutual Relations of the Granitic Rocks of the Ryoke Metamorphic Belt in Central Japan, Earth Science, Vol.26, 5, 205-216 (in Japanese with English abstract).

(11) Ishihara, S. and Suzuki, Y. (1969): Basement granites of the Toki Uranium Deposits in Tono region, Report, Geol. Surv. Japan, 232, 113-127 (in Japanese with English abstract).

(12) Itoigawa, J. (1980): Geology of the Mizunami district, central Japan, Monograph of the Mizunami Fossil Museum, No.1. 1-50 (in Japanese).

(13) Kaizuka, S., Kiso, T., Machida, T., Ota, Y. and Yoshikawa, T.(1964): Geomorphic development of the drainage basins of the Kiso and the Yahagi, Central Japan, Geographical Review, 37, 35-48 (in Japanese with English abstract).

(14) The Research Group for Active Faults (1980): Active faults in Japan, Tokyo University Press, 186-195 (in Japanese).

(15) JNC (2000): Regional Hydrogeological Study Project Results from 1992-1999 Period, JNC Technical Report, JNC TN7400 2000-014 (in Japanese with English abstract).

(16) White, M. J., C del Olmo (1996): The Application of Geological Computer Modeling Systems to the Characterization and Assessment of Radioactive Waste Repositories, Proc., The International Conference on Deep Geological Disposal of Radioactive Waste, Canadian Nuclear Society, 3-235-244.

(17) White, M. J., Humm, J. P. et al. (1998): GEOMASS : Geological Modeling Analysis and Simulation Software for the Characterization of Fractured Hard Rock Environments, Proc. The third Aspo International Seminar, Oskarshamn, June 10-12 1998, SKB TR-98-10, 233-242.

(18) McEwen, T. (1995): The Scientific and Regulatory Basis for the Geological Disposal of Radioactive Waste, Chapter 8, 239-320, John Wiley &Sons.

(19) Briggs, I. C. (1974): Machine Contouring Using Minimum Curvature, Geophysics, 39, 39-48.

(20) PNC (1994): Uranium Deposits in Japan, PNC Technical Report, PNC TN7420 94-006 (in Japanese).

(21) PNC (1995): Uranium Resources in the Tono area and its vicinity, PNC Technical Report, PNC TN7420 95-005 (in Japanese).

(22) Sugihara, K., Yoshioka, H., Imai, H. and Matsui, H. (1992): Outline of shaft excavation effects Project in Neogene sedimentary rocks, Proceedings of the Symposium on Underground Space 1992, Japan Society of Civil Engineers, 185-194 (in Japanese with English abstract).

(23) Inoue, D., Mizuochi, Y. and Sakurada, H. (1992): Geological Characteristics of "Linearment" and its Evaluation on Fractured System, Journal of the Japan Society of Engineering Geology, vol.33, 3, 25-34 (in Japanese with English abstract).

(24) Koide, K. and Yanagizawa, K. (1994): Examination of study area for Regional Hydrogeological Study using characteristics of linearment distribution, Program of 229th Meeting, Geological Survey of Japan, 3 (in Japanese).

(25) Kobayashi, K. and Koide, K. (1995): Division of geological structure based on the characteristics of linearment distribution, Proceeding of 1995 Meeting of Chubu Branch, Japan Society of Engineering Geology, 13-16 (in Japanese).

(26) Yamanoi, T., Wakamatu, H., Wachi, T. and Odagawa, S. (1997): Geological Survey on Regional Scale in Tono Area, JNC Technical Report, JNC 7440 2000-027 (in Japanese with English abstract).

(27) Shinohara, N. (1999): High Frequency Tensor CSMT & MT soundings in TONO Area, JNC Technical Report, JNC TJ7420 99-007 (in Japanese with English abstract).

(28) Yoneda, S. (1994): Seismic Refraction Survey at the Tono Research Field (1), JNC Technical Report, JNC TJ7308 94-007 (in Japanese with English abstract).

(29) Kawamura, T., Ito, T., Hasegawa, K. and Yabuuchi, S. (1996): Seismic reflection study using the Mini Impactor (CJM-MINI65) for the Tsukiyoshi fault, Tono, Central Japan, Proceeding of 104th Annual Meeting of the Geological Society of Japan, 521 (in Japanese).

(30) Ogata, N., Koide, K., Maekawa, K. and Inaba, H. (1996): Location and depth of boreholes excavated for the geoscientific research, PNC Technical Report, PNC TN7420 96-008 (in Japanese).

(31) Katayama, N. et al. (1974): "Genesis of uranium deposits of the Tono mine, Japan", IAEA-SM-183/11.

(32) Ogata, N., Osawa, H., Nakano, K., Yanagizawa, K. and Nishigaki, M. (1994): Relationships among Lithology, Permeability and Resistivity and their Application to Modelling of Hydrogeology, Journal of the Japan Society of Engineering Geology, Vol.32, 6, 51-62 (in Japanese with English abstract).

(33) Yanagizawa, K., Imai, H., Ogata, N., Osawa, H. and Watanabe, K. (1992): Shaft Excavation Effect Project on Groundwater Flow –Case Study at the Test Shaft in the Tono Mine, Central Japan-, Journal of the Japan Society of Engineering Geology, 33, No.5, 32-49 (in Japanese with English abstract).

(34) Abe, M., Ishikawa, K. and Kai, M. (2000): Core observations to grasp geological structure, JNC Technical Report, JNC TJ7440 2000-015 (in Japanese with English abstract).

(35) Yoshida, H., Osawa, H., Yanagizawa, K. and Yamakawa, M. (1989): Analysis of Fracture System in Granitic Rock -Case Study for the Granitic Rock, Gifu Prefecture, Japan- Journal of the Japan Society of Engineering Geology, 30, No. 3, 11-22 (in Japanese with English abstract).

(36) Sakuma, H., Tsubota, K., Olsson, O. and Lundmark, L. (1988): Case Study of RAMAC System in TOKI GRANITE, Proceedings of the 78th Conference of the Society of Exploration Geophysicists of Japan, 305-309 (in Japanese with English abstract).

(37) Oyanagi, M., Hirooka, S. and Sugihara, N. (1999): Seismic Survey using Controllable Vibratory Source, JNC Technical Report, JNC TJ7420 99-005 (in Japanese with English abstract).

(38) Oyanagi, M., Hirooka, S. and Iwasaki, T. (1999): Seismic Reflection Survey at Shomasamabora Site, JNC Technical Report, JNC TJ7420 99-020 (in Japanese with English abstract).

(39) Nishide, S., Kubota, R., Kawanishi, S., Nishiuchi, T., Tanase, A. and Baba, H. (1999): Drilling Survey (MIU-1) of Mizunami Underground Research Laboratory Project in Shobasama-bora site, JNC Technical Report, JNC TJ7440 98-001 (in Japanese with English abstract).

(40) Ishikawa, K., Mezaki, Y., Suzuki, H., Kai, M., Watanabe H., Fujimori, S. and Ishikawa J. (1999): Investigation program in borehole MIU-2 for the Mizunami Underground Research Laboratory project in the Shobasama site, JNC Technical Report, JNC TJ7420 99-016 (in Japanese with English abstract).

(41) Toyokura, I., Hashii, T., Nagoe, S., Ito, T., Sugimori, T., Sugita, N. and Masaeda, H. (2000): Drilling Survey (MIU-3) of Mizunami Underground Research Laboratory Project in Shomasama-bora site, JNC Technical Report, JNC TJ7440 2000-022 (in Japanese with English abstract).

(42) I.C.Briggs (1974): Machine Contouring Using minimum Curvature, Geophysics, Vol.39, p.39-48.
(43) Kikuchi, K. (1990): An introduction to geotechnics, Doboku-kogaku-sha (in Japanese).
(44) Fujii, N. (1968): "Genesis of the fireclay deposits in Tajimi-Toki district, Gifu Prefecture, Central Japan", Rept. Geol. Surv. Japan, No.230, 1-56.
(45) JNC (1999): Working programme for MIU-4 Borehole Investigations, JNC Technical Report, JNC TN7410 99-007.
(46) Suyama, Y. and Saegusa, H. (2000): Geological Modelling and Groundwater Flow Simulation in the Regional Hydrogeological Study Project, JNC Technical Report, JNC TJ7400 2000-012 (in Japanese with English abstract).
(47) Imai, H. and Yanagizawa, K. (1990): Overviews of groundwater flow analysis code : TAGSAC, PNC Technical Report, PNC TN7410 90-026 (in Japanese with English abstract).
(48) Inaba, H., Takeuchi, S., Okazaki, H., Saegusa, H. and Ogata, N. (1998): Simulation of groundwater flow in Tono mine, JNC Technical Report, PNC TN7410 98-001 (in Japanese with English abstract).
(49) Groundwater Handbook Editorial Committee (1989): Groundwater Handbook, Construction Industry Investigation Committee (in Japanese).
(50) Todd, D.K. (1989): Groundwater Hydrology Second Edition, John Wiley & Sons.
(51) Yahata, T. (1975): Soil Physics, University of Tokyo Press (in Japanese).
(52) Odagawa, S., Saegusa, H., Ogata, N., Wakamatsu, H. and Okazaki, H. (1999): Estimation of groundwater recharge from the subsurface to the rock mass around Tono Mine and a plan for the future study, Proceedings of Workshop on Rock Hydraulics, 13-18 (in Japanese with English abstract).
(53) Saegusa, H., Inaba, H., Koide, K. and Ogata, N. (1998): Simulation of regional scale groundwater flow in Tono area, PNC Technical Report, PNC TN7410 98-004 (in Japanese with English abstract).
(54) TGC (2000): Report on the DH-1 borehole investigations, JNC Technical Report, JNC TN7400 2000-006 (in Japanese).
(55) TGC (2000): Report on the DH-2 borehole investigations, JNC Technical Report, JNC TN7400 2000-007 (in Japanese).
(56) TGC (2000): Report on the DH-3 borehole investigations, JNC Technical Report, JNC TN7400 2000-008 (in Japanese).
(57) Yamauchi, D., Miyahara, T., Takeuchi, S. and Odagawa, S. (2000): Water Balance Observation Results Around the Mizunami Underground Research Laboratory, JNC Technical Review, No.9, 103-114, JNC Technical Report, JNC TN1340 98-001 (in Japanese with English abstract).
(58) Saito, M. and Sakamori, K. (2000): Manipulation of hydraulic heads measured continuously in the JNC's observation holes, JNC Technical Report, JNC TN7440 2000-017 (in Japanese with

English abstract).

(59) Toyama, S., Wakamatsu, H. and Okazaki, H. (2000): The installed of the groundwater place meter at the Shoma-sama site, JNC Technical Report, JNC TJ7420 2000-005 (in Japanese with English abstract).

(60) JNC (1999): Second Progress Report on Research and Development for the Geological Disposal of HLW in Japan, H12 : Project to Establish the Scientific and Technical Basis for HLW Disposal in Japan, Supporting Report 1 Geological Environment in Japan, JNC Technical Report, TN1400 99-021 (in Japanese ; also available in English, JNC TN1410 2002-002).

(61) Ogata N., Wakamatsu, H., Umeda, K. and Yanagizawa, K. (1995): Estimation of Subsurface Groundwater Flow by the River Runoff and Water Quality - A Case Study at the Tono Area, Central Japan -, Journal of the Japan Society of Engineering Geology, Vol.36, 1, 2-13 (in Japanese with English abstract).

(62) Toyama, S., Wakamatsu, H. and Odagawa, S. (2000): Compilation of Soil Moisture and Groundwater Level Data, JNC Technical Report, JNC TJ7440 2000-026 (in Japanese and English abstract).

(63) Saito, M., Ishizaki, S. and Sakamori, K. (2000): Manipulation of hydraulic heads measured/surveyed in the regional hydrogeological study area, JNC Technical Report, JNC TJ7440 2000-010 (in Japanese with English abstract).

(64) Shimo, M. and Nishijima, N. (2000): Crosshole Hydraulic Test between MIU-2 and MIU-3 Holes, JNC Technical Report, JNC TJ7400 2000-011 (in Japanese with English abstract).

(65) Onishi, A., Kubota, R., Kawanishi, S., Tanase, A. and Igeta, T. (1999) Investigative Drilling for the Study of the Regional Ground Water Flow System (2) -DH-9-, JNC Technical Report, JNC TJ7440 98-002 (in Japanese with English abstract).

(66) Matsunaga, T., Ikeda, N., Nagai, Y., Saito, M., Kudo, S., Akashi, T., Shigeno, M. and Kawamura, T. (1999): Investigation of Regional Flow Groundwater (DH-11), JNC Technical Report, JNC TJ7440 2000-023, vol.2 (in Japanese with English abstract).

(67) Shimo, M. and Nishijima, N. (2000): Regional Groundwater Simulation using Heterogeneous Equivalent Continuum Model, JNC Technical Report, JNC TJ7400 2000-008 (in Japanese with English abstract).

(68) Kikuchi, K., Mito, Y. and Honda, M. (1992): Stochastic Modelling of Rock Joint Distribution, Part 2: Joint Characteristic Elements and the Probabilistic Space Model, Journal of the Japan Society of Engineering Geology, 33, No.5, 19-31 (in Japanese with English abstract).

(69) Ohno, H. and Kojima, K. (1993): Fractal on the Spatial Distribution of Fractures in Rock Mass, Part 2 : Fractal Characteristics and Variability of Fractal Distribution, Journal of the Japan Society of Engineering Geology, 34, No.2, 12-26 (in Japanese with English abstract).

(70) Shimo, M. and Yamamoto, H. (1996): Groundwater Flow Simulation for Fractured Rocks using an equivalent Heterogeneous Continuum Model, Taisei Corporation Annual Report, 29, 257-262 (in Japanese).

(71) Ishizuka, M., Noda, M., Shiogama, Y. and Adachi, T. (1999): Design Study of Underground Facility of the Mizunami Underground Research Laboratory, JNC Technical Report, JNC TJ1400 99-001 (in Japanese with English abstract).

(72) CRIEPI (Central Research Institute of Electric Power Industry) and FEPC (Federation of Electric Power Companies) (1999): Study on Execution Techniques for High-level Radioactive Waste Disposal (in Japanese).

(73) Yin, J. and Cornet, F. H. (1995): Integrating hydraulic data and focal plane solution for regional stress determination. Proc. International Workshop on Rock Stress Measurement at Great Depth, 13-18.

(74) Brudy, M. and Zoback, M. D. (1993): Compressive and tensile failure of boreholes arbitrarily-induced to principal stress axis: application to the KTB borehole, Int. J. Rock. Mech. Min.. Sci., 1035-1038.

(75) Sugita, N., Arakawa, T., Lin, W., Masaeda, H., Nakajima, M., Sakaue, A., Narumi, A. and Oguchi, N. (1998): Measurement on Physical Property of Core Samples from MIU-1 Drill Hole in Laboratory, JNC Technical Report, JNC TJ7440 99-018 (in Japanese with English abstract).

(76) Hata, K. and Ouchi, H. (1998): Measurement of the initial stress in rock cored from MIU-1 borehole, JNC Technical Report, JNC TJ7440 98-003 (in Japanese with English abstract).

(77) Kato, H. (1998): *In situ* stress measurement in AN-1 borehole using hydraulic fracturing, JNC Technical Report, JNC TJ7420 99-013 (in Japanese with English abstract).

(78) Matsui, H. (1999): The results of the investigation on Rock mechanics in AN-1 and MIU-1 boreholes, JNC Technical Report, JNC TN7420 99-004 (in Japanese with English abstract).

(79) Kato, H. (1998): In situ stress measurement in MIU-2 borehole using hydraulic fracturing, JNC Technical Report, JNC TJ7440 98-003 (in Japanese with English abstract).

(80) Kuriyagawa, M., et al. (1988): Application of hydraulic fracturing to three dimensional in-situ stress measurements, Proc. 2nd Workshop on hydraulic fracturing stress measurements, 307-340.

(81) Matsui, H., Maeda, N. and Yoshikawa, K. (2000): The results of the investigation on Rock mechanics in MIU-2 borehole and the geomechanical conceptual model in Toki granitic body of hanging wall of Tukiyoshi fault, JNC Technical Report, JNC TN7420 2000-001 (in Japanese with English abstract).

(82) Association for the development of earthquake prediction (1990): Horizontal strain in Japan (in Japanese).

(83) Kato, H. (2000): *In-situ* stress measurement in MIU-3 borehole using hydraulic fracturing, JNC Technical Report, JNC TJ7430 2000-005 (in Japanese with English abstract).

(84) Matsui, H., Maeda, N. and Yoshikawa, K. (2001): The results of the geomechanical investigations in the MIU-3 borehole and the conceptual geomechanical model of the Toki granitie in Shobasama area, JNC Technical Report, JNC TN7420 2001-001 (in Japanese with English abstract).

(85) Kato, H. (1999): In situ stress measurement in 99SE-02 borehole using hydraulic fracturing, JNC Technical Report, JNC TJ7430 2000-001 (in Japanese with English abstract).

(86) Maeda, N., Sato, T., Matsui, H. and Sugihara, K. (1999): Estimation of applicability of stress measurement methods and three dimensional stress state in soft sedimentary rock, Proceeding of the '99 JAPAN-KOREA JOINT SYMPOSIUM ON ROCK ENGINEERING, 277-284.

(87) JNC (1998): Annual Report of Geoscientific Research in the MIU Project (1997), JNC TN7400 99-003 (in Japanese).

(88) JNC (2000): Annual Report of Geoscientific Research in the MIU Project (1999), JNC TN7410 2001-003 (in Japanese).

(89) JNC (1999): Annual Report of Geoscientific Research in the MIU Project (1998), JNC TN7400 2000-001 (in Japanese).

(90) PNC (1998): Annual Report of Geoscientific Research in the MIU Project (1996), PNC TN7410 97-042 (in Japanese).

(91) Shinohara, N. (1999): Field Application of the Borehole Sparker Source, JNC Technical Report, JNC TJ7420 99-006 (in Japanese with English abstract).

(92) Nakano, K., Takeuchi, R., Hirata, Y., Goto, K. and Nishigaki, M. (1996): Application of New Hydraulic Test Equipment to Deep Underground in Crystalline Rocks, The Proceeding of the 31st Conference of the Japanese Geotechnical Society, 2145-2146 (in Japanese).

(93) Koide, K., Nakano, K. and Ogata, N.. (1998): Current Status of Development of Groundwater Investigation and Simulation Methodologies in the PNC's Geoscientific Study Programme, Journal of Nuclear Fuel Cycle and Environment, Vol.4, 2, 59-71 (in Japanese with English abstract).

(94) Hama, K., Seo, T., Teshima, K., Nakano, K., Nakajima, Y., Shimazaki, S. and Nishizaki, M. (1995): Development of 1,000m-class water sampling equipment, Proceeding of 1995 Fall Meeting of the Japanese Association of Groundwater Hydrology, 20-25 (in Japanese).

(95) Sato, T. and Kato, H. (1998): Current status of development of 1,000m class initial stress measuring equipment using a stress release method, Proceeding of 1998 Meeting of the Mining and Materials Processing Institute of Japan, session (A), 41-44 (in Japanese).

(96) Kumazawa, M., Nakajima T. and Hasada, Y. (1998): Introduction to general theory and practice of EM ACROSS, Proceeding of 1998 Autumn Meeting of the Seismological Society of Japan, B07 (in Japanese with English abstract).

(97) Saito, H., Kawase, K., Sugihara, K. and Yamamoto, J. (2000): Application of Virtual Reality Technology to Activities for Offering Information for the General Public in the Mizunami Underground Research Laboratory Project, JNC Technical Review, 7, 93-98, JNC Technical Report, JNC TJ1340 2000-002 (in Japanese with English abstract).

(98) Stanfors, R. et al. (1997): Aspo HRL - Geoscientific evaluation. 1997/3. Results from pre-investigations and detailed site characterization. Comparison of predictions and observations. Geology and Mechanical stability, SKB Technical Report 97-04.

(99) Rhen, I. et al. (1997): Aspo HRL - Geoscientific evaluation. 1997/4. Results from pre-investigations and detailed site characterization. Comparison of predictions and observations. Geohydrology, groundwater chemistry and transport of solutes, SKB Technical Report 97-05.

(100) Rhen I. et al. (1997): Aspo HRL - Geoscientific evaluation. 1997/2. Results from pre-investigations and detailed site characterization, SKB Technical Report 97-03.

(101) Tsuboya, T. (1997): MIU – Mizunami Underground Research Project, Radioactive Waste Research, Vol.3, 2, 109-114 (in Japanese with English abstract).

(102) Mikake, S., Sugihara, K. and Nagasaki, Y. (2000): Development of Research Program and Design Concept of the Mizunami Underground Research Laboratory, JNC Technical Review, 6, 105-113, JNC Technical Report, JNC TN1340 2000-001 (in Japanese with English abstract).

Appendix 1 :

Overview of the MIU-1 borehole investigations

Appendix 1 (1) Overview of the MIU-1 Borehole Investigations

35°22'52.732" N, 137°13'37.516" E, 220.074 masl
Coordinate X: 5488.826, Y: -68629.358, Z: 220.074

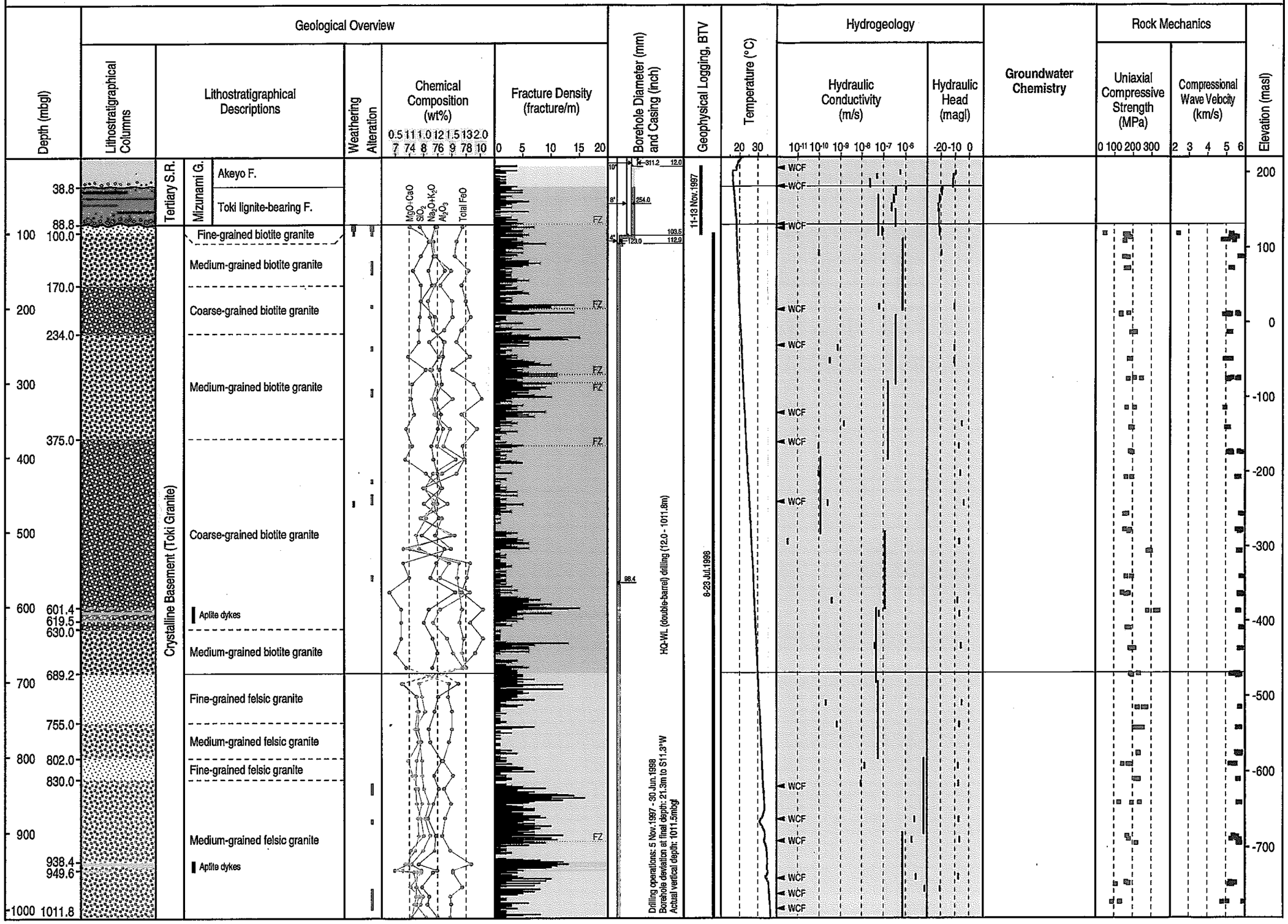

Appendix 1 (2) Overview of the MIU-1 Borehole Investigations

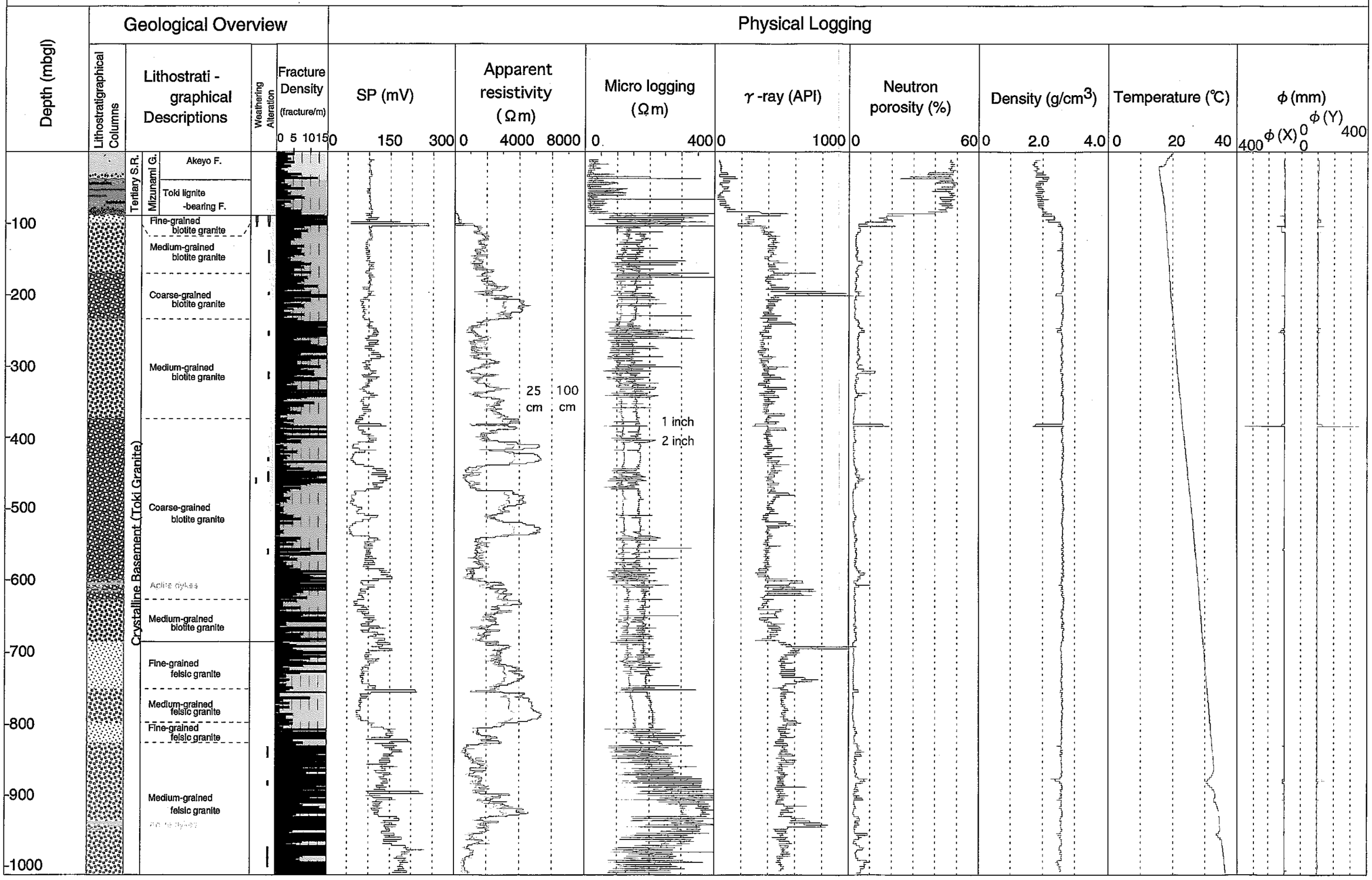

Appendix 2 :

Overview of the MIU-2 borehole investigations

Appendix 2 (1) Overview of the MIU-2 Borehole Investigations

35°22'55.2310" N, 137°13'35.3175" E, 223.755 masl
Coordinate X: 5433.295, Y: -68552.402, Z: 223.755

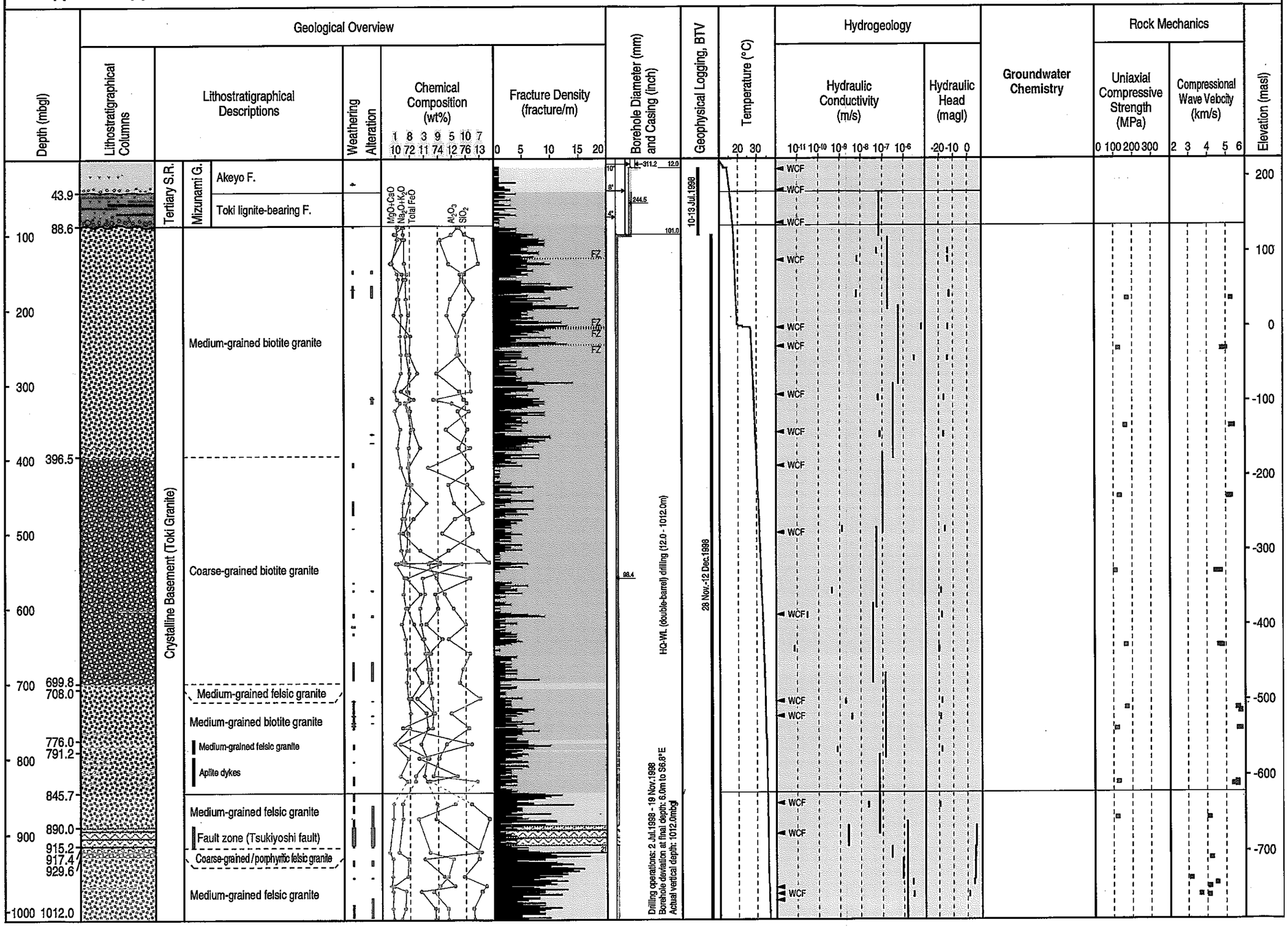

Appendix 2 (2) Overview of the MIU-2 Borehole Investigations

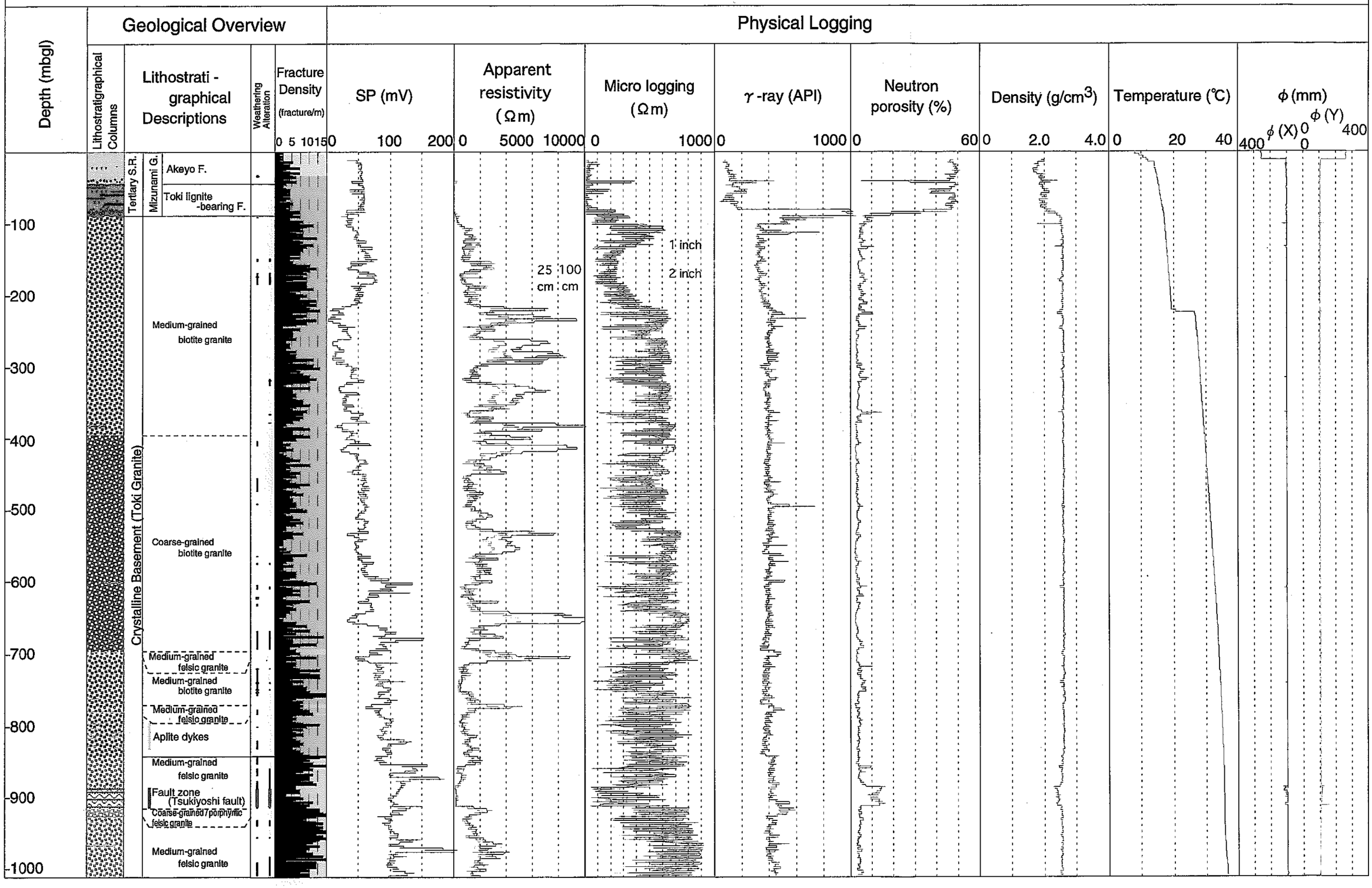

Appendix 3 :

Overview of the MIU-3 borehole investigations

Appendix 3 (1) Overview of the MIU-3 Borehole Investigations

35°22'58.3845" N, 137°13'31.6317" E, 230.475 masl
Coordinate X: 5340.231, Y: -68455.291, Z: 230.475

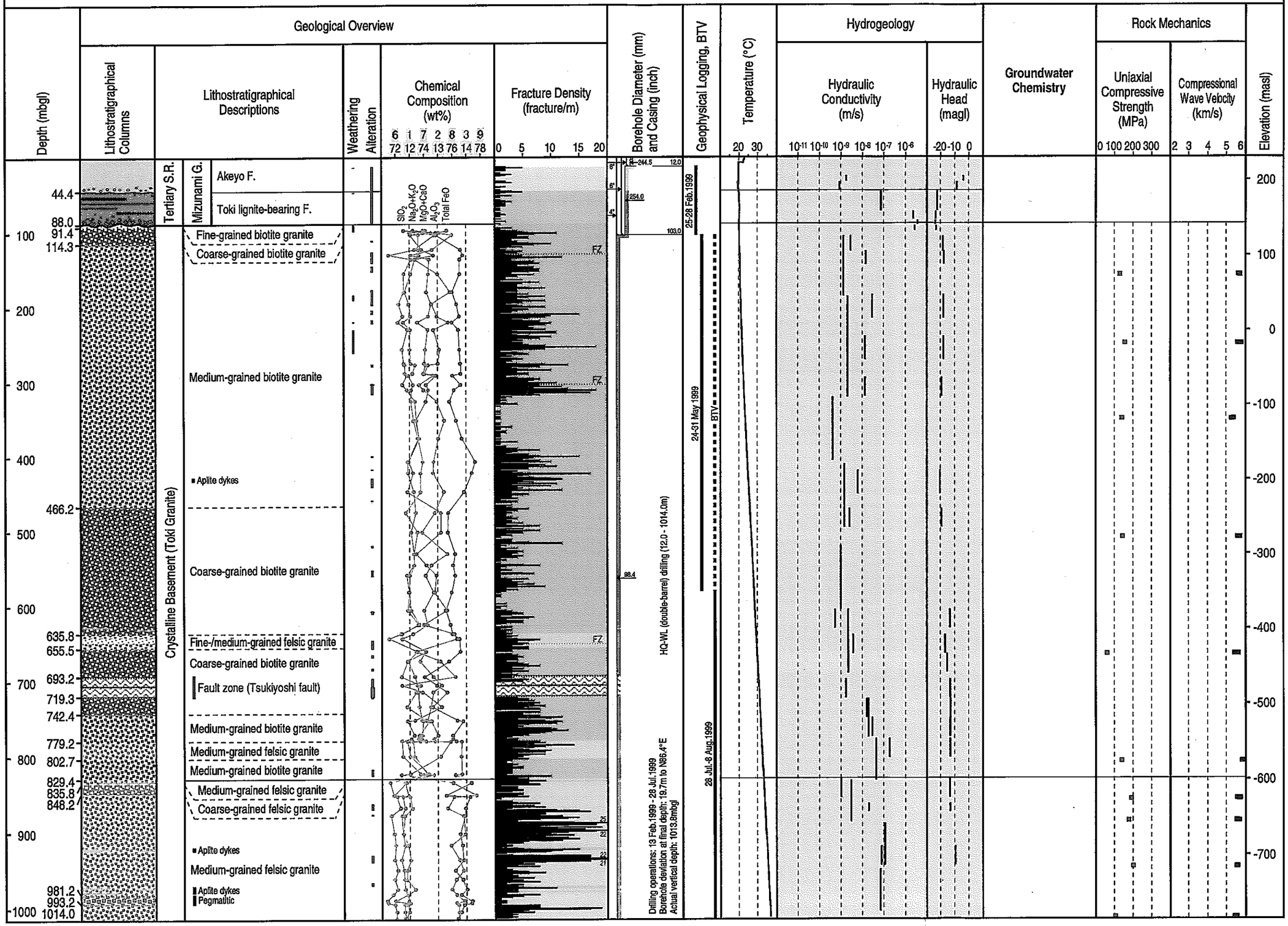

Appendix 3 (2) Overview of the MIU-3 Borehole Investigations